LBL-10593

Lawrence Berkeley Laboratory

UNIVERSITY OF CALIFORNIA

Materials & Chemical Sciences Division

Time Domain Multiple Quantum NMR

D.P. Weitekamp
(Ph.D. Thesis)

November 1982

Prepared for the U.S. Department of Energy under Contract DE-AC03-76SF00098

LBL-10593

TIME DOMAIN MULTIPLE QUANTUM NMR

By

Daniel P. Weitekamp

Ph.D. Thesis

November 1982

Department of Chemistry and

Lawrence Berkeley Laboratory

University of California, Berkeley, CA 94720

This work was supported by the Director, Office of Energy Research, Office of Basic Energy Sciences, Materials Sciences Division of the U. S. Department of Energy under Contract Number DE-AC03-76SF00098.

The United States Department of Energy has the right to use this thesis for any purpose whatsoever including the right to reproduce all or any part thereof.

TIME DOMAIN MULTIPLE QUANTUM NMR

Copyright © 1982

Daniel Paul Weitekamp

ABSTRACT

The development of time domain multiple quantum nuclear magnetic resonance is reviewed through mid 1982 and some prospects for future development are indicated. Particular attention is given to the problem of obtaining resolved, interpretable, many quantum spectra for anisotropic magnetically isolated systems of coupled spins. New results are presented on a number of topics including the optimization of multiple quantum line intensities, analysis of noise in two dimensional spectroscopy, and the use of order selective excitation for cross polarization between nuclear spin species.

ACKNOWLEDGEMENTS

It is a pleasure to acknowledge Alex Pines and my many colleagues and collaborators in multiple quantum NMR at Berkeley. Their contributions to this monograph go far beyond the work cited. Their insights, criticism, questions and friendship made my job both more fruitful and more enjoyable. Special thanks go to Joel Garbow, Rob Tycko and Yu-Sze Yen for proofreading and assistance with the manuscript and to Dione Carmichael and Cordelle Yoder for expert typing. Financial support through the National Science Foundation Graduate Fellowship program is appreciated.

To my parents,

Margaret and Dan

TABLE OF CONTENTS

		Page
I.	INTRODUCTION	1
II.	FUNDAMENTAL PRINCIPLES AND PHENOMENA	6
	A. Why NMR Was a Single Quantum Spectroscopy	6
	1. Motivation	6
	2. The Hamiltonians and the Density Operator	9
	3. The Single Quantum Fourier Transform Experiment	13
	B. Multiple Quantum Fourier Transform NMR	16
	1. The Three Pulse Experiment	16
	2. The General Form of the Pulse Sequence	19
	3. Notation	22
	4. Comparison with Single Quantum NMR	23
	C. Frequency Selective Excitation	25
	1. Background	25
	2. Applications	26
	a. The three level system	26
	b. Sequential two frequency excitation	27
	c. Selective multiple quantum pulses on resonance	29
	d. Simultaneous weak irradiation with two frequencies	30
	e. Double quantum rotary phenomena	30
	f. Double quantum decoupling	32
	g. Chemical shift powder patterns	33
	h. Double quantum deuterium spectra with magic angle spinning	36
	i. Multiple quantum spin tickling	39

TABLE OF CONTENTS (continued)

Page

D. Separation of the Transition Orders. 39

1. Transition Frequencies in the Off-Resonance Rotating Frame 39

2. Labeling of Coherence by the rf Phase of the Preparation Period 41

a. Order dependent phase shifts 41

b. Phase Fourier transformation 43

c. Time proportional phase incrementation 43

d. Implementation of small phase shifts 44

e. Related approaches to separation of the transition orders. 45

E. Consequences and Uses of Static Field Inhomogeneity. . 48

1. Spin Echoes in The Evolution Period. 48

2. Coherence Transfer Echoes. 53

3. Coherence Transfer Echo Filtering (CTEF) 55

4. Total Spin Coherence Transfer Echo Spectroscopy (TSCTES) 61

a. The problems which are solved by TSCTES. . . . 61

b. The pulse sequence 62

c. Single quantum TSCTES spectra. 64

d. Multiple quantum TSCTES spectra. 66

e. Limitations. 66

5. Diffusion in Field Gradients 67

6. Zero Quantum Coherence 68

a. Introduction 68

b. Relaxed performance conditions for zero quantum NMR. 68

c. Alternative excitation and detection methods for zero quantum coherence 69

TABLE OF CONTENTS (continued)

Page

F. Information Content and Symmetry Considerations. . . . 72

1. The Number of Transitions. 72

a. The general case 72

b. The role of permutation group symmetry 73

2. Time Reversal and Spin Inversion Parity. 75

a. Symmetry operations. 75

b. Degeneracy of bilinear Hamiltonians. 77

c. Operators with definite parity 78

d. Dynamic constraints on parity. 78

e. Applications 81

3. Information Content in Multiple Quantum Line Positions. 81

a. The questions. 81

b. The relative orientation of chemical shift tensors in powder patterns 82

c. The relative signs of J couplings in weakly coupled systems. 86

d. Isolation of signals from components of mixtures 87

e. The measurement of molecular order in anisotropic phases. 89

III. EXCITATION DYNAMICS FOR MANY LEVEL SYSTEMS 96

A. The Similarity of Preparation and Mixing 96

1. Motivation 96

2. Time Reversal Experiments. 96

3. General Approach to Matching Mixing and Preparation 98

4. Spin Inversion Transitions and Associated Echo Phenomena. 101

TABLE OF CONTENTS (continued)

Page

a. Introduction 101

b. Transition frequencies 102

c. Prescription for obtaining spin inversion transitions in phase 103

B. Statistical and Computational Aspects of Multiple Quantum Excitation 104

1. Line Intensities for Nonselective Excitation . . . 104

a. The statistical model of equal average line intensities. 104

b. Analytical expressions for line intensities for sequences of several strong pulses 109

c. Exact computation of line intensities. 109

d. Experimental determination of excitation functions. 112

2. The Maximization of Signal Energy in the Detection Period 113

a. Signal power and signal energy 113

b. The signal power for nonselective excitation . 116

c. The peak in signal power for matched preparation and mixing. 118

d. Signal power for an optimally excited group of lines. 120

e. Spatial removal of H_2. 122

f. Pulsed spin locking in t_2. 122

3. Fluctuations in the Excitation Function - t_1 Noise 125

a. The phenomenon 125

b. Simple formalism for t_1 noise. 126

c. Demonstration of the multiplicative nature of t_1 noise 129

d. The minimization of t_1 noise 130

TABLE OF CONTENTS (continued)

Page

e. Repetition rate 132

f. Reduction of t_1 noise by coherence transfer echo filtering 133

C. Order Selective Excitation. 135

1. Motivation. 135

2. Even or Odd Selection. 137

3. Excitation of Zero Quantum Transitions of Definite Spin Inversion Parity. 140

4. Average Hamiltonian Theory (AHT). 141

5. Phase Cycling. 144

a. Frequency domain picture. 144

b. AHT of phase cycling. 145

6. Subcycle Design. 151

a. The requirements for a successful subcycle. . . . 151

b. Time reversal sandwiches. 153

c. Stretched. 158

d. Selecting against n = 0 terms in the excitation Hamiltonian 158

e. A subcycle for liquids. 161

7. The Order of Selectivity. 162

a. Overview. 162

b. Zero-order selectivity. 162

c. First-order selectivity. 164

d. Higher order selectivity. 167

TABLE OF CONTENTS (continued)

Page

8. Subspace Dynamics and Line Intensities 167

a. Overview. 167

b. The available magnetization 168

c. Dynamical simplifications for n-quantum selection 173

d. Optimum line intensities. 178

9. Selective Population Inversion. 182

a. Motivation. 182

b. Two level and quasi-two-level systems 182

c. The quasi-four-level system (QFLS) 183

IV. MULTIPLE QUANTUM PROCESSES WITH TWO SPIN SPECIES. 191

A. Motivation 191

1. Doubly Rotating Frane Formalism. 191

2. Outline. 193

B. Cross Polarization and Multiple Quantum Coherence. . . . 194

1. Background. 194

a. Static Fields. 194

b. Hartman-Hahn matching. 194

c. Multiple quantum cross polarization. 197

d. Cross polarization by ADRF. 197

e. Total cross polarization. 198

2. Spin Polarization Exchange with Total Transfer of Entropy by Resonant Selection. 200

a. Motivation. 200

b. Heteronuclear phase cycling. 201

TABLE OF CONTENTS (continued)

Page

3. Multiple Quantum Cross Polarization of Quadrupolar Spins 205

C. The Spectroscopy of Heteronuclear Multiple Quantum Coherence. 207

1. Overview. 207

2. Pulse Sequences for HMQ Spectroscopy. 209

3. Techniques for Determining $\mathcal{H}_{IS}$ in Anisotropic Phases. 214

V. RELAXATION. 218

A. Overview. 218

1. Reversibility and Irreversibility. 218

2. Relaxation Times as Constraints. 220

B. Longitudinal Relaxation Times. 222

1. Master Equation Description for the Individual Populations. 222

2. Other Descriptions of the Quasi-constants. 222

C. Transverse Relaxation Times. 226

1. Complete Characterization of the Spectral Densities. . 226

2. Enhanced and Reduced Sensitivity to Fluctuations . . . 227

3. Correlations in Fluctuating Fields. 229

4. Spin Locking of Multiple Quantum Coherence. 230

5. Exchange. 234

REFERNCES 238

I. INTRODUCTION

In the last few years a class of time domain nuclear magnetic resonance experiments has been developed which makes accessible all possible transition frequencies and relaxation times in groups of coupled spins. These experiments are strikingly simple, requiring in many cases only a few radio frequency pulses. Yet they comprise a powerful and still largely unused approach to measuring the couplings and spectral densities which characterize a spin system.

The simple concept underlying all of these experiments is that by recording an NMR signal in one time period as a function of a preceding variable time, it is possible to map out features of the system which would not be manifest in a single free induction decay (f.i.d.) signal or its Fourier transform, the single quantum spectrum.

In retrospect it is apparent that this concept has played a role in the development of nuclear magnetic resonance for several decades. The earliest spin echo experiments in liquids led to the observation of echo amplitude modulation as a function of pulse spacing[1]. The explanation of this modulation constituted the discovery of the scalar or J coupling between spins[2], which had been masked by poor magnet homogeneity.

In solid state studies, the observation of the quadrupole echo[3] in high field was accompanied by smaller forbidden echoes whose intensity depended on the finite length of the first pulse. The explanation was found to be a coherent superposition between states differing by two in their Zeeman quantum number. This coherence, though not directly detectable, led to a signal after a second pulse[3].

In the last decade various experiments in which the f.i.d. is observed as a function of a prior time variable have been developed by a

number of research groups. The use in NMR of 2D arrays of signal $S(t_1,t_2)$ and their conversion by double Fourier transformation to spectra $S(\omega_1,\omega_2)$ was first proposed in an unpublished lecture[4].

Experiments aimed at monitoring the evolution of forbidden multiple quantum coherence between high field eigenstates developed without reference to this particular means of data analysis[5-8] and also as a special case of the generalized 2D experiment[9]. Little of the work covered in this monograph makes use of two dimensional displays of data. Nearly all of it, however, involves repeated recording of a transient as a function of a variable prior period of coherent evolution. In this sense, it will be referred to as 2D NMR.

The scope of this work does not encompass the whole of the burgeoning literature in the field of 2D NMR. Reviews of this field have appeared[10-12]. The focus will be only on studies of time domain (or Fourier transform) multiple quantum NMR. At least one literature review of multiple quantum NMR has appeared[13], which includes reproductions of many of the early results. I hope that the present work presents pedagogically the principal time domain multiple quantum phenomena appearing in the literature through mid 1982. In addition a number of new results and possible extensions are included. No claim to a balanced coverage of the literature is made, though the intent is to alert the reader to those topics which are not treated in any depth. I apologize in advance for the possible oversights. In the interest of cohesiveness, the notation of the original work has often been distilled away and with it, no doubt, some of the flavor.

The approach taken is to incorporate experimental results into the theoretical discussion as it is developed. These illustrative examples

are, as a matter of convenience, largely from the work of the Berkeley group directed by Alex Pines.

Figure 1 is a proton multiple quantum spectrum of benzene partially oriented in a liquid crystal[14-16]. It is presented here to serve as a point of reference for introduction of the sections to follow. This system, whose energy level structure is well-known from its single quantum spectrum[17], has served as the testing ground for many of the developments of time domain multiple quantum NMR. The spectrum consists of well resolved lines at positions determined by the energy differences between individual pairs of the 2^6 spin eigenstates of this isolated system of 6 spin ½ nuclei.

Section II begins with a discussion of the traditional NMR experiments and their relationship to time domain multiple quantum NMR. After a consideration of some general features, much of the early work is reviewed in Section IIC. Attention then turns in Section IID to the methods of separating the spectral lines by their transition order n, which is the difference in Zeeman quantum number between the states connected. This feature is evident in Figure 1 where n runs from zero through six. Section IIE discusses the many facets of magnetic field inhomogeneity, including methods for eliminating its effect on the linewidth. One such method was employed to obtain Figure 1. The information content of the line positions is considered in Section IIF along with symmetry operations on the spatial and spin coordinates of the Hamiltonians.

Section III takes up the interactions of the spin systems with the radiation field and how these determine the line intensities and the signal-to-noise ratio. A major theme is the means by which the technique

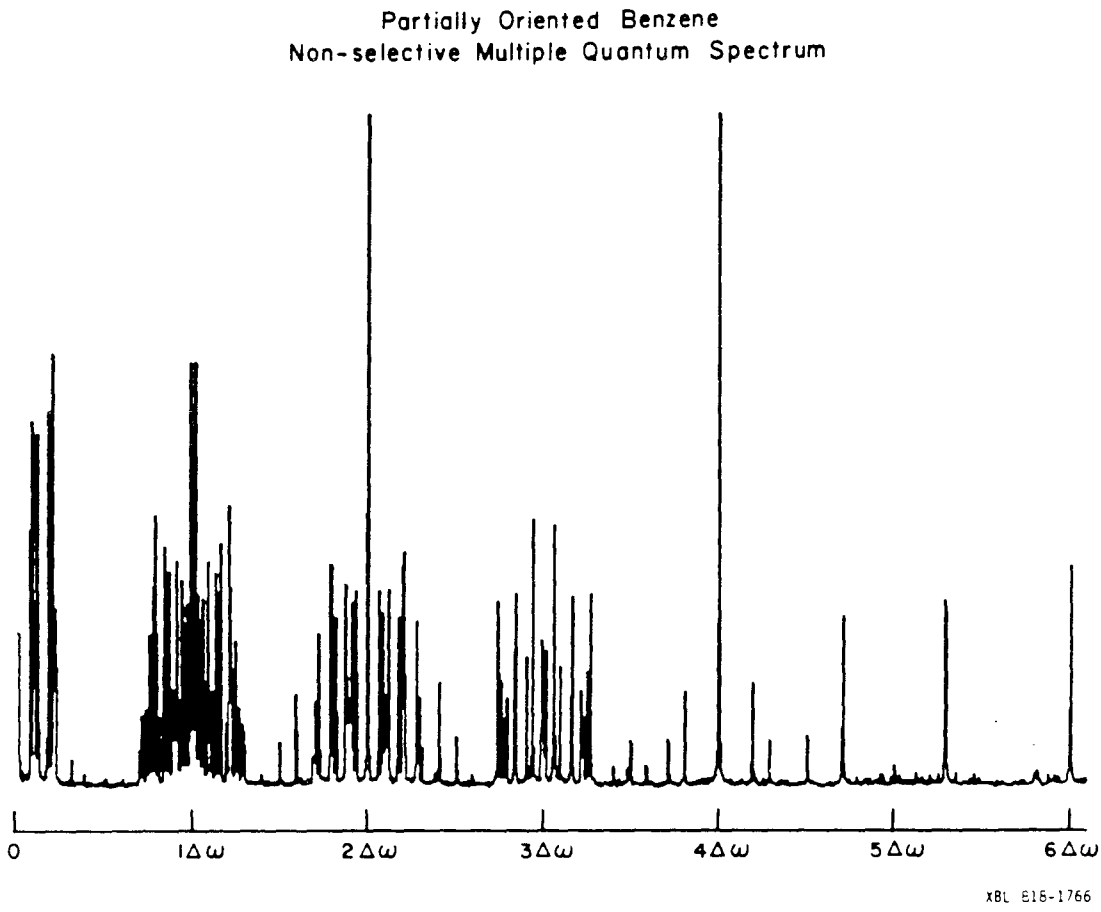

Figure 1. Fourier transform multiple quantum NMR spectrum of benzene partially oriented in a nematic liquid crystal. This highly symmetrical six proton system has been used as a prototype to demonstrate a variety of multiple quantum phenomena. The spectrum shown here is a typical nonselective experiment in which all allowed coherent superpositions of pairs of states are prepared and detected. Note that the transitions appear in separated spectra according to the change in Zeeman quantum number. The complexity of each decreases from left to right until for the highest order spectrum labeled $6\Delta\omega$ there is a single transition. The pulse sequences and analysis required to obtain and interpret such a spectrum are reviewed in Section II.

[By permission from S. Sinton, "NMR Studies of Oriented Molecules", Ph.D. dissertation, University of California, Berkeley, 1981, published as Lawrence Berkeley Laboratory Report LBL-13604).

may be extended to larger systems by minimizing noise (Sec. IIIB) and making the most efficient use of the equilibrium nuclear magnetization (Sec. IIIB and IIIC).

Section IV considers the extensions of multiple quantum techniques to systems of two or more different spin species. The role of multiple quanta is considered in the exchange of order between spin systems and in the spectroscopy of heteronuclear systems.

Section V treats relaxation processes. These irreversible processes determine the line widths of spectra such as Figure 1, limit the range of systems for which such spectra may be obtained, and at the same time are among the most informative phenomena measurable by time domain multiple quantum NMR.

II. FUNDAMENTAL PRINCIPLES AND PHENOMENA

A. Why NMR Was a Single Quantum Spectroscopy

1. Motivation

The usual NMR experiments are designed to observe the frequencies and intensities of the magnetic dipole transitions of a system of nuclei in a magnetic field[18]. In the low power continuous wave (CW) experiment, a precessing magnetization proportional to the perturbing rf field is created when the resonance condition is met for one of these transitions. In the Fourier transform (FT) experiment, an intense brief pulse of radiation creates a transverse magnetization which precesses with components at the same resonant frequencies found in the CW experiment.

The identity of the spectra obtained by the two methods is a remarkable fact[19-21]. In each case the absorption spectrum may be written in the limit of infinitely sharp lines as

$$S(\omega) \propto \sum_{i>j} |\langle i|I_+|j\rangle|^2 \, \delta(\omega - \omega_{ij}) \tag{2.1}$$

The states $|i\rangle$ and $|j\rangle$ are the eigenstates of the unperturbed internal spin Hamiltonian $\mathcal{H}_{int}$ which characterizes the system whose total spin angular momentum components are I_x, I_y, and I_z. The matrix elements are of the raising or lowering operators.

$$I_\pm = I_x \pm iI_y \tag{2.2}$$

In the usual high field limit

$$[\mathcal{H}_{int}, I_z] = 0 \tag{2.3}$$

and

$$I_z|i\rangle = M_i|i\rangle \tag{2.4}$$

The Zeeman quantum number M_i is a good quantum number and the only non-zero matrix elements of I_+ are between eigenstates with

$$n_{ij} \equiv \Delta M_{ij} \equiv M_i - M_j \tag{2.5}$$

equal to ±1. Thus $I_\pm$ are single quantum operators and the spectrum described by (2.1) is a single quantum spectrum.

Figure 2 shows a schematic energy level diagram for a system of coupled spins in a large magnetic field. The particular Zeeman quantum numbers are appropriate to a system of N spin ½ nuclei. The solid arrows indicate allowed single quantum transitions, the matrix elements of which appear in (2.1). The dashed arrows indicate those transitions not observed in the usual experiments. In fact the majority of the transitions are multiple quantum transitions and their observation may be desirable for a number of reasons. The single quantum spectrum may be ambiguous; it might arise from any number of Hamiltonians or may be insensitive to some quantity of interest. The single quantum spectrum may be too complex; the number of lines may be so great that resolving or assigning individual lines becomes impossible. The single quantum spectrum may not contain sufficient information to fully characterize the Hamiltonian or the relaxation of the system. In each case the difficulty might be resolved if we were able to observe the transitions which are forbidden by the $n \equiv \Delta M = \pm 1$ selection rule.

In CW NMR the single quantum selection rule arises from the assumption that the perturbing rf field H_1 is small. The expression (2.1) arises then from first order perturbation theory. If the rf power is

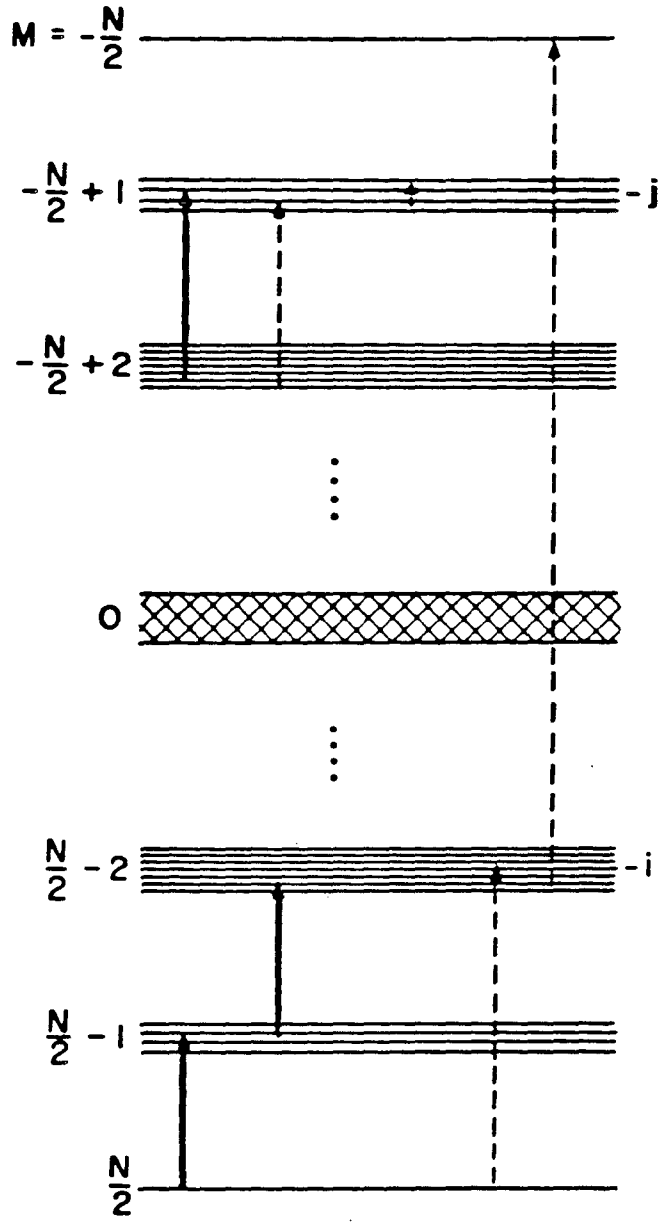

XBL 7710-10019

Figure 2. Schematic representation of the high field energy level diagram for N coupled spins 1/2 . The energy levels are grouped into manifolds according to their Zeeman quantum number M. The energy difference between adjacent manifolds is $\hbar\omega_0$ where ω_0 is the Larmor frequency used for irradiation and detection. The structure within each manifold is due to the chemical shifts and the couplings between spins. The solid arrows indicate some of the magnetic dipole allowed single quantum transitions which are detected in conventional NMR. The dashed arrows indicate dipole forbidden transitions which are, however, allowed in the Fourier transform multiple quantum experiments.

increased, the single quantum lines become broad and new absorption lines appear with intensities proportional to higher powers of H_1. This phenomenon of CW multiple quantum NMR was observed over twenty years ago [22-23]. It has been extensively analyzed by high order perturbation theory[24].

While some few applications have been made[13], CW multiple quantum NMR is both difficult and clumsy. Line shapes and positions depend on the amplitude of H_1 as well as on the chemically interesting unperturbed Hamiltonian and relaxation processes. Perhaps the greatest single difficulty is that the different resonant processes occurring in a given frequency range are distinguished only by the dependence of their lineshapes on rf intensity. Consequently, they are not easily sorted out from one another in a complex system.

These problems would vanish if we could observe the multiple quantum transitions without the complications of the perturbing rf field. In the usual Fourier transform experiment, the single quantum transitions are observed in just this way. The perturbing field is absent during the time that the system is exhibiting its eigenfrequencies through a f.i.d. The principal subject of this work is experiments which allow the measurement of multiple quantum interferograms analogous to the single quantum f.i.d.

To describe first the single and then the multiple quantum Fourier transform experiments we will use a rotating frame density operator formalism[25,26].

2. The Hamiltonians and the Density Operator

The resonant rotating frame is the interaction representation where the large average interaction of the spins with the applied

static field has been transformed away. This has the consequence that the trivial evolution (precession) of the system at the Larmor frequency and its harmonics is demodulated leaving only the much slower evolution due to rf irradiation, chemical shift differences, couplings between spins and, in the case of spins $I \geq 1$, couplings between the nuclear quadrupole moment and the molecular electric field gradients.

The Hamiltonian describing these interactions for a single spin species may be written

$$\mathcal{H}_{tot} = \mathcal{H}_{rf} + \mathcal{H}_{int} \tag{2.6}$$

The term describing the interaction of the spins with the rf field is

$$\mathcal{H}_{rf} = -\omega_p(I_x\cos\psi - I_y\sin\psi) - \Delta\omega I_z \tag{2.7a}$$

$$= -\omega_p I_\psi - \Delta\omega I_z \tag{2.7b}$$

where ψ is the phase of the radiation with respect to a spectrometer reference frequency and $\omega_p = \gamma H_1$ if the linearly polarized rf irradiation has amplitude $2H_1$. The internal Hamiltonian of the system consists of two sets of terms.

$$\mathcal{H}_{int} = \mathcal{H}^Z + \mathcal{H}^{ZZ} \tag{2.8}$$

The terms linear in the individual spin angular momenta are

$$\mathcal{H}^Z = -\sum_i \omega_{zi} I_{zi} - \omega_z(\vec{r})I_z \tag{2.9}$$

where ω_{zi} are the chemically shifted resonance frequencies of the individual spins relative to the spectrometer reference frequency defining

the rotating frame. The spatially dependent offset $\omega_z(\vec{r})$ is included in the internal Hamiltonian as a reminder that even in the absence of chemical shifts, all molecules in the sample are not isochronous. The convention used will be that $\sum_i \omega_{zi} = 0$ and $\int \omega_z(\vec{r})d\vec{r} = 0$, which is consistent with the incorporation of any net offset into (2.7).

The terms which are bilinear in the spin angular momenta are

$$\mathcal{H}^{zz} = \mathcal{H}^D_{II} + \mathcal{H}^Q_I + \mathcal{H}^J_{II} \tag{2.10}$$

The first two transform as second rank tensor operators. The direct dipolar interaction

$$\mathcal{H}^D_{II} = -\sum_{i<j} D'_{ij}(3I_{zi}I_{zj} - I_i \cdot I_j) \tag{2.11}$$

is the single most important term for most of the applications to be discussed. For $I < 1$ it is the largest internal term. Furthermore it has a straightforward geometric interpretation (Sec. IIF3). The primes will be used to denote parameters written in radians $\sec^{-1}$ when the unprimed symbol is conventionally expressed in Hz.

For $I \geq 1$ the quadrupole term

$$\mathcal{H}^Q_I = \sum_i (\omega_{Qi}/3)(3I^2_{zi} - I(I+1)) \tag{2.12}$$

will usually dominate the single quantum dynamics. The possibility of sidestepping this large term with multiple quantum transitions forms the basis of some of the earlier applications of the technique (Sec. IIC2).

The indirect or scalar coupling

$$\mathcal{H}^J_{II} = -\sum_{i<j} J'_{ij}\, \underset{\sim}{I}_i \cdot \underset{\sim}{I}_j \tag{2.13}$$

is at once the smallest and most recalcitrant term. The impossibility of manipulating this interaction with intense rf fields is both a rationale for and a complication in the excitation of high quantum coherence.

The density operator of the system of spins will usually start off at equilibrium in a static field H_0. This may be expressed as

$$\rho(0) = bI_z, \qquad b = \frac{-\gamma\hbar H_0}{kT(2I+1)^N} \tag{2.14}$$

The high temperature (Curie law) limit has been assumed and the term proportional to the identity operator has been dropped since it has no dynamics. Furthermore, the high field limit has been assumed; the only ordering of the spins at equilibrium is along the field direction and this ordering is far from complete. The constant b in (2.14) is appropriate to N nuclei of spin I and gyromagnetic ratio γ.

A consequence of dropping the identity operator is that in this notation

$$\mathrm{Tr}\ \rho(t) = 0 \tag{2.15}$$

(rather than unity) expresses conservation of probability. For periods of time over which relaxation is negligible the traces of higher powers of ρ are also conserved. For example

$$\mathrm{Tr}(\rho^2(t)) = \mathrm{Tr}(\rho^2(0)) \tag{2.16}$$

expresses conservation of the norm (squared) of the density operator viewed as a vector in a Hilbert space called Liouville space, which is the phase space of the spin system.

In nearly all of the examples to follow, the sample will consist of an ensemble of isolated groups of coupled spins. Such groups occur on molecules in liquids and often in liquid crystals because the couplings between molecules are motionally averaged to zero by diffusion. In solids such isolated groups occur through chemical or isotopic dilution, aided in some cases by spin decoupling. The techniques discussed are in many cases not limited to such isolated groups, but do find their most elegant applications in such samples, because of the possibility of observing resolved transitions.

3. The Single Quantum Fourier Transform Experiment

The simplest time domain experiment begins with a resonant pulse of intense rf magnetic field sufficiently brief that the internal Hamiltonian may be neglected during the pulse. The time development during the pulse is described by

$$\rho(t_p) = \exp(-i\omega_p t_p I_y) I_z \exp(i\omega_p t_p I_y) = I_x \tag{2.17}$$

where ω_p is the nutation frequency and $\omega_p t_p = \pi/2$. The system now develops under the influence of the unperturbed Hamiltonian so that

$$\rho(t) = \exp(-i\mathcal{H}_{int} t) I_x \exp(i\mathcal{H}_{int} t) \tag{2.18}$$

The operator for the observable transverse magnetization is

$$M_- = \gamma\hbar I_- = \gamma\hbar(I_x - iI_y) \tag{2.19}$$

The operator is non-Hermitian because it actually represents two quantum mechanical observables. Suppressing the constants, the complex f.i.d. signal in the two audio frequency channels of the phase sensitive heterodyne detector is

$$S(t) = \mathrm{Tr}(\rho(t)I_+) \tag{2.20}$$

Expanding the density operator given by (2.18) in the eigenbasis of a spatially homogeneous $\mathcal{H}_{int}$ gives

$$\rho(t) = \sum_{i,j} \langle i|I_x|j\rangle|i\rangle\langle j| \exp(-i\omega_{ij}t) \tag{2.21}$$

where $\omega_{ij} = \omega_i - \omega_j$ and

$$\mathcal{H}_{int}|i\rangle = \omega_i|i\rangle \tag{2.22}$$

have been used. Taking the trace (2.20) in this basis gives the single quantum free induction signal without any decay

$$S(t) = \frac{1}{2} \sum_{i>j} |\langle i|I_+|j\rangle|^2 \exp(-i\omega_{ij}t) \tag{2.23}$$

Fourier transformation shows the equivalence to (2.1).

This derivation demonstrates that the restriction to single quantum transitions, an apparent linear response, occurs despite the fact that ω_p during the pulse was arbitrarily intense. There are two significant aspects to this well-known result.

The first is that the density operator $\rho(t)$ contains only single quantum coherence: superpositions of states coherent over the sample and satisfying $n_{ij} = \pm 1$ for all finite $\rho_{ij}(\tau)$. This is a corollary of the high temperature approximation. The initial operator I_z is the $n = 0$ component of a spherical tensor operator[27] $T_n^{\ell\alpha}$ of rank $\ell = 1$. The label α is needed since generally more than one tensor operator of the same rank is required to form a complete basis in Liouville space. Any rotation can only result in other components of the same tensor operator.

The only other components are $n = \pm 1$, since $|n| \leq \ell$. The result of a $\pi/2$ rotation, as in (2.17), is the sum of the $n = \pm 1$ components, which is I_x. Since n is conserved by both $\mathcal{H}_{int}$ and by any relaxation processes[28,29], only single quantum coherence exists at any time after a single brief pulse.

Thus it is the particular initial condition of equilibrium at high temperature which assures the identity of the relative line intensities for the CW and FT experiments[19]. Other nonequilibrium initial conditions and their consequences for single quantum NMR have been discussed[20,21,30,31]. These include systems which have been adiabatically demagnetized to a state of dipolar order[30] or dynamically polarized to spin temperatures sufficiently low that the quasi-equilibrium density operator is nonlinear in the spin angular momenta[31]. Such initial conditions contain tensor operators with rank $\ell > 1$ and give multiple quantum coherence upon a single pulse. This has been demonstrated for the case of dipolar order[32].

Aside from the nature of the initial condition, the second aspect of the one pulse experiment which makes it single quantum is that the expectation value of transverse magnetization in (2.20) indicates the measurement at successive times of a single quantum operator. Because of our inability to measure any spin observables of the system other than oscillating magnetization, only single quantum coherence is directly detectable. Thus even for an arbitrary initial condition, free evolution offers no direct evidence of any multiple quantum coherence which may exist. The multiple quantum coherence is invisible.

B. Multiple Quantum Fourier Transform NMR

1. The Three Pulse Experiment

Although n is conserved under free evolution, the tensor operator rank ℓ is not, in general, conserved if $\mathcal{H}_{int}$ contains terms which are bilinear in the single spin angular momentum components. These are just the terms collected as $\mathcal{H}^{zz}$ in (2.10). In liquids, where $\mathcal{H}_I^Q$ and $\mathcal{H}_{II}^D$ vanish, the chemical shifts of (2.9) are necessary in conjunction with $\mathcal{H}_{II}^J$ to cause evolution away from the $\ell = 1$ operator present after a single brief pulse. This is so since $\mathcal{H}_{II}^J$ (2.13) is a scalar operator. For arbitrary values of its parameters it commutes with $\underset{\sim}{I}$.

Thus some time after the initial pulse, on the order of the inverse of the couplings, the density operator expanded as a sum of tensor operators has the form

$$\rho(t) = \sum_{\ell,\alpha,\pm 1} \rho_{\ell,\alpha,\pm 1}(t)\ T_{\pm 1}^{\ell\alpha} \tag{2.24}$$

where the time dependence is in the coefficients $\rho_{\ell,\alpha,n}(t)$. All values $\ell \leq 2NI$, the total spin of the system, are possible.

If at time $t = \tau$ a second brief rf pulse is given[9], then[15]

$$\rho(\tau) = \sum_{\ell,\alpha,n} \rho_{\ell,\alpha,n}(\tau)\ T_n^{\ell\alpha} \tag{2.25}$$

with no restrictions on the indexes other than $|n| \leq \ell$. The second pulse need not differ in any way from the first pulse, which gave only single quantum coherence. The appearance of all orders n of coherence after the second pulse is a result of the internal Hamiltonian having brought the ensemble to a state capable of engaging in coherent exchange of several photons with the radiation field.

The relationship between the operators $T_n^{\ell\alpha}$ and the off-diagonal eigenoperators $|i><j|$ of an eigenbasis expansion is easily discerned from the defining property[27]

$$[I_z, T_n^{\ell\alpha}] = nT_n^{\ell\alpha} \tag{2.26}$$

and the related property

$$[I_z, |i><j|] = n_{ij}|i><j| \tag{2.27}$$

which follows from (2.4) and the definition (2.5). Thus the operators $T_n^{\ell\alpha}$ span that part of Liouville space consisting of coherent superpositions of states with $n_{ij} = n$. Operators in either basis set will be called n-quantum operators. The eigenoperator basis will prove most convenient, but the tensor operators will make occasional appearances because of their particularly simple transformation properties under rotations.

Having prepared multiple quantum coherence we are still faced with the problem of how to follow its free evolution in analogy to the way that the f.i.d. follows the single quantum evolution. The detection system is only sensitive to oscillating magnetization which corresponds to the rotating frame operators I_x and I_y. Thus a third pulse is required to convert the unobserved multiple quantum operators into $n = \pm 1$ operators which may then evolve into a signal.

This three pulse sequence[9] is shown in Figure 3. The preparation time τ is fixed and, in the simplest version, the components of the oscillating magnetization are sampled at a fixed time t_2. The evolution time t_1 is incremented after each shot and the pulse sequence is repeated. The resulting signal in the two channels of the phase sensitive detector

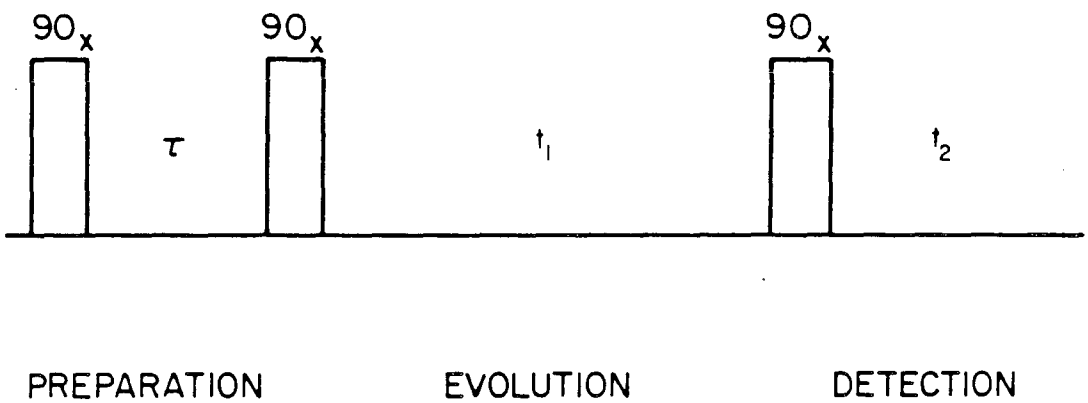

XBL 8112-13040

Figure 3. The three pulse sequence. A sequence of three $\pi/2$ pulses is perhaps the conceptually simplest method of obtaining multiple quantum spectra. For this purpose the sequence is repeated with increasing values of the evolution period t_1 and the magnetization is sampled at one or more points in t_2. Fourier transformation with respect to t_1 gives a spectrum containing in general the rotating frame frequencies of lines of all multiple quantum orders. However, the sequence is frequently inadequate in that it does not lead to the greatest possible line intensities.

is a one dimensional complex function

$$S(\tau,t_1,t_2) = Tr(\rho(\tau,t_1,t_2)I_+) = S_x(\tau,t_1,t_2) + iS_y(\tau,t_1,t_2) \quad (2.28)$$

This signal traces the evolution of that multiple quantum coherence which can be prepared in a time τ and detected at a time t_2. It is a multiple quantum interferogram and the complex Fourier transform with respect to t_1 of each component $S_\alpha(\tau,t_1,t_2)$ is a multiple quantum spectrum $S_\alpha(\tau,\omega_1,t_2)$, $\alpha = (x,y)$. More generally, the data is recorded at many points t_2, leading to a two dimensional data array and the possibility of a two dimensional Fourier transform with respect to the variables t_1 and t_2[9]. Aspects of two dimensional data analysis are mentioned in Section IIF3 and Section IIIB2. The nature of the parametric dependence on τ is discussed in Section IIIB1.

2. The General Form of the Pulse Sequences

Figure 4 shows schematically the general form of most of the experiments which will be discussed. The preparation period extends for a time τ and may contain two or more strong pulses or any irradiation sequence extending over a time comparable to or greater than the inverse of the bilinear coupling frequencies. The density operator at the end of preparation will be referred to as $\rho(\tau) \equiv \rho(t_1 = 0)$.

The evolution period t_1 is characterized by some secular high field Hamiltonian $\mathcal{H}_1$ which may be free evolution under $\mathcal{H}_{int}$ or may be an effective Hamiltonian resulting from a pulse sequence during t_1. It will prove convenient to define $\mathcal{H}_1$ as containing no net offset; like $\mathcal{H}_{int}$ it is in the rotating frame in which the sum of the chemical shifts is zero. Formally, its energy level diagram differs from that of Figure 2 in that the large splittings between different Zeeman manifolds are absent.

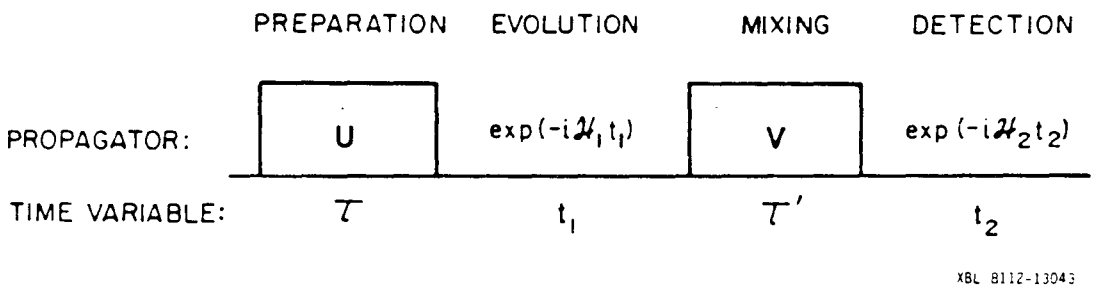

Figure 4. General form for most Fourier transform multiple quantum pulse sequences. The preparation and mixing periods, are characterized by the propagators U and V respectively. They contain one or many pulses and extend over a period comparable to or longer than the inverse of the couplings between spins or the electric quadrupole couplings. The evolution and detection periods are described by effective Hamiltonians $\mathcal{H}_1$ and $\mathcal{H}_2$ respectively and often consist simply of free evolution under the internal Hamiltonian. The period t_1 is incremented to give successive points in the time domain signal. The multiple quantum transition frequencies observed in the Fourier transform with respect to t_1 are differences between pairs of eigenvalues of $\mathcal{H}_1$.

Section IID1 describes the role of the offset term on the multiple quantum experiment.

The number N_1 of different points t_1 for which the pulse sequence is repeated is determined by the range of transition frequencies and the attainable or desired resolution. The sampling rate theorem states that each sinusoidal component of the time domain signal must be sampled more than twice per cycle to avoid losing information or aliasing high frequency components to lower frequency[33]. This may be expressed as $N_1 = 2\nu_N/R$. The Nyquist frequency ν_N is chosen to be greater than the expected line frequencies and will depend on $\mathcal{H}_1$ and on offset terms. The resolution R is in Hz per point. The increment in t_1 between shots is $\Delta t_1 = (2\nu_N)^{-1}$.

The mixing period τ'[34] will be a useful concept in those experiments where the irradiation after t_1 consists of more than a single short pulse. As will be shown in Section IIA, the requirements of the mixing period mirror those of the preparation period. For this reason they will usually be referred to jointly as excitation periods. If mixing consists of only a short pulse at time t_1, then the detection period variable t_2 will have its origin after that pulse, as in Figure 2, and the variable τ' is not needed.

The detection period requires little special comment. Since only single quantum transitions are directly detectable the filters are set as in a single pulse Fourier transform experiment, so that all single quantum (magnetic dipole) radiation can contribute to the signal. Manipulation of the detection period Hamiltonian $\mathcal{H}_2$ in order to maximize signal energy is discussed in Section IIIB2.

3. Notation

For later reference a notation is set down here which indicates a convenient approach to calculating the signal resulting from any sequence of the general type of Figure 4. Consider one component of the magnetization at time t_2. This is

$$S_\alpha(\tau,t_1,\tau',t_2) = \mathrm{Tr}(\rho(\tau,t_1,\tau',t_2)I_\alpha), \qquad \alpha = x,y,z \tag{2.29}$$

The density operator needed (neglecting relaxation) is

$$\rho(\tau,t_1,\tau',t_2) = \exp(-i\mathcal{H}_2 t_2)V(\tau')\ \exp(-i\mathcal{H}_1 t_1)U(\tau)\rho(0)U^+(\tau)$$
$$\exp(i\mathcal{H}_1 t_1)V^+(\tau')\ \exp(i\mathcal{H}_2 t_2) \tag{2.30}$$

Define the operators

$$\rho(\tau) = U(\tau)\rho(0)U^+(\tau) \tag{2.31}$$

and

$$I_\alpha(-t_2,-\tau') = V^+(\tau')\ \exp(i\mathcal{H}_2 t_2)I_\alpha\ \exp(-i\mathcal{H}_2 t_2)V(\tau') \tag{2.32}$$

The signal becomes

$$S_\alpha(\tau,t_1,\tau',t_2) = \mathrm{Tr}(\exp(-i\mathcal{H}_1 t_1)\rho(\tau)\ \exp(i\mathcal{H}_1 t_1)I_\alpha(-t_2,-\tau')) \tag{2.33}$$

This expression is useful when expanded in the eigenbasis of $\mathcal{H}_1$ as

$$S_\alpha(\tau,t_1,\tau',t_2) = \sum_{i,j} \rho_{ij}(\tau)\alpha_{ji}(-t_2-\tau')\ \exp(-i\omega_{ij}t_1) \tag{2.34}$$

The subscripted coefficients may be viewed as the matrix elements

$$\rho_{ij}(\tau) = \langle i|\rho(\tau)|j\rangle \tag{2.35}$$

$$\alpha_{ji}(-t_2,-\tau') = \langle j|I_\alpha(-t_2,-\tau')|i\rangle \tag{2.36}$$

or equivalently as the expansion coefficients in the eigenoperator basis;

$$\rho(\tau) = \sum_{i,j} \rho_{ij}(\tau)|i\rangle\langle j| \tag{2.37}$$

$$I_\alpha(-t_2,-\tau') = \sum_{ij} \alpha_{ji}(-t_2,-\tau')\ |j\rangle\langle i| \tag{2.38}$$

The notation of (2.29) - (2.38) incorporates several biases which will permeate the remaining sections. In (2.29) the possibility is allowed that the z component of magnetization is measured. This will prove to be a convenient fiction for calculation although the actual experiment would include a $\pi/2$ pulse to convert this to precessing magnetization. The definitions in (2.31) and (2.32) and their use in (2.34) focus attention on the evolution period eigenfrequencies ω_{ij} and collect all other time development into an operator accounting for prior time (preparation) and another accounting for subsequent time (mixing and detection). The expansion in the non-Hermitian eigenoperators $|i\rangle\langle j|$ satisfying

$$[\mathcal{H}_1,|i\rangle\langle j|] = \omega_{ij}|i\rangle\langle j| \tag{2.39}$$

rather than the Hermitian pseudospin ½ operators[35,36], reflects a preference for phase factors over sines and cosines. For typographical and conceptual simplicity, all relaxation effects are omitted wherever practical.

4. Comparison with Single Quantum NMR

Comparison of the multiple quantum signal (2.34) and the single quantum signal (2.23) reveals a number of fundamental differences.

The most important difference, of course, is that the coefficients of (2.34) will be finite for pairs of states with $n_{ij} \neq \pm 1$. The question of which such pairs occur will depend on the symmetry of $\mathcal{H}_1$ (Sec. IIF1) and on the particular excitation sequences (Sec. III).

While the Fourier coefficients $|\langle i|I_+|j\rangle|^2$ are real and positive for all lines in the single quantum experiment, the coefficients $\rho_{ij}(\tau)\alpha_{ji}(-t_2,-\tau')$, which are the line amplitudes of the multiple quantum spectrum, are generally complex quantities with phases which differ from line to line. The result is that such spectra usually cannot be presented in absorption mode. The usual expedient is to present magnitude spectra. Magnitude spectra of realistic line shape functions have broader wings than the properly phased absorption spectra. Methods of obtaining certain lines properly phased are discussed in Sections IIE4, IIIA4, and IIIC8.

A third difference is that while (2.23) describes with a single set of coefficients the complex signal formed from the two orthogonal channels of the phase sensitive detector (2.34) requires, in general, a different set of coefficients for the two channels. In Section IIE3 experiments will be described for which the multiple quantum signal in the two channels as a function of t_1 comprise a Hilbert transform pair[33], just as they do in a single quantum experiment.

A final difference is that while the coefficients of (2.23) are readily calculated after solving for the eigenvalues and eigenvectors of $\mathcal{H}_{int}$, the coefficients of (2.34) require a dynamical calculation including the interaction with the radiation. This means that predicting intensities of individual multiple quantum transitions quantitatively is often difficult. For large spin systems excited by complex irradiation sequences

such prediction is impractical. One exceptionally simple recourse is discussed in Section IIE4. Computational and approximation methods are reviewed in Section IIIB1.

C. Frequency Selective Excitation

1. Background

The emphasis so far and in most of this work is on experiments using only strong pulses. These are rf pulses for which the condition $|\omega_p|>|\omega_{ij}|$ is met. This inequality states that the nutation frequency is greater than any of the frequencies associated with the rotating frame internal Hamiltonian. All transitions are simultaneously resonant in the sense that the spectral intensity of the pulse is large over the spectral width (transform limited bandwidth) and the net number of photons exchanged is limited by the system, not by the source intensity (highly nonlinear interaction). The power of the strong pulse approach is that it leads to excitation methods of great generality and simplicity, which are largely independent of the details of the internal Hamiltonian. Most importantly, they are applicable to large systems with closely spaced transition frequencies. Strong pulse methods of selectively excitating certain transition orders are the subject of Section IIIC.

In this section, frequency selective, or narrow-band, excitation is reviewed. The restriction on rf field strength in these experiments is roughly that $|\omega_p| < |\omega_{ij} - \omega_{kl}|$. This states that the radiation is sufficiently weak that it may be tuned to be resonant with transitions between particular pairs of states, while not perturbing the populations of or coherence between other states. These methods are principally of interest in systems with only a few levels. This is because the transitions are more likely to be well resolved and, as importantly, because

one would not know where to begin doing frequency selective experiments on a system of many like spins. For spins with large quadrupole splittings the frequency selective methods are indispensable, since even the strongest pulses available cannot satisfy $|\omega_p|>|\omega_Q|$.

The theoretical description of weak rf with a spin system starts out by treating the rotating frame rf term using perturbation theory. The result in the limit of well resolved transitions and weak irradiation is that the two levels, which are resonantly connected by the radiation, behave like an isolated spin ½. An effective gyromagnetic ratio may be associated with this pseudo-spin, which will differ for each pair of states. Bloch equations[18] and the associated model of the density operator as a vector in three dimensions are used to describe the excitation dynamics. In the following section a brief review is given of the elegant ways in which such two level problems have been strung together to observe multiple quantum coherence and other multiple quantum phenomena.

2. Applications

a. The three level system. A system with three unequally spaced energy eigenstates has received nearly exhaustive attention as the prototype multilevel system. Several detailed presentations of the results have appeared[35-41]. In high field NMR any three successive Zeeman levels which can be radiatively connected without involving other levels will be amenable to the approaches of this section. The m = 1/2, -1/2, and -3/2 levels of $^{27}Al(I = 5/2)$ in a simple crystal of Al_2O_3 were the basis set for several early developments[5,6,42-44].

A spin 1 nucleus in a molecular electric field gradient is the simplest system on which time domain multiple quantum experiments can be performed[7,45]. An isomorphic problem is that of two isochronous spin ½ nuclei with a direct dipolar coupling. Here the triplet states comprise

a three level system, which is unconnected by the radiation to the singlet state. The energy level diagram labelled for the spin 1 system is shown in Figure 5. The convention used here is to label the states $|1\rangle$, $|2\rangle$ and $|3\rangle$ in order of ascending energy. The dipole allowed single quantum transitions are $|1\rangle \rightarrow |2\rangle$ and $|2\rangle \rightarrow |3\rangle$. The dipole forbidden transition $|1\rangle \rightarrow |3\rangle$ is double quantum.

b. Sequential two frequency excitation. One approach to preparing the double quantum coherence involves successive irradiation at each of the two single quantum frequencies[5,46]. A $\pi/2$ pulse at the $|2\rangle \rightarrow |3\rangle$ frequency ($\pi/2(\omega_{23})$) is followed by a $\pi(\omega_{12})$ pulse. The first pulse creates coherence between $|2\rangle$ and $|3\rangle$ and the second transfers this to coherence between $|1\rangle$ and $|3\rangle$ since it interchanges the coefficients of states $|1\rangle$ and $|2\rangle$.

It might seem that such an approach would be faster than the method of two hard pulses separated by a delay, since here no delay between pulses is necessary. This is, of course, not the case since while the strong pulses could be arbitrarily short, the two weak pulses must be of duration $\sim\omega_Q^{-1}$ in order to be selective. Thus the preparation time is comparable.

After the evolution period a selective π mixing pulse at one of the allowed frequencies leads to a detectable f.i.d. at the other allowed frequency.

Various combinations of two selective pulses in AX_n, AB, and AA'XX' systems have also been demonstrated[8,47-49].

An interesting view point for discussion of experiments which detect forbidden transitions by sequential irradiation at two frequencies is the notion of "spin interferometry"[8,50-52]. Since a selective pulse

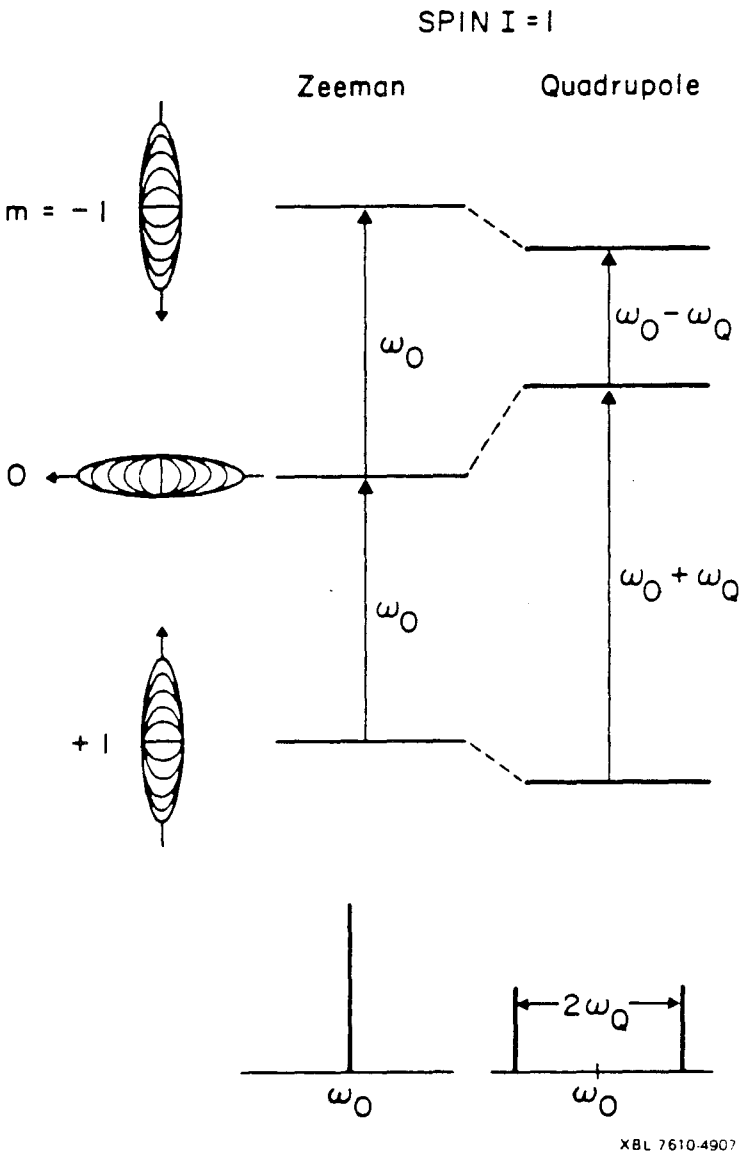

Figure 5. Energy level scheme and spectra for a spin 1 nucleus in an electric field gradient. This is the simplest system which can support multiple quantum transitions in the sense of this work. At left is a schematic illustration of the orientation with respect to a vertical magnetic field of the nuclear charge distribution (ellipsoidal) and magnetic moment (arrow) in each of the three Zeeman eigenstates. The sum of the Zeeman and electric quadrupole terms gives the energy levels at the right. The single quantum spectrum at lower right is a doublet with splitting $2\omega_Q$ while the double quantum transition at lower left is independent of ω_Q in high field and measures only the Zeeman interaction. [By permission from A. Pines, S. Vega, and M. Mehring, Phys. Rev. B 18, 112 (1978).]

may leave a certain eigenstate temporarily unperturbed, the coefficient of this state is viewed as a reference with respect to which the phase of other coefficients are measured.

Various combinations of frequency selective and nonselective pulses for exciting multiple quantum coherence have been discussed[9,38,53,54]. The motivations vary from simple experimental convenience to a desire to introduce a level specific label into an otherwise broadband experiment.

c. Selective multiple quantum pulses on resonance. A second approach to exciting double quantum coherence is a weak pulse at the center frequency $(\frac{1}{2})\omega_{13}$[6,7]. A double quantum pulse nutation angle may be defined for the pseudospin ½ system consisting of levels $|1\rangle$ and $|3\rangle$. For the spin 1 system this is[38]

$$\theta_{DQ} = (\omega_p^2/\omega_Q)t_p, \qquad \omega_p << \omega_Q \tag{2.40}$$

A $\pi/2(\frac{1}{2}\omega_{13})$ pulse or double quantum $\pi/2$ pulse completely transfers the initial longitudinal magnetization into $n = \pm 2$ coherence. If the same pulse is used for mixing, then the magnetization must be brought into the transverse plane for detection by another pulse, preferably intense. In practice quadrupolar echoes are sometimes incorporated into the mixing period in order to remove the signal from the immediate region of the pulse[38,54].

Resonant population inversion by a selective double quantum pulse has been demonstrated in $^{33}Na(I = 3/2)$[55]. The triple quantum selective resonant pulse for the I = 3/2 case has been discussed theoretically[35,36] and demonstrated experimentally[53]. In this case there is a single quantum transition which is simultaneously resonant.

d. Simultaneous weak irradiation with two frequencies. The central single quantum transition for half integral spins is often the only detectable one since the satellites are spread over a large range of frequencies by inhomogeneity in ω_Q. For large ω_Q the transfer of coherence between the triple quantum coherence and this detectable line is inefficient. For this reason methods were developed for modulating the central frequency to create sidebands which irradiate and indirectly detect the satellites. This allowed efficient preparation of the triple quantum coherence from the equilibrium magnetization and efficient mixing back to the easily detected central transition[53].

Even in the three level system interesting effects are seen for simultaneous but unequal weak irradiation at the two single quantum transitions[44,51]. The vector density operator model appropriate to this situation has the coefficients of the three coherences as the three orthogonal components. The rotation axis, about which the vector precesses, depends on the ratio of the amplitudes of the two frequency components. In this way the three coherences are continually interconnected during the irradiation.

e. Double quantum rotary phenomena. Frequency selective pulses are not only useful in the excitation periods of experiments of the type depicted in Figure 4, which lead to spectra of the unperturbed internal Hamiltonian. They have also been used to demonstrate various analogs of rotary phenomena normally associated with the dynamics of long intense pulses[18].

The upper trace of Figure 6 shows the rotary decay under frequency selective double quantum irradiation[7]. The amount of longitudinal magnetization remaining after increasing periods of such irradiation is

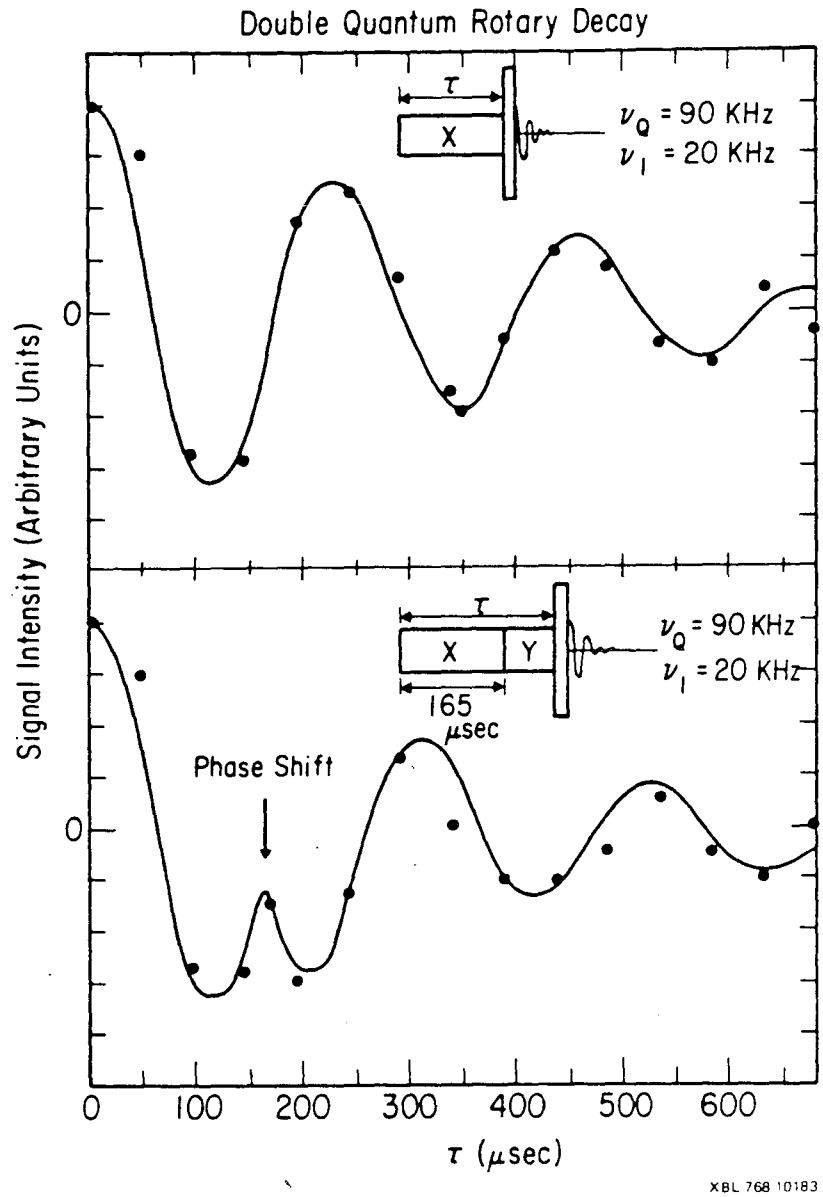

Figure 6. Double quantum rotary decay of the carboxyl deuterons of crystalline oxalic acid dihydrate. The experimental points represent the magnetization remaining after the indicated period of double quantum nutation as measured by the signal after a final hard pulse. The solid line is the theoretical sinusoidal dependence on the angle θ_{DQ} given by (2.40) with damping added. In the lower figure the sense of nutation was reversed at 165 μsec by a phase shift of $\pi/2$, thus demonstrating the proportionality of the apparent phase shift to number of quanta. [By permission from S. Vega and A. Pines, in "Magnetic Resonance and Related Phenomena" (H. Brunner, K. Hausser, and D. Schweitzer, eds.), p. 395. Baltz Offsetdruck, Hemsbach, 1976.]

assessed by measuring the single quantum signal immediately after a strong $\pi/2$ pulse. The $\cos\theta_{DQ}$ dependence of (2.40) is evident. This is the double quantum analog[6] of transient nutation[56].

In the lower trace of Figure 6 a similar experiment is shown in which the rf phase of the double quantum pulse was shifted by $\pi/2$ for times greater than 165 μsec[7]. The direction of double quantum nutation clearly reverses, which for ordinary nutation requires a phase shift of π.

This is the first demonstration of a concept which has been central to the development of multiple quantum spectroscopy: phase shifts of ϕ in the radiation appear effectively as shifts of $n\phi$ for an n quantum process. This notion is crucial to methods for separately detecting (Sec. IID) and exciting (Sec. IIIC) specific orders of multiple quantum coherence in large systems. In addition it is used in multiple quantum spin locking[7,43,55] which will be taken up in Section VC4.

Other rotary echoes[42-44] and rotary saturation[43] experiments have been performed on the Al_2O_3 three level system with the different types of frequency selected radiation already mentioned.

f. Double quantum decoupling. Another effect of double quantum nutation is observed in the spectrum of a heteronucleus coupled to the spin 1 nucleus. Resonant rf is found to decouple deuterons from neighboring protons even though ω_p is much less than the deuterium spectral width which is proportional to ω_Q. Deuterium decoupling in anisotropic phases is thus much easier than might have been anticipated and this is due to the greater allowedness of double quantum over single quantum transitions for weak resonant fields. This observation was first made in a liquid crystal sample[57] and analyzed by perturbation theory[58] and computer diagonalization[58,59].

The extension to solids allowed high resolution chemical shift spectra of dilute protons to be measured[60]. This is an alternative to the multiple pulse line narrowing techniques used on fully protonated material[61-63]. Quantitative theoretical expressions for the decoupling efficiency as a function of internal and rf Hamiltonians have been derived and compared with solid state measurements of proton linewidths[64,65].

Figure 7 shows the dependence of the linewidth of residual protons in perdeuterated dimethyl sulfoxide on the deuterium rf field strength[64]. The sudden onset of decoupling takes place when the double quantum nutation frequency of (2.40) is comparable to the heteronuclear coupling.

g. Chemical shift powder patterns. One of the principal applications of multiple quantum spectroscopy of quadrupolar nuclei is the measurement of the chemical shift in inhomogeneously oriented samples[45]. The orientation dependence of ω_Q in the first order high field quadrupole Hamiltonian (2.12) leads to single quantum powder patterns hundreds of kHz in width. It does not, however, affect the double quantum transition frequency since the $M = \pm 1$ levels are shifted in the same way by ω_Q. Thus its spectrum is dominated by the chemical shift term if second order quadrupole terms[18] can be neglected. Since the excitation of the multiple quantum coherence is a sensitive function of ω_Q (and thus of crystallite orientation) some care is needed to obtain a powder pattern representative of the chemical shift tensor[38,54].

Figure 8a shows a simulation of the double quantum powder pattern of d-1 benzene[54] at a temperature where rapid motion about the six-fold axis is occurring. Gaussian broadening convoluted with the calculated spectra increases from left to right. The most prominent feature in the intensity pattern is the absence of double quantum coherence for those

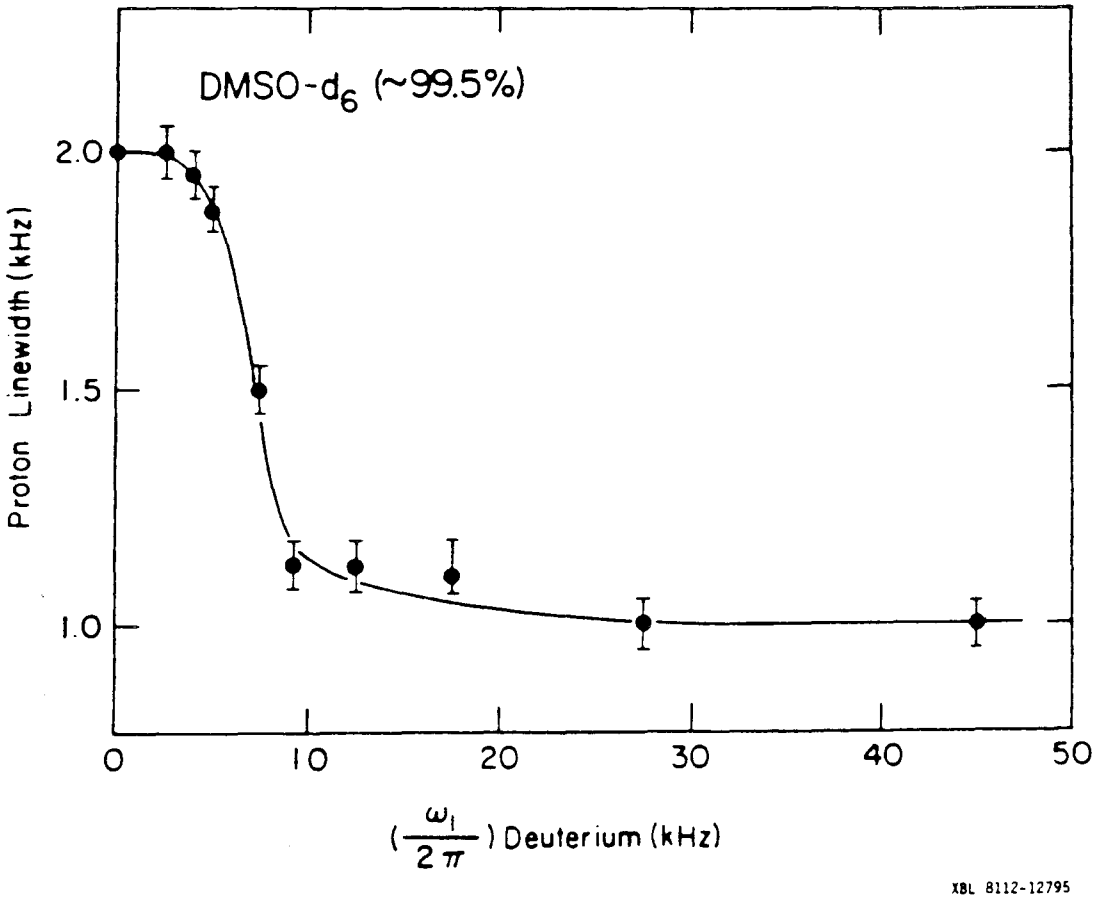

Figure 7. Double quantum decoupling of deuterium. The linewidth of the residual protons in perdeuterated dimethyl sulfoxide is plotted as a function of the deuterium nutation frequency (ω_1 here is ω_p in the text). The sudden onset of effective decoupling is characteristic of the double quantum process, which depends quadratically on the rf field strength. The solid curve is a fit to the detailed theory. [By permission from A. Pines, S. Vega, and M. Mehring, Phys. Rev. B 18, 112 (1978).]

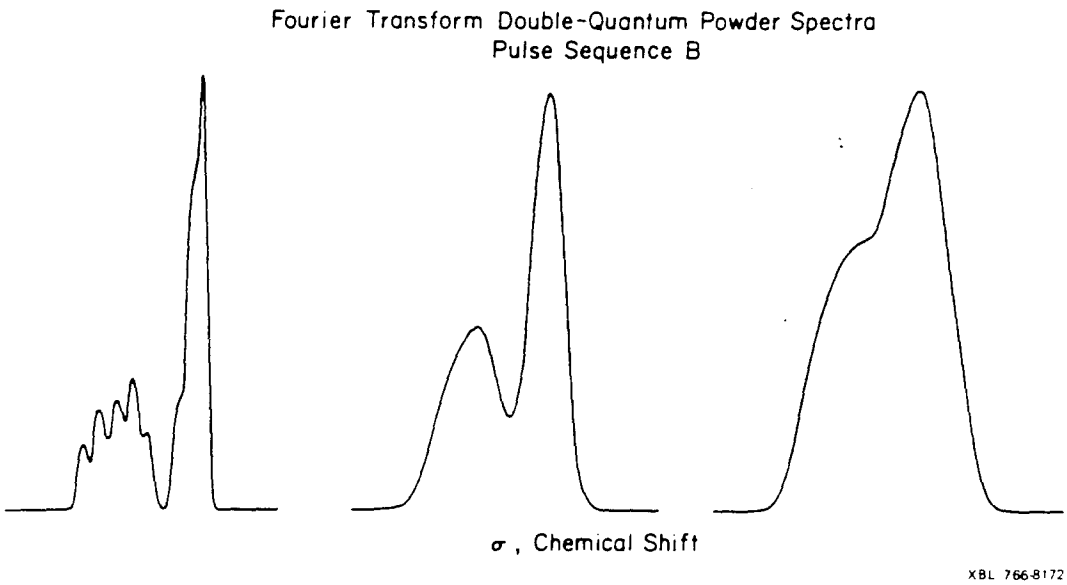

Figure 8. a) Simulated double quantum deuterium powder patterns of d-1 benzene undergoing rapid motion about the six-fold axis. The simulation is for a preparation pulse of amplitude $\omega_p/2\pi$ = 20 kHz and length 25 μsec. Mixing consisted of two orthogonal pulses with $\omega_p/2\pi$ = 50 kHz and lengths 3 and 4.5 μsec separated by 100 μsec. Sampling was at the quadrupolar echo 100 μsec after the last pulse. Three convolutions of the computed stick spectrum with increasingly wide Gaussian broadening functions appear from left to right.

molecules whose six-fold axis is oriented at the "magic angle" $\cos^{-1}(1/\sqrt{3})$. For these molecules, $\omega_Q = 0$. No double quantum coherence is possible without help from some bilinear coupling.

The experimental spectrum is shown in Figure 8b[54] and closely matches the right most simulation in Figure 8a. Though this is not a very sensitive test of the simulation it was possible to measure the chemical shift anisotropy of 6.5 ± 1.0 ppm. The uncertainty is presumably due to residual dipolar broadening.

h. Double quantum deuterium spectra with magic angle spinning. Rotation of the sample at the magic angle, $\theta_m = \cos^{-1}(1/\sqrt{3})$, has long been used to reduce those anisotropic terms of the spin Hamiltonian which transform spatially as second rank tensors[66]. The extension of this technique to deuterated compounds offered a method of obtaining hydrogen isotropic chemical shifts from polycrystalline compounds[67]. Because the principal purpose of the sample spinning is to average away the large first order quadrupole interaction, the technique is very sensitive to rotor alignment[68].

Despite the averaging to zero of the quadrupole interaction over a rotor cycle, it is still possible to observe the double quantum coherence since its excitation takes place in a fraction of a rotation period[69]. Figure 9 illustrates an advantage of the double quantum method for obtaining the isotropic chemical shift of deuterium in powder samples. Small rotor alignment errors which destroy the single quantum line narrowing have little effect on the double quantum spectrum. This is because the double quantum transition is invariant to the first order quadrupole interaction and the rotation need only be accurate enough to diminish dipolar and chemical shift anisotropy broadening.

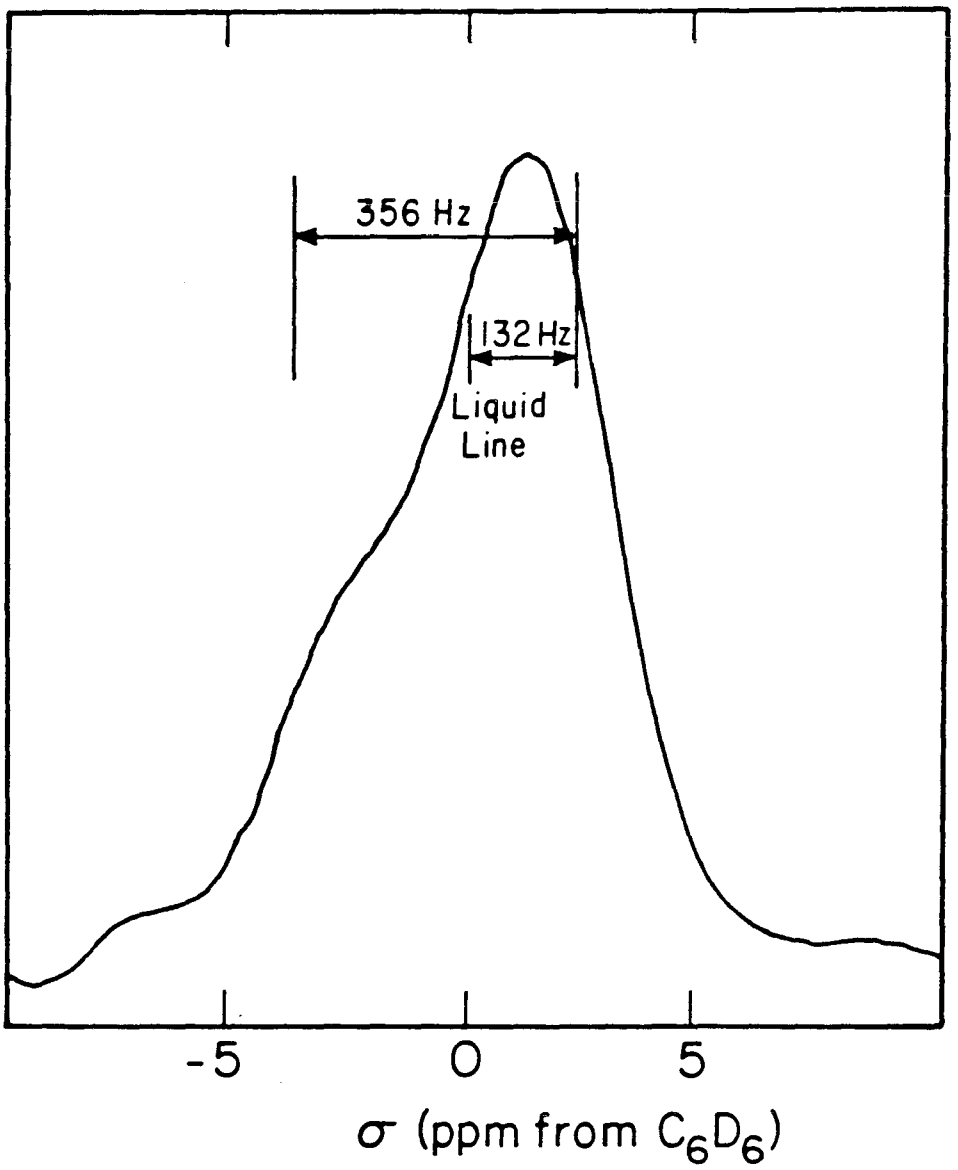

XBL 764-1092

Figure 8. b) Experimental double quantum spectrum of 10% d-1 benzene in protonated benzene at 4.2 Tesla with proton decoupling. The pulse sequence is that simulated in a). The spectrum reveals the chemical shift anisotropy to be 6.5 ± 1 ppm, while the single quantum spectrum would be dominated by the much larger first order quadrupole terms. [Figures 8 a) and b) by permission from D. E. Wemmer, "Some Double Resonance and Multiple Quantum NMR Studies in Solids", Ph.D. Dissertation, University of California, Berkeley, 1978, published as Lawrence Berkeley Laboratory Report LBL-8042.]

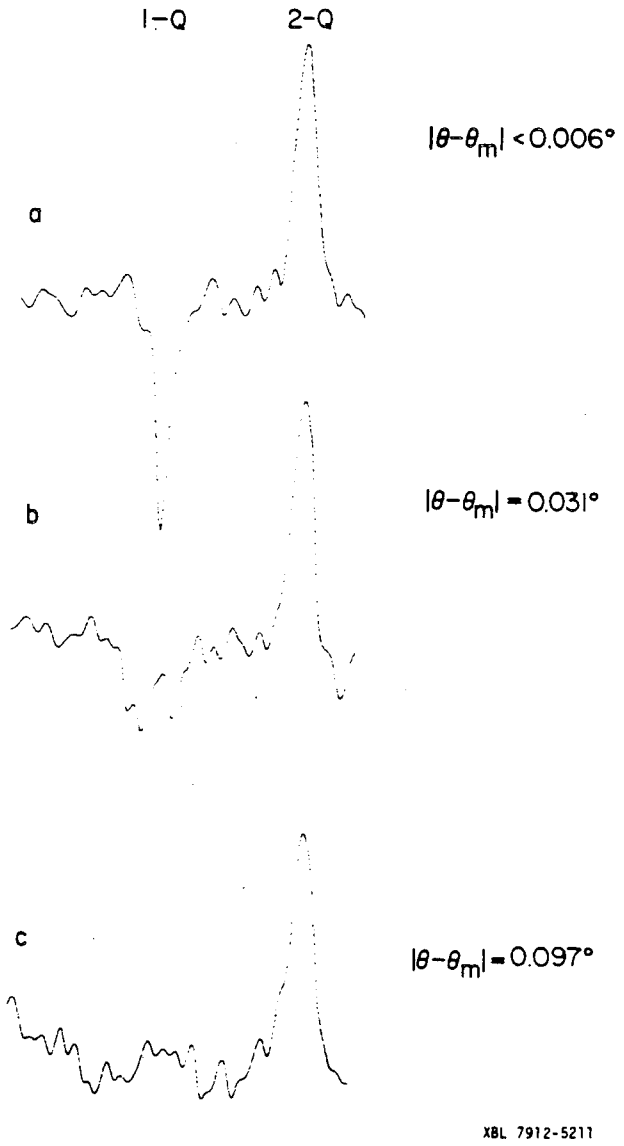

Figure 9. Sensitivity to rotor misset of single and double quantum deuterium spectra with magic angle sample spinning. The sample is 28% randomly deuterated polycrystalline ferrocene rotating at 1.1 kHz. The single and double quantum spectra are shown in a, b, and c for increasingly large missets of the spinner axis from the magic angle θ_m. Even slight misadjustments lead to reintroduction of the quadrupolar broadening in the single quantum spectrum. The double quantum transition is inherently insensitive to the quadrupole interaction and remains sharp for small rotor missets, allowing easy measurement of the isotropic chemical shift.

[By permission from R. Eckman, L. Müller, and A. Pines, Chem. Phys. Lett. 74, 376 (1980).]

i. Multiple quantum spin tickling. In most of the schemes reviewed so far, the frequency selective irradiation was used during the preparation and mixing periods. An exception was double quantum spin decoupling (Sec. IIC2f). Another case where frequency selective irradiation is used during the evolution period is in time domain spin tickling. The effect of such weak irradiation on the spectra obtained from multiple quantum interferograms has been discussed in some detail[70]. It is suggested that such experiments will prove useful in elucidating the assignment of lines to an energy level scheme.

D. Separation of the Transition Orders

1. Transition Frequencies in the Off-Resonance Rotating Frame

In order to interpret the profusion of transitions which arise with the breaking of the selection rule, it is convenient to separate them according to their transition order $n \equiv \Delta M$. In terms of the energy level diagram (Fig. 2) this would appear to be a simple matter since the frequency differences of order $n\omega_o$ insure that lines of one order will be separated from those of a neighboring order by the Larmor frequency. In practice this large difference is unavailable, since it is precisely the Larmor terms which are removed in the rotating frame. In fact an energy level diagram properly drawn for the resonant rotating frame would show overlap of the different Zeeman manifolds. In this frame, transitions of all orders have a similar spectral range determined by the spin couplings and the chemical shifts which lift the degeneracy of states with the same M. Since all of the coherences are necessarily detected only through their modulation of the magnetic dipole radiation near ω_o, they are not readily distinguishable in this frame.

One method of changing the spectral range of the different orders is to move the heterodyne detector reference frequency off resonance. This introduces the term $-\Delta\omega I_z$ into the rotating frame Hamiltonians (2.7). This term commutes with the evolution Hamiltonian $\mathcal{H}_1$ so the eigenoperators $|i\rangle\langle j|$ do not change, but the eigenfrequencies are shifted. If the eigenfrequencies on resonance were given by

$$[\mathcal{H}_1, |i\rangle\langle j|] = \omega_{ij}|i\rangle\langle j| \tag{2.41}$$

then by (2.27) they are given off resonance by

$$[(\mathcal{H}_1 - \Delta\omega I_z), |i\rangle\langle j|] = (\omega_{ij} - n_{ij}\Delta\omega)|i\rangle\langle j| \tag{2.42}$$

In the time domain, this corresponds to multiplying each term of (2.34) by $\exp(in_{ij}\Delta\omega t_1)$. The offset $\Delta\omega$ is chosen to be large enough so that the lines of each order do not overlap with adjacent orders. Typically the required offset is about the full width of the single quantum spectrum, but other orders may be somewhat wider. Note that the Nyquist frequency, determined by the increment Δt_1 in the evolution period, must be greater than $2I\Delta\omega$.

This method of separating transitions according to n has a number of disadvantages which render it quite unsatisfactory. On most spectrometers the irradiation frequency and the reference frequency are the same and setting the latter off resonance would lead to ineffective excitation. This is not a profound problem since a resonant irradiation frequency separate from the reference could be generated. A second problem is that by centering the pass band at the edge of the single quantum spectrum it is necessary to digitize at least twice as rapidly in t_2 as would be

necessary on resonance. Again this is not a fundamental objection, but only an experimental inconvenience. The crucial objection to using an off-resonance detector frequency for separating transition orders is that it cannot work in those experiments which use spin echoes during the evolution period. The full treatment of these experiments is postponed until Section IIE. At this point it is only necessary to note that the offset term also includes the inhomogeneous term $-\omega_z(\vec{r})I_z$ of (2.9). Since experiments designed to remove this inhomogeneity from the evolution also remove the modulation needed to distinguish the transition orders, other methods of separation are needed. These methods are the subject of the next section.

2. Labeling of Coherence by the rf Phase of the Preparation Period

a. Order dependent phase shifts. What is desired is a method of separating coherences of different order in those experiments where an offset is not present during evolution. The clue to such methods lies in the dependence of the coherence on the rf phase[7]. Consider some arbitrary irradiation sequence during the preparation period of Figure 4. The propagator is

$$U(\tau) = T \exp(-i \int_0^\tau \mathcal{H}(t)dt) \tag{2.43}$$

with

$$\mathcal{H}(t) = -\omega_p(t)I_{\psi(t)} - \Delta\omega(t)I_z + \mathcal{H}_{int} \tag{2.44}$$

T orders the products of operators so that those with earlier time arguments are to the right[71]. $\mathcal{H}_{int}$ is the secular, internal, time independent spin Hamiltonian (2.8). The time dependence is all from the rf

term (2.7) and enters through the experimental quantities $\omega_p(t)$, $\psi(t)$, and $\Delta\omega(t)$ which allow for arbitrary variation of the rf amplitude and phase and of the resonant frequency (within the rotating wave approximation). Next consider preparation by the same irradiation sequence, but with all rf phases shifted by an angle ϕ. The new Hamiltonian is obtained by the substitution of $I_{\psi(t)+\phi}$ for $I_{\psi(t)}$. This is equivalent to substituting the operator $\exp(i\phi I_z)\,\mathcal{H}(t)\,\exp(-i\phi I_z)$ for $\mathcal{H}(t)$. The new propagator is $U(\tau,\phi) = \exp(i\phi I_z)U(\tau)\,\exp(-i\phi I_z)$ and the new density operator prepared is

$$\rho(\tau,\phi) = U(\tau,\phi)\rho(0)U^{+}(\tau,\phi) \tag{2.45}$$

Suppose that $\rho(0)$ contains only $n=0$ operators. This is the case for a system initially at equilibrium as well as for those non-equilibrium initial conditions which are specifiable by population differences in the eigenbasis of a secular Hamiltonian. Then

$$\rho(\tau,\phi) = \exp(i\phi I_z)\rho(\tau)\,\exp(-i\phi I_z) \tag{2.46}$$

If the density operator is decomposed into parts transforming as n-quantum operators so that $\rho(\tau) = \sum_n \rho_n(\tau)$, then

$$\rho(\tau,\phi) = \sum_n \exp(in\phi)\rho_n(\tau) \tag{2.47}$$

and (2.37) becomes

$$\rho(\tau,\phi) = \sum_{ij} \rho_{ij}(\tau)\,\exp(in_{ij}\phi)\,|i\rangle\langle j| \tag{2.48}$$

This demonstrates that the rf phase of the preparation period tags the coherences prepared with a phase factor distinct for each order n. These

factors show up as phase dependent modulation of the signal expressed by (2.34) and may be used to sort out the different contributions to the signal by order. There are two methods for performing this sorting.

b. Phase Fourier transformation. The first is the method of phase Fourier transformation (PFT)[14,72]. This requires the collection of a data set $S_\alpha(\tau,t_1,\tau',t_2,\phi)$ in the manner described in Section IIB, but repeated for different values of ϕ between zero and 2π. This data set is at least two dimensional, since t_1 and ϕ are varied independently. A Fourier transformation may now be performed in each of these dimensions: a transformation with respect to t_1 with ω_1 as the conjugate variable and a transformation with respect to ϕ with n as the conjugate variable. In Section IIB2 the number of points required in the t_1 dimension was discussed in terms of a Nyquist frequency. The sampling rate theorem[33] may be applied in the ϕ dimension as well. If n_{max} is the highest order coherence, then ϕ must take a minimum of $(2n_{max}+1)$ values to retain all information in the transform with respect to ϕ.

c. Time proportional phase incrementation. An alternative approach is the method of time proportional phase increments (TPPI)[15,73]. Suppose that in (2.48) the angle is set to $\phi = \Delta\omega t_1$. In practice this means that the phase of the radiation used for preparation is incremented by $\Delta\phi = (\Delta\omega)(\Delta t_1)$ when the evolution time is incremented by Δt_1. The effect is a phase factor in (2.34) of $\exp(in_{ij}\Delta\omega t_1)$. This is precisely the same modulation which was found in Section IID1 to be caused by a homogeneous offset term $-\Delta\omega I_z$ appended to $\mathcal{H}_1$. Now, however, it appears as an artifact of the preparation period and the offset may be eliminated during evolution without collapsing the lines of different n into the same frequency range. The separation of lines by

order is achieved in the Fourier transform with respect to t_1. The phase Fourier transform and the additional dimension in the data array are eliminated. The total amount of time and data storage required is nearly the same for either method. This is because the apparent offset requires that the evolution period increment Δt_1 be decreased by a factor $2n_{max}$ or more to accommodate the spectra of all orders without overlap or aliasing. An example of a TPPI spectrum is shown in Figure 1.

TPPI results in a t_1 interferogram which is $2n_{max}$ as long as a single quantum FID at the same resolution. Hybrid experiments can be useful for keeping within the capacities of the available Fourier transform software. For example, a pair of TPPI signals with initial ($t_1 = 0$) preparation phase differing by π can be added and subtracted to give, respectively, the even quantum signal and the odd quantum signal. This allows $\Delta\omega$ to be half as large without overlap of orders occurring. Thus Δt_1 can be twice as long and each t_1 transform has half as many points.

The precise formal equivalence of TPPI with a homogeneous offset term added to $\mathcal{H}_1$ allows the treatment of various preparation periods without explicit mention of TPPI. The fictitious offset may always be accounted for as if due to a homogeneous offset during the evolution period and the preparation propagator rf phase is then treated as though it were constant for all t_1.

d. Implementation of small phase shifts. The increments in rf phase of π/n_{max} or less which are needed for the PFT and TPPI experiments are not as yet common capabilities of commercial spectrometers. Digitally addressed 8-bit variable delay lines are commercially available and have been successfully used[15]. A method based on digital synthesis of phase shifted waves has also been implemented[74].

Another method of generating phase shifts, illustrated in Figure 10, is to switch the frequency of the spectrometer reference wave for a period of time between pulses. Phase coherent frequency switching is a commonly available feature of commercial rf synthesizers. The phase shift obtained is $\phi = \Delta\omega t$, where now $\Delta\omega$ is the frequency shift which is maintained for the time t. This suggests a particularly simple implementation of TPPI, in which the frequency shift is made during the free evolution period t_1[75].

e. Related approaches to separation of the transition orders. In the two approaches discussed above, PFT and TPPI, and the various hybrid versions, the phase shifting is restricted to the pulses of the preparation period. It is possible to achieve a similar labeling of coherence by variation of the phase of other pulses.

If a π pulse is used in t_1, it alone may be phase shifted on successive shots to give a modulation of what was n quantum coherence at time $t_1 = 0$ by $\exp(i2n\phi)$. This is a consequence of the general fact that a coherence transfer from order n to order n' is accompanied by an extra phase factor $\exp(i(n-n')\phi)$, where ϕ denotes the phase of the rf effecting the transfer relative to some arbitrary reference. For a perfect π pulse $n' = -n$ only. Systematic variation of the phase of the pulse at $t_1/2$ has been used to eliminate artifacts due to other coherence transfers resulting from pulse imperfections[73].

An entirely different way of labeling the n quantum coherence with a factor $\exp(in\phi)$ has been demonstrated[76] which only requires the usual four equally spaced rf phases. A familiar result of angular momentum theory is that a rotation about an arbitrary axis can be achieved by a series of three rotations about two orthogonal axes, which may be chosen

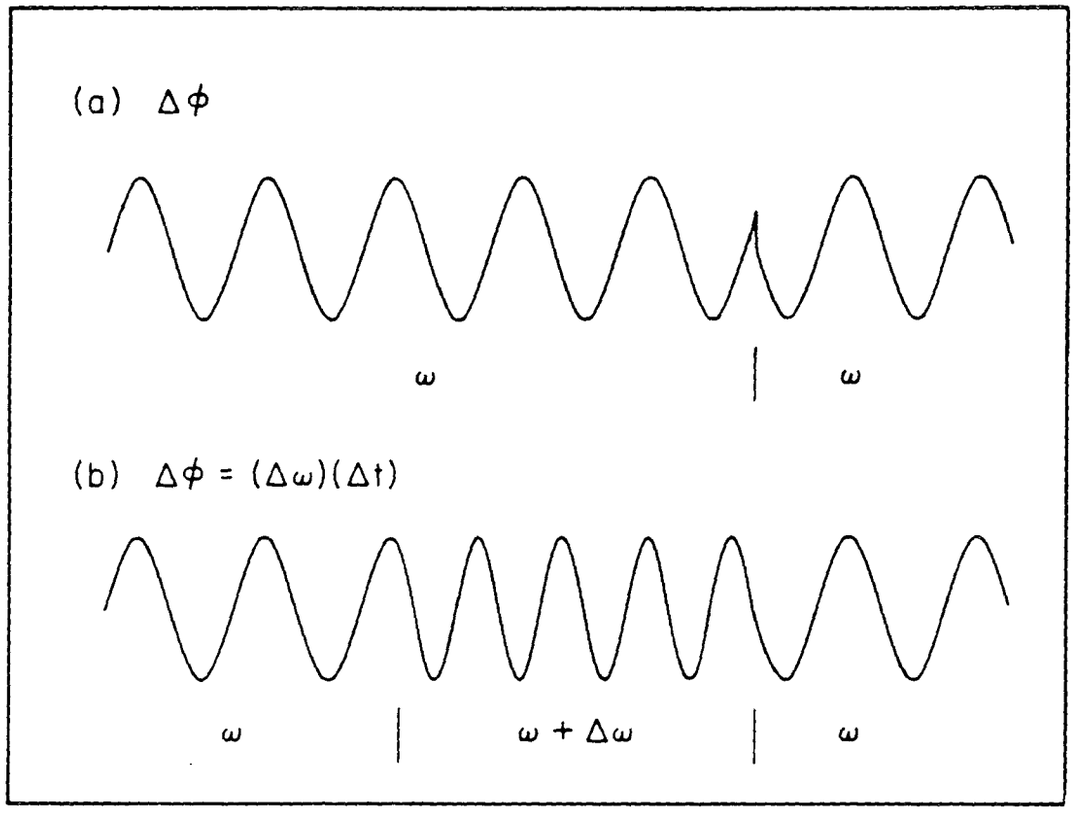

XBL 8112-12801

Figure 10. Implementation of phase shifts of the rf. In a) the phase shift $\Delta\phi$ takes place suddenly as, for example, by digital synthesis or by switching to a carrier wave which has followed a different pathlength. In b) the same phase shift is obtained by shift in frequency by $\Delta\omega$ for a time Δt.

as fixed. In the usual Euler rotation angle convention these are chosen to be the y and z axes. Since the rotations which describe intense resonant rf pulses are rotations about axes in the transverse plane, the axes x and y are the convenient choice here.

The trick is to use pulses of the canonical phases to achieve an effective rotation about z, which serves to label according to n. The result needed is[76]

$$\exp(i(\pi/2)I_x \exp(-i\theta I_y)\exp(-i(\pi/2)I_x) = \exp(i\theta I_z) \qquad (2.49)$$

The sequence of three pulses indicated on the left (composite z-pulse) can be given at any time during the evolution period. In practice they were combined with the final $\pi/2$ pulse of the preparation period. Instead of $2n_{max}$ values of rf phase, one needs $2n_{max}$ pulse angles θ which are used on successive shots.

The limitations inherent in this method need to be noted. The first is that the nutation frequency ω_p must be much greater than the spectral width. This is implicit in the neglect of the internal Hamiltonian during the composite pulse. This condition can be difficult or impossible to attain, particularly in anisotropic systems.

Secondly, inhomogeneity of ω_p over the sample volume is translated linearly into a misset of θ and thus of the modulation factor $\exp(in\theta)$. While rf phase accuracy of 1% is routine, rf field strength inhomogeneity of 1% is only obtained with samples which fill a fraction of the coil volume. Thus the method of composite z-pulses is not as generally applicable as methods based on phase or frequency jumps.

E. Consequences and Uses of Static Field Inhomogeneity

1. Spin Echoes in the Evolution Period

In Section IID1 the dependence of the multiple quantum transition frequencies on the frequency offset term $\Delta\omega I_z$ was considered as a way of separating spectra of different orders n. The problem with this approach is that due to variations in the static field strength the offset is inhomogeneous over the volume of the sample. The consequence of this inhomogeneity is a line broadening proportional to n. This is depicted in Figure 11 for the six proton system of oriented benzene[54].

The solutions to this problem include the technically difficult one of improving the field homogeneity until it is not linewidth limiting or the relatively simple one of incorporating a spin echo[1] into the multiple quantum evolution period[6,15,73]. A coherence which evolves during the first half of the evolution as an n quantum operator accumulates a phase factor $\exp(in\omega_z(\vec{r})t_1/2)$. A π pulse at $t_1/2$ converts this operator to a -n quantum operator which at time t_1 has accumulated a factor $\exp(-in\omega_z(\vec{r})t_1/2)$. Neglecting diffusion, these factors cancel and the evolution at t_1 is independent of $\omega_z(\vec{r})$.

While correct, this description neglects other possible effects of the π pulse on the evolution. The propagator for the evolution period with a π_x pulse at $t_1/2$ is

$$\exp((-i\mathcal{H}_{int} + \omega_z(\vec{r})I_z)t_1/2)\ \exp(i\pi I_x)\ \exp((-i\mathcal{H}_{int} + \omega_z(\vec{r})I_z)t_1/2) \quad (2.50)$$

Implicit in (2.50) is that ω_p is much greater than the range of offset frequencies so that a good π pulse is delivered over the entire sample volume. Defining the operator

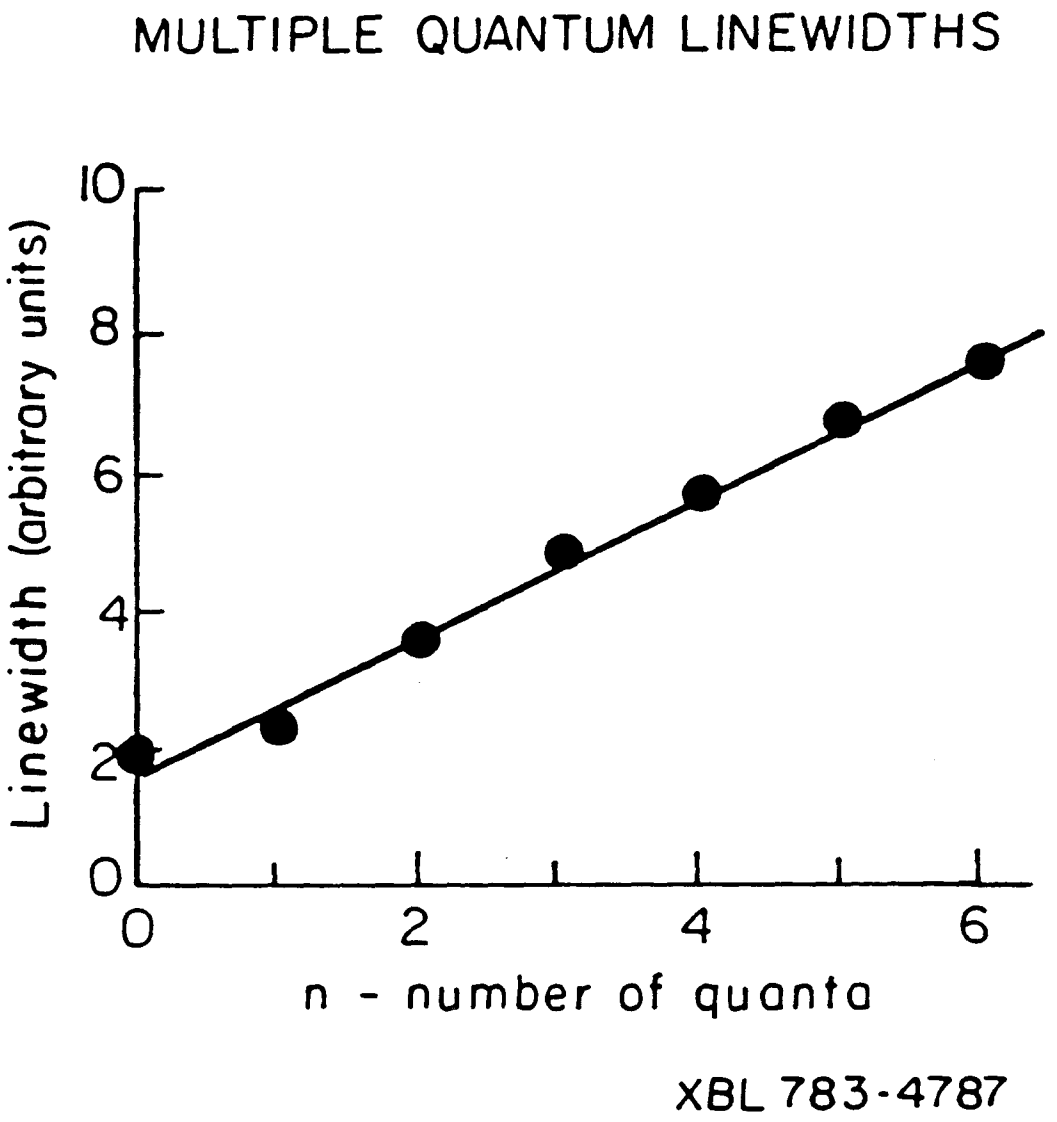

Figure 11. The effect of magnet inhomogeneity on multiple quantum linewidths. The widths of individual transitions of partially oriented benzene are linear in the order of the transitions. This inhomogeneous broadening is eliminated by sequences with a π pulse at $t_1/2$.
[By permission from D. E. Wemmer, "Some Double Resonance and Multiple Quantum NMR Studies in Solids", Ph.D. dissertation, University of California, Berkeley, 1978 published as Lawrence Berkeley Laboratory Report LBL-8042.]

$$\mathcal{H}'_{int} = \exp(-i\pi I_x)\ \mathcal{H}_{int}\ \exp(i\pi I_x) \tag{2.51}$$

the propagator (2.50) can be rewritten as

$$\exp(i\pi I_x)\ \exp(-i\mathcal{H}'_{int}t_1/2)\ \exp(-i\mathcal{H}_{int}t_1/2) \tag{2.52}$$

$\mathcal{H}'_{int}$ is obtained from $\mathcal{H}_{int}$ by simply changing the sign of all the linear (Zeeman) terms $\mathcal{H}^z$ (2.9). As desired, the dependence on $\Delta\omega(r)$ has vanished. The factor $\exp(i\pi I_x)$ may be thought of as part of the mixing period and is of no concern here.

If $[\mathcal{H}_{int},\mathcal{H}'_{int}] = 0$ then these exponents in (2.52) may be added. The resulting evolution is equivalent to that resulting from an average Hamiltonian

$$\mathcal{H}_1 = \frac{1}{2}\ (\mathcal{H}_{int} + \mathcal{H}'_{int}) \tag{2.53}$$

There are two common cases where the commutator is zero. One is the weak coupling limit, which occurs when chemical shift differences greatly exceed the spin couplings. This situation occurs often in liquids and is the basis of J spectroscopy[77]. The second case for which the commutator effectively vanishes is the other extreme where the chemical shift differences between pairs of spins are negligible compared to the couplings of the spins. This situation occurs for some solids and for some molecules oriented in liquid crystal phases where the direct dipolar couplings or electric quadrupole couplings dominate the spectrum. Both situations can occur for the same system if for every pair of spins the difference in Zeeman terms is either negligible or much greater than the coupling.

A more complicated analysis is required for an echo spectrum in a system for which $[\mathcal{H}_{int},\mathcal{H}'_{int}]$ is significant (comparable couplings and chemical shift differences). This case has been treated for single quantum spectra[78a]. The generalization to multiple quantum spectra[78b] is straightforward in principle. Each frequency observed in ω_1 is the average of two frequencies which would be observed in a perfect magnet: one frequency of order n and one of order -n. A computer program for calculating such spectra has been written[79].

Figure 12 shows how this averaging comes about. On the left the coherence before the π pulse is represented on an energy level diagram by arrows connecting states in coherent superposition. Only two coherences are shown for simplicity. In the center the result of a π pulse is shown for the case $[\mathcal{H}_{int},\mathcal{H}'_{int}] = 0$. Because there is a one-to-one correspondence between coherences before and after the π pulse, an average Hamiltonian (2.53) suffices. On the right, the result of a π pulse on the same two coherences is shown when the commutator does not vanish. There is a one-to-many correspondence between the coherences present before and after the pulse. The spectrum obtained in ω_1 is the superposition resulting from one such correspondence for each prepared eigenoperator. The net result is far more apparent transition frequencies than there are eigenoperators.

This proliferation of line frequencies could possibly be an aid to line assignment, since only transitions belonging to the same irreducible representation and having the same value of $(m_i + m_j)$ as well as $(m_i - m_j)$ give rise to average frequency lines. However, in general the multiplicity of lines observed is counterproductive to our goal of high resolution. Spectral analysis is complicated and the signal-to-noise ratio is reduced.

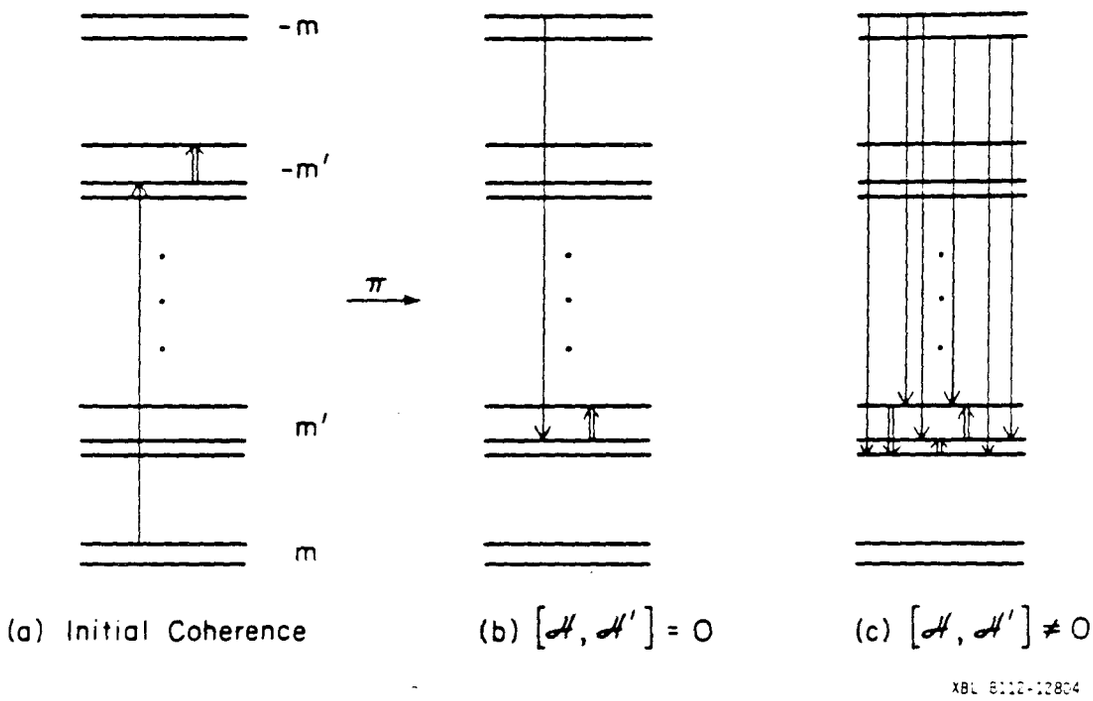

Figure 12. Coherence transfer due to a π pulse. In part a) two coherences exisiting before the π pulse are indicated by the single and the double arrow. In part b) each of these has been transferred to a single other coherence having the opposite value of the Zeeman quantum numbers. This occurs when the spin Hamiltonians $\mathcal{H}$ and $\mathcal{H}'$ (2.51) commute. When they do not commute, the situation in part c) occurs after the π pulse. This leads to a spectrum with many lines corresponding to the averages of the frequencies occurring before and after the π pulse.

A related proposal for removing inhomogeneity which does not increase the number of transitions is the use during evolution of a train of π pulses. For closely spaced pulses an effective $\mathcal{H}_1$ containing only bilinear terms is achieved. This will not be discussed further here. An easier approach, total spin coherence transfer echo spectroscopy, is taken up in Section IIE4.

2. Coherence Transfer Echoes

The different rates of dephasing and rephasing for each order, which were noted in the previous section as a source of inhomogeneous line broadening, lead also to a more useful phenomenon, the coherence transfer echo[3,5,80].

This differs from the familiar spin echo in that it depends on a change in $|n|$, rather than only a change in the sign of n as occurs with an ideal π pulse. The result is that the echo may be retarded or advanced according to the difference in n before and after the pulse.

Figure 13a sketches the pulse sequence for a simple demonstration of the phenomenon[80]. The preparation period contains a π pulse at $\tau/2$ so that a normal single quantum spin echo occurs at the time of the second $\pi/2$ pulse. This insures that the density operator existing after the second $\pi/2$ pulse is independent of magnet inhomogeneity. Evolution for a period t_1 results in an accumulated phase factor $\exp(in\omega_z(\vec{r})t_1)$ for n quantum coherence. The mixing pulse converts some of this coherence to $n = \pm 1$ operators which accumulate during t_2 a phase factor $\exp(\pm i\omega_z(\vec{r})t_2)$. At times such that $t_2 = |n|t_1$ the factors cancel for all $\omega_z(\vec{r})$.

Such an approach is not useful for obtaining multiple quantum spectra. Although the signals from each n are separated, the times t_2 at which the echoes occur vary with t_1. The signal array formed by sampling these echoes would be a function of both t_1 and t_2 and the points

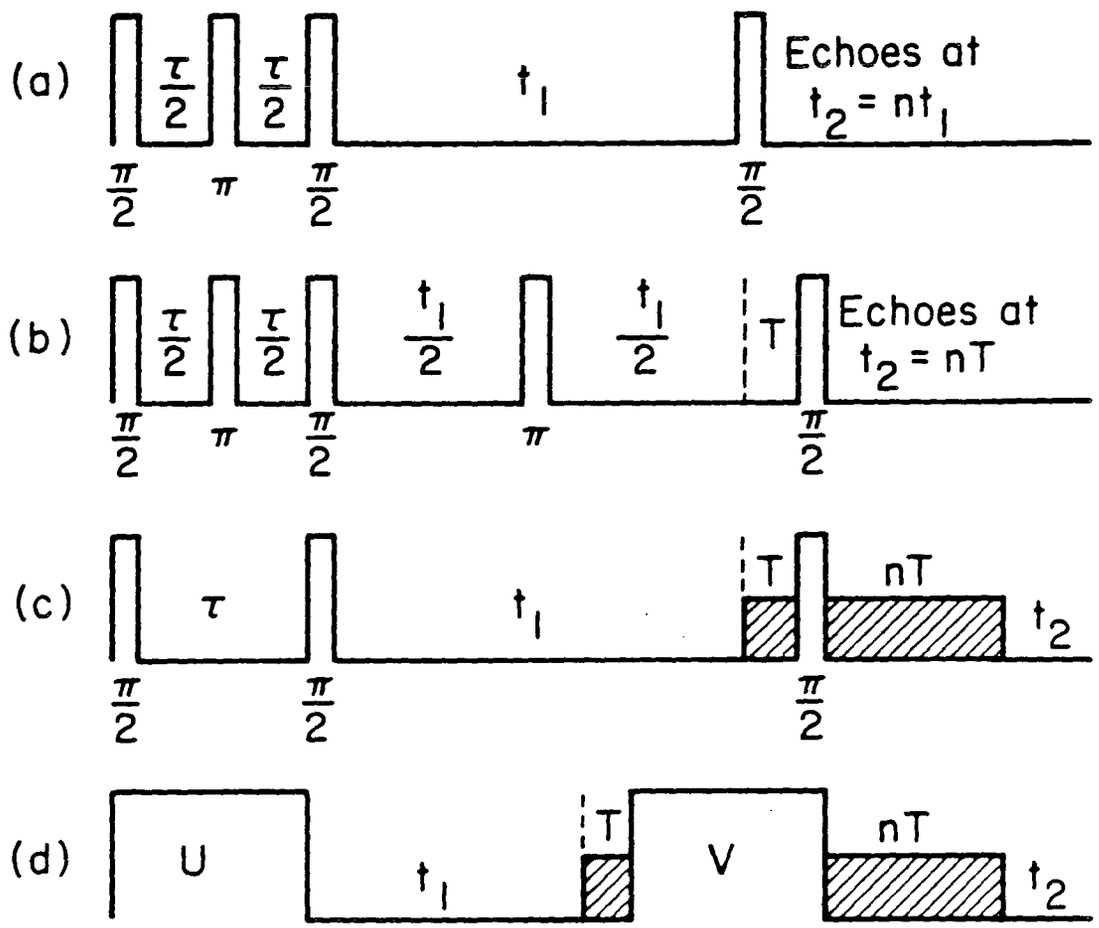

XBL 8112-12798

Figure 13. Pulse sequences involving coherence transfer echoes. In parts a) and b) the magnet is assumed to be inhomogeneous. The preparation period of length τ incorporates a π pulse to insure a coherent initial condition. In part a) dephasing of n-quantum coherence during t_1 at a rate proportional to n is followed by mixing to single quantum coherence and rephasing at a common rate leading to separate echoes for each n at $t_2 = nt_1$. In part b) the inhomogeneity is compensated within the evolution period by the π pulse at $t_1/2$. A dephasing of the n-quantum coherence for a fixed time T leads to separated echoes at time $t_2 = nT$ independent of t_1. Thus Fourier transformation with respect to t_1 gives homogeneous multiple quantum spectra. In parts c) and d) the static field is assumed to be homogeneous. In part c), pulsed field gradients are used to selectively echo a single order n of coherence. Part d) is similar, but indicates that for lengthy mixing periods involving many pulses and indicated by the propagator V, the interval between dephasing and rephasing may become large and eventually lead to loss of echo amplitude through diffusion.

of constant t_2 needed for a Fourier transform with respect to t_1 would not be echo points for all t_1. Thus the inhomogeneity during evolution leaves the multiple quantum lines broad. Sharp ridges occur in the 2D Fourier transform at the angles $\tan^{-1}(1/n)$[80].

3. Coherence Transfer Echo Filtering (CTEF)

Figures 13b shows a variation[81-83] which can be used for obtaining separated multiple quantum spectra free of inhomogeneous broadening. An extra constant period of multiple quantum evolution of length T is inserted before the mixing pulse. In addition a π pulse is given at the center $t_1/2$ of the variable evolution period. Now the accumulated phase factor depends only on T and the echoes occur at $t_2 = |n|T$ independent of t_1.

Figure 14 shows the signal in t_2 for one value of t_1 using the pulse sequence of Figure 13b and a sample of oriented benzene. Six equally spaced echoes are visible at times $t_2 = |n|T$. Significantly, the signal is present in both channels of the phase sensitive detector and the signal from a given order cannot be adjusted into one channel for all t_1. This is a characteristic of coherence transfer experiments: the signal in t_2 is phase modulated, rather than amplitude modulated, as a function of t_1.

To prove that this is generally the case recall that it is possible to combine the two Hermitian observables I_x and I_y into the linear combinations $I_\pm = I_x \pm iI_y$. One linear combination or the other can arbitrarily be assigned to the phase sensitive detector. If we choose to detect the combinations I_+ then the signal is $Tr(\rho I_-)$, due to the nature of the trace operation as an inner product. The detected operator (2.32) needed for the experiment of Figure 13b is

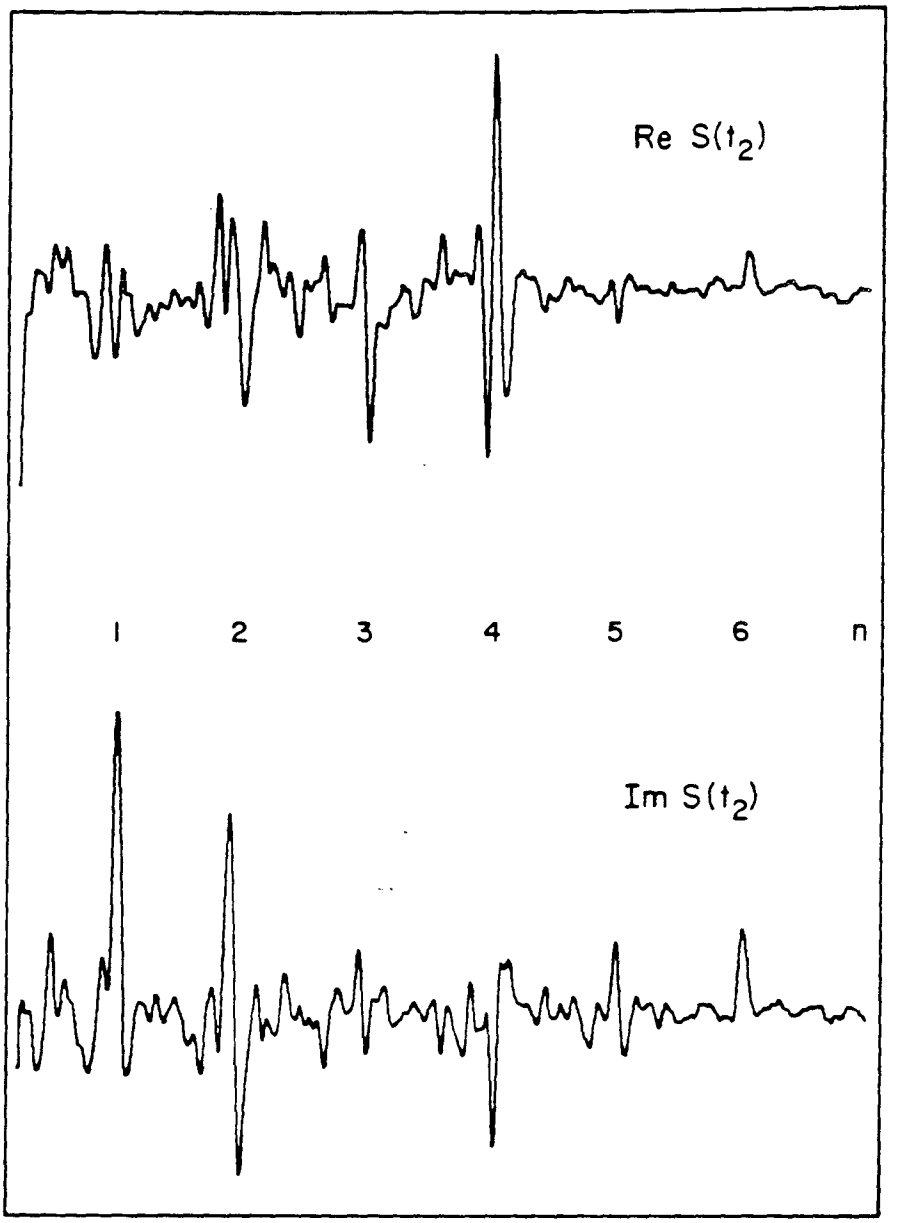

XBL 8112-12796

Figure 14. Coherence transfer echoes in t_2. The detection period signal in the two audio channels of the phase sensitive detector is shown for a sample of oriented benzene using the pulse sequence of Figure 13b with the parameters τ = 4 msec, t_1 = 33.28 msec, and T = 3 msec. The phase difference between the first two $\pi/2$ pulses was $\sim\pi/4$ so that all orders are prepared (Sec. IIIC2). The separation between echoes is T. The decay of each echo in a few hundred μsec is due to the static magnetic field inhomogeneity. By sampling at a particular echo maxima it is possible to obtain the signal due to a single order n. See Figure 15.

$$I_-(-(t_2+T),\vec{r}) = V^\dagger(T)\ \exp(i\mathcal{H}_{int}t_2)I_-\ \exp(-i\mathcal{H}_{int}t_2)V(T) \qquad (2.54)$$

where $\mathcal{H}_2$ has been set equal to $\mathcal{H}_{int}$ and the mixing propagator is

$$V(T) = \exp(-i(\pi/2)I_y)\ \exp(-i\mathcal{H}_{int}T) \qquad (2.55)$$

Note that the dephasing period T is formally part of mixing though it precedes the mixing pulse. The dependence on the position in the sample which is not noted explicitly in (2.55) is through the term $-\omega_z(\vec{r})I_z$ of $\mathcal{H}_{int}$ (2.8).

Since this inhomogeneity term commutes with the rest of $\mathcal{H}_{int}$ it is possible to express (2.54) in terms of a primed detected operator which would be relevant in a homogeneous field:

$$I_-(-(T+t_2),\vec{r}) = \exp(-i\omega_z(\vec{r})TI_z)\ \exp(+i\omega_z(\vec{r})t_2)I'_-(-(T+t_2)) \qquad (2.56)$$

Expanding in the basis set of $\mathcal{H}_1$ gives

$$I_-(-(T+t_2),\vec{r}) = \sum_{ij}(x'_{ji}(-(T+t_2))-iy'_{ji}(-(T+t_2))\exp(-i\omega_z(\vec{r})(n_{ij}T-t_2))|j><i| \qquad (2.57)$$

The signal (2.34) becomes

$$S_+(\tau,t_1,(T+t_2),\vec{r}) = \sum_{ij}\rho_{ij}(\tau)(x'_{ji}(-(T+t_2)-iy'_{ji}(-(T+t_2))$$

$$\exp(-i[\omega_z(\vec{r})(n_{ij}T-t_2)+\omega_{ij}t_1]) \qquad (2.58)$$

If $\omega_z(\vec{r})n_{ij}T$ ranges over all angles then integration over $\vec{r}$ cancels out the signal contribution from all orders except $n_{ij} > 0$ and even these only survive in the neighborhood of $t_2 = n_{ij}T$ as evidenced by Figure 14.

The restriction to positive n_{ij} has as a corollary that the dependence on t_1 is through a phase factor $\exp(-i\omega_{ij}t_1)$ since there is no complex conjugate term in the sum to make this real. Thus both channels of the receiver are necessary to collect the full signal, regardless of whether this would have been the case without the introduction of the coherence transfer echoes.

Figure 15 shows an example of what will be called coherence transfer echo filtering (CTEF). In the upper trace all of the orders prepared are detected by eliminating the period T of Figure 13b, placing a π pulse at $t_2 = \tau/2$ and sampling at $t_2 = \tau$. The separation of orders was achieved with the TPPI method discussed in Section IID2. In the lower trace the sequence of Figure 13b was used with $T = t_2/4 = \tau/4$ to detect only the $n = 4$ spectrum.

The approach of Figure 13b is not generally satisfactory with respect to signal-to-noise ratio since only the t_2 points near the echo maxima may be used to construct the multiple quantum FID. As discussed further in Section IIIB2 maximization of signal-to-noise ratio requires use of the signal over as long a period in t_2 as the natural decay time allows. Furthermore it is sometimes desirable to correlate the single quantum and multiple quantum spectra by two dimensional display of the spectra[72]. For this a complete f.i.d. in t_2 is needed.

The original version of the CTEF experiment[81], appropriate to homogeneous magnets, is shown in Figure 13c. It is assumed ideally that the only significant inhomogeneity of the static field is during the shaded periods of length T and nT during which times a reproducible current is delivered to a gradient coil intentionally dephasing or rephasing the ensemble. The full f.i.d. arising from one order is collected

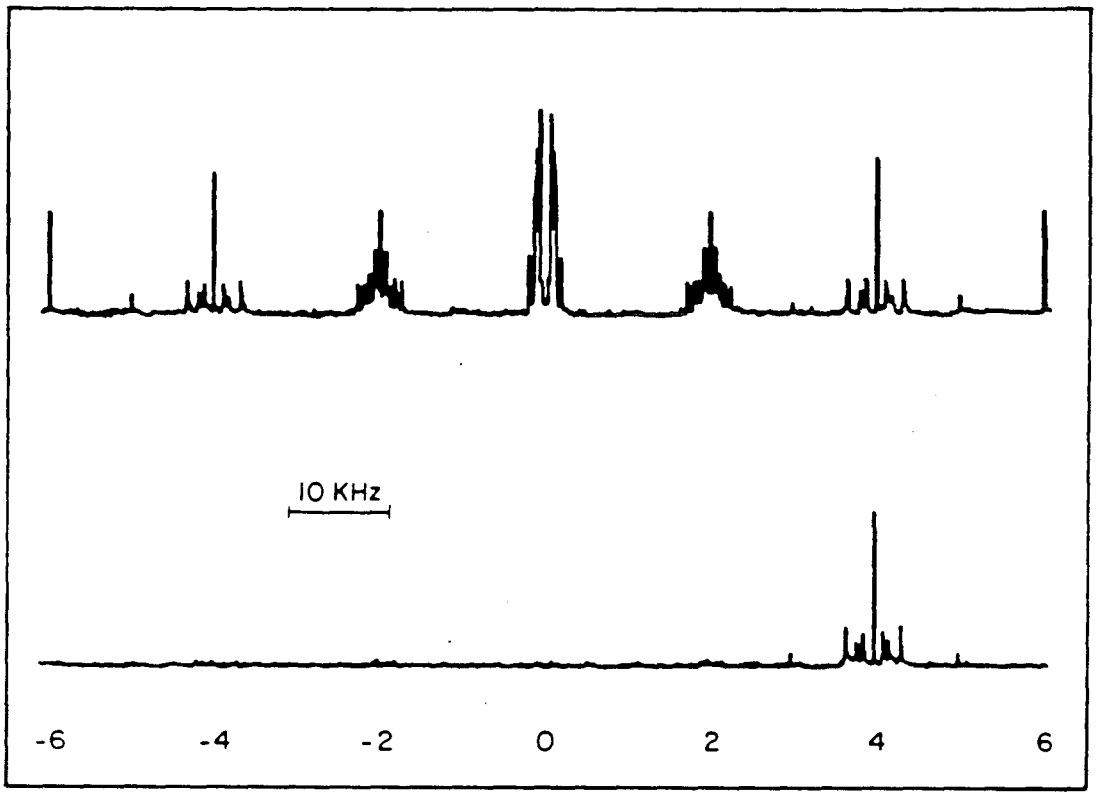

XBL 6112-12799

Figure 15. Coherence transfer echo filtering. The top trace is a spectrum of oriented benzene obtained with the sequence of Figure 3 augmented with π pulses at $\tau/2$, $t_1/2$ and $t_2 = \tau/2$. Sampling is at $t_2 = \tau = 4$ msec. Note that only even orders appear (Sec. IIIC2). The lower trace was obtained by removing the π pulse in t_2 and adding a fixed delay $T = \tau/4$ before the mixing pulse to give the sequence of Figure 13(b). Now only the $n = 4$ spectrum contributes to the signal at $t_2 = \tau = 4T$. The signals from other orders echo at other points in t_2. See Figure 14.

in t_2. Figure 13d indicates the generalization of this approach to the situation where a more complicated preparation and mixing sequences are used. As in Figure 4 these are indicated by their propagators U and V.

It is important to recognize that in the CTEF methods signal is always lost. The sequence of Figure 13b suppresses signal for most values of t_2, while those of Figure 13c and d suppress signal for most values of n. This is in contrast to the methods of Section IID which separated the signal from particular orders without suppressing that from any order.

There are auxiliary considerations which make the suppression of coherence by field gradients a valuable tool despite the fact that some signal energy is lost. Since only transitions of a single order appear, there is no need to disentangle the signal from different orders by PFT or TPPI. For a given resolution in ω_1, this reduces the minimum time needed to obtain a spectrum by a factor of 2N for N coupled spin ½ nuclei. This reduction in minimum experimental time is accompanied by an equivalent reduction in minimum data storage capacity required to obtain a spectrum of a given resolution. Of course, the accumulated signal is reduced by this same factor even for those transitions which are observed and is reduced ideally to zero for the suppressed transitions. If however, the signal-to-noise ratio is adequate and only one or a few transition orders are of interest then a genuine time advantage is achieved. This is particularly true if order selective excitation techniques (Sec. IIIC) are used which enhance the signal intensity of the selected order at the expense of others.

There is still another advantage to suppressing coherence with field gradients which arises because of instrumental instabilities during the

course of a two dimensional experiment. Such instability gives rise to a noise contribution, the multiplicative t_1 noise, which is minimized by suppressing extraneous transitions. Thus, a signal-to-noise gain may be obtained in this way for the observed lines without increasing their intensity or the experimental time. The achievable gain by this mechanism is dependent on a complex of performance conditions including instrument instability. The concept of multiplicative t_1 noise and its suppression are treated in Section IIIB3.

4. Total Spin Coherence Transfer Echo Spectroscopy (TSCTES)

a. The problems which are solved by TSCTES. In Section IIE1 the difficulty was noted that if $[\mathcal{H}_1,\mathcal{H}_1'] \neq 0$ the spectrum obtained in ω_1 by putting a π pulse at $t_1/2$ contains lines at the sums and differences of the frequencies which would be observed without a π pulse in an ideally homogeneous magnet. Such a set of lines is not directly interpretable in terms of an energy level diagram; indeed there are more lines than would be expected for any reasonable model Hamiltonian. The simulation of intensities for such a spectrum requires a calculation based on the details of the excitation and the parameters of $\mathcal{H}_1$. As discussed in Section IIIB1 there are practical limits on the complexity of systems for which dynamical intensity calculations are feasible. One feature of the method to be described is that it supplies relative line intensities which are exactly calculable independent of excitation dynamics. Exact knowledge of relative intensities is an aid to line assignment during spectral analysis.

A second potential drawback of the usual spin echo method is that the chemical shift differences are not readily measured from the resulting spectra. Their effect on the transition frequencies either vanishes

entirely or is muted, appearing only through their noncommutation with the bilinear terms. The TSCTES line positions have full sensitivity to chemical shift differences between coupled spins.

Finally, it is possible with TSCTES to obtain spectra of any order n with properly phased lines. This applies not only to spin inversion transitions (Sec. IIIA4), but also to the more interesting class of lines which carry information on the bilinear terms of $\mathcal{H}_1$. This phasing of lines improves resolution relative to that obtained with magnitude spectra and guarantees that spectral intensity is not lost through the destructive interference of unresolved transitions.

b. The pulse sequence. The general form of the TSCTES experiment is shown in Figure 16[84]. It differs from the scheme of Figure 4 in that the evolution period has been divided unequally into two parts by one or more rf pulses indicated by W.

The total spin coherence (n = N for N spins ½) is prepared by the preparation sequence indicated by U. Its evolution during time nt_1/N is determined entirely by the offset terms, as it commutes with all chemical shift differences as well as with the bilinear terms of $\mathcal{H}_{int}$. The propagator W transfers this coherence to lines of other orders including some particular order n of interest. A coherence transfer echo occurs after further free evolution for the period t_1. For $n \neq \pm 1$ this is invisible and is mixed to magnetization by the mixing propagator V.

As for the case where a π pulse is employed at $t_1/2$, the Fourier transform with respect to t_1 is independent of offset terms and thus of magnet inhomogeneity. The transfer of coherence by W is again a one-to-many correspondence (Fig. 12), but now, because of the uniqueness of the total spin coherence, the signal from only one such correspondence is

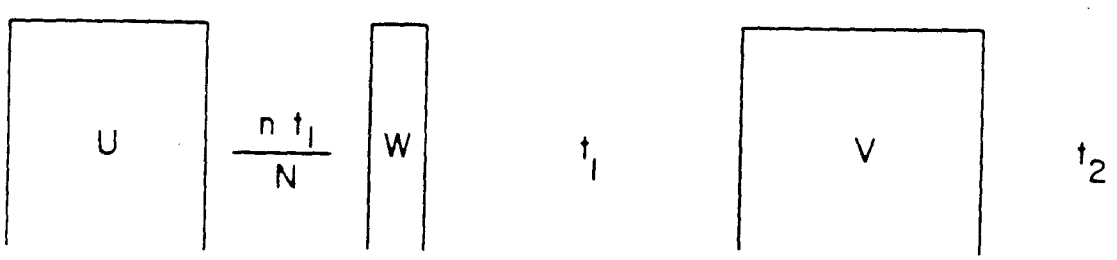

XBL 811-7537

Figure 16. General form of the pulse sequence for total spin coherence transfer echo spectroscopy. The propagator U is designed to prepare total spin (N-quantum) coherence. This dephases for a period nt_1/N at which time it is converted to n-quantum coherence by W. This coherence evolves for a time t_1 during which it also rephases. Mixing to observable single quantum coherence is accomplished with V. Fourier transformation with respect to t_1 gives an n-quantum spectrum free of broadening by magnet inhomogeneity, yet sensitive to chemical shift differences.

observed. The resulting spectrum contains only one line for each eigenoperator which is present during t_1 and which is connected by W to the total spin coherence.

c. Single quantum TSCTES spectra. Figure 17 shows the comparison between an ordinary one pulse single quantum spectrum and the n = -1 TSCTES spectrum for oriented acetaldehyde[84]. Comparison of parts a) and b) demonstrates the removal of magnet inhomogeneity. The simulation in part c) demonstrates that a spectrum sensitive to chemical shift differences and with calculable relative line intensities can be obtained. The complex amplitudes of the lines are given to within a common phase factor by

$$\rho_{ij}(\tau)(x_{ji} + iy_{ji}) = \rho_{N/2,-N/2}(\tau)d^{N}_{N,-1}(\theta)\langle i|T^{N}_{-1}|j\rangle\langle j|I_{+}|i\rangle \qquad (2.59)$$

The notation on the left is similar to that of (2.34-2.36), with $t_2 = 0$ and no mixing period. Both channels of the phase sensitive detector are considered simultaneously for the same reason as in Section IIE3: the echo condition holds only for transitions where the order of coherence changes sign and the detector is here arbitrarily taken as measuring n = -1. The factor $\rho_{ij}(\tau)$ on the left might also be written $\rho_{ij}(\tau+nt_1/N)$ since the $n_{ij} = -1$ coherence is created at this time. However, the dependence on nt_1/N is only dephasing and this is precisely what the echo removes.

The first factor on the right is the coefficient of the total spin coherence prepared by the propagator U. The second factor is a Wigner rotation matrix element[27], which expresses the efficiency with which single quantum coherence is prepared from the total spin coherence by a pulse of nutation angle θ. These factors are common to all lines. The

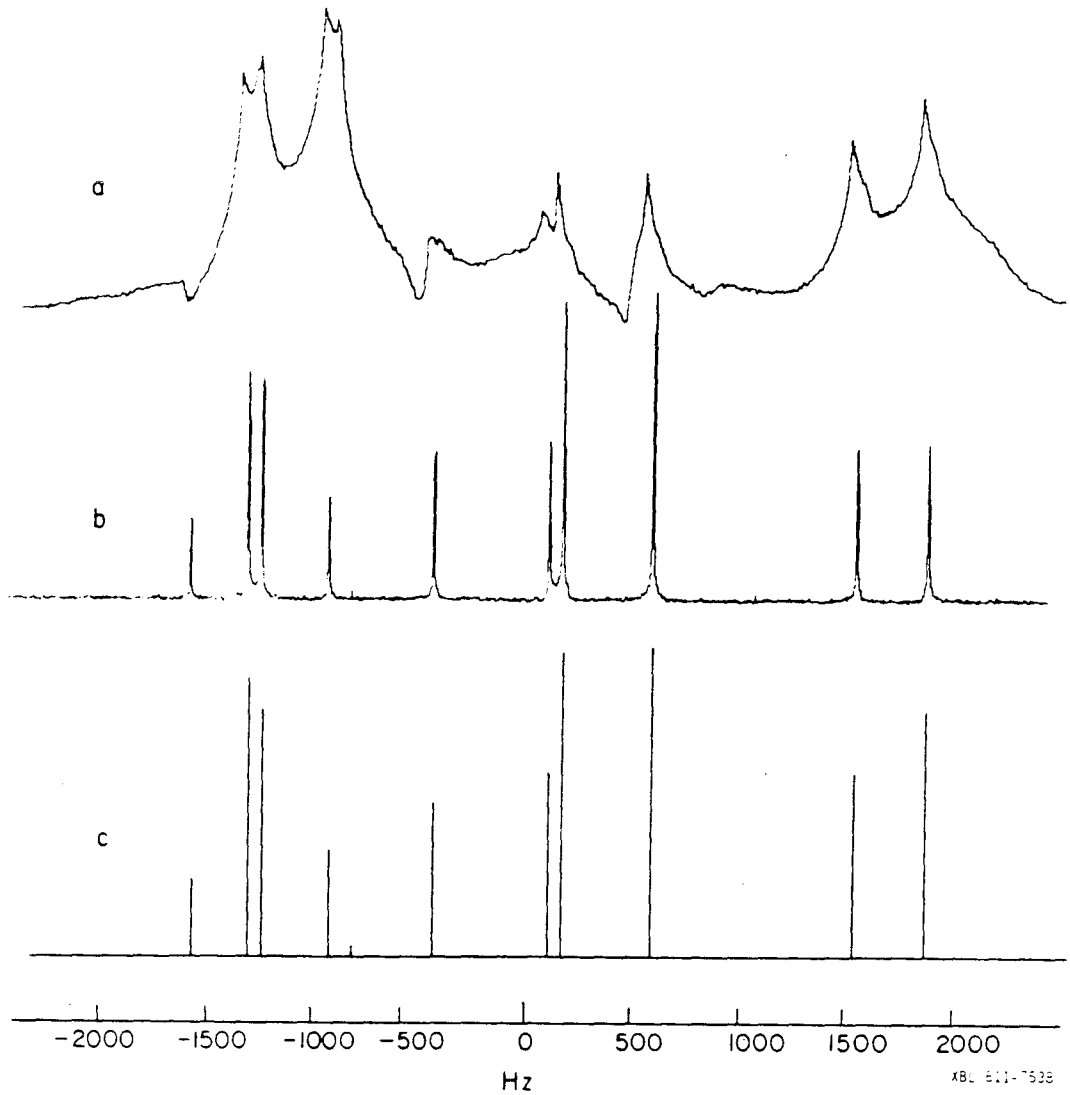

Figure 17. Removal of magnetic field broadening by total spin coherence transfer echo spectroscopy (TSCTES). Trace a) is the normal single quantum spectrum of acetaldehyde oriented in a nematic liquid crystal obtained by Fourier tranformation of the f.i.d. after a single pulse. It indicates inhomogeneous broadening of greater than 1 ppm. Trace b) is the TSCTES single quantum magnitude spectrum which is free of inhomogeneous broadening. Trace c) is the simulated spectrum which gives the paramaters J_{AB} = 2.8 Hz, ν_{AB} = 1360.9 Hz, D_{AB} = -179.0 Hz, D_{BB} = 458.6 Hz. The line amplitudes are given by (2.59). Unlike the usual single quantum spin echo methods TSCTES is sensitive to chemical shift differences and does not increase the number of transitions over that expected from the energy level diagram. When applied to multiple quantum spectra TSCTES gives phased lines of easily calculable relative intensities.

third factor expresses the extent to which a particular line is represented in this coherence. The fourth factor is the usual magnetic dipole detection period matrix element.

The phase of the lines is not indicated in the magnitude spectra of Figure 17 nor obvious in (2.59). It turns out that within a common phase factor all transitions are either absorptive or emissive, a point demonstrated and discussed elsewhere[85].

d. Multiple quantum TSCTES spectra. The extension to higher order spectra[85] is straightforward. The most useful form of the experiment uses a mixing propagator V which forces the coherence of interest back through the total spin coherence before the final mixing to detectable coherence. In this case line amplitudes are given by

$$\rho_{ij}(\tau)\alpha_{ji}(-\tau',-t_2) = \rho_{N/2,-N/2}(\tau)\alpha_{-N/2,N/2}(-\tau',-t_2)(d^N_{N,n}(\theta))^2|\langle i|T^N_n|j\rangle|^2 \tag{2.60}$$

The first three factors on the right are common to all lines of the chosen order n. The last two factors are non-negative and real. This is sufficient to give all lines with a common phase, if the only inhomogeneity in the ensemble is that of the static magnetic field. Since the total spin transition is a spin inversion transition, the product of the first two factors on the right can also in principle be made non-negative and real for a wider class of inhomogeneities by the methods of Section IIIA4.

e. Limitations. The most obvious limitation of the TSCTES method is that it depends on excitation of the extreme coherence. The theoretical limit on the magnetization available to this coherence is discussed in Section IIIC8. This small fraction of the total magnetization

is further divided up among the lines of the observed order n and in addition much is wasted in unobserved orders, which do not satisfy the echo condition. Quantitative expressions for the efficiency are given elsewhere[85].

Another major limitation is that while the method preserves chemical shift differences within a group of coupled spins, it is incapable of measuring differences between isolated systems. Thus the shift differences cannot be referenced to a standard with the same accuracy with which they are measured.

Finally, the lines observed with TSCTES always belong to the totally symmetric representation. This can be inconvenient since transitions of other representations may be more sensitive to certain combinations of Hamiltonian parameters which one would like to extract from the spectra.

5. Diffusion in Field Gradients

Translational diffusion along magnetic field gradients has long been recognized as a cause of irreversible dephasing in NMR[1,86]. Since the motion of the molecule gives the offset term of the Hamiltonian a random time dependence, a π pulse in the middle of the evolution does not lead to perfect rephasing of coherence. The decay depends on the order of the transition. For a single π pulse at $t_1/2$ the signal due to prepared n-quantum coherence decays as

$$\exp[(-t_1/T_2) + (-n^2\gamma^2G^2Dt_1^3/12)] \qquad (2.61)$$

This is the well-known single quantum result[86] for a gradient G and diffusion constant D, but the gyromagnetic ratio is effectively increased by n. This greater sensitivity to diffusion has been used to measure the anisotropic diffusion of methylene chloride[87a] (n = 2) and benzene[87b] (n = 6) in liquid crystal solvents.

For diffusion measurements large field gradients are introduced intentionally. Decay due to diffusion processes also can appear in the presence of residual field inhomogeneities. For example, in the three pulse sequence of Figure 3 (or the four pulse sequence obtained by adding a π pulse at $t_1/2$), the inhomogeneous dephasing which occurs during the preparation period is echoed for $t_2 = \tau$. Diffusion may cause this echo to be diminished in amplitude even at $t_1 = 0$. Such interference of diffusion effects with the performance of multiple quantum experiments is only a problem if the magnet inhomogeneity is quite poor and only then in liquids. It is mentioned here only because it does set an upper bound on the degree of inhomogeneity which can be effectively removed by the various echo phenomena of the preceding sections.

6. Zero Quantum Coherence

a. Introduction. Coherent superpositions among states in the same Zeeman manifold have a number of features which distinguish them from their higher quantum analogues. These unique properties make the $n = 0$ spectra of coupled spin systems accessible with somewhat simpler instrumentation than required for the full multiple quantum experiment. In addition, the zero quantum coherences may be prepared not only by the rf pulse sequences discussed so far, but also by methods which in principle need not involve any irradiation. One other zero quantum peculiarity, an extra quantum number, is taken up in Section IIIC3.

b. Relaxed performance conditions for zero quantum NMR. The three pulse sequence of Figure 3 suffices to give the $n = 0$ transitions with linewidths unaffected by magnetic field inhomogeneity[9]. As noted in Section IID1 (2.42), the dependence of the transition energy on the offset term is proportional to n and thus vanishes for these

transitions[9]. The only remaining dependence of these line positions on the field strength in the high field limit is through the differences in chemical shifts. These differences $(\omega_{zi} - \omega_{zj}) = (\sigma_i - \sigma_j)\omega_0$ are linear in the Larmor frequency but with coefficients $(\sigma_i - \sigma_j)$ of parts per million instead of unity as with the offset term. The limiting fractional resolution then is the product of the fractional inhomogeneity and the fractional shift difference $(\sigma_i - \sigma_j)(\lesssim 10^2$ ppm). Thus even casual conditions of field inhomogeneity (1 ppm) would give an inhomogeneous contribution of about one part in 10^{10}. This is almost always negligible compared to broadening due to T_2. This allows zero quantum spectra to be recorded at high resolution without a π pulse at $t_1/2$, thus avoiding the complications of simulating the effect of this pulse (Sec. IIE1).

Since all other coherence will rapidly decay during t_1 in an inhomogeneous field, it is possible to make use of this decay to observe only the n = 0 contribution to the signal by starting t_1 at a value several times the inhomogeneous decay time T_2^*. This obviates the need for the many rf phases required by the PFT and TPPI methods of separating signals of different order (Sec.IID2). This may be viewed as a special case of the CTEF methods discussed in Section IIE3.

Zero quantum spectra of weakly coupled liquid systems have recently been discussed[88].

c. Alternative excitation and detection methods for zero quantum coherence. The close kinship between zero quantum coherence and populations, which is evidenced by their similar indifference to magnetic field gradients, has consequences also for possible means of creating zero quantum coherence. Suppose that a system of spins is suddenly subjected to a change in its Hamiltonian. Suppose furthermore that

$$[\mathcal{H}_{new}, \mathcal{H}_{old}] \neq 0 \tag{2.62}$$

so that a different set of eigenstates is needed for each Hamiltonian. Let these states be solutions to the Schrodinger equations

$$\mathcal{H}_{new}|i\rangle = \omega_i|i\rangle \tag{2.63a}$$

$$\mathcal{H}_{old}|i'\rangle = \omega_i'|i'\rangle \tag{2.63b}$$

If the system initially has no coherences, then its density operator can be expressed as a sum of number operators for the old eigenstates

$$\rho(0) = \sum_{i'} \rho_{i'i'}(0)|i'\rangle\langle i'| \tag{2.64}$$

Immediately after the sudden change from $\mathcal{H}_{old}$ to $\mathcal{H}_{new}$ the density operator is the same, but now it is appropriate to rewrite it in the basis of the new eigenstates. Thus

$$\rho(0) = \sum_{i'} \sum_{j,k} \rho_{i'i'}(0)\, T_{ji'}T_{i'k}|j\rangle\langle k| \tag{2.65}$$

where T is the transformation operator relating the two bases. For free evolution under $\mathcal{H}_{new}$, $\rho(t)$ is given simply by multiplying each term $|j\rangle\langle k|$ by $\exp(-i\omega_{jk}t)$. Such off diagonal terms ($j \neq k$) will exist so long as $[\rho(0), \mathcal{H}_{new}] \neq 0$. Thus a sudden change between noncommuting Hamiltonians may induce oscillating terms in the density operator without the application of any rf. An early example of this phenomenon is the oscillations in the magnetization induced by rapid switching between low magnetic fields[89].

If the experiment takes place in high field then

$$[\mathcal{H}_{old}, I_z] = [\mathcal{H}_{new}, I_z] = 0 \tag{2.66}$$

and both Hamiltonians and the transformation operator T block factor according to Zeeman quantum number. Thus the sum in (2.65) is restricted to terms with $m_{i'} = m_j = m_k$. The result is that only zero quantum coherence can be created by a change from one high field spin Hamiltonian to another in a system originally lacking coherence.

One of the earliest observations of zero quantum coherence was, in fact, made with such a preparation method[20,90]. The change in Hamiltonian was due to a chemical association between photo-fragments, which during their history as free radicals had developed nuclear spin polarizations (chemically induced dynamic nuclear polarization)[91].

In principle, this means of preparing zero quantum coherence by reaction is more general and need not involve free radical reactions. If reactants A and B with different magnetizations combine rapidly in such a manner that strong couplings between spins on A and spins on B are created then zero quantum coherence will be created. The difference in magnetization could be achieved simply by bringing one species into the magnetic field immediately before mixing so that it would be initially unpolarized. It is worth noting that n = 0 coherence excited in this way is created instantaneously, while if the evolution Hamiltonian $\mathcal{H}_1 = \mathcal{H}_{new}$ did commute with $\mathcal{H}_{old}$ or $\rho(0)$ a finite preparation period would be necessary.

Zero quantum coherence has also been detected in an unorthodox manner[92]. After preparation by large angle pulses, small fractions of the coherence were mixed to n = 1 operators by small angle pulses at regular intervals. In this way the mixing and detection processes coexist with the continued evolution of the bulk of the coherence and the

experiment becomes one dimensional. Because field gradient pulses were used before each mixing pulse to eliminate interferences, the method is peculiar to n = 0 coherence.

F. Information Content and Symmetry Considerations

1. The Number of Transitions

a. The general case. The most striking feature of multiple quantum spectra, such as that of Figure 1, is that the number of transitions of a given order n falls rapidly with n, while the spectral range is roughly constant. The combinatorial origin of this effect is evident from Figure 2. The density of states falls with M and the high order spectra consist of transitions connecting these sparse manifolds. In the absence of permutational symmetry in $\mathcal{H}_{int}$, all transitions are allowed in the sense that some sequence of pulses can be found which will excite the corresponding coherence. For the vast majority of coherences $|i\rangle\langle j|$, the sequence of three $\pi/2$ pulses (Fig. 3) will lead to a finite line amplitude $\rho_{ij}\alpha_{ji}$ in (2.34). Special cases of lines which are allowed, but not with this sequence, are mentioned in Section IIIC3 and IVC. Various other aspects of line intensity are treated in IIIB and IIIC.

The number of transitions for the general case, where there is no permutational symmetry, serves as an upper bound for any particular system. For N spins ½ there are 2^N states and the density operator may be viewed as a vector in a 4^N dimensional Hilbert space (Liouville space). The number of operators characterized by each value of n is a well-known combinatorial problem[28,29].

There are $N!/(N/2+M_i)!(N/2-M_i)!$ kets with eigenvalue M_i of I_z to which may be appended any of the $N!/(N/2+M_j)!(N/2-M_j)!$ bras with

eigenvalue M_j to form an outer product operator $|i><j|$ characterized by n_{ij} (2.5). The same difference n_{ij} may be obtained by other combinations of M_i and M_j so that the total number of n quantum operators is the sum

$$Z_n = \sum_{M-M'=n} \binom{N}{N/2+M}\binom{N}{N/2+M'} = \binom{2N}{N+n} \tag{2.67}$$

The case n = 0 is special in that the $\binom{2N}{N}$ zero quantum operators consist of 2^N number operators describing the populations (diagonal elements of ρ) and the other

$$Z_o = [\binom{2N}{N} - 2^N] \tag{2.68}$$

are coherences between pairs of states in the same Zeeman manifold. In reference 29 Z_o was defined as one half this quantity in recognition of the fact that the zero quantum transition frequencies for $\omega_1 < 0$ are mirrored for $\omega_1 > 0$. The definition (2.68), on the other hand, counts off-diagonal matrix elements. The sum of all such elements is

$$\sum_{n=-N}^{N} Z_n = 4^N - 2^N \tag{2.69}$$

b. The role of permutation group symmetry. The selection rules of magnetic resonance are particularly simple since the interaction with the radiation acts only on the spin degrees of freedom. The full Hamiltonian including the rf term has the same symmetry as the internal Hamiltonian with regard to permutation of nuclear indices. A consequence is that no transitions are induced by the rf fields between states belonging to different irreducible representations of the permutation group. This is as true for multiple quantum as for single quantum

NMR. The initial condition $\rho(0)$ has the permutation symmetry of $\mathcal{H}_{int}$ and this is preserved through any sequence of pulses. This requires that all finite terms of the density operator have matrix elements only between states of the same irreducible representation. This restriction reduces the number of possible coherences when there is permutation symmetry.

Neglecting relaxation mechanisms, which may have a lower symmetry than $\mathcal{H}_{int}$, it is possible to treat the dynamics within each irreducible representation as a separate problem. In any case, the eigenstates of $\mathcal{H}_1$ have at least the symmetry of $\mathcal{H}_{int}$ and the enumeration and/or construction of symmetry adapted states is a usual prelude to detailed consideration of a particular system. There is nothing peculiar to multiple quantum NMR in these steps, since the states are the same as enter into the single quantum calculations. The applications of group theory to these problems are reviewed in numerous texts[93-95]. A minor wrinkle in practice is deciding, ultimately by spectral simulation, which molecular motions are sufficiently fast to increase the symmetry of $\mathcal{H}_{int}$ by motional averaging.

If the number of states belonging to each irreducible representation has been enumerated for each value of M, then the number of possible transitions is easily arrived at by allowing all transitions within the irreducible representation. Examples for different values of n and various permutation symmetries have appeared[29,96-99].

An enumeration of transitions for only the few highest orders often suffices in applications, since these are the best resolved and most easily assigned spectra. A rule for counting n = N-2 quantum lines in spin ½ systems without chemical shifts has been proposed, which does not

require the enumeration of the number of states in the relevant manifolds which belong to each irreducible representation[97,98]. It is not repeated here as at least one counterexample is known: the case of two inequivalent correlated methyl groups[100]. The usual group theoretical methods give the correct answer.

2. Time Reversal and Spin Inversion Parity

a. Symmetry operations. That time reversal symmetry should play any role in magnetic resonance is at first glance unlikely, since it is the difference in Zeeman energy of states differing only in the sign of their spin angular momentum which makes the technique possible. However, since the effect of transformation to the rotating frame is to remove to a good approximation the terms linear in spin angular momenta, many of the spin Hamiltonians which arise are, in fact, invariant to the simultaneous reversal of all angular momenta. This will be the case when the residual Zeeman terms, the chemical shifts and magnet inhomogeneity, are negligibly small on the time scale of interest or when pulse sequences are so designed that on average these terms do not contribute to the dynamics.

Consider a system characterized by a Hamiltonian $\mathcal{H}_1$ without Zeeman terms. All the other terms in the resonant rotating frame Hamiltonian, collected as $\mathcal{H}^{zz}$ in (2.10), are bilinear in spin angular momenta. A consequence is that such a Hamiltonian has an extra symmetry element which does not depend on the particular value of the Hamiltonian parameters nor involve permutation of spin labels. One such spin-space symmetry element is already familiar: any high field spin Hamiltonian is invariant to rotation about the magnetic field direction (Eq. 2.3).

The extra group element for a bilinear Hamiltonian can be taken to be the time reversal operation. The conventional definition of this operation is[101]

$$K = \exp(-i\pi I_y)K_0 \tag{2.70}$$

For a spin system, K_0 has the effect of complex conjugation and of changing the sign of all I_{yi} operators. The form (2.70) is useful for operations on bracket notation expressions. For operator expressions written in terms of the components of spin angular momenta it is sufficient to remember that

$$K\underset{\sim}{I}_i K^\dagger = -\underset{\sim}{I}_i \tag{2.71}$$

and

$$K(i)K^\dagger = -i \tag{2.72}$$

where $i = \sqrt{-1}$ in (2.72).

Time reversal is clearly very closely associated with the operation of giving π pulses. In fact, it turns out to be useful to introduce additional operations which may also be symmetry operations for a bilinear spin Hamiltonian. These are

$$\Pi_x \equiv \exp(-i\pi I_x) \tag{2.73}$$

$$\Pi_y \equiv \exp(-i\pi I_y) \tag{2.74}$$

A useful labeling scheme for eigenstates of bilinear Hamiltonians is to define spin inversion pairs by the operation

$$\Pi_x|i\rangle \equiv |\bar{i}\rangle \tag{2.75}$$

which is reciprocal. In terms of the simple product basis, $|\bar{i}>$ is obtained from $|i>$, or vice versa, by replacing all the individual spin states $|\beta>$ by $|\alpha>$ and all the $|\alpha>$ by $|\beta>$.

b. Degeneracy of bilinear Hamiltonians. A secular bilinear Hamiltonian (2.10) is invariant to all three of the operations introduced. For such an operator, $\mathcal{H}_1 = \mathcal{H}^{zz}$,

$$K\mathcal{H}_1 K^{\dagger} = \Pi_x \mathcal{H}_1 \Pi_x^{\dagger} = \Pi_y \mathcal{H}_1 \Pi_y^{\dagger} = \mathcal{H}_1 \tag{2.76}$$

A corollary is that if

$$[\mathcal{H}_1, |i><j|] = \omega_{ij} |i><j| \tag{2.39}$$

then

$$[\mathcal{H}_1, |\bar{i}><\bar{j}|] = \omega_{ij} |\bar{i}><\bar{j}| \tag{2.77}$$

This states that the transitions associated with these spin inversion eigenoperators are degenerate. Note also that if

$$[I_z, |i><j|] = n_{ij} |i><j| \tag{2.27}$$

then

$$[I_z, |\bar{i}><\bar{j}|] = -n_{ij} |i><j| \tag{2.78}$$

Thus these transitions are only degenerate if the different orders $\pm n$ are not separated by any of the various schemes of Section IID.

Similarly, there are repeated eigenvalues even in orders with different $|n|$. These are of the form

$$\omega_{ij} = \omega_{i\bar{j}} \tag{2.79}$$

which states that for a bilinear $\mathcal{H}_1$, there will be a line at distance ω_{ij} from the center of order $n_{ij} = M_i - M_j$, and an identically placed line in order $n_{i\bar{j}} = M_i + M_j$.

c. Operators with definite parity. Because of the degeneracy (2.77) it is reasonable to consider sums and differences of these operators which transform in a particularly simple way under the transformations associated with Π_x, Π_y and K. Table 1 lists Hermitian combinations of the eigenoperators of $[\mathcal{H}_1,]$ which have the properties:

$$\Pi_\varepsilon A \Pi_\varepsilon^\dagger = P_\varepsilon^A A, \qquad \varepsilon = x,y \tag{2.80a}$$

and

$$KAK^\dagger = P_K^A A \tag{2.80b}$$

These operators form an alternative basis for expanding the density operator at various points in a multiple quantum pulse sequence. No explicit use of the basis, however, is necessary to exploit the symmetry arguments. Notice that each operator is characterized by a definite value of $|n|$, but contains operators with n having either sign. For even values of n, $(P_x^A P_y^A) = 1$; for odd values $(P_x^A P_y^A) = -1$. These are the same factors by which even or odd operators, respectively, are multiplied when rotated by π around the z spin axis.

The operators $I_{x\pm}^{ij}$ and $I_{y\pm}^{ij}$ are coherences, while $I_{z\pm}^{ij}$ are population differences.

d. Dynamic constraints on parity. Since the numbers $P_{x,y,K}^A$ take values of ± 1, they will be referred to as parity quantum numbers. Their usefulness derives from the constraints on these quantum numbers during time development under Hamiltonians of definite parity.

Table I. Operators of Definite Parity

A Relation to Pseudo-Spin Operators	Operator Definitions	P_x^A	P_y^A	P_K^A
$I_{x+}^{ij} = I_x^{ij} + I_x^{\bar{i}\bar{j}}$	$= \frac{1}{2}(\lvert i\rangle\langle j\rvert + \lvert j\rangle\langle i\rvert) + \frac{1}{2}(\lvert \bar{i}\rangle\langle \bar{j}\rvert + \lvert \bar{j}\rangle\langle \bar{i}\rvert)$	1	$(-)^{n_{ij}}$	$(-)^{n_{ij}}$
$I_{x-}^{ij} = I_x^{ij} - I_x^{\bar{i}\bar{j}}$	$= \frac{1}{2}(\lvert i\rangle\langle j\rvert + \lvert j\rangle\langle i\rvert) - \frac{1}{2}(\lvert \bar{i}\rangle\langle \bar{j}\rvert + \lvert \bar{j}\rangle\langle \bar{i}\rvert)$	-1	$(-)^{n_{ij}+1}$	$(-)^{n_{ij}+1}$
$I_{y+}^{ij} = I_y^{ij} + I_y^{\bar{i}\bar{j}}$	$= \frac{-i}{2}(\lvert i\rangle\langle j\rvert - \lvert j\rangle\langle i\rvert) - \frac{i}{2}(\lvert \bar{i}\rangle\langle \bar{j}\rvert - \lvert \bar{j}\rangle\langle \bar{i}\rvert)$	1	$(-)^{n_{ij}}$	$(-)^{n_{ij}+1}$
$I_{y-}^{ij} = I_y^{ij} - I_y^{\bar{i}\bar{j}}$	$= \frac{-i}{2}(\lvert i\rangle\langle j\rvert - \lvert j\rangle\langle i\rvert) + \frac{i}{2}(\lvert \bar{i}\rangle\langle \bar{j}\rvert - \lvert \bar{j}\rangle\langle \bar{i}\rvert)$	-1	$(-)^{n_{ij}+1}$	$(-)^{n_{ij}}$
$I_{z+}^{ij} = I_z^{ij} + I_z^{\bar{i}\bar{j}}$	$= \frac{1}{2}(\lvert i\rangle\langle i\rvert - \lvert j\rangle\langle j\rvert) + \frac{1}{2}(\lvert \bar{i}\rangle\langle \bar{i}\rvert - \lvert \bar{j}\rangle\langle \bar{j}\rvert)$	1	1	1
$I_{z-}^{ij} = I_z^{ij} - I_z^{\bar{i}\bar{j}}$	$= \frac{1}{2}(\lvert i\rangle\langle i\rvert - \lvert j\rangle\langle j\rvert) - \frac{1}{2}(\lvert \bar{i}\rangle\langle \bar{i}\rvert - \lvert \bar{j}\rangle\langle \bar{j}\rvert)$	-1	-1	-1

Suppose that at some point $\rho(t)$ contains an operator A with parity given by the numbers P_x^A, P_y^A, and P_K^A. If time development now occurs under some Hamiltonian $\mathcal{H}$, we would like to know what parity quantum numbers characterize A(t) defined by

$$A(t) = \exp(-i\mathcal{H}t)A \exp(i\mathcal{H}t) \tag{2.81}$$

Lemma 1. Assume that

$$[\Pi_x, \mathcal{H}] = 0 \tag{2.82}$$

or equivalently

$$\Pi_x \mathcal{H} \Pi_x^\dagger = \mathcal{H} \tag{2.83}$$

Then it follows that

$$\Pi_x A(t) \Pi_x^\dagger = P_x^A A(t) \tag{2.84}$$

Thus P_x^A is a constant of the motion. An identical proof holds for P_y^A.

Lemma 2. Assume that

$$K\mathcal{H}K^\dagger = -\mathcal{H} \tag{2.85}$$

Then

$$K \exp(-i\mathcal{H}t)K^\dagger = \exp(-i\mathcal{H}t) \tag{2.86}$$

and

$$KA(t)K^\dagger = P_K^A A(t) \tag{2.87}$$

Thus time reversal parity is a constant of the motion under Hamiltonians of odd time reversal parity.

Theorem: For $\mathcal{H} = -\omega_P I_x$ (a strong θ_x pulse), the parity P_y^B of an operator B which appears in A(t) (2.81) and is of the form defined in Table 1 is given by

$$\Delta = (P_x^A P_y^A)(P_x^B P_y^B). \tag{2.88}$$

The quantity Δ is +1 if A and B are both even quantum or both odd quantum. If one is even and the other odd, then $\Delta = -1$. The proof of the theorem is most easily obtained by inspection of Table 1. Starting in any row, we are confined by Lemma 1 to set $P_x^B = P_x^A$ and by Lemma 2 to set $P_K^B = P_K^A$. With these restrictions an operator B with a different value of $(-)^n$ then the operator A must also have a different parity under a π_y pulse. An identical theorem holds with x and y interchanged.

e. Applications. Time reversal arguments are used in Section IIIA to develop relationships between preparation and mixing periods. Parity considerations are used in Section IIIC2 to predict in which channel of the phase sensitive detector a signal resulting from a given order of coherence will occur and in Section IIIC3 to develop selection rules for n = 0 transitions. Operators with definite parity are used in Section IIIC9 to describe an excitation sequence in which a population inversion of two levels $|i\rangle$ and $|j\rangle$ takes place selectively without the appearance of a corresponding coherence $|i\rangle\langle j|$.

3. Information Content in Multiple Quantum Line Positions

a. The questions. There are a number of issues which might come under the heading of information content. Some of these have been raised already. It is abundantly clear that there exist situations where the increased resolution or the simplicity of interpretation make the multiple quantum spectra of a given system preferable to the single

quantum spectrum. The number of such situations will surely grow as the technique becomes more widely considered by practicing spectroscopists. The motivation in a given situation may be unresolved or unassignable lines due to a short T_2 or an accidental degeneracy or the chemical heterogeneity of the sample. Other crucial uses of multiple quantum spectra appear when magnet inhomogeneity (Sec. IIE4) and relaxation effects (Sec. 5) are considered. This section begins with a considerably narrower question: Are there spin Hamiltonians for which analysis of the multiple quantum spectra is able to supply information which is absent even in the ideal single quantum spectrum? The answer in principle is yes and two such situations are discussed. This is followed by a review of some of the areas where multiple quantum techniques have proven in practice to be valuable for obtaining easily interpreted resolved spectra.

b. The relative orientation of chemical shift tensors in powder samples. Multiple pulse line narrowing sequences[61-63] result in the effective removal of the direct dipolar couplings between homonuclei. The average Hamiltonian which suffices to explain the spectrum for many applications is

$$\mathcal{H}_1 = -\kappa \sum_i \omega_{z\,i} \underset{\sim}{I}_i \cdot \underset{\sim}{n} \qquad . \qquad (2.89)$$

The chemical shift terms are scaled down by a factor κ and quantized along the direction in spin space of a unit vector $\underset{\sim}{n}$. Both effects depend on the particular pulse sequence used. The scalar parts of the indirect or J couplings do survive these pulse sequences, but are usually negligible at the resolution attainable in rigid solids. In this limit,

the single quantum spectrum consists of a discrete line for each chemical shift. The sample is effectively a collection of isolated spins during the multiple pulse sequence. The frequencies of these lines are proportional to the component of the individual chemical shift tensors along the magnetic field;

$$\omega_{zi} = \omega_o \sigma^i_{zz} \tag{2.90}$$

The rotating frame frequency has been taken as coincident with the zero of the chemical shift scale.

The measured component depends on the principal components and the orientation of the molecule fixed chemical shift tensor in the laboratory frame according to[63]

$$\sigma^i_{zz} = \sigma^i_{11}\cos^2\alpha_i\sin^2\beta_i + \sigma^i_{22}\sin^2\alpha_i\sin^2\beta_i + \sigma^i_{33}\cos^2\beta_i \tag{2.91}$$

The Euler angles (α_i, β_i) relate the principal axes of the tensor to the laboratory frame. They can be extracted by rotating a single crystal about one or more axes. This information can be combined with knowledge (from diffraction studies) of the molecular orientation with respect to the crystal axes to yield the orientation of each shielding tensor in the molecular frame. This molecular frame orientation is essential for the interpretation of the observed chemical shift in terms of electronic structure or partial molecular ordering.

A drawback of this single quantum multiple pulse approach is the requirement for single crystals. It is only through the rotation plots that the orientations of the individual spin chemical shift tensors can be related to one another or to a common molecular frame. This is a

consequence of the fact that both the coherence for the single quantum experiment and the Hamiltonian (2.89), are sums of single spin operators.

Since many molecules cannot be obtained as crystals sufficiently large for rotation studies, a means of determining the relative and molecular frame orientations of the shift tensors in powder samples is desirable. The powder patterns resulting from the unperturbed Hamiltonian including direct dipolar couplings in principle contain this information, since the dipolar coupling tensors have an obvious relation to the molecular frame. This approach is of limited usefulness as the single quantum powder spectrum of even a small spin system has few resolved features. Multiple quantum NMR might make possible the extension of such analyses to larger molecules, since the spectral structure due to $\mathcal{H}^D$ diminishes in the high orders.

An intriguing possibility is to combine the multiple pulse Hamiltonian (2.89) with a multiple quantum initial condition at $t_1 = 0$. Although the spins evolve effectively independently during t_1, their preparation as a coupled system guarantees that this evolution is much more informative than the single quantum multiple pulse experiment. In order to simplify the analysis of such an experiment, discussion will be restricted to the case where $\underset{\sim}{n}$ of (2.89) is z. Such multiple pulse line narrowing sequences are known[61]. The case of $\underset{\sim}{n} \neq z$ is similar, but leads to a greater number of superimposed powder patterns in the spectrum of a given order, because n is then not conserved during t_1.

The eigenstates of (2.89) with $\underset{\sim}{n} = z$ are simply the simple product states. This fact makes it convenient to analyze the evolution during t_1 directly in the operator basis

$$I_{+i} = |\alpha_i\rangle\langle\beta_i|$$

$$I_{-i} = |\beta_i\rangle\langle\alpha_i|$$

$$I^{+}_{0i} = |\alpha_i\rangle\langle\alpha_i|$$

$$I^{-}_{0i} = |\beta_i\rangle\langle\beta_i| \qquad (2.92)$$

Any product of these operators consisting of one operator for each spin i constitutes an eigenoperator. For example the total spin coherence (n = N) evolves according to the symmetric sum of the individual chemical shifts:

$$[\mathcal{H}_1, \prod_{i=1}^{N} I_{+i}] = -\kappa(\sum_{i=1}^{N} \omega_{zi}) \prod_{i=1}^{N} I_{+i} \qquad (2.93)$$

The same result with $\kappa = 1$ applies even without the multiple pulse sequence and so provides a method of measuring κ. The n = (N-1) spectrum consists of N-1 contributions determined by the sum of all but one chemical shift:

$$[\mathcal{H}_1, I^{\pm}_{oi} \prod_{j\neq i} I_{+j}] = -\kappa(\sum_{j\neq i} \omega_{zj}) I^{\pm}_{oi} \prod_{j\neq i} I_{+j} \qquad (2.94)$$

This analysis can be extended to smaller absolute values of n, to obtain eigenfrequencies proportional to all sums and differences of the ω_{zi}. However, the number of lines becomes large rapidly.

The significance of measuring the shifts as sums or differences becomes apparent when the rotation patterns or the powder patterns are considered. The relevant spatial factor is now the laboratory field component of a molecular tensor formed by the appropriate sums or differences of individual spin tensors. The sums in (2.94) for example are

$$\sum_{j\neq i} \omega_{zj} = \omega_0 (\sum_{j\neq i} \sigma^j_{zz}) \equiv \omega_0 \, \sigma^{\neq i}_{zz} \tag{2.95}$$

Such a molecular N-1 chemical shift tensor is, like the individual spin tensors, second rank. Both its orientation in the molecule and its principal components depend on the relative orientations of the single spin tensors.

The complete characterization of the Hamiltonian (2.89) requires the specification of all these relative orientations as well as the overall orientation in the molecule. In simple situations where some symmetry element restricts the possible orientations, this information will be accessible even from powder spectrum. Multiple quantum spectra supply the orientational information implicit in summing shift tensors and single quantum spectra supply the principal components of the individual spin shift tensors. For the general unsymmetric case, correlation with bilinear couplings (homonuclear or heteronuclear) appears to be necessary to specify the shift tensor orientations in the molecular frame from a powder sample. This correlation may be accomplished by allowing the bilinear couplings to act simultaneously or in a separate epoch of a multidimensional experiment.

c. The relative signs of J couplings in weakly coupled systems. A common situation in liquid state NMR in high magnetic field is the limit of weak coupling where $(\omega_{zi} - \omega_{zj}) >> J_{ij}$ for all spins which are not fully equivalent. The effective Hamiltonian may be written

$$\mathcal{H}_1 = -\sum_i \omega_{zi} I_{zi} + \sum_{i<j} J'_{ij} I_{zi} I_{zj} \tag{2.96}$$

The single quantum spectrum is first order; it consists of symmetrical multiplets centered at the frequencies ω_{zi}. It contains no information

on the signs of the J_{ij}. The eigenstates of (2.96) are still the simple product states and so in analogy to (2.94) the n = (N-1) eigenoperator equation is

$$[\mathcal{H}_1, I^{\pm}_{oi} \prod_{j\neq i} I_{+j}] = -\sum_{j\neq i} (\omega_{zj} \pm J'_{ij}/2) I^{\pm}_{oi} \prod_{j\neq i} I_{+j} \tag{2.97}$$

This corresponds to a spectrum of N doublets centered at the frequencies

$$-\sum_{j\neq i} \omega_{zj} = -\sum_{j=1}^{N} \omega_{zj} + \omega_{zi} \tag{2.98}$$

Thus the shifts differ from the single quantum spectrum only by a sign and a constant. Since each doublet splitting is the algebraic sum of all the couplings to a given spin, information on the relative signs is available, which was absent in the single quantum spectrum.

An analogous situation of weak coupling, involving at least one heteronucleus, occurs in oriented systems where the sign of the coupling contains geometric information. This is discussed in Section IVC.

d. Isolation of signals from components of mixtures. A commonly encountered difficulty in NMR spectral interpretation is the interference between signals from different molecular species or isolated spin species. Some help is provided by the simple fact that a multiple quantum spectrum of order n can only arise from a spin system with total spin $I \geq n/2$. Thus the creation of a high order coherence can be used to label a part of the magnetization as arising from a coupled group of spins above a certain size and to discriminate absolutely against signal arising from smaller spin systems. It was early recognized[15] that this fact would make possible proton multiple quantum spin labelling experiments in liquid crystals, even in partially deuterated host species

having levels of proton impurity so high that the single quantum spectrum of the protonated guest would be obscured. Multiple quantum studies of liquid crystals are reviewed in the following section.

In liquid state NMR the mixed nature of even chemically pure samples has long been apparent from the small satellite lines seen in both ^{1}H and ^{13}C spectra within about 100 Hz of most strong resonances. These satellites are due to those molecules having a ^{13}C nucleus near the nucleus associated with the so-called parent resonance. In ^{13}C spectra a given satellite thus belongs to the spectrum of one of those rare molecular species (about 1 part in 10^4) having two ^{13}C nuclei in a particular pair of nearby sites. Aside from the sensitivity problem associated with the scarcity of these molecules at natural abundance, there is a dynamic range problem, since the parent lines due to species with one ^{13}C are a hundred times larger. This problem has been nicely solved[102-107] by preparing double quantum coherence in those species having nearby ^{13}C nuclei and using the properties of this coherence under phase shifting (Sec. IID2) to isolate signals from such pairs. The correlation of the double and single quantum spectra leads to 2D spectra from which the connectivity of the carbon skeleton is easily deduced[105,106]. For some applications incrementation of the period of double quantum coherence is unnecessary since double quantum frequencies suffice[102,103]. The double quantum period then serves only to label the magnetization observed as having come from spin pairs. Related applications with proton spectra have been anticipated[102].

Additional possibilities for isolating signals from mixtures arise when the multiple quantum spectra of systems of two different spin species are considered. This is taken up in Section IVC.

e. The measurement of molecular order in anisotropic phases. The form of the various terms of $\mathcal{H}_{int}$ (2.8-2.13) derives from the decomposition of the Hamiltonian into double tensor operators according to its transformation properties under the distinct sets of rotations associated with the spatial and spin angular momenta of the molecule[18,62,63]. The spatial factor takes the form of an expectation value of a spherical harmonic over the non-spin degrees of freedom (e.g., 2.91). For the purposes of calculating the unitary time development or the line positions this is usually just a motionally averaged constant. In this section a review is made of those few multiple quantum studies of anisotropic media where the information content of these constants is a principal finding. Chemical shift investigations of quadrupolar nuclei have already been mentioned in Section IIC2, while in Section IIF3b the possibility of obtaining the relative orientation of shift tensors in powders was discussed. Studies involving two nuclear species are deferred to Section IVC.

The single quantum NMR of anisotropic interactions is the subject of several textbooks[62,63,95] and is frequently reviewed[108-113]. The systems studied include solids, absorbed species, liquids partially oriented by electric or magnetic fields, and liquid crystals. The study of liquid crystals and guest molecules dissolved in and oriented by liquid crystal solvents has been a particularly active field of study for over a decade and continues to be so. The questions studied are the domain structure of the various mesophases, the structure and probability of different molecular conformers, and the ordering of the molecules with respect to the symmetry axes of the liquid crystal and of applied fields.

The principle interactions measured for the purpose of answering these questions are the same ones that make multiple quantum coherence so accessible in oriented systems: the electric quadrupole (2.12) and the direct dipolar (2.11) interactions. The quadrupolar coupling parameter of (2.12) and Figure 5 is given by

$$\omega_{Qi} = 3eQ_i V^i_{zz}/4I_i(2I_i-1) \tag{2.99}$$

where

$$V^i_{zz} = V^i_{33}[\langle(\tfrac{1}{2})(3\cos^2\theta_i-1)\rangle + (\eta_i/2)\langle\cos 2\phi_i \sin^2\theta_i\rangle] \tag{2.100}$$

This expression indicates how the measurable field gradient V^i_{zz} depends on the principal values in the molecular frame, which enter as V^i_{33} and through the asymmetry parameter

$$\eta_i = (V^i_{11} - V^i_{22})/V^i_{33} \tag{2.101}$$

The bracketed spherical harmonic functions describe the time averaged orientation of the principal axes of the field gradient tensor with respect to the magnetic field. Implicit in the form (2.100) is the assumption that the magnitude of the field gradient tensor is not also significantly time dependent as a result of the molecular motions which average its orientation.

In most quadrupolar nuclei in partially ordered systems, the relaxation due to the time dependence of the interaction broadens the spectroscopic lines to the point where their observation is both difficult and of little interest. The most notable exception is deuterium, which has been intensively used as a spin label. In the majority of such studies the resolution is only sufficient to resolve a pair of lines for

each orientationally distinct spin. The spectral substructure due to the dipolar couplings

$$D_{ij} = -\frac{h\gamma_i\gamma_j}{4\pi^2} \langle \frac{1}{2} (3\cos^2\theta_{ij} - 1) r_{ij}^{-3} \rangle \qquad (2.102)$$

is usually unresolved. This may be due to an inhomogeneity of $\mathcal{H}_Q$ over the sample or to irreversible dephasing. In both cases the spectral splittings due to the dipolar couplings may be better resolved in those high quantum transitions which are insensitive to $\mathcal{H}_Q$. This is because for such transitions the linewidth is independent of secular quadrupolar terms which are frequently the greatest source of broadening in the single quantum spectra. This concept is taken up again in Section VC.

The first measurements of dipolar couplings between deuterons by double quantum NMR were made on selectively labeled solids[54]. These were followed by similar experiments on liquid crystals in which the dipolar couplings among at most three specifically deuterated chain positions were observed with protons decoupled[114]. These were found to be consistent with a model of molecular ordering based on the measurement of quadrupole couplings at a greater number of sites[114].

Though a marked improvement in the ability to resolve dipolar couplings between deuterons was obtained in the double quantum spectra, it was soon realized that the amount of synthetic chemistry necessary to pursue this approach in liquid crystals was prohibitive. Furthermore, the dipolar interaction is far stronger and the dephasing times longer for protons. Thus protons give higher resolution information for greater internuclear distances r_{ij} than do deuterons. A major disadvantage of any proton dipolar spectrum is that the assignment of lines is difficult since there are no quadrupolar splittings nor large chemical shifts to give rise to subspectra for individual sites.

The analysis of single quantum proton dipolar spectra of liquid crystals is a well-developed technique based on computer simulations in which the parameters D_{ij} are determined by iterative processes[115-117]. A spectral width of several kHz and individual linewidths of several Hz are typical for solutes dissolved in liquid crystals. For the liquid crystals themselves, which are somewhat more ordered, the ratio of spectral width to linewidth is also in the range of 10^2 - 10^3. From (2.67) it is found that $Z_1 = 10^4$ for N = 8. The consequence is that for systems of more than about eight coupled protons the single quantum spectrum has little resolved structure and consequently yields little information on the D_{ij}.

The role for multiple quantum spectroscopy in this field is clear. By making accessible the far simpler high order spectra, it makes possible the analysis of larger systems of coupled spins. This reduces the requirement for isotopic labeling since larger protonated molecules or parts of molecules may be examined in a single experiment. The applications to studies of molecular conformation and ordering by proton multiple quantum NMR are as yet few.

Figure 18a shows the multiple quantum spectra of the eight proton system of the liquid crystal 4-cyano-4'-n-pentyl-d_{11}-biphenyl[16,96,118]. The line positions were interpreted[96] in terms of dipolar couplings motionally averaged over the energetically equivalent conformers obtained by independently flipping either phenyl ring by 180°. The fitting parameters were bond distances, order parameters describing the equivalent biaxial ordering of the conformers, and the dihedral angle between the rings at the potential minimum. This angle was found to be 32°. Figure 18b and 18c are approximate simulations of the line intensities[118] and are discussed in Section IIIB1.

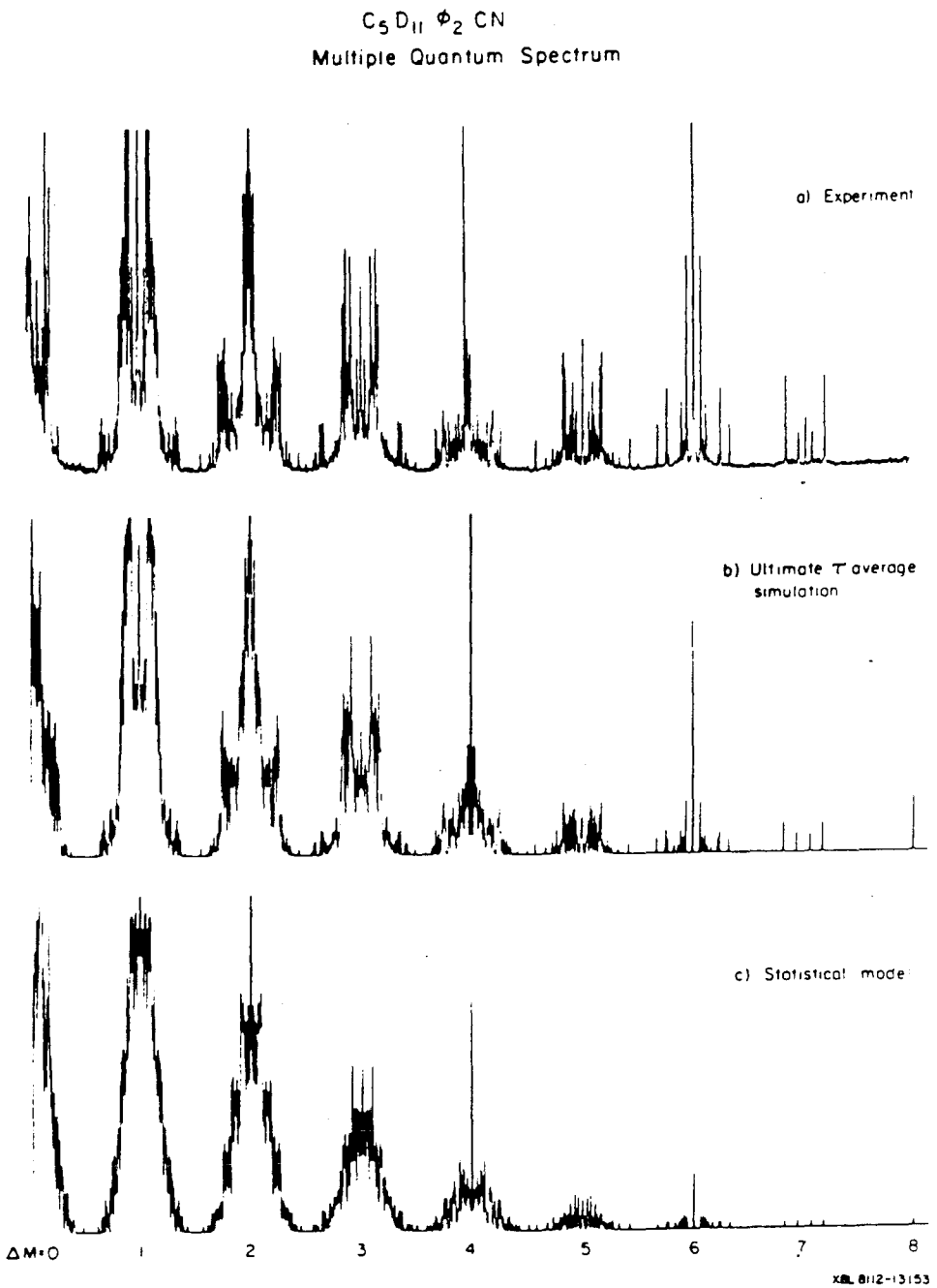

Figure 18. Simulation of experimental multiple quantum line intensities by approximate methods. Part a) is the experimental spectrum of the eight proton system of 4-cyano-4'-n-pentyl-d_{11} biphenyl (Ref. 96). The pulse sequence ($\pi/2-\tau-\pi/2-t_1/2-\pi-t_1/2-\pi/2-\tau$-sample) was used to collect 16 K interferograms in t_1 for each of six values of τ between 0.4 and 1.4 msec. The upper half (500 kHz) of the Fourier transform with respect to t_1 is displayed. The strongest lines in the $\Delta M = n = 0,1,2$, and 4 spectra are off scale. The simulation of part b) was obtained by calculating the rotation operator matrix elements which determine the average of the transition magnitude over all values of τ with the restriction $t_2 = \tau$ (ref. 126). The statistical model of part c) assigns unit strength to each transition. [By permission from S. Sinton and A. Pines, Chem. Phys. Lett. 76, 263 (1980) and J. B. Murdoch, "Computer Studies of Multiple Quantum Spin Dynamics", Ph.D. dissertation, University of California, Berkeley, 1982].

Another application of multiple quantum NMR to molecules oriented in liquid crystals is a study of the six methyl protons of 2,3 dimethylmaleic anhydride in a nematic solvent[119]. The spectra of different orders were simulated for the case that the methyl groups are correlated by gearing and for the case that on average no positional correlation exists. Even consideration of only the number of lines in the n = 4 spectrum enabled long time correlation effects to be ruled out.

A considerably more complicated problem of motional averaging is posed by the alkane region of liquid crystals and dissolved molecules. At each carbon-carbon single bond three local minima are found in the torsional potential[120]. Two of these, the gauche conformations, are mirror images, while the third is the lower energy trans conformation. The full specification of the time averaged conformation in terms of rotamer probabilities, structure and ordering is a subject of much current inquiry. Proton nuclear magnetic resonance can provide the value of the time averaged dipolar coupling (2.102) for every pair of protons within about four methylene units of one another. This provides a far larger and more diverse data base for model building than can be provided by deuterium quadrupole splittings. This base can be further augmented by measuring carbon-proton dipolar couplings by the methods of Section IVC.

The proton multiple quantum spectra of $CD_3 - (CH_2)_4 - CD_3$ dissolved in a nematic liquid crystal has recently been obtained[99]. Preliminary spectral simulation consisted of fitting the n = 5,6, and 7 quantum spectra by assuming the geometry of the conformers, calculating Boltzmann probabilities for "feasible" conformers according to the number of gauche bonds, and varying a single uniaxial order parameter. Even this simple

approach appears to distinguish between sets of feasible conformers, the best fit being found when only nearly linear conformers are included. Excluded were those conformers with adjacent gauche bonds.

In the applications so far of proton multiple quantum NMR to conformational problems in liquid crystals, only the simple pulse sequence of Figure 3 has been used, augmented with π pulses to remove effects of magnet inhomogeneity. The practical limits to the number of spins using this approach appears to be about $n = 8$. For larger systems the high quantum signals become prohibitively weak. The reasons for this problem are discussed in Sections IIB and IIB2 and techniques for overcoming it by efficient order selective excitation are taken up in Section IIIC.

III. EXCITATION DYNAMICS FOR MANY LEVEL SYSTEMS

A. The Similarity of Preparation and Mixing

1. Motivation

It has been emphasized since (2.34) that the amplitudes and phases of the multiple quantum transitions are a product of a factor from the preparation period and another from the mixing period. In the TSCTES experiment discussed in Section IIE4, the relative phases and intensities are easily calculated. In the next few sections questions of line intensities and phase are examined for more general cases. The principal concerns are how the excitation periods can be designed to give the largest signals and when they can be expected to give phased lines. The results will be useful in deriving estimates of the signal available in nonselective (Sec. IIIB) and order selective (Sec. IIIC) experiments on large spin systems.

2. Time Reversal Experiments

Consider the following gedanken experiment. A system initially at equilibrium is prepared by a propagator $U(\tau)$, evolves for time t_1 and is mixed with propagator $V = U^\dagger$. The z-magnetization immediately after mixing is by (2.34)

$$S_z(\tau,t_1,\tau,0) = \sum_{ij} \rho_{ij}(\tau) z_{ji}(-\tau) \exp(-i\omega_{ij}t_1) \tag{3.1}$$

The assumption $V = U^\dagger$ allows this to be rewritten

$$S_z(\tau,t_1,\tau,0) = \sum_{ij} |\rho_{ij}(\tau)|^2 \exp(-i\omega_{ij}t_1) \tag{3.2}$$

since

$$\rho(\tau) = UI_zU^\dagger = V^\dagger I_z V = I_z(-\tau) \tag{3.3}$$

This signal could be measured by giving a $\pi/2$ pulse at $t_2 = 0$ and recording the initial transverse magnetization. For notational purposes though, it is preferable to leave the "signal" along z. The multiple quantum expression (3.2) is a Fourier series with positive coefficients as was the single quantum expression (2.23). It differs in that it is a real signal (one channel) and thus it does not distinguish positive and negative frequencies. The signal at zero time is however identical in each case. This is so because

$$\sum_{ij} |\rho_{ij}(\tau)|^2 = \mathrm{Tr}(\rho^2(\tau)) = \mathrm{Tr}(\rho^2(0)) = \mathrm{Tr}(I_z^2) \tag{3.4}$$

and

$$\mathrm{Tr}(I_z^2) = \mathrm{Tr}(I_x^2) = \sum_{ij} |\langle i|I_x|j\rangle|^2 = 2 \sum_{i<j} |\langle i|I_x|j\rangle|^2 \tag{3.5}$$

This is the largest instantaneous signal which the system can emit. It is the sum of the line intensities and the first point in time both for the single quantum f.i.d. and for the multiple quantum interferogram when $V = U^\dagger$. Nothing has been specified about the distribution of intensity among the different transitions. The sum in (3.2) may contain any or all of the system matrix elements, including diagonal elements which contribute signal only to $\omega_1 = 0$ upon Fourier transformation with respect to t_1.

The condition $V = U^\dagger$ is equivalent to a reversal of time or, in practice, a change in the sign of the effective Hamiltonian responsible for the excitation. It is an idealization which can be experimentally approached in certain circumstances. It has little to do with the mathematical operation of Section IIF2. Reversal of the sign of the

direct dipolar Hamiltonian $\mathcal{H}^{D}_{II}$ (2.11) is well-known from the "magic echo" experiments[121]. These demonstrated that the rapid decay of the f.i.d. in a rigid solid in a time comparable to $M_2^{-\frac{1}{2}}$, the inverse square root of the second moment of the spectrum, is in fact not an irreversible phenomenon.

There is another approach to devising effective Hamiltonians whose sign can be changed. Suppose that the preparation propagator can be written as

$$U(\tau) = \exp(-i\mathcal{H}\tau) \tag{3.6}$$

and that furthermore

$$\exp(i\phi I_z)\mathcal{H} \exp(-i\phi I_z) = -\mathcal{H} \tag{3.7}$$

for some ϕ. In such a case it would easily be possible to obtain experimentally

$$V(\tau) = \exp(i\phi I_z)U(\tau) \exp(-i\phi I_z) = U^{\dagger}(\tau) \tag{3.8}$$

since U and V are related simply by a phase shift through ϕ of all the irradiation. Pulse sequences which give effective Hamiltonians which approximate (3.7) are discussed in Section IIIC6.

3. General Approach to Matching Mixing and Preparation

In this section a proof is developed which shows that for an arbitrary preparation period pulse sequence, there is an experimentally realizable mixing period sequence, which guarantees maximum average signal intensity at the end of the mixing period. Unlike the case of the previous section where time reversal was invoked to obtain the lines in phase, here the lines will for the most part have unknown phases.

This has the consequence that overlapping lines in ω_1 could cancel out. Thus it will be necessary to assume that the transitions of interest are resolved in ω_1. A corollary of the existence of the different phases is that the signal maximum need not come at $t_1 = 0$. Thus an average of the signal over t_1 is the quantity which is maximized.

As a starting point recall the general preparation period propagator of Section IID2:

$$U(\tau) = T \exp(-i \int_0^\tau \mathcal{H}(t)dt) \tag{2.43}$$

with

$$\mathcal{H}(t) = -\omega_p(t) I_{\psi(t)} - \Delta\omega(t) I_z + \mathcal{H}_{int} \tag{2.44}$$

Here there is no general way of reversing the sense of time, but it is certainly possible to reverse the experimental manipulations of amplitude ($\omega_p(t)$), phase ($\psi(t)$) and offset ($\Delta\omega(t)$) which define $U(\tau)$. For each of these define a starred function such that

$$\omega_p^*(t) \equiv \omega_p(\tau - t) \tag{3.9a}$$

$$\psi^*(t) \equiv -\psi(\tau - t) \tag{3.9b}$$

$$\Delta\omega^*(t) \equiv \Delta\omega(\tau - t) \tag{3.9c}$$

and let the mixing period propagator be dictated by these such that:

$$V(\tau) = T \exp(-i \int_0^\tau \mathcal{H}^*(t)dt) \tag{3.10}$$

$\mathcal{H}^*(t)$ is obtained from (2.44) by substituting the starred for unstarred functions.

The relationship between these two time dependent Hamiltonians may be written as

$$K_o \mathcal{H}(t) K_o^{+} = \mathcal{H}^{*}(\tau - t) \tag{3.11}$$

where from (2.70) it can be seen that

$$K_o = \Pi_y^{+} K \tag{3.12}$$

Thus

$$K_o U(\tau) K_o^{+} = T \exp(i \int_o^{\tau} \mathcal{H}^{*}(\tau - t) dt) \tag{3.13a}$$

$$= V^{+}(\tau) \tag{3.13b}$$

The relationship between the prepared and detected operators (2.31-2.32) is now seen to be:

$$K_o \rho(\tau) K_o^{+} = K_o U(\tau) I_z U^{+}(\tau) K_o^{+} \tag{3.14a}$$

$$= V^{+}(\tau) K_o I_z K^{+} V(\tau) \tag{3.14b}$$

$$= I_z(-\tau) \tag{3.14c}$$

Therefore

$$\rho_{ij}^{*}(\tau) = z_{ij}(-\tau) \tag{3.15}$$

The star here indicates complex conjugation. In this last step it was assumed that $|i\rangle$ and $|j\rangle$, the eigenstates of $\mathcal{H}_1$, have real coefficients when expressed in the simple product basis. This is always the case, or for degenerate states can be made so, since all of the terms in $\mathcal{H}_{int}$ which might appear in $\mathcal{H}_1$ have real matrix representations in the simple product basis and are diagonalized by unitary transformations.

Since both $\rho(\tau)$ and $I_z(-\tau)$ are Hermitian (2.34) becomes

$$S_z(\tau,t_1,\tau,0) = \sum_{ij} \rho_{ij}^2(\tau) \exp(-i\omega_{ij}t_1) \tag{3.16}$$

The magnitudes are the same as if $V = U^\dagger$ as in (3.2), but now the phases are not obvious since the numbers $\rho_{ij}(\tau)$ are in general complex. Equation (3.16) holds even for the three pulse sequence (Fig. 3) as can be seen by considering that the addition of a fourth $\pi/2$ pulse at $t_2 = \tau$ would put it into the form assumed here, in which each preparation pulse is matched by a mixing pulse and the expectation value of I_z is calculated at $\tau' = \tau$ (Fig. 4).

Aside from the possibility of degenerate transitions destructively interfering, the signal intensity averaged over t_1 is the same as if the lines were all in phase. In the next section it will be shown that for the most common type of degeneracy the transitions may be obtained in phase and thus at least for these the problem of destructive interference can be avoided.

4. Spin Inversion Transitions and Associated Echo Phenomena

a. Introduction. The results of the last section have special significance for a small class of transitions which satisfy the reciprocal relationship

$$\Pi_x |i\rangle\langle j| \Pi_x^\dagger = |j\rangle\langle i| \tag{3.17}$$

These spin-inversion transitions, between states which are interchanged by inversion of all the spins, have also been called Class 1 transitions[73]. In any system, the total spin transition is a member of this class. Other members of this class are found in orders differing from the highest by multiples of two. In this section the properties of these

transitions are developed including a prescription for obtaining them all in phase under very general conditions.

b. Transition frequencies. An important property of spin-inversion transitions is that their eigenfrequencies do not depend on the bilinear terms of $\mathcal{H}_1$. This may be proved as follows. By definition

$$[\mathcal{H}_1, |i\rangle\langle j|] = \omega_{ij}|i\rangle\langle j| \tag{2.39}$$

while the commutator with

$$\mathcal{H}_1' = \Pi_x \mathcal{H}_1 \Pi_x^{\dagger} \tag{3.18}$$

is

$$[\mathcal{H}_1', |i\rangle\langle j|] = [\mathcal{H}_1', \Pi_x |j\rangle\langle i| \Pi_x^{\dagger}] \tag{3.19a}$$

$$= \Pi_x [\mathcal{H}_1, |j\rangle\langle i|] \Pi_x^{\dagger} \tag{3.19b}$$

$$= -\omega_{ij}|i\rangle\langle j| \tag{3.19c}$$

Adding gives

$$[(\mathcal{H}_1 + \mathcal{H}_1'), |i\rangle\langle j|] = 0 \tag{3.20}$$

The sum of $\mathcal{H}_1$ and $\mathcal{H}_1'$ is just the bilinear terms $\mathcal{H}^{zz}$ (2.10) so ω_{ij} must be independent of these.

The dependence of ω_{ij} on the linear terms $\mathcal{H}^{z}$ (2.9) is somewhat more subtle. The obvious situation where transitions satisfying (3.17) occur is when there are no chemical shifts. In this case ω_{ij} depends only on the off resonance and static field inhomogeneity terms[73]. More generally transitions of this type may depend on those chemical shift differences which commute with $\mathcal{H}^{zz}$. For weakly coupled systems, this

includes all the chemical shift differences. For strongly coupled systems, the difference between the chemical shift of a group of fully equivalent spins and the sum of the shifts of all spins will be measurable from a spin-inversion transition frequency.

c. Prescription for obtaining spin inversion transitions in phase. It has been recognized from calculations on anisotropic systems of coupled protons[122] and deuterons[123] that the basic pulse sequence of Figure 2 with or without a π pulse at $t_1/2$ and with arbitrary pulse phases produces transition amplitudes with phases independent of τ for spin-inversion transitions.

A related observation is that the same pulse sequence applied to a powder sample of deuterons gives a sharp maximum or echo in the signal at $t_2 = \tau$[124,125]. This echo is not the familiar stimulated echo[1] which is mediated by population gratings during t_1, but rather is due to double quantum coherence during t_1. It represents a refocussing during t_2 of the loss of coherence which occurred during τ as a result of a distribution of quadrupole frequencies. The existence of this echo demonstrates that the phase of the double quantum spectrum $S(\tau,\omega_1,t_2=\tau)$, obtained by t_1 Fourier transformation of the double quantum interferogram, has a constant phase for all ω_1. Here coupling between deuterons is assumed to be negligible.

By a simple extension of the results of Section IIIA3, the spin inversion transitions can be obtained in phase for an arbitrary preparation period pulse sequence. Suppose that the mixing period specified by (3.10) is supplemented by a Π_x pulse. This may come at t_1 if chemical shifts are being measured or at $t_1/2$ if Zeeman terms are to be removed. In either case the defining property (3.17) guarantees that the coefficients of $|i\rangle\langle j|$ and $|j\rangle\langle i|$ are exchanged. Since these coefficients are

complex conjugates (3.15) is replaced by

$$\rho^*_{ij}(\tau) = z_{ji}(-\tau) \tag{3.21}$$

for all spin-inversion transitions. Thus these special transitions are in phase with coefficients $|\rho_{ij}(\tau)|^2$ in the same way that all transitions were in phase for the hypothetical case of perfect time reversal in Section IIIA2.

An interesting feature of this result is that the phase of the lines is invariant to inhomogeneities of the internal or rf Hamiltonians, with the exception that a satisfactory π pulse was assumed to be delivered to the entire ensemble. For the three pulse sequence of Figure 2, the π pulse is equivalent in this regard to a change in phase of the mixing pulse and is therefore unnecessary. A corollary of this persistence of the phase in spite of possible inhomogeneities is that there are echo phenomena associated with each of the spin inversion transitions.

One application where this property of the spin inversion transitions is relevant is in the use of high order transitions to measure the sums and differences of chemical shift tensors in powders. This is discussed in Section IIF3. In such a case there is an orientational inhomogeneity leading to an inhomogeneity of all anisotropic terms in $\mathcal{H}_{int}$. This does not prevent the recording of absorption phase powder patterns for the spin inversion transitions even for a general preparation period.

B. Statistical and Computational Aspects of Multiple Quantum Excitation

1. Line Intensities for Nonselective Excitation

a. The statistical model of equal average line intensities. Once some sequence of irradiation has been settled upon for use during the excitation periods, it is in principle possible to calculate

the coefficients of (2.34). Some such calculations have been performed and are reviewed in the following sections. For many spin systems and pulse sequences of interest calculations are impractical. This may be because they require as input the very parameters which the experiment is designed to reveal or because the complexity of the spin system or the pulse sequence makes them impractical with current computing technology. For these reasons a rough statistical picture of the line intensities is a valuable guide. A statistical view is particularly appropriate for those sequences for which $\rho_{ij}(\tau)$ has a complicated dependence on τ. The prime example is the three pulse sequence of Figure 3 with a system of strongly coupled spins. Since most or all of the single quantum frequencies enter the dynamics, the experimental reality is that a given line will appear with widely fluctuating phase and amplitude as τ is varied. This suggests that the quantities $\rho_{ij}(\tau)$ be treated as random variables, with the parameter τ specifying different events. In order that these events be plausibly independent, the interval between values of τ should be greater than a correlation time related to the inverse of the frequencies characteristic of U. A plausible choice of the correlation time is $M_2^{-\frac{1}{2}}$ where M_2 is the second moment of the single quantum spectrum. For differences in τ of several times $M_2^{-\frac{1}{2}}$ the elements of $\rho(\tau)$ will appear largely uncorrelated and can be taken as independent events providing information on the unknown distributions governing each $\rho_{ij}(\tau)$. For times τ greater than a few correlation times these distributions are approximated as stationary or independent of τ.

There may be any number of constraints on these distributions, depending on the dynamical symmetry of the propagator U and the symmetry of the initial condition. For example, the dynamics factors rigorously into a separate problem for each irreducible representation of the

permutation group as discussed in Section IIF1. A common situation is that there are N_T elements $\rho_{ij}(\tau)$ which, on the basis of symmetry considerations may be nonzero. In the absence of relaxation these are constrained by conditions of the form

$$\sum_{ij}{}' \, |\rho_{ij}(\tau)|^2 = C \tag{3.22}$$

where the prime indicates a restricted summation, as for example within an irreducible representation. C is the norm squared of some known part of the initial condition. An example of such a relation is (3.4), which is the unrestricted case which holds even when no particular dynamical symmetry is present.

Given such a constraint, the simplest statistical hypothesis is that as long as τ is greater than a few inverse spectral widths then all transitions are equally probable. For the unrestricted case, where all the magnetization is dispersed among N_T matrix elements, this means

$$\overline{|\rho_{ij}(\tau)|^2} = \mathrm{Tr}(\rho^2)/N_T \tag{3.23}$$

where the bar indicates an average over many values of τ.

For the case of preparation and mixing matched so that (3.2) or (3.16) holds, (3.23) expresses the assumption that on average all lines have the same intensity. This will be called the statistical model.

It is worth recalling for a moment the suppressed constant b of (2.14) which appears on the right hand side (3.23) if that equation is interpreted as an estimate of magnetization per matrix element prepared. With this in mind, the numerator of (3.23) increases linearly with the number N of spins in the coupled system. Alternatively stated, the numerator is independent of N if the total number of spins in the sample

is held constant. The denominator N_T however typically grows as 4^N for spins ½ leading to a rapid decrease in signal-to-noise ratio with N for statistical excitation. The statistical model then is that on average equal fractions of the equilibrium magnetization detected in t_2 will be found to be oscillating as a function of t_1 at any frequency ω_{ij}.

This hypothesis was tested for an eight spin system as depicted in Figure 18c[118]. The variation in intensity comes from the piling up of degenerate and nearly degenerate transitions. Comparison with the experimental spectrum of Figure 18a shows that, while some of the spectral intensity features are reproduced, the hypothesis does not hold up well for individual lines. Moreover the intensity of the high order lines are systematically underestimated by as much as an order of magnitude. This latter feature is largely a peculiarity of systems in which most of the dipolar couplings have the same algebraic sign. It is discussed further elsewhere[126].

Another view of the statistical model is obtained by summing the line intensities within a given order and plotting these sums as a function of order n. This is depicted by the broad line in Figure 19[98] for the six spin system of partially oriented benzene. The approximately Gaussian decline in spectral intensity with order n is accounted for by the statistical model since the quantitites Z_n of (2.67) approach a Gaussian distribution for large N.

The success of the statistical model is not a quantitative one. Its importance is as a simple model which is independent of the particular system. As shown in Figure 19, the model suffices to frame the essential problem of nonselective excitation sequences: the vast bulk of the magnetization appears in the numerous low order transitions. In

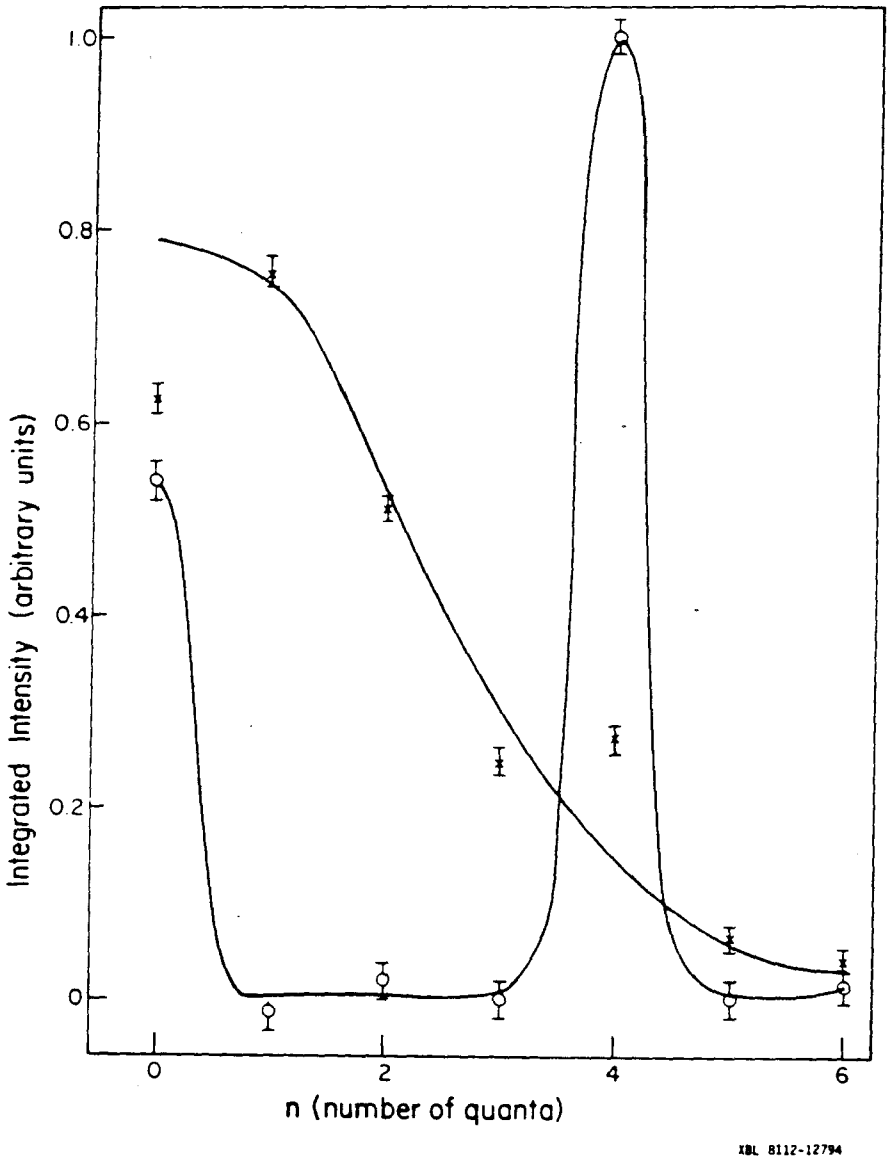

Figure 19. The problem with nonselective excitation. The closed circles are the intensities of different orders n integrated over all lines in the order for a nonselective experiment on partially oriented benzene using the sequence of Figure 3 with a π pulse at $t_1/2$. The roughly Gaussian decrease in intensity with n is due to the decrease in the number of transitions with n. The bulk of the magnetization appears in the more numerous lower order transitions. The open circles are from an order selective sequence like that used to obtain Figure 31 and discussed in Sections IIIC5 through IIIC8. Here the magnetization is concentrated in particular orders.

large systems where these spectra are unresolved, the magnetization is wasted. What is needed is a means for causing the signal intensity to peak in the high order spectra as shown by the narrow curve of Figure 19. This subject is deferred to Section IIIC.

b. Analytical expressions for line intensities for sequences of several hard pulses. For spin systems whose single quantum spectrum and f.i.d. are readily calculated by hand, the multiple quantum spectrum obtained with a series of hard pulses is also straightforwardly derived, but the calculation is tedious for more than a few spins and a few pulses. Various results have appeared for the three pulses sequence of Figure 3 and analogues of it formed by adding π pulses or modifying the pulse angles. Spin ½ systems treated include the AB system with three pulses[9], and the AB system with π pulses in τ[127] and t_1[78b]. A_2[35,36], A_3[35,36] and A_N[126] systems with dipolar coupling have been discussed. The use of π pulses with these systems does not complicate the problem since there are no chemical shift differences.

For deuteron (spin 1) systems hard pulse line intensity calculations have been reported for one spin[35,36,38,41,73], two identical spins[54], two and three nonidentical spins with dipolar couplings neglected during preparation and mixing periods[114], and three identical spins with dipolar coupling included[123].

c. Exact computation of line intensities. It is normally possible to ascertain the parameters of the internal spin Hamiltonian from the spectral frequencies alone. Intensity information does not explicitly enter in the iterative analysis of the most widely used computer routines[115]. Rather, the intensities are calculated after the final determination of the eigenvectors and eigenvalues and used to confirm that the assignments are reasonable. The same philosophy has

been applied to the analysis of proton multiple quantum spectra of oriented molecules, but the situation is complicated by the dependence of the line intensities on τ. This has led to two different approaches for the nonselective experiments.

The first approach is to define a line intensity which is independent of the excitation time. This is done for the three pulse sequence by formally averaging over the single quantum time development of the preparation and mixing periods to obtain analytical expressions for $\overline{|\rho_{ij}(\tau)|^2}$ [126]. When the limits of the integration are taken to infinity such an average is dependent only on the eigenvectors and the nutation angles of the pulses at the beginning and end of the evolution period. This type of calculation is illustrated by Figure 18b[118] and is called an ultimate τ average. In its agreement with the experimental spectrum of Figure 18a, it is considerable more satisfying than the statistical model. The remaining discrepancy is largely due here to the statistical nature of the experiment rather than the calculation. The experiment[96] was performed for six values of τ over the range 0.4 to 1.4 msec and thus only approximates the ultimate τ average.

Such an ultimate average is an idealization which can never be realized experimentally for a complex system with recurrence times greater than T_2. A more relevant calculation is needed. This is an exact dynamic calculation for those particular values of τ used in the experiment. Computer programs for performing such calculations have been written which are capable of simulating even quite complex pulse sequences for small groups of spins[118]. For the three pulse sequence, eight spins ½ is practical and an example of such a calculation is compared with experiment in Figure 20[16]. The spin system is again the ring protons

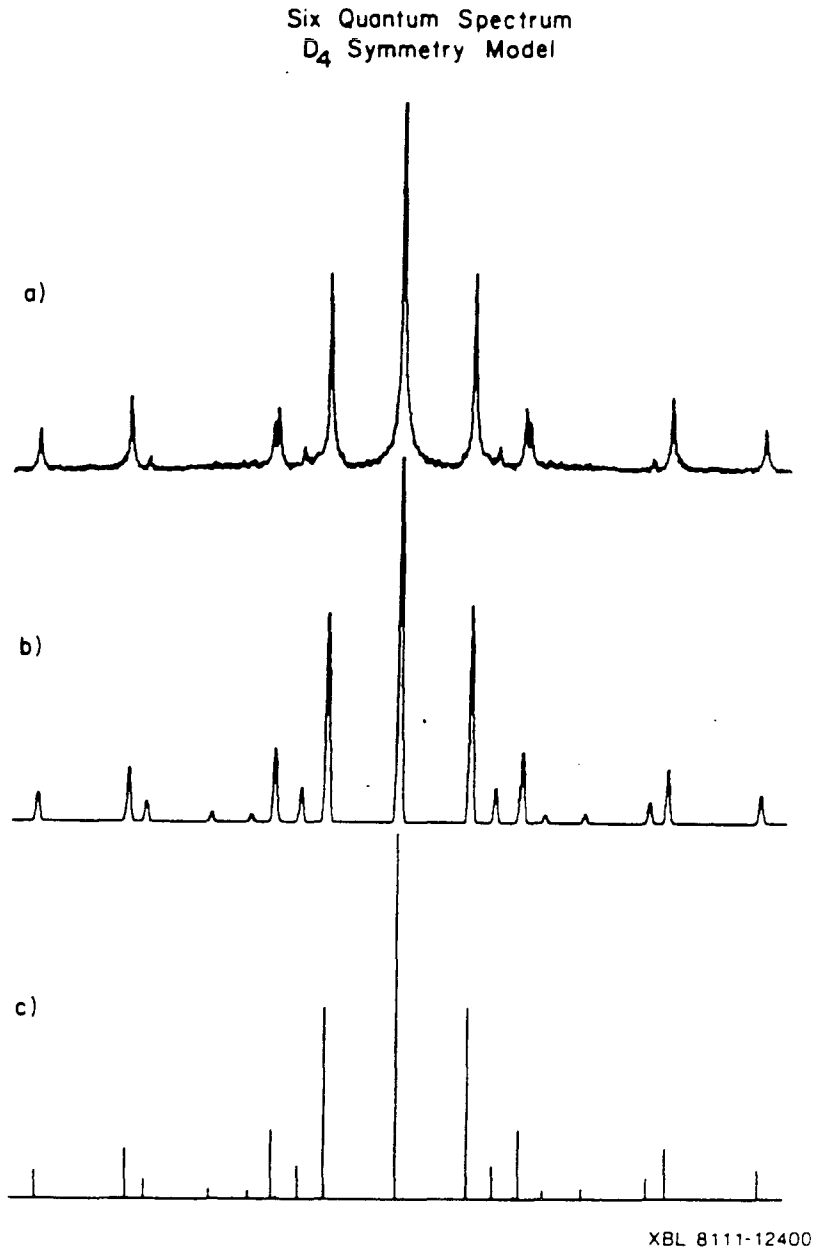

Figure 20. Exact calculation of line intensities for nonselective excitation. The spectrum is the n = 6 region of the nematic liquid crystal 4-cyano-4'-n-pentyl-d_{11} biphenyl. The experiment used to obtain part a) is similar to that described in the caption of Figure 18. Part b) and part c) were obtained by exact computer simulation of the preparation and mixing using the actual experimental values of τ and spin couplings obtained from an initial simulation of frequencies only. In part b) a broadening function was convoluted with the stick spectrum of c). [By permission from S. Sinton, "NMR Studies of Oriented Molecules", Ph.D. dissertation, University of California, Berkeley,1981, published as Lawrence Berkeley Laboratory Report LBL-13604.]

of 4-cyano-4'-n-pentyl-d_{11} biphenyl. Experiment and simulation are the sum of magnitude spectra for six values of τ. The agreement is much improved over that found with the ultimate average. Residual error is presumably due to certain symmetry constraints placed on the parameters D_{ij}, which are only approximately correct for the actual molecule.

Additional computer calculations have been performed for order selective excitation sequences. Discussion of these is deferred to Section IIIC.

d. Experimental determination of excitation functions. The computations discussed in the last section require as input the parameters or the eigenvectors of $\mathcal{H}_{int}$. Since these are often the object of the experiment, they are not usually available *a priori* to guide the choice of excitation times. It has been common to repeat the experiment several times using equally or randomly spaced values of τ and then summing the resulting magnitude spectra. The spectra of both Figure 1 and Figure 18 were obtained in this way. This approach becomes inefficient if only the transitions of the high order spectra are desired. This is because a given value of τ may result in little or no intensity for the desired lines. The extreme case is when only the total spin coherence in $\rho(\tau)$ is of interest as in the TSCTES experiment of Section IIE4.

In order to avoid performing the full experiment over all values of t_1 only to find that the excitation is inefficient, it is desirable to have a quicker way of evaluating $|\rho_{ij}(\tau)|$ for the lines of interest over a range of τ or over some other excitation period parameter. One approach to this is the method of parameter proportional phase increments (PPPI)[128]. This experiment is performed with a fixed value of t_1, but a variable excitation period parameter. With each increment in the

excitation parameter, the phase of the preparation period radiation is incremented. In the example of Figure 21, the parameter is the length of the excitation periods which are incremented together. The pulse sequences is that of Figure 3, but augmented by π pulses at $\tau/2$, $t_1/2$ and $t_2 = \tau/2$. Sampling was at $t_2 = \tau$.

The Fourier transform of the resulting signal is shown in Figure 21b. The signal from different orders is clearly separated in analogy to TPPI (Sec. IID2), but now the frequencies present are sums and differences of those characteristic of U and V. The only reason for performing this Fourier transform is to allow the signal from all but one order to be deleted. Inverse Fourier transformation again gives a signal as a function of the excitation parameter. The magnitude of this complex excitation function is shown in Figure 21d. It is an experimental measurement of the amount of the magnetization which has been excited to a particular order. For the case of the total spin coherence it is proportional to $|\rho_{N/2,-N/2}(\tau)|^2$.

As is evident from Figure 21d, the signal intensity at the best values of τ is considerably larger than the average intensity one would obtain with arbitrarily chosen values of τ. This result holds in systems of a few spins even for the lower order spectra[129]. For systems of more than about eight coupled protons, it is experimentally difficult to locate times for which the simple nonselective sequence used here gives line intensities much greater than the average values.

2. The maximization of signal energy in the detection period.

a. Signal power and signal energy. So far the discussion has been in terms of the line amplitudes which are the Fourier coefficients of (2.34), or the average magnitude of these quantities as given in (3.23). These quantities are proportional to magnetization. Another

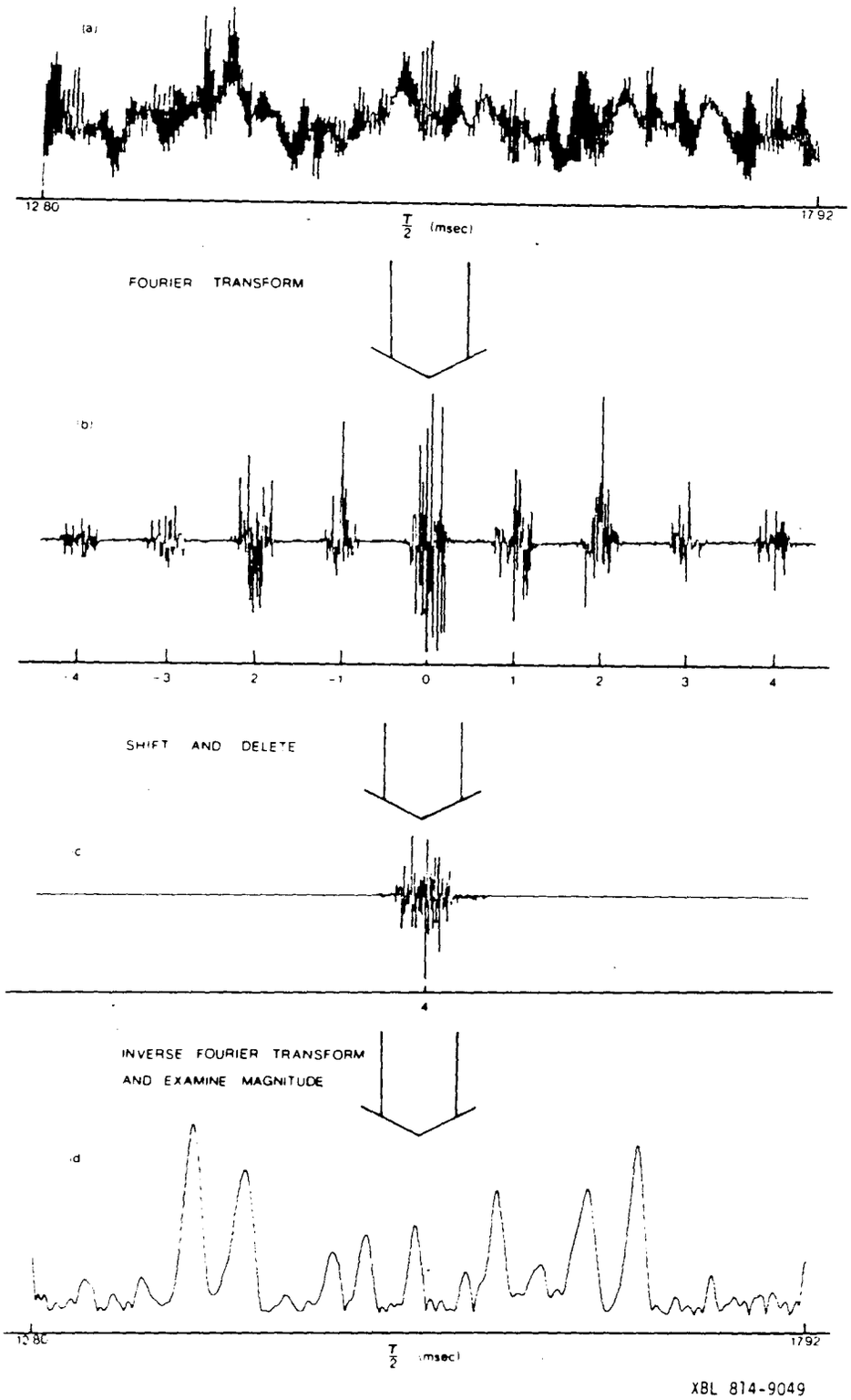

Figure 21. (Caption next page)

Figure 21. Data manipulation for the PPPI search procedure. The sample is the N = 4 proton system of partially oriented acetaldehyde also used in Figure 17. The signal in a) was obtained with the sequence ($\pi/2 - \tau/2 - \pi - \tau/2 - \pi/2 - t_1/2 - \pi - t_1/2 - \pi/2 - \tau/2 - \pi - \tau/2$ - sample) by incrementing the excitation periods and simultaneously incrementing the phase. Fourier transformation separates out the signal contributions from each order just as in TPPI (Sec. IID2c), however the frequency information in b) describes how each order is excited rather than how it evolves. This is put into useful form by excising the signal from one order as in c) and examining the magnitude of the inverse Fourier transform in d). This excitation function of the original parameter $\tau/2$ shows for which values the n = 4 coherence magnitude is maximized.

useful measure is the signal power associated with a given transition or group of transitions. This is proportional to the square of magnetization. The relevant measure of signal power for a given point in t_2 is the average over t_1. This may be defined as

$$\langle S_\alpha^2(\tau,\tau',t_2)\rangle \equiv (1/t_1') \int_0^{t_1'} S_\alpha^2(\tau,t_1,\tau',t_2)dt_1 \tag{3.24a}$$

$$= (2\pi/t_1') \int_{-\infty}^{\infty} |S_\alpha(\tau,\omega_1,\tau',t_2)|^2 d\omega_1 \tag{3.24b}$$

The second equality is the Rayleigh (or Parseval, or Plancherel) theorem[33], which states the equivalence of the time and frequency averages.

The integral of signal power over the detection period variable t_2 is the signal energy. Signal energy is proportional to the time required to achieve a given signal-to-noise ratio[130], barring instrumental instabilities, the effect of which is considered statistically in Section IIB3. The signal energy enters naturally when weighting procedures[130, 131] are used to optimize sensitivity with a given data set.

The expression (3.24) for the signal power can be evaluated using (2.34) in the limit of resolved lines in ω_1 and negligible relaxation:

$$\langle |S_\alpha(\tau,\tau',t_2)|^2\rangle \simeq \sum_{ij} |\rho_{ij}(\tau)|^2 |\alpha_{ji}(-t_2,-\tau')|^2 \tag{3.25}$$

The equality holds if there are no degeneracies and the contribution on the right from a given transition is correct if that ω_{ij} is not degenerate. The possibility of inequality arises from interference between degenerate transitions. The relation (3.25) for the total signal power can be taken as a sufficiently accurate estimate, as long as the fraction

of the power associated with degenerate lines in ω_1 is small. Often only a limited number of multiple quantum transitions are of interest and then the sum on the right may be restricted, for example to those terms with a common value of n_{ij}. In this and subsequent expressions for signal power and energy a factor of b^2 (2.14) is suppressed on the right hand side.

It was noted in Section IIIA3 that when preparation and mixing periods are similar so that (3.16) holds, then the magnitudes of transitions resolved in ω_1 are as great as for the hypothetical case of (3.2), where reversal of the excitation dynamics during mixing is assumed. For this special case ($t_2 = 0$ for sequences of the form of Fig. 4) the average (3.25) of the signal power over t_1 becomes

$$<|S_z(\tau,\tau,0)|^2> \simeq \sum_{ij} |\rho_{ij}(\tau)|^4 \tag{3.26}$$

b. The signal power for nonselective excitation. For sequences like Figure 3 where mixing consists of a single pulse, the mixing period variable τ is omitted. In this case (3.25) and (3.26) become, respectively,

$$<|S_z(\tau,t_2)|^2> \simeq \sum_{ij} |\rho_{ij}(\tau)|^2 |z_{ji}(-t_2)|^2 \tag{3.27}$$

and

$$<|S_z(\tau,t_2=\tau)|^2> \simeq \sum_{ij} |\rho_{ij}(\tau)|^4 \tag{3.28}$$

The question then arises of how, in a statistical sense, the signal at $t_2 = \tau$ compares with that at other values of t_2. This question may be addressed by contemplating a simultaneous averaging of signal power over τ and t_2 so that (3.27) becomes

$$\overline{<|S_z(\bar{t}_2)|^2>} \simeq \sum_{ij} \overline{|\rho_{ij}(\tau)|^2 |z_{ji}(-t_2)|^2} \tag{3.29}$$

The variable $\bar{t}_2 = t_2 - \tau$ is seen to be relevant by considering the two cases $\bar{t}_2 = 0$ and $\bar{t}_2 >> M_2^{-\frac{1}{2}}$.

For $\bar{t}_2 >> M_2^{-\frac{1}{2}}$ the two factors in each term are uncorrelated and so the mean of the product is the product of the means. Thus

$$\overline{<|S_z(\bar{t}_2 >> M_2^{-\frac{1}{2}})|^2>} \simeq \sum_{ij} \overline{|\rho_{ij}(\tau)|^2} \, \overline{|z_{ji}(-t_2)|^2} \tag{3.30a}$$

$$= \sum_{ij} (\overline{|\rho_{ij}(\tau)|^2})^2 \tag{3.30b}$$

If the statistical model of equal average line intensities is assumed then this sum of N_T terms may be estimated from (3.23) as

$$\overline{<|S_z(\bar{t}_2 >> M_2^{-\frac{1}{2}})|^2>} \simeq (Tr(\rho^2))^2/N_T \tag{3.31}$$

This is just N_T^{-1} of the signal power after a $\pi/2$ pulse delivered at equilibrium.

To put this into more familiar light it may be compared to the average signal power in a similarly idealized single quantum f.i.d. corresponding to a spectrum $S(\omega)$ containing Z_1 resolved lines of equal amplitude. This is

$$\overline{|S(t)|^2} = (Tr(\rho^2))^2 / Z_1 \tag{3.32}$$

Another useful quantity is the signal power per line which is obtained by dividing (3.31) by N_T and (3.32) by Z_1. Thus the totally nonselective experiment with sampling of all the signal power in t_2 should with these considerations, take about

$$(N_T/Z_1)^2 \simeq (4^N/Z_1)^2 \simeq 4N \tag{3.33}$$

times as long to obtain the same signal-to-noise ratio for some resolved transition as the single quantum Fourier transform experiment on the same system.

Neglected so far is a further loss of signal in the multiple quantum experiment due to its two dimensional nature[131]. In averaging over the evolution period in (3.24) to obtain (3.25) relaxation was neglected. This is an unrealistic approximation since, while the excitation periods may well be shorter than T_2, the evolution period must extend to several times T_2 in order to measure the natural linewidths. This leads to an extra reduction of

$$r_{2D} = (1/t_1') \int_0^{t_1'} [\exp(-t_1/T_2)]^2 dt_1 \tag{3.34a}$$

$$= (T_2/2t_1')(1 - \exp(2t_1'/T_2) \tag{3.34b}$$

in the average signal power. This factor is typically about 0.1 to 0.5 depending on the resolution desired.

On the other hand, large improvements are possible in the signal power over that of the nonselective multiple quantum experiment. These are discussed at the end of this section and in Section IIIC8.

c. The peak in signal power for matched preparation and mixing. In making comparison with the single quantum experiment, the signal power at some typical value of t_2, as given by (3.30) and (3.31) was used. The estimate (3.30b) may be viewed as the sum of the squares of the second moments of the distributions characterizing the quantities $|\rho_{ij}(\tau)|$. However, at $\bar{t}_2 = 0$, the same process of averaging over τ gives

$$\overline{<|S_z(\bar{t}_2 = 0)|^2>} \simeq \sum_{ij} |\rho_{ij}(\tau)|^4 \tag{3.35}$$

which is the sum of fourth moments for the same distributions. Since fourth moments are greater than or equal to the square of second moments, a peak in signal power is expected at $t_2 = \tau$ relative to other values of t_2.

The magnitude of this peak has been examined by exact computer simulation[126]. It is found that for most transitions the decrease in intensity away from $t_2 = \tau$ is consistent with a model where ρ_{ij} has a Gaussian distribution in the complex plane:

$$P(\rho_{ij}) = (\pi\sigma^2)^{-1} \exp(-|\rho_{ij}|^2/\sigma^2) \tag{3.36}$$

Such a result is consistent with a view of nonselective excitation as a random walk in Liouville space. More specifically, (3.36) is a natural estimate if the attainment of a particular value of ρ_{ij} after preparation is viewed as the result of a large number (Z_1) of steps, one for each single quantum transition frequency which enters the excitation dynamics[126]. The various powers of ρ_{ij} which enter into the signal magnitude and power are evaluated over the distribution by equating $|\rho_{ij}| \equiv r$ and performing the two dimensional integrals:

$$\overline{r^k} = \int_0^\infty \int_0^{2\pi} r^k \, P(r) r dr d\phi \tag{3.37}$$

The results are

$$|\rho_{ij}|^2/|\rho_{ij}| = 4/\pi \simeq 1.27 \tag{3.38a}$$

$$|\rho_{ij}|^4/|\rho_{ij}|^2 = 2 \tag{3.38b}$$

The ratio of (3.38a) gives the average signal magnitude at $t_2 = \tau$ relative to other values of t_2. This value was confirmed by calculation for a variety of dipolar coupled spin systems at many values of τ and t_2[126]. The ratio of (3.38b) is the ratio of (3.30) to (3.35) and thus describes the peak in signal power at $\bar{t}_2 = 0$.

For the spin inversion transitions, the two dimensional Gaussian of (3.36) is replaced by a one dimensional Gaussian[126]. This is consistent with the fact that the phase of the spin inversion transitions is independent of τ.

The peaking of signal power at $t_2 = \tau$ in the nonselective experiment is not a large effect typically amounting to about 1.27 in magnitude or 2 in power relative to that signal found at other values of t_2. A corollary of this is that for a nonselective experiment, in which most matrix elements of $\rho(\tau)$ have about equal probability, the particular Hamiltonian effective during t_2 has little effect on the total signal energy. In the next section this will be seen to be an exceptional and undesirable situation, though it corresponds to the way in which most experiments have been performed until recently.

d. Signal power for an optimally excited group of lines. As discussed in Section IIIB1, it can be very inefficient to perform the full multiple quantum experiment with arbitrarily chosen excitation parameters. It is possible to find excitation sequences which are far better than the statistical average for some limited set of transitions. Let G be the ratio of the greatest possible signal magnitude per line obtainable for some group of lines and the average value (3.23) (with $N_T = (4^N - 1)$ for N spins ½) obtained with many values of τ using the statistical model. For larger systems the practical attainment of highly nonstatistical $|\rho_{ij}(\tau)|$ requires the order selective methods of Section

IIIC and the calculation of G is deferred to Section IIIC8.

At the point of matched preparation and mixing, the signal power for such a hypothetically optimized excitation is increased over that in (3.31) by a factor of G^2. However, this point of maximum signal power is fleeting, lasting only for a time on the order of the inverse single quantum spectral width. This behavior is clear in Figure 21d where each peak in signal magnitude vanishes in $\sim 10^2$ μsec. In practice the preparation period would be fixed at the favorable value and the decrease in signal power as t_2 progressed would be by a factor of G to G times the statistical value. For optimized sequences of the form of Figure 4, the signal power averaged over t_1 as a function of t_2 is thus expected to have the approximate form

$$\langle |S_z(\tau,\tau,t_2)|^2 \rangle \simeq N_T (\mathrm{Tr}(\rho^2)/4^N)^2 (G^2 \exp(-M_2 t_2^2) + G) \exp(-2t_2/T_2) \qquad (3.39)$$

The first factor is the number of transitions $N_T \ll 4^N$ which are optimally excited. The second factor is the estimate of the statistical model for the signal power per transition when $N_T \simeq 4^N$. The third factor expresses the way in which the signal power exceeds this estimate at different points in t_2 when such optimal excitation is assumed. The fourth factor is the irreversible decay of the f.i.d. at a rate T_2^{-1}. In writing (3.39), the possibility of a recurrence at $t_2 \gg M_2^{-\frac{1}{2}}$ of a signal power comparable to the maximum at $t_2 = 0$ has been excluded by construction. Thus this expression is only applicable for larger systems. The symmetric four spin system of Figure 21d is evidently too small, since it shows substantial recurrence in a few milliseconds. The probability of significant recurrence in a time $\sim T_2$ clearly depends on the complexity and resolution of the single quantum spectrum, but will usually be negligible for $N \gtrsim 8$.

e. Spatial removal of $\mathcal{H}_2$. The peak in signal power, which results from a favorable mixing period, could be prolonged if the free rotating frame evolution of the system could be halted at the point of matched preparation and mixing. This requires the effective removal of the nonscalar part of the detection period Hamiltonian $\mathcal{H}_2$. In anisotropic systems this entails removal of the dominant terms $\mathcal{H}^Q$ and $\mathcal{H}^D$. In many liquid crystal systems, diffusion causes rapid molecular rotation about a unique direction in the sample. In principle, it is possible to reorient this crystal axis during t_2 to the magic angle $\cos^{-1}(1/3)$ with respect to the static field. If this is done, diffusion motionally averages the anisotropic terms of $\mathcal{H}_2$ to zero. Such a sample reorientation would be impractical to achieve mechanically in a time $M_2^{-\frac{1}{2}}$. Another possibility for samples with an anisotropic electric susceptibility is to reorient them with electric fields[132].

f. Pulsed spin locking in t_2. Instead of trying to remove $\mathcal{H}_2$ by manipulation of its spatial part, the spins themselves may be manipulated by rf to achieve the same end. Perhaps the simplest method of eliminating evolution in t_2 is pulsed spin locking[133,134]. This is identical to CW spin locking[135-137] except that the rf is repetitively gated off to allow sampling of the nuclear magnetization. The method is nearly immune to the subtle pulse errors which limit the popularity of the more elaborate line narrowing sequences needed to observe chemical shifts in anisotropic systems. Spin locking eliminates the disappearance of the magnetization into unobservable coherence. The only remaining evolution is the irreversible decay characterized by an exponential time constant $T_{1\rho}$.

To see how pulsed spin locking can increase the signal energy available in a two dimensional experiment, consider the case of optimal excitation where the signal power is approximated by (3.39). Only the case $M_2^{-\frac{1}{2}} << T_2/2$ is relevant since $M_2^{-\frac{1}{2}}$ is a lower bound on τ and relaxation during preparation and mixing is being neglected. Furthermore, unless this inequality holds there will generally be no time to efficiently excite high order coherence (Sec. VA). In this limit, integration of (3.39) gives the average signal energy per shot for a group of N_T optimally excited lines as

$$E_{opt}^{f.i.d.} \simeq N_T(Tr(\rho^2)/4^N)^2(G^2(\pi/4M_2)^{\frac{1}{2}} + GT_2/2) \tag{3.40}$$

Now suppose that instead of allowing free evolution in t_2, $\mathcal{H}_2$ is effectively removed by pulsed spin locking. The signal power replacing (3.39) becomes

$$<|S_z(\tau,\tau,t_2)|^2> \simeq N_T(Tr(\rho^2)/4^N)^2 G^2 \exp(-2t_2/T_{1\rho}) \tag{3.41}$$

and the signal energy becomes

$$E_{opt}^{s.l.} \simeq \alpha N_T(Tr(\rho^2)/4^N)^2 G^2 T_{1\rho}/2 \tag{3.42}$$

The factor α is the fraction of time that the receiver is actually available during the pulse sequence, taking into account both the pulse duty cycle and any period after each pulse needed for ring down. At high Larmor frequencies it should be possible even in rigid protonated solids to keep $\alpha > 0.2$ with the typically achieved probe quality factors of $Q \simeq 10^2$.

As will become clear when G is calculated in Section IIIC8, the second term of (3.40) will often be negligible compared to the first. In such a case the relative time advantage of detection of multiple quantum coherence with pulsed spin locking is the energy ratio

$$E_{opt}^{s.l.}/E_{opt}^{f.i.d.} = \alpha T_{1\rho}(M_2/\pi)^{\frac{1}{2}} \qquad (3.43)$$

This may exceed 10^4 in a protonated solid as has been confirmed in preliminary studies[138].

In liquid crystals a ratio of 10^2 - 10^3 is anticipated. Here dielectric heating can be expected to change the molecular ordering during high duty cycle spin locking. This is not necessarily a problem as the evolution period is unaffected and the temperature can equilibrate before the next shot.

Another possibility is to minimize heating by spin locking at high duty cycle only for as long in t_2 as it takes to accomplish a reduction of $\mathcal{H}_2$ by rotation of the sample to the magic angle.

There are situations where it is desirable to correlate[9,72] the multiple quantum lines in ω_1 with the single quantum lines in ω_2 through 2D Fourier transformation. One of these is mentioned in Section VC. In these cases elimination of the t_2 dynamics must be forgone, along with any subsequent gain in signal energy. In such cases that the single quantum spectrum is well resolved this gain will be less than that given by (3.43) and will be proportional to Z_1.

As an aside, it should be noted that the notion of increasing sensitivity by line narrowing in t_2 is not restricted to multiple quantum NMR. Other areas which would benefit from it are single quantum wide line studies of spectral moments, powder patterns, diffusion or spin-lattice relaxation times. In each case it is only necessary to put the

usual evolution in t_1 and augment it by a detection period t_2 incorporating line narrowing. The time advantage given by (3.43) is appropriate also to T_1 applications. For comparison to single quantum studies it should be multiplied by r_{2D} given by (3.34) since a 1D experiment is being made into a 2D experiment.

3. Fluctuations in the Excitation Function - t_1 Noise

a. The phenomenon. Elsewhere in this work statistical arguments are used in order to estimate expectation values which are, in principle at least, exactly calculable and whose thermodynamic fluctuations are negligible. In this section the practical difficulties are examined of magnetization measurements which depend not only on the initial state of the spin systems, but on the experimental ability to reproducibly perturb the system and record its response.

The statistics of the reproducibility of experimental manipulations enters into 2D spectroscopy in a fundamentally different and more troublesome way than in the more familiar 1D experiment. As a simple example consider the effect of a small rf pulse instability. In the single pulse Fourier transform experiment the only effect of a small change in pulse amplitude is to slightly decrease the magnitude of the f.i.d. from the maximum value it attains with a well-adjusted $\pi/2$ pulse. Similarly, a small jitter from shot to shot in the pulse phase relative to the spectrometer reference only leads to some slight cancellation of signal when successive shots are averaged together. In both cases the fluctuation is likely to go unnoticed if it is small, since it leads to no spurious frequency components in the spectrum and only a marginal increase in the performance time needed to obtain a desired ratio of signal-to-noise. Even in a more elaborate one dimensional experiment in which,

for example, only certain transitions are excited by a tailored sequence of pulses, the magnetization which is excited, whether intentionally or otherwise, is certain to be found only at its eigenfrequencies.

The situation changes qualitatively in any experiment in which a Fourier transform is performed on an interferogram, collected point by point on successive shots. Fluctuations in the phase or amplitude of the magnetization are now converted to the frequency domain, whether or not these fluctuations are due to the systematic and intentional variation of the evolution time or to the vagaries of the apparatus.

The manifestations of these instrumental fluctuations in a two dimensional spectrum is a ridge of noise running along the ω_1 axis at each value of ω_2 at which there is a transition. This effect has been noted previously and has been termed t_1 noise[129,140]. In this section a simple and largely phenomenological formalism for t_1 noise is developed. This leads to a crucial distinction between additive noise and multiplicative noise and a demonstration that t_1 noise is multiplicative. Finally some strategies are discussed for the minimization of t_1 noise, particularly in multiple quantum experiments.

b. Simple formalism for t_1 noise. As a starting point, reconsider (2.34), the general expression for the signal as a function of the experimental time variables. For notational simplicity we will take just one term from the sum and suppress all but the evolution time as explicit variables. A new quantity

$$S'_{ij}(t_1) \equiv \rho_{ij}\alpha_{ji}(1+a_{ij})\exp(-i\omega_{ij}t_1) \tag{3.44}$$

$$= S_{ij}(t_1) + N_{ij}(t_1) \tag{3.45}$$

is defined which represents the signal from a single coherence present during t_1. This differs from one term of (2.34) in that a random variable a_{ij} has been introduced to account for the possibility of fluctuations other than those due to the oscillation $\exp(-i\omega_{ij}t_1)$.

In principle the fluctuations could be due to nearly any part of the spectrometer: the static magnetic field, the rf pulses reaching the spins, or even the receiver itself. Except perhaps for receiver instabilities, it is easy to imagine a given instrumental fluctuation having greater or lesser effects on different lines, so a possibly different random variable is allowed for each pair of subscripts. The random variable is likely to depend on other implicit variables as well, most notably the design of the excitation sequences.

For our purposes here however, it will suffice to make some statistical assumptions about the random variable. The fluctuations are taken to be small

$$\langle |a_{ij}|^2 \rangle^{\frac{1}{2}} \ll 1 \tag{3.46}$$

and of zero mean

$$\langle a_{ij} \rangle = 0 \tag{3.47}$$

Since we are interested in the ω_1 spectrum, (3.44) needs to be Fourier transformed:

$$S'_{ij}(\omega_1) \equiv (1/2\pi)\int_0^\infty S'_{ij}(t_1)\ \exp(-i\omega_1 t_1)dt_1 \tag{3.48a}$$

$$= \rho_{ij}\alpha_{ji}[\delta(\omega_{ij}-\omega_1) + \int_0^\infty a_{ij}(t_1)\exp(-i(\omega_{ij}-\omega_1)t_1)dt_1] \tag{3.48b}$$

$$\equiv S_{ij}(\omega_1) + N_{ij}(\omega_1) \tag{3.49}$$

This is the sum of the desired signal, represented in (3.48b) by the δ function, and a noise term. The random variable has been written as a function of t_1, which is only meant to indicate that each successive value of t_1 is an event at which a_{ij} may take on a new value.

By definition, the noise has no systematic dependence on t_1. Experimentally, this means that it averages incoherently during repeated accumulation. The best that can be done is to calculate its spectral density. For this the Wiener-Khintchine theorem is appropriate: the power spectral density is the Fourier transform of the autocorrelation function. The latter is given by

$$R_{ij}(\Delta t_1) = \langle N_{ij}(t_1)N^*_{ij}(t_1 + \Delta t_1)\rangle \tag{3.50a}$$

$$= \langle a_{ij}(t_1)a^*_{ij}(t_1 + \Delta t_1)\rangle\langle S_{ij}(t_1)S^*_{ij}(t_1 + \Delta t_1)\rangle \tag{3.50b}$$

The brackets indicate an average over t_1 or over many experiments. The factoring of this average in (3.50b) follows if the instability of the instrument is not caused by the signal level.

At this point another assumption about the nature of the fluctuations is convenient. Each successive shot is separated in real time by a delay, on the order of a spin lattice relaxation times T_1, during which the longitudinal magnetization tends toward equilibrium. There will be no correlation between the value of the random variable at successive values of t_1, if the fluctuations responsible for the t_1 noise occur on a time scale much shorter than this delay. This assumption corresponds to a δ function correlation function for a_{ij}. The required power spectral density is then

$$<|N_{ij}(\omega_1)|^2> = (1/2\pi)\int_{-\infty}^{\infty} R_{ij}(\Delta t_1)\ \exp(-i\omega_1\Delta t_1)d(\Delta t_1) \tag{3.51a}$$

$$= (1/2\pi)\int_{-\infty}^{\infty} <|a_{ij}|^2>\delta(\Delta t_1)<S_{ij}(t_1)S^*_{ij}(t_1+\Delta t_1)>\exp(-i\omega_1\Delta t_1)d(\Delta t_1) \tag{3.51b}$$

$$= (1/2\pi)<|a_{ij}|^2><|S_{ij}|^2> \tag{3.51c}$$

The square root of this quantity is the r.m.s. noise in the spectrum. The noise is proportional to the signal; it is multiplicative. The noise associated with a line at any frequency $\omega_1 = \omega_{ij}$, is spread over the entire range of ω_1; it is white.

c. Demonstration of the multiplicative nature of t_1 noise. A convenient way to assess the contribution of t_1 noise to the total noise is to perform the pulse sequence of interest with a fixed value of t_1. On successive shots only the storage address of the signal is incremented. The resulting data array is, in the absence of noise, completely flat in one dimension. The r.m.s. deviation in this dimension of the actual signal from its mean value is a measure of the noise.

In order to test the hypothesis of multiplicative noise it is necessary to vary the signal size. A convenient way to do this, while holding other aspects of the experiment constant, is to vary the repetition rate of the pulse sequence. After a period of several times T_1, the initial condition for each further repetition of the sequence reaches a steady-state, even though the repetition period may be less than T_1. The steady-state value of the initial density operator, and hence of the signal size, increases with increasing delay between repetitions until this delay is sufficiently long to allow full equilibration.

The result of such an experiment is shown in Figure 22. The pulse sequence is that of Figure 13b. The sample is acetaldehyde in a nematic

solvent. The linear relationship between signal magnitude and r.m.s. noise is confirmed.

The point at zero signal magnitude was obtained by sampling after the echo train (see Fig. 14) had passed. In other experiments it was confirmed that the noise at zero signal is the same for an array of data points sampled at a rate equal to the audio filter cut off frequency or at intervals on the order of one second. This demonstrates that the intercept in Figure 22 is just the usual additive (detector-limited) rf noise.

The extra noise due to the 2D nature of the experiment is entirely multiplicative. This rules out the possibility of a slow spectrometer baseline drift contributing to the t_1 noise, since such a mechanism would be additive, that is, independent of the signal magnitude.

Finally, the receiver noise figure was shown to be independent of signal magnitude, by injecting test signals in the size range (10^{-13} - 10^{-10} watts) of the nuclear signals. This strongly suggests that the instability is in the excitation of the spins and not in the detection process.

d. The minimization of t_1 noise. Many of the usual remedies for poor signal-to-noise ratio are futile in the limit where multiplicative noise is dominant. Increasing the sample size, lowering the sample or the spin temperature, or working at a higher static field all increase signal size, but the noise increases proportionally. The t_1 noise is nuclear magnetization out of control. Decreasing the detector noise is also of no use, when it is already a negligible contribution.

Obviously the most direct and desirable way to minimize t_1 noise would be to identify and correct the instrumental instabilities responsible

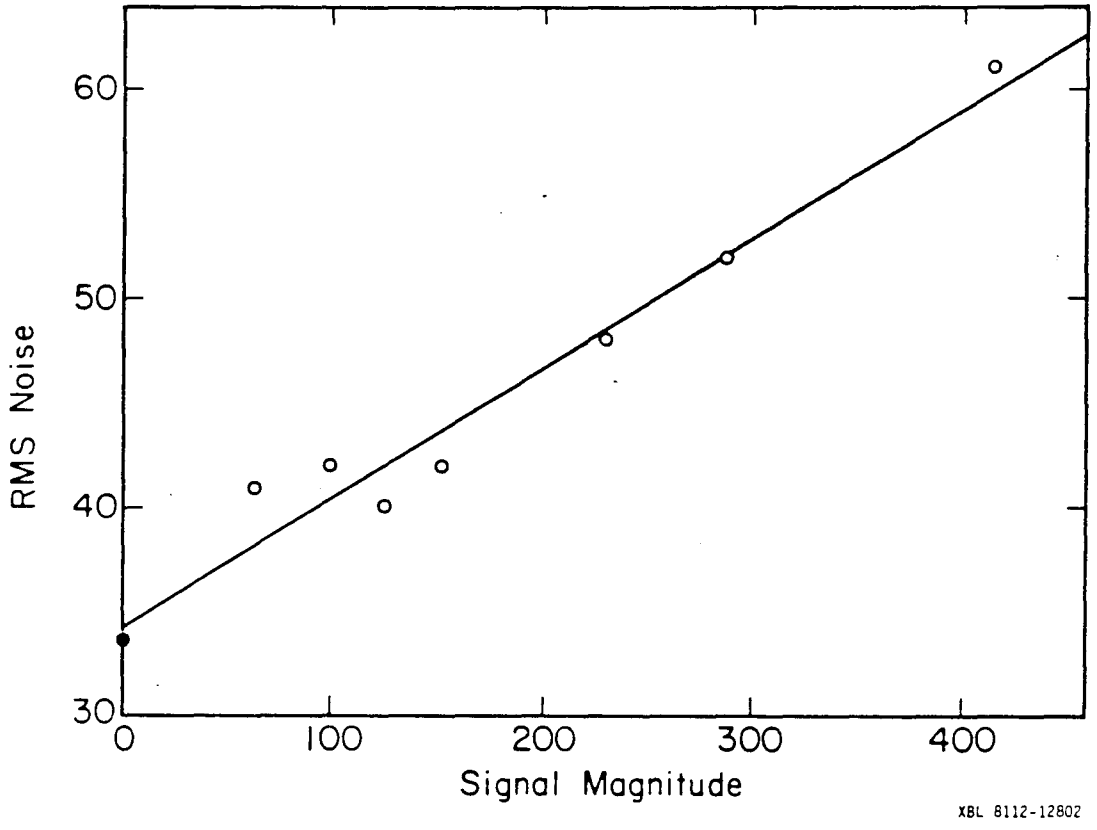

Figure 22. The multiplicative nature of t_1 noise. The signals are from the n = 2 coherence transfer echo of oriented acetaldehyde using the pulse sequence of Figure 13b. The intervals were fixed at the values (in msec) $\tau/2 = 25$, $t_1/2 \doteq 21.28$, $T = 3$. In order to obtain the different points, the signal magnitude was varied by changing the delay between repetitions of the sequence to different values $\lesssim T_1$. The root-mean-square deviation of the steady-state signal magnitude from its mean is proportional to that mean. The intercept at zero signal is just the usual additive (detector limited) rf noise, which is present even in a one dimensional experiment.

or, if possible, design pulse sequences less sensitive to instability. There is no fundamental reason to believe that for any given situation the problem cannot be made negligible relative to detector-limited noise. On the other hand, the problem does exist and due to its multiplicative nature is most likely to be dominant under precisely those conditions where excellent S/N would otherwise be anticipated. For this reason it is worthwhile to consider strategies for its minimization.

e. Repetition rate. At any point on the line of Figure 22, the r.m.s. noise will accumulate as $(N_s)^{\frac{1}{2}}$, where N_s is the number of shots. This is true regardless of the mixture of additive and multiplicative noise so long as both are random variables with zero mean (by definition) and smooth spectral density (by assumption). The signal magnitude, at any particular level per shot, accumulates linearly with N_s.

Thus it is evident that there is an optimum repetition rate in the neighborhood where additive and multiplicative noise are comparable. At higher repetition rates the ratio of signal-to-noise per shot decreases rapidly toward zero; at lower repetition rates there is a reduction in total shots per unit of time without significant gain in signal-to-noise ratio per shot. This argument is necessarily qualitative since the line in Figure 22 is obtained with a fixed value of t_1. If the coefficients $<|a_{ij}|>^2$ of (3.51) do vary from line to line a somewhat different line would be found for another t_1 or for the full 2D experiment.

Nevertheless, it is certainly true that the usual recommendations for choosing repetition rates for 1D experiments[141] or for 2D experiments with t_1 noise neglected[131] lead to less than optimal time performance when t_1 noise dominates. More rapid repetition is desirable.

As repetition rates are increased, closer consideration must be given to the interaction between successive shots. Coherence of all orders $n \geq 1$ can in principle be destroyed by field gradients between shots. Nonequilibrium population differences and $n = 0$ coherence, on the other hand, will in general be part of the steady-state initial condition achieved with rapid repetition rates. This is not necessarily a problem, but would alter slightly line intensities predicted on the basis of $\rho(0) = I_z$.

f. Reduction of t_1 noise by coherence transfer echo-filtering. According to (3.51) there is a contribution to the t_1 noise associated with each spectral line. It follows that, other factors being equal, the fewer lines detected, the smaller tha noise will be. The CTEF methods discussed in Section IIE3 allow only that signal from a single order to reach the receiver. Thus only that multiplicative noise associated with the observed transitions can possibly appear in the spectrum.

An example of this effect is shown in Figure 23, which is an expanded view of the $n = 4$ region of Figure 15. The noise magnitude is reduced by a factor of about 2 by preventing the signal from other orders from reaching the receiver.

Even in an ideal n-quantum selective experiment (Sec. IIIC8), there is always a large undesirable contribution to the magnetization at the receiver. This is due to that part of the equilibrium magnetization in the nonselected Zeeman manifolds which is left unperturbed by the preparation propagator, but which finally appears as transverse magnetization after mixing. Since it does not evolve during t_1, it corresponds to a line at $\omega_1 = 0$. If however, its amplitude fluctuates because of instabilities, it becomes a source of t_1 noise and could fruitfully be eliminated by CTEF using the pulse sequence of Figure 13d.

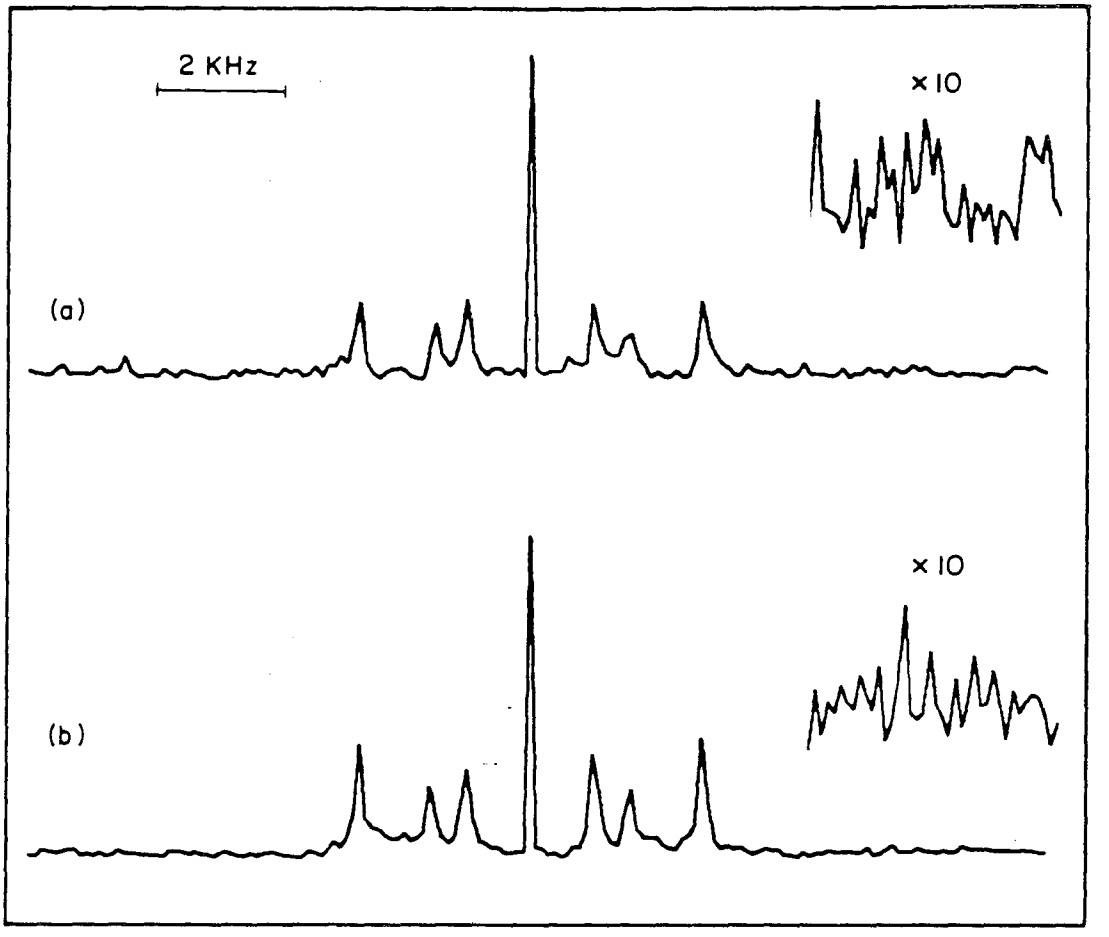

XBL 8112-12800

Figure 23. The reduction of t_1 noise by CTEF. Parts a) and b) are expanded images of the n = 4 regions of the upper and lower traces respectively, of Figure 15. The seven line spectrum is identical, but the noise, magnified in the insets, is reduced by about a factor of 2 with CTEF. This is a consequence of the filtering out of the t_1 noise associated with transitions of other orders.

C. Order Selective Excitation

1. Motivation

In the previous sections a recurring theme has been the spectral simplification and the increase in resolution which characterize the high order spectra of coupled spin systems. The practical realization of this resolution enhancement requires that the desired spectra be obtainable with adequate signal-to-noise ratio. In Section IIIB2 the dependence of signal power on the number of transitions was noted for the statistical limit in which all line intensities are assumed to be equal. While this limit is never precisely realized, it is approximately applicable when the excitation periods are of adequate length to excite the highest order coherences and are not specifically designed to favor particular transitions. Regardless of whether the intensity distributions of different transition orders are equal, they do share in the same initial magnetization.

The excitation sequences to be discussed in this section are designed to narrow the accessible part of Liouville space to that characterized by restricted values of n. In this way the density operator is forced to proceed more directly to regions in which the initial magnetization is distributed predominantly among the desired coherences.

It is important to distinguish this notion of channeling the magnetization into coherence with certain values of n from methods discussed in earlier sections. An analogy to synthetic chemistry will clarify the relationships among the different approaches. The isolated spectrum of a certain order n is the goal. Its chemical analog is a sample of a certain pure compound.

In Section IID2 methods were reviewed of sorting out the signals resulting from different orders of coherence on the basis of their characteristic modulation as the relative phases of the radiation within a pulse sequence were varied. The requisite variations in phase were between one shot and another. The roughly analogous chemical procedure would be the chromatographic separation of a complex reaction product mixture into its pure components.

In Section IIE3 the use of field gradients for suppressing coherence was discussed. This had the advantage of reducing the minimum time needed to perform the experiment, but did not increase the signal energy per shot associated with a given order n. The analogous chemical separation might be the precipitation of a single low yield product from a reaction vessel and the disposal of the remaining products.

In Section IIIB1d a method was noted of searching for relatively good excitation times. In principle a simple excitation sequence can result in the maximum possible signal power for a given transition or a given order. This is routinely achieved in simple systems for which the form of the excitation dynamics can be calculated in advance. As the size of the system and the complexity of the single quantum spectrum grows, the occurrence of significantly non-statistical maxima in the excitation function becomes increasingly brief and rare. The search over τ in the nonselective excitation sequence becomes essentially a random walk in a large fraction of the entire Liouville space. A time $\tau \lesssim T_2$ is available for searching before irreversible dephasing destroys all coherence. The probability of achieving significantly non-statistical intensities for the relatively few high order transitions of interest decreases rapidly as the dimension of the Liouville space increases. A

chemical analogy would be an attempt to optimize the yield of a reaction by systematic variation of reaction conditions. Some measure of success is likely, but when there are many possible products the chances of a very high yield are poor.

In the order selective sequences of this section an activist approach is taken to the problem of bringing the system to that small region of Liouville space characterized by large intensities for coherences of certain orders n. Trains of pulses with spacings comparable to $\|\mathcal{H}_{int}\|^{-1}$ are applied during the preparation and mixing periods in order to create an effective Hamiltonian under which the initial density operator can only evolve by the exchange of groups of n photons with the radiation field. The result is that high order coherences can be excited with nearly ideal efficiency without prior detailed knowledge of the internal Hamiltonian. The analogy would be synthesis by enzymatic catalysis. The reaction proceeds swiftly and selectively to the thermodynamic limit.

2. Even or Odd Selection

The simplest order selective experiments are those which prepare only even quantum coherence or only odd quantum coherence[54,142]. In a system with a bilinear internal Hamiltonian, the simplest resonant two pulse preparation sequence (Fig. 3) is even selective or odd selective depending on the relative phases of the two $\pi/2$ pulses. In order to remove the effects of static field inhomogeneity, resonance offset and chemical shifts, the practical even or odd selective experiment involves one or more π pulses during τ. As discussed in Section IIE1, one pulse suffices unless $[\mathcal{H}_{int},\mathcal{H}'_{int}] \neq 0$ (intermediate coupling) in which case a train of π pulses serves to remove the Zeeman terms.

Assuming that a bilinear effective Hamiltonian has been achieved the preparation propagator can be written without loss of generality as

$$U(\tau) = \exp(i(\pi/2)I_x)\ \exp(-i\mathcal{H}^{zz}\tau)\ \exp(-i(\pi/2)I_\gamma) \tag{3.52}$$

The first $\pi/2$ pulse has been chosen to be of arbitrary phase γ (2.7) and the second $\pi/2$ pulse is an x pulse. Since we already know that variation of the overall phase of the preparation period only has the effect of modulating phase factors in $\rho(\tau)$ (2.48), it is only the relative phase of the preparation pulses which is of concern here.

The last factor in (3.52) can be rewritten as

$$\exp(-i(\pi/2)I_\gamma) = \exp(i\gamma I_z)\ \exp(-i(\pi/2)I_x)\ \exp(-i\gamma I_z) \tag{3.53a}$$

$$= \exp(-i(\pi/2)I_x)\ \exp(i\gamma I_y)\ \exp(-i\gamma I_z) \tag{3.53b}$$

With the further substitution

$$\exp(-i\mathcal{H}^{yy}\tau) \equiv \exp(i(\pi/2)I_x)\ \exp(-i\mathcal{H}^{zz}\tau)\ \exp(-i(\pi/2)I_x) \tag{3.54}$$

the prepared density operator becomes

$$\rho(\tau) = \cos\gamma\ \exp(-i\mathcal{H}^{yy}\tau)I_z\ \exp(i\mathcal{H}^{yy}\tau)$$

$$-\sin\gamma\ \exp(-i\mathcal{H}^{yy}\tau)I_x\ \exp(i\mathcal{H}^{yy}\tau) \tag{3.55}$$

This has the form of a two term initial condition acted upon by an effective Hamiltonian $\mathcal{H}^{yy}$. This Hamiltonian is of the same form as (2.10) except that I_{yi} and I_{zi} are interchanged for all spins. Since $\mathcal{H}^{zz}$ consists of tensor operators of rank two and rank zero, $\mathcal{H}^{yy}$ can contain $n = \pm 2$ terms as its highest order components. In fact, it can contain only terms with $n = 0$ and $n = \pm 2$, since it is invariant to a rotation of π about I_z and thus is even quantum.

This same invariance to a π_z rotation holds for the entire first term of (3.55). Thus it contains only operators with even n. All possible even values of n may appear for all $|n| \leqslant 2NI$.
Similarly the second term contains only odd quantum operators since it inverts under a π_z rotation.

Even selection then is simply a matter of choosing $\sin\gamma = 0$ ($\pi/2$ pulses with a phase difference of $\pi/2$), while odd selection corresponds to $\cos\gamma = 0$ ($\pi/2$ pulses with a phase difference of zero or π). An example of an even quantum selective spectrum appears in Figure 15.

If both even and odd quantum coherence are prepared, for example, by choosing $\gamma = \pi/4$, then it is still possible to detect them separately even without labeling the coherence by the overall preparation phase (Sec. IID2) or by coherence transfer echo filtering (Sec. IIE3). This is because under the conditions that $\mathcal{H}_2$ conserves spin inversion parity (Sec. IIF2) and a $\pi/2$ pulse is used for mixing, the signal resulting in t_2 from even and odd coherences will be out of phase by 90°. Therefore it is adjustable into separate channels of the phase sensitive detector.

To see this, consider that the detected operators (2.32) for a $(\pi/2)_x$ mixing pulse are:

$$I_x(-t_2) = \exp(-i(\pi/2)I_x)\ \exp(i\mathcal{H}^{zz}t_2)I_x\ \exp(-i\mathcal{H}^{zz}t_2)\ \exp(i(\pi/2)I_x) \quad (3.56a)$$

$$= \exp(i\mathcal{H}^{yy}t_2)I_x\ \exp(-i\mathcal{H}^{yy}t_2) \quad (3.56b)$$

and

$$I_y(-t_2) = \exp(-i(\pi/2)I_x)\exp(i\mathcal{H}^{zz}t_2)I_y\ \exp(-i\mathcal{H}^{zz}t_2)\ \exp(i(\pi/2)I_x) \quad (3.57a)$$

$$= \exp(i\mathcal{H}^{yy}t_2)I_z\ \exp(-i\mathcal{H}^{yy}t_2) \quad (3.57b)$$

Comparison with the two terms of $\rho(\tau)$ in (3.55) demonstrates the segregation of even and odd signals into separate channels. Setting $t_2 = \tau$ exemplifies the concept of similar preparation and mixing dynamics.

3. Excitation of Zero Quantum Transitions of Definite Spin Inversion Parity

In Section IIF2 the definition (2.75) was introduced of states $|i\rangle$ and $|\bar{i}\rangle$ which are interconverted by a Π_x pulse. This interconversion is associated with a change of M_i to $-M_i$. The set of states in the M = 0 manifold is therefore closed under the action of a π pulse. If $\mathcal{H}_1$ commutes with the spin inversion operators, then states within this manifold can be chosen as simultaneous eigenstates of internal energy, Zeeman energy and spin inversion parity. They satisfy the condition

$$|\bar{i}\rangle = \pm|i\rangle \tag{3.58}$$

This fact was noted in an early analysis of the single quantum spectrum of oriented benzene[17], but the spin inversion symmetry label has no consequences for the single quantum selection rules.

The transitions between these states also have definite spin inversion parity:

$$\Pi_{x,y}|i\rangle\langle j|\Pi^{\dagger}_{x,y} = \pm|i\rangle\langle j| \tag{3.59}$$

The plus sign (gerade) applies for transitions between states of the same parity and the minus sign (ungerade) for transitions between states of opposite parity.

Recall that for preparation by a bilinear internal Hamiltonian and two $\pi/2$ pulses (3.55) the even quantum terms have the same spin inversion parity as I_z, which is ungerade. We immediately can conclude that such a

preparation sequence does not prepare gerade even-quantum coherence. The only off diagonal operators $|i><j|$ which occur exclusively in gerade Hermitian operators (Table 1) represent gerade M = 0 zero-quantum transitions. Thus these are forbidden with the usual preparation by two $\pi/2$ pulses.

The simplest way to violate this selection rule is change the pulse angle of the second preparation pulse to $(\pi/2 - \theta)$. This may be viewed as giving a $\theta_{\bar{x}}$ pulse to the density operator of (3.55). The question is whether this new density operator will contain the gerade M = 0 zero-quantum coherence which was forbidden for a precise $\pi/2$ pulse.

A prediction is easily made on the basis of parity arguments. The first term in (3.55) has the spin inversion parity of I_z, which is described by the ordered pair $(P_x,P_y) = (-1,-1)$. Since a $\theta_{\bar{x}}$ pulse cannot change P_x, this term does not contain the desired coherence, which is described by (1,1).

The odd quantum term in (3.55) has the spin inversion parity of I_x, which is given by (1,-1). The $\theta_{\bar{x}}$ pulse acting on this term can create even-quantum terms of the type (1,1). Thus the prediction is that the gerade M = 0, n = 0 coherence will be maximized at $\sin\gamma = \pm 1$ and the last preparation pulse must not be a multiple of $\pi/2$. In fact, the previously allowed ungerade transitions now become forbidden. As usual the mixing must match preparation for optimal signal intensity. These predictions have been confirmed by both experiment and computation on partially oriented benzene using a $\pi/4$ pulse at the end of preparation and for mixing[126].

4. Average Hamiltonian Theory (AHT)

The development of more highly order selective excitation

sequences relied heavily on the theoretical machinery of coherent averaging theory, also known as average Hamiltonian theory (AHT)[61-63]. This formalism provides a recipe for replacing the time dependent Hamiltonian describing a complex irradiation sequence with a time independent effective Hamiltonian. The effective Hamiltonian produces, within limits, the same dynamics. This formalism has been presented pedagogically in two highly recommended monographs[62,63]. The barest of reviews will be presented in this section in order to introduce notation essential to later discussion. More recent developments of the theory will be introduced as needed.

Coherent averaging theory is designed for those situations in which a periodic and cyclic perturbation is applied to the spin system. For the purposes here, this will always be a sequence of rf irradiation described by $\mathcal{H}_{rf}(t)$. The total Hamiltonian is

$$\mathcal{H}_{tot} = \mathcal{H}_{int} + \mathcal{H}_{rf}(t) \tag{3.60}$$

The requirement for periodicity, if $\mathcal{H}_{int}$ is constant, is

$$\mathcal{H}_{rf}(t + N_c t_c) = \mathcal{H}_{rf}(t) \tag{3.61}$$

where t_c is the period or cycle time and N_c is some integral number of cycles. Cyclic means that

$$U_{rf}(N_c t_c) = T \exp(-i \int_0^{N_c t_c} \mathcal{H}_{rf}(t)dt) = 1 \tag{3.62}$$

where T is the Dyson time-ordering operator. The calculation proceeds by transforming to the interaction representation defined by $U_{rf}(t)$. When $\mathcal{H}_{rf}(t)$ consists of a sequence of pulses, this representation is known as the toggling frame. It is the representation in which the

action of the pulses survives only in so much as they render the transformed internal Hamiltonian time dependent. This Hamiltonian in the toggling frame is then

$$\tilde{\mathcal{H}}_{int} = U_{rf}^{-1}(t)\, \mathcal{H}_{int}\, U_{rf}(t) \tag{3.63}$$

The next step is to use the Magnus expansion to replace this time dependent Hamiltonian by a time independent Hamiltonian

$$\mathcal{H} = \tilde{\mathcal{H}}^{(0)} + \tilde{\mathcal{H}}^{(1)} + \tilde{\mathcal{H}}^{(2)} + \ldots \tag{3.64}$$

This is the effective Hamiltonian. The leading term is the average Hamiltonian given by

$$\tilde{\mathcal{H}}^{(0)} = \int_0^{t_c} \tilde{\mathcal{H}}_{int}(t)dt \tag{3.65}$$

For many purposes it is a good approximation to $\mathcal{H}$. The higher order terms $\tilde{\mathcal{H}}^{(k)}$ are correction terms proportional to t_c^k. They have the form of integrals over commutators of the operator $\tilde{\mathcal{H}}_{int}(t)$ evaluated at different times. If such commutators do not vanish, then (3.64) is roughly an expansion in $\|\mathcal{H}_{int}\| t_c$ which largely restricts its usefulness to short cycle times for which the leading terms dominate.

The cyclic condition (3.62) implies that at times $t = Nt_c$, the toggling frame and rotating frame coincide. With the restriction that we only consider the density operator at these times, its rotating frame dynamics may be calculated using the leading term or terms of (3.64), rather than the time dependent Hamiltonian.

In practice it is often desirable to perform a nested series of AHT expansions. This is useful whenever there are several different

periodicities present in the time dependent Hamiltonian. The most rapid time dependence is dealt with first leading to a piecewise constant effective Hamiltonian. Each successively slower periodicity takes the form of a continuous or sudden switching of this effective Hamiltonian. It in turn is removed by a subsequent expansion. This process results in a sequence of effective Hamiltonians which may be used to calculate the dynamics on successively longer time scales.

This approach of nesting has computational advantages over the alternative of calculating a single effective Hamiltonian for the longest time scale. The number of distinct time intervals or different modulation frequencies appearing in the integrals of each expansion is minimized. In practice, each expansion is rapidly convergent so the effective Hamiltonian carried on to the next step consists of only the leading terms of (3.64) which are relatively easy to calculate. Most importantly, physical insight is gained of the approximations and dynamics of each time scale. This approach is implicitly used whenever one starts with rotating frame Hamiltonians, which themselves are derivable by AHT[62,63].

5. Phase Cycling

a. Frequency domain picture. Phase cycling[143-145] is the term used to describe an irradiation sequence which consists of n subcycles which are identical except that the phase of the rf is shifted by $2\pi/n$ in going from one to another. Each subcycle, as well as the entire sequence, is a cycle in the sense of AHT. Phase cycling is the most fundamental architectural theme in the often baroque order selective excitation sequences.

Figure 24 is a schematic diagram of phase cycling[98]. On the left is depicted an infinite irradiation sequence consisting of a carrier at the

Larmor frequency ω_0 which is instantaneously shifted in phase by $2\pi/n$ at intervals of $\Delta\tau_p$. The average frequency with which the phase advances is $\omega_c = 2\pi/n\Delta\tau_p$. The right side of Figure 24 sketches the relationship of the spectrum of this phase modulated irradiation to the absorption line of the spin system at ω_0. The nearest Fourier component of the irradiation is at $(\omega_0 - \omega_c)$. The next nearest component is at $\omega_0+(n-1)\omega_c$ and is weaker by a factor of n. Now consider what energy conserving processes are possible which exchange photons between the spin system and the radiation field. The lowest order such process is that involving (n-1) photons at $(\omega_0 - \omega_c)$ and one photon at $\omega_0 + (n-1)\omega_c$. This sums to an n photon process resonant at $n\omega_0$.

This frequency domain picture of how phase cycling can lead to order selective excitation is satisfyingly simple, but misleadingly so. The notion of lower order processes being nonresonant is not compelling, since in the actual sequences to be described intense brief pulses will be used having transform limits in excess of $n\omega_c$ and of the absorption line. Furthermore, the irradiation within each subcycle $\Delta\tau_p$ will not be continuous, but will itself consist of trains of pulses (Sec. IIIC6). Finally, the cycle of n phases will not always be the longest period, but will become a unit within a longer cycle (Sec. IIIC7). In order to deal with these exigencies another viewpoint is needed.

b. AHT of phase cycling. The subcycles themselves are AHT cycles with cycle time $\Delta\tau_p << T_2$ and have effective Hamiltonians (detailed in Sec. IIIC6)

$$\mathcal{H}_\phi = \exp(i\phi I_z)\, \mathcal{H}_{\phi=0}\, \exp(-i\phi I_z) \quad . \tag{3.66}$$

The overall phase ϕ of the radiation, which takes the values $\phi = (0, 2\pi/n,$

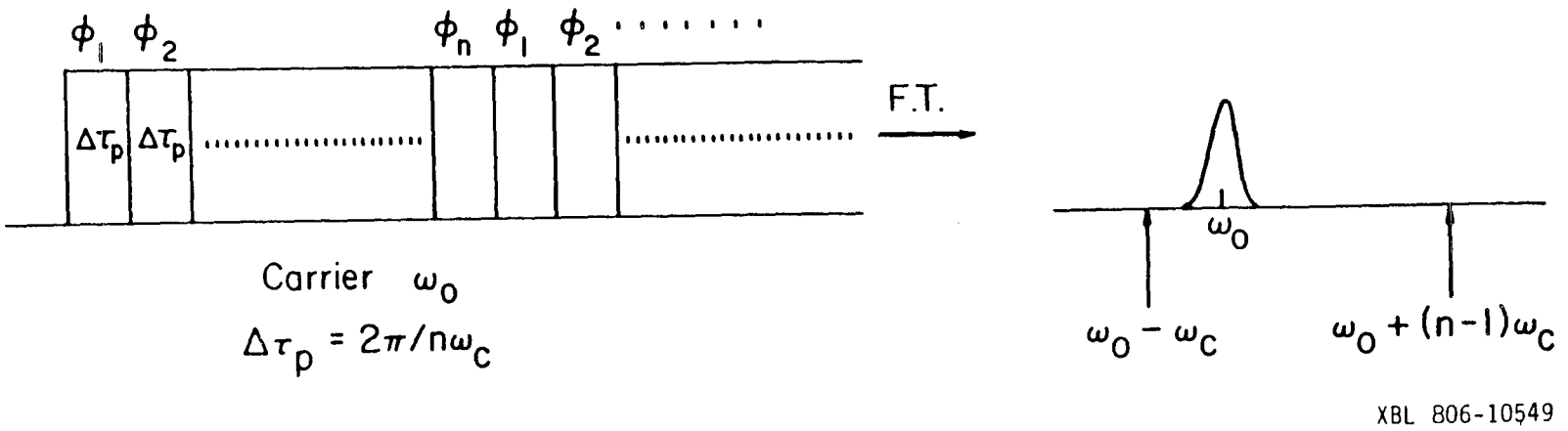

Figure 24. Phase cycling and the frequency domain interpretation of order selective excitation. On the left, constant amplitude radiation at frequency ω_0 is phase shifted by $2\pi/n$ every $\Delta\tau_p = 2\pi/n\omega_c$ seconds. On the right, the single quantum spectrum centered at ω_0 is shown flanked by arrows at the two dominant frequencies in the Fourier transform of the irradiation. A resonant n-quantum process at $n\omega_0$ results from a combination of (n-1) quanta at frequency $\omega_0 - \omega_c$ and one quantum at frequency $\omega_0 + (n-1)\omega_c$. Lower order processes are nonresonant. Practical sequences use more complex sequences of pulses within each subcycle of length $\Delta\tau_p$.

$4\pi/n \ldots 2\pi(n-1)/n)$, is all that distinguishes one subcycle from another. The relationship between the subcycle Hamiltonians is easily appreciated by evaluating an arbitrary matrix element of (3.66) in a high field eigenbasis:

$$\langle i|\mathcal{H}_{\phi}|j\rangle = \exp(in_{ij}\phi)\langle i|\mathcal{H}_{\phi=0}|j\rangle \tag{3.67}$$

The subcycle Hamiltonians of interest are, of course, largely off-diagonal (nonsecular) in this basis. They are designed to cause excitation of multiple quantum coherence when the initial condition is secular. In this regard they are analogous to the excitation Hamiltonian $\mathcal{H}^{yy}$ which appeared in the analysis of the even or odd selective experiment (Sec. IIIC2).

AHT can be used to obtain an effective Hamiltonian for the phase cycled sequence using the effective subcycle Hamiltonians of (3.66) as a starting point. The time dependence which is to be removed by this procedure comes only from the phase shifting between subcycles. Thus $\mathcal{H}_{\phi=0}$ is playing the role of $\mathcal{H}_{int}$ in (3.60-3.65). This is an example of nesting.

The first term or average Hamiltonian is readily expressed in terms of (3.66) since the integral appearing in (3.65) is just the sum over subcycles:

$$\tilde{\mathcal{H}}^{(0)} = (\Delta\tau_p/t_c) \sum_{\ell=0}^{n-1} \exp(i(2\pi\ell/n)I_z)\, \mathcal{H}_{\phi=0}\, \exp(-i(2\pi\ell/n)I_z) \tag{3.68}$$

Evaluating a particular matrix element using (3.67) gives

$$\langle i|\tilde{\mathcal{H}}^{(0)}|j\rangle = \langle i|\mathcal{H}_{\phi=0}|j\rangle\delta(nk-n_{ij}) \tag{3.69}$$

The significance of this is that the phase cycled sequence has an average

Hamiltonian which only connects states differing in Zeeman quantum numbers by nk, where k is any integer. In other words, this average Hamiltonian only allows the system to exchange photons in groups of n with the radiation field, which is ultimately responsible for the non-secular character of $\tilde{\mathcal{H}}^{(0)}$.

A couple of notational comments are needed here. The symbol n, which has been used to denote the order of coherence excited, is here being used to indicate a property of the excitation process; specifically, it indicates here the multiple by which the order of coherence can be changed by this excitation process. With this in mind, the meaning of n should be clear from context. An operator is called nk-quantum (selective) if its expansion in spherical tensor operators (2.25) includes only terms $T_{nk}^{\ell\alpha}$. This term may be applied to Hamiltonians, the propagators constructed from them or the density operators resulting from the action of such propagators.

The other notational comment concerns a second use of the word "order". An excitation sequence whose average Hamiltonian satisfies (3.69) will be called zero-order nk-quantum selective. Sequences selective to higher order are discussed in Section IIIC7.

The role of phase cycling can now be clarified by using this average Hamiltonian to make an approximate propagator

$$U^{(0)}(\tau) \equiv \exp(-i\tilde{\mathcal{H}}^{(0)}\tau) \tag{3.70}$$

which implies repetition of the phase cycled sequence until τ has elapsed. If the initial condition is, as usual, Curie law magnetization, the prepared density operator is

$$\rho(\tau) \simeq U^{(0)}(\tau) I_z \, U^{(0)\dagger}(\tau) \tag{3.71a}$$

$$= \sum_{ij} \rho_{ij}(\tau)\delta(nk - n_{ij}) |i\rangle\langle j| \tag{3.71b}$$

as is easily seen by noting that the set of nk-quantum operators is closed under multiplication. An alternate way of viewing this result is that both I_z and $\tilde{\mathcal{H}}^{(0)}$ are invariant to rotations of $2\pi/n$ about I_z and thus so is this approximation to $\rho(\tau)$.

Figure 25 graphically illustrates the constructive and destructive interference of the subcycles at this level of approximation. The case depicted is zero-order 4k-quantum selective preparation. Each arrow represents the complex coefficient ρ_{ij} of a particular coherence $|i\rangle\langle j|$ of a given order n_{ij} excited by a single subcycle. The phase shift between arrows placed head to tail is $2\pi n_{ij}/4$. The trajectories from left to right correspond to respectively, n_{ij} = 1, 2, 3, and 4. Only for the 4-quantum coherence is there any net excursion from the initial condition after the four subcycles.

It is worth emphasizing that the cancellation of the excitation which occurs for $n_{ij} \neq nk$ is not a dissipative process associated with an increase in entropy or reduction in the norm of ρ. Rather it is a closed trajectory in Liouville space. It is akin to a round trip. A familiar analog in a restricted region of Liouville space is the nutation which the magnetization undergoes when four closely spaced $\pi/2$ pulses are applied. The great simplicity of the average Hamiltonian approach arises largely from the fact that such extraneous cyclic processes are suppressed from view leaving only the net dynamics in the foreground.

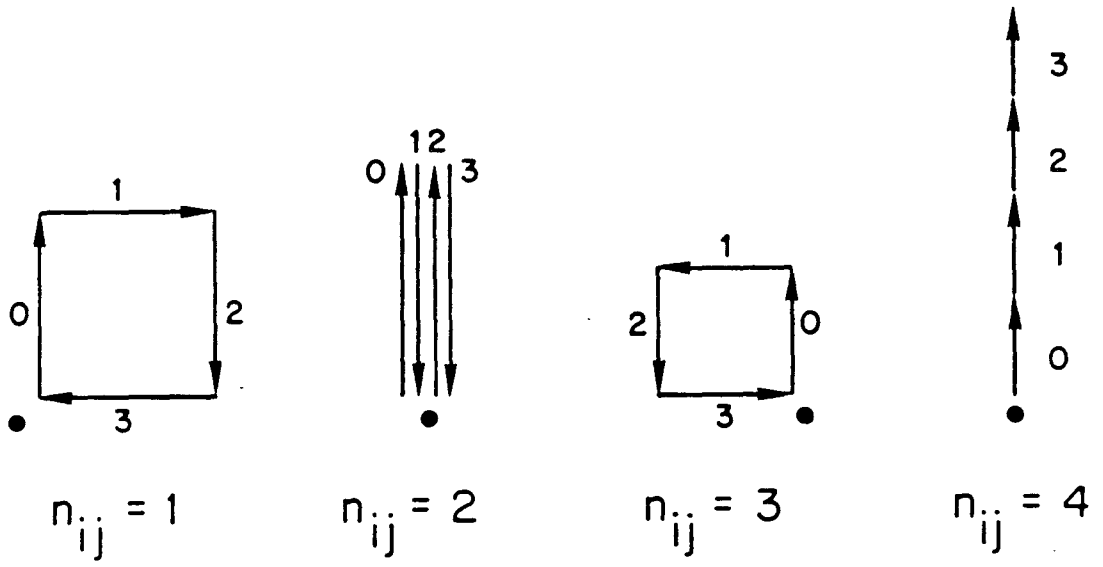

XBL 8112-12908

Figure 25. Schematic illustration of the excursions in Liouville space of the coherence of different orders n_{ij} = 1,2,3, and 4 during one cycle of zero-order 4k-quantum selective excitation. The rf phase of each subcycle is indicated by the numbers in units of $\pi/2$, the phase shift necessary to select for n_{ij} = 4 coherence. These rf phase shifts appear as rotations of $n_{ij}\pi/2$ between the increments to the coherence amplitudes from successive subcycles. The instantaneous coherence magnitude is the distance from a point on the trajectory to the origin near the dot. Only for the selected n_{ij} = 4 coherence is there a net magnitude after a full cycle of four subcycles.

6. Subcycle Design

a. The requirements for a successful subcycle. The comparison of a cycle of four phase shifted subcycles to four $\pi/2$ pulses is imprecise in an important respect. The return of the $n_{ij} \neq 4$ trajectories to the origin in Figure 25 depended on the approximation that the excursion due to each subcycle was small. A better analogy in the three dimensional Liouville space of a two level system is to visualize the excursions of the equilibrium magnetization vector as four equal angle pulses are given in rapid succession with a phase shift of $\pi/2$ in between pulses. For small pulse angles the tip of the magnetization vector will trace out a square on the unit sphere. For larger pulse angles, the square will distort and the net trajectory will no longer be zero.

Figure 26 sketches the analogous situation in some subspaces of the larger Liouville space which is needed to describe a many level system subjected to four phase cycled subcycles. Here the dynamics is assumed to proceed to a greater degree than in Figure 25. The cycle has started to become nonselective; even for the coherences with $n_{ij} \neq 4$, there is a net excursion at the end of the cycle.

Mathematically, this comes about because the subcycle Hamiltonians (3.66) do not commute. This leads to significant correction terms in the series of the form (3.64) describing the effective cycle Hamiltonian. When these terms are too large then (3.68) is no longer the only important term and (3.70) is a poor approximation to the actual propagator. This can be expected to occur when $\|\mathcal{H}_\phi\| \Delta\tau_p$ becomes comparable to unity.

The obvious expedient then to preserve selectivity is to keep $\Delta\tau_p$ small. The trouble with this approach is that a subcycle sequence

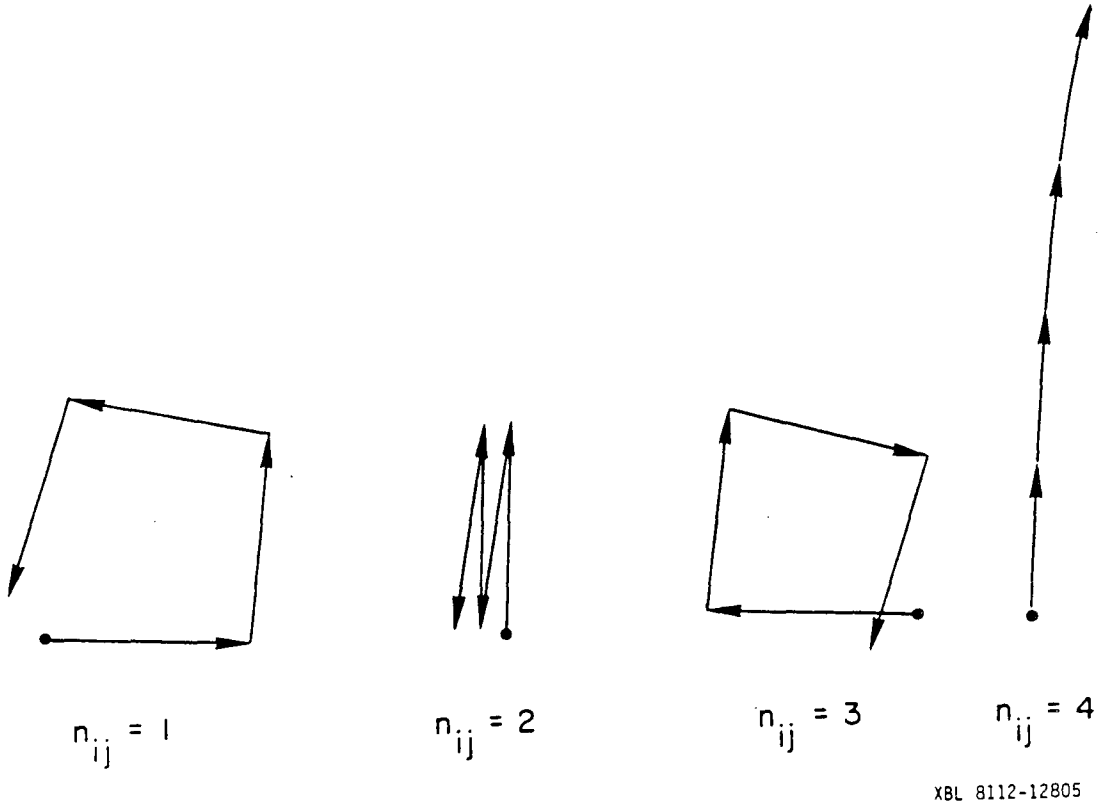

Figure 26. Illustration of a failure of selectivity of a zero-order selective excitation sequence. When the effect of a single subcycle becomes too large, the linearization of the dynamics is no longer a good approximation. This is indicated by the slight curvature of the arrows for each subcycle. The result is a net excitation of the non-selected coherences n_{ij} = 1, 2, and 3, indicated by their failure to return to the origin after a full cycle. Compare with Figure 25.

extending in time for less than $\sim M_2^{-\frac{1}{2}}$ will tend to be selective without being effective. This is illustrated by Figure 27. A subcycle which is too short will excite preferentially low order coherence. At the end of the cycle the selected high order coherence is hardly present. Within limits, this can be remedied by repeating the cycle. The relaxation times of the system set a bound however on the length of the excitation periods. This is discussed further in Section VA. In the remainder of this section some specific schemes are described which lead to effective subcycle Hamiltonians, which successfully tread the thin line between a cycle which is nonselective and one which is ineffective.

b. Time reversal sandwiches[143-145]. One scheme for designing a useful subcycle sequence is sketched in Figure 28a[145]. The first period T of the subcycle consists of a pulse sequence having an average Hamiltonian $\mathcal{H}_p$ which is time reversible in the sense of Section IIIA2; by some manipulation the sign of $\mathcal{H}_p$ must be reversed to give $-\mathcal{H}_p'$ in the period T', such that $\mathcal{H}_p'T' = -\mathcal{H}_p T$. This condition states that in the limit that the central period of length $\Delta\tau_p'$ vanished, the subcycle would have a propagator of unity. An example of this limit is the magic echo experiment[121] for which

$$\mathcal{H}_p = \mathcal{H}_{II}^{D,yy} = \exp(i(\pi/2)I_x)\ \mathcal{H}_{II}^{D}\ \exp(-i(\pi/2)I_x) \tag{3.72}$$

is achieved by a pair of $\pi/2$ pulses as in the even selective experiment of Section IIIC2, while

$$\mathcal{H}_p' = -(\tfrac{1}{2})\ \mathcal{H}_{II}^{D,yy} \tag{3.73}$$

is obtained by a train of equally spaced $\pi/2$ pulses. For this case $T' = 2T$ is required. Note that in writing (3.72) and (3.73) the small

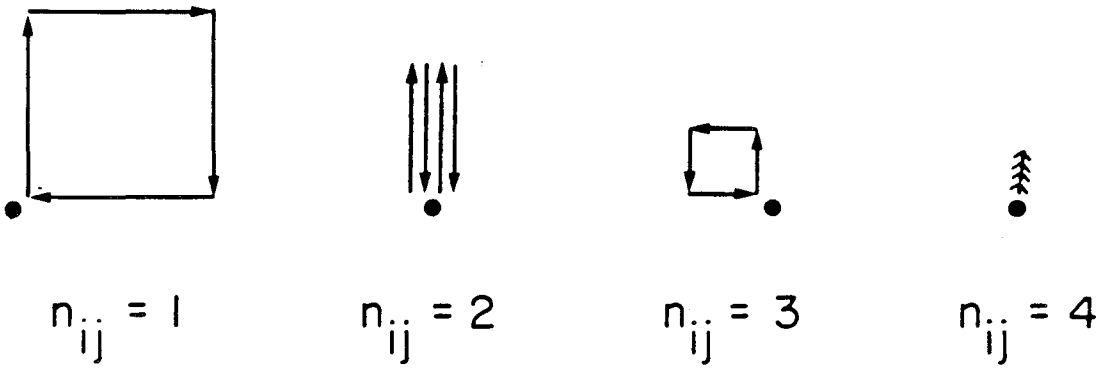

XBL 8112-12808

Figure 27. Illustration of the failure of an order selective excitation cycle to prepare high quantum coherence. If the subcycle inadequately excites the desired high order coherence, then the cycle is ineffective, though formally selective. To some extent this problem can be alleviated by repeating the cycle or incorporating it into more complex cycles (Sec. IIIC7). Eventually irreversible relaxation sets an upper bound on the length of the excitation periods (Sec. VA2). Compare with Figure 25.

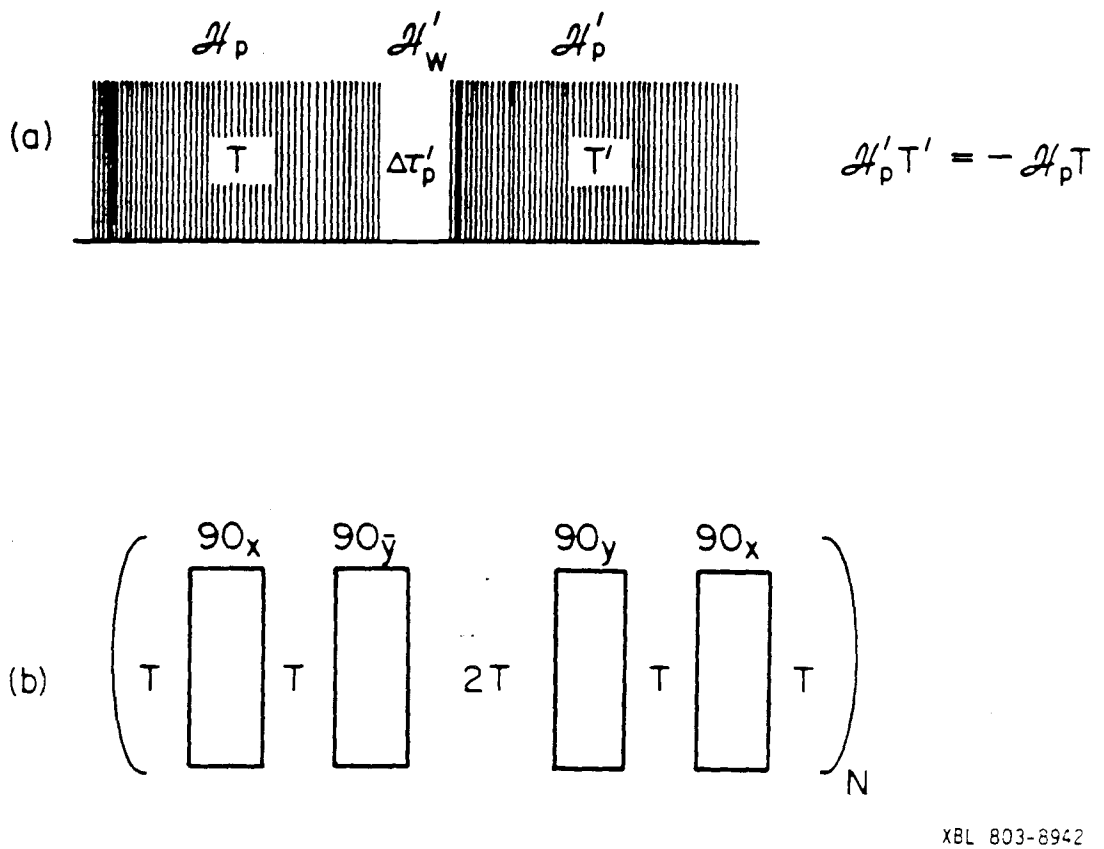

Figure 28. Subcycle architecture for order selective excitation in anisotropic systems. Two different ways are shown of causing the dipolar couplings between the spins to act in a nonlinear fashion in the effective subcycle Hamiltonian. In a) a time reversal sandwich is depicted. The two closely shaded regions T and T' have average Hamiltonians of opposite sign and act as a multiple quantum rotation (3.75) on the Hamiltonian $\mathcal{H}'_w$ of the central interval. In b) one cycle of the WAHUHA or WHH-4 line narrowing sequence is shown. By using an interval T too large for effective line narrowing high rank correction terms are made significant in the effective Hamiltonian.

term $\mathcal{H}_{II}^{J}$ is neglected. Since these scalar operators are unaffected by the pulse sequences, the time reversal is only approximate.

An alternative pulse sequence for obtaining a reversible $\mathcal{H}_p$ is that shown in Figure 29. Here the spacing between $\pi/2$ pulses is alternately $2\tau''$ and τ''. The phase alternation corrects for pulse angle errors[145,146]. This sequence gives (with $\phi' = 0$)

$$\mathcal{H}_p = (1/3)(\mathcal{H}_{II}^{D,yy} - \mathcal{H}_{II}^{D,xx}) \tag{3.74}$$

where again $\mathcal{H}_{II}^{J}$ is neglected as small. This Hamiltonian contains no diagonal operators, but is rather a 2-quantum operator. A consequence is that a phase shift of all the pulses by $\pi/2$ gives $\mathcal{H}_p' = -\mathcal{H}_p$.

To see why the time reversal sandwich is a useful form for the subcycle of an order selective sequence, consider its average Hamiltonian which can be written

$$\tilde{\mathcal{H}}_{\phi=0}^{(0)} = (\Delta\tau_p'/\Delta\tau_p)\exp(i\mathcal{H}_p T)\mathcal{H}_w \exp(-i\mathcal{H}_p T) \tag{3.75}$$

The norm of this is just

$$\|\tilde{\mathcal{H}}_{\phi=0}^{(0)}\| = (\Delta\tau_p'/\Delta\tau_p)\|\mathcal{H}_w\| \tag{3.76}$$

and thus it can be kept small by keeping $\Delta\tau_p' << \Delta\tau_p$. Typically $\mathcal{H}_w = \mathcal{H}_{int}$; that is $\Delta\tau_p'$ is free evolution.

Unlike $\mathcal{H}_{int}$ however, the operator (3.75) has been transformed by the time reversal sandwich so that it contains operators of all ranks when $\|\mathcal{H}_p\| T \gtrsim 1$. In effect, the dipolar terms ultimately responsible for creating high order coherence have been forced to act nonlinearly. This is the trick necessary to prevent the situation of Figure 27 in which the subcycle creates too little high quantum coherence.

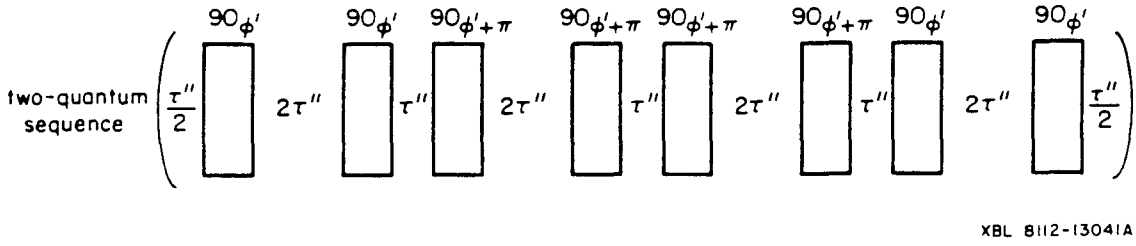

Figure 29. Pulse sequence for creating 2-quantum average Hamiltonian. This sequence of $\pi/2$ pulses gives an average Hamiltonian (3.74) linear in the dipolar couplings, but containing only the nonsecular $n = \pm 2$ operators. The sign of the average Hamiltonian is reversed when all pulses are shifted in phase by $\pi/2$, making it a useful ingredient when time reversal is called for. It is used, for example, in the shaded portions of Figure 28a and Figure 30b.

c. Stretched line narrowing sequences[145,147]. One of the principal applications of AHT has been the development of sequences whose effective Hamiltonian is to a good approximation independent of $\mathcal{H}_{II}^{D}$ [61-63,148,149]. The simplest such sequence, WHH-4,[61] is shown in Figure 28a. While the motivation for these sequences has been to observe chemical shifts in solids they can also be contorted to serve as subcycles for order selective excitation. The most important modification is to stretch out the intervals between pulses so that $\mathcal{H}_{II}^{D}$ is not effectively removed, but shows up in significantly large correction terms. Since these correction terms involve commutators of $\mathcal{H}_{int}(t)$ at several different times, $\mathcal{H}_{II}^{D}$ is once again forced to act in a highly nonlinear fashion. As with the time reversal sandwiches, this gives rise to an effective subcycle Hamiltonian $\mathcal{H}_{\phi}$ whose norm is small and adjustable and which is rich in high order operators. An advantage of such sequences over the time reversal sandwiches is the relative simplicity of the pulse programmer needed to implement them and the lower duty cycle, which minimizes sample heating.

d. Selecting against n = 0 terms in the excitation Hamiltonian. The method of phase cycling as described so far (Sec. IIIC5) selects out of the subcycle Hamiltonians $\mathcal{H}_{\phi}$ the nk-quantum operators which then become the average Hamiltonian $\bar{\mathcal{H}}^{(0)}$ for the cycle as described by (3.69). In the typical application, $n > N/2$ so that the only values of k possible are $k = 0, \pm 1$. Given such an nk-quantum selective Hamiltonian it might seem that the $kn = 0$ transitions would acquire the bulk of the magnetization since they are by far more numerous. This is not necessarily the case for two reasons. First of all the zero quantum operators never appear to first order in τ since zero quantum operators

in $\mathcal{H}$ commute with $\rho(0) = I_z$. Secondly, it is only a subset of the zero quantum transitions which are accessible even to higher order in τ. This is discussed in greater detail in Section IIIC8.

There are, however, two quite distinct reasons for designing sequences which are n-quantum selective, rather than only nk-quantum selective. The first, which has been discussed previously[145], is that by reducing the number of finite matrix elements in the leading terms of the effective Hamiltonian expansion, the size of nonselective correction terms may be reduced. In this view n-quantum selection is primarily important when the selectivity would otherwise be dubious. It is a form of good housekeeping. A chemical analogy would be the wisdom of starting with pure reagents, particularly when the possible reactions of the impurities are not well understood.

The second reason for selecting against zero quantum terms in the effective excitation Hamiltonian is that for many cases, the dynamics becomes qualitatively simpler in their absence. This has nothing to do with selectivity itself. It is as if the removal of a certain reagent led to a totally different and more straight-forward reaction mechanism. These dynamical simplifications are taken up in Sections IIIC8 and IIIC9.

The trick needed to obtain cycles that are n-quantum selective is a combination of phase cycling and time reversal. It is sketched in Figure 30[145]. In part a) an overview of one n-quantum selective cycle is indicated. Each of the 2n blocks is a subcycle obtained from the one to its left by incrementing the overall phase of the radiation by π/n and in addition reversing the sign of the subcycle Hamiltonian, which may require additional phase shifts within the subcycle. The idea here is that the phase shift by π/n gives an extra sign change to the n-quantum terms

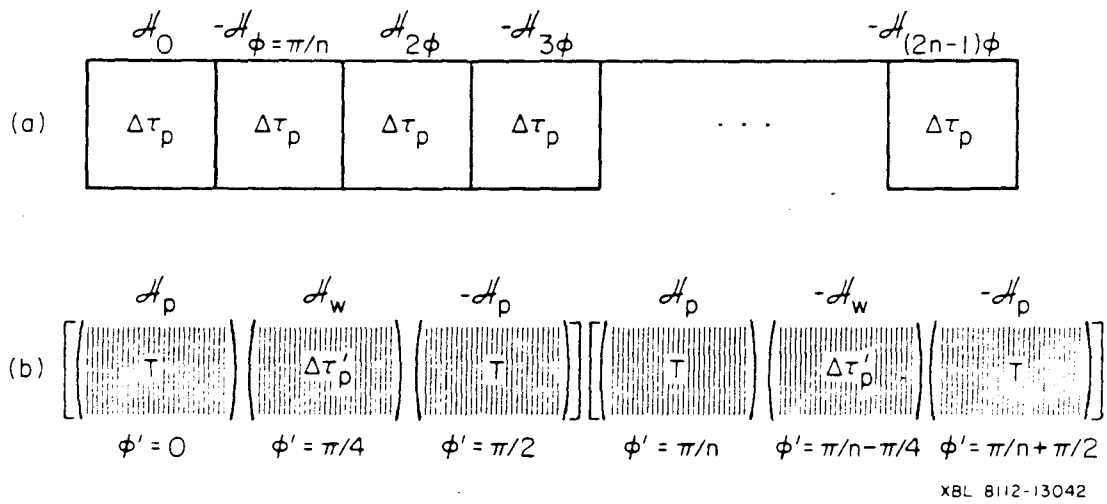

Figure 30. Cycle for zero-order n-quantum selective excitation. This cycle combines phase cycling with time reversal in order to select for orders (2k + 1)n as described in the text. In this way the zero quantum terms are eliminated from the average Hamiltonian $\mathcal{H}^{(0)}$ of the cycle. Part a) shows the block diagram of 2n subcycles indicating phase shifts and time reversals. Part b) shows how the first two subcycles of part a) could be implemented using the 2-quantum pulse sequence of Figure 29.

(and generally $n(2k+1)$-quantum terms) which cancels the overall sign change experienced by all orders. Thus the $n=0$ operators average to zero and only orders $n(2k+1)$ survive in the average Hamiltonian for the cycle.

Figure 30b is an expanded view of the first two blocks in Figure 30a showing how this cycle can be implemented. The closely spaced lines represent the 2-quantum sequence of Figure 29 repeated for the periods of time indicated. The phase ϕ' in that figure is indicated below each use of the sequence in Figure 30b. The relative change of ϕ' by $\pi/2$ between successive periods labeled $\mathcal{H}_p$ and $-\mathcal{H}_p$ creates a time reversal sandwich just as in Figure 28. The relative change of ϕ' by $\pi/4$ between $\mathcal{H}_p$ and $\mathcal{H}_w$ insures that they do not commute and thus high rank operators are created. To date no experiments with this sequence have been reported.

e. A subcycle for liquids. To date homonuclear multiple quantum experiments in liquids[9,12b,29,70,72,80,81,88,92,102-107,127] have been done with nonselective sequences, with frequency selective sequences (Sec. IIC) or at best with sequences selective for even or odd coherence. A subcycle appropriate for liquids has been proposed and demonstrated by computer calculation on the four spin AB_3 system of CH_3OH[150]. The subcycle pulse sequence is simply $(\pi/2)_x - \pi_x - (\pi/2)_x$. A pulse spacing of 12 msec was found to be adequate for $n=4$ in the simulation of the sequence at 270 MHz. Nearly ideal (Sec. IIIC8) preparation of the total spin coherence was found after 576 msec.

7. The Order of Selectivity

a. Overview. The process of phase cycling with some increment of $2\pi/n$ between subcycles was shown in Section IIIC5 to give an effective Hamiltonian $\mathcal{H}$ whose leading term, the average Hamiltonian $\tilde{\mathcal{H}}^{(0)}$, is an nk-quantum operator. This fact alone does not guarantee that any such zero-order selective cycle is useful, since it does not establish that $\tilde{\mathcal{H}}^{(0)}$ has the desired off-diagonal matrix elements nor whether $\tilde{\mathcal{H}}^{(0)}$ is large relative to the other, possibly nonselective terms in the series (3.64), nor even that this series is convergent. To a great extent these concerns are the province of the subcycle design, which was taken up in Section IIIC6.

In this section an experimental example of zero-order nk-quantum selective excitation will be discussed and then a brief review made of sequences which are selective to higher order. A sequence is said to be j-order nk-quantum selective if in the AHT series expansion of its effective Hamiltonian all terms up to and including $\tilde{\mathcal{H}}^{(j)}$ are nk-quantum operators.

b. Zero-order selectivity. An experimental example of order selective excitation on the N = 9 proton system of 1-bromo-butane[98] is shown in Figure 31. The upper trace was obtained with the three pulse sequence of Figure 3 supplemented with a π pulse at $t_1/2$. A single value of $\tau = 4.0$ msec was used for this spectrum, but extensive exploration of other τ values up to several times this value failed to discover substantially more favorable distributions of the magnetization among the lines. As in Figure 18, this is a case where the statistical model of equal average transition intensities gives an approximate picture of the spectral intensity. The lower trace shows a zero-order

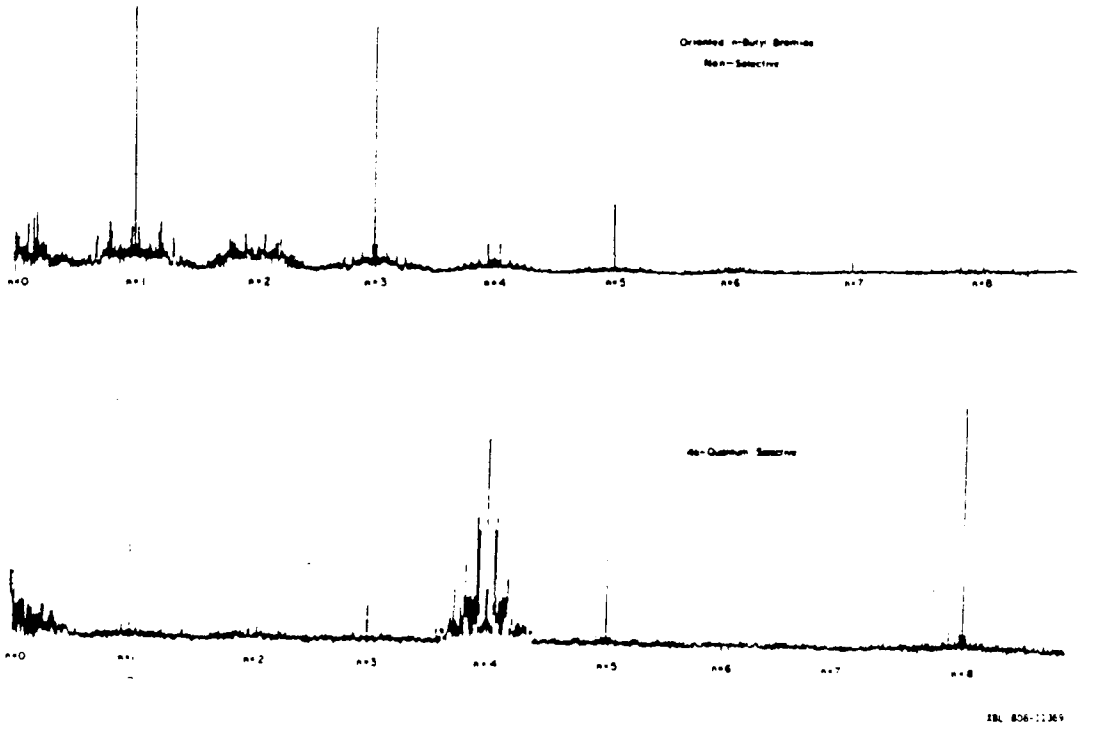

Figure 31. Experimental demonstration of zero-order 4k-quantum selective excitation on an N = 9 proton system. The sample is n-butyl bromide dissolved in the nematic phase of p-octylphenyl-2-chloro-4- (p-heptylbenzoyloxy) benzoate (Eastman 15320). For the upper trace the pulse sequence is the nonselective one of Figure 3 with a π pulse at $t_1/2$ and with τ = 4.0 msec. For the lower trace the order selective pulse sequence is of the form of Figure 4 with a π pulse at $t_1/2$. The excitation (preparation and mixing) periods each consist of two cycles of four phase cycled subcycles. The subcycle form is in Figure 28a with the sequence during T and T' given in Figure 29. The intervals are T = T' = 720 μsec, $\Delta\tau_p'$ = 15 μsec and τ'' = 4.2 μsec. The $\pi/2$ pulses are 3.5 μsec long. The order selective experiment restricts the magnetization to the n = 0, 4, and 8 coherences, thereby increasing their sensitivity.

4k-quantum selective experiment. The enhancement at $n = 4$ and $n = 8$ of about an order of magnitude is qualitatively consistent with the order of magnitude reduction in the number of transitions excited[98]. Much greater enhancements are possible when selecting for n closer to N, as is discussed quantitatively in Section IIIC8. Both 6k-quantum and 8k-quantum sequences have also been demonstrated[146].

It is of some interest to note that though the same number of shots were taken in the nonselective and selective experiments, the noise appears to be somewhat greater in the more complex selective experiment. This was frequently observed[146] and is a manifestation of the multiplicative t_1 noise discussed in Section IIIB3. This problem is not fundamental and can certainly be minimized by the methods mentioned there or eliminated by more stable instruments.

c. First-order selectivity. A well-known theorem from AHT is that a cycle which is symmetric in the sense that

$$\mathcal{H}_{int}(t) = \mathcal{H}_{int}(t_c - t) \tag{3.77}$$

has no contributions $\tilde{\mathcal{H}}^{(j)}$ for odd j[61]. The selectivity of a cycle can thus be extended to $\tilde{\mathcal{H}}^{(1)}$ by symmetrizing it so that this term vanishes. The sense of this symmetrization is shown in Figure 32[145]. Part a) shows again the block diagram of subcycles for zero-order nk-quantum selectivity. The first-order analog is obtained by repeating the same set of subcycles in reverse order.

A schematic illustration of how this improves the selectivity is shown in Figure 33. In part a) is a picture of the trajectory of a $n_{ij} = 1$ coherence amplitude during zero-order 4k-quantum selective

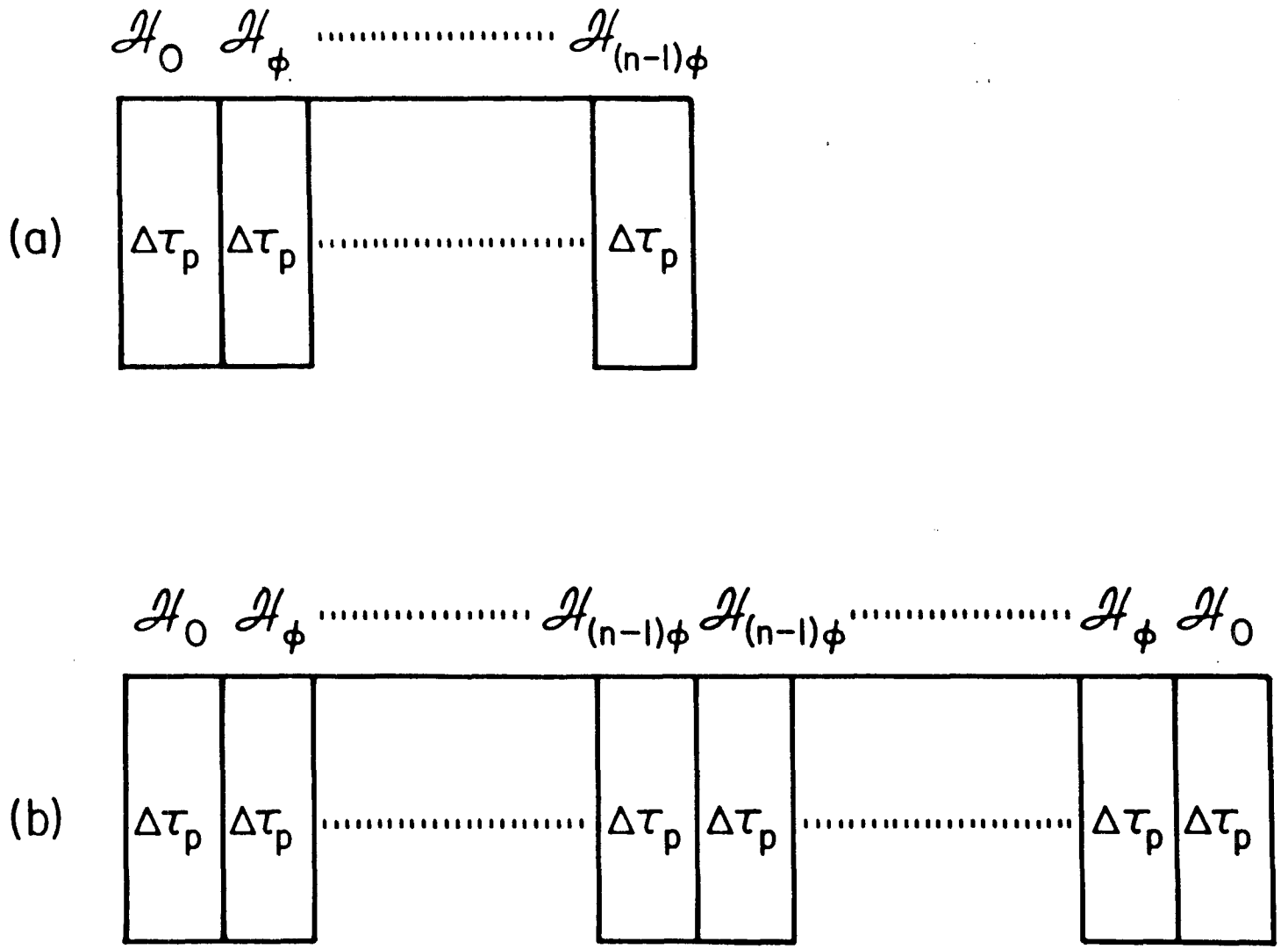

Figure 32 (caption next page)

XBL 803-8899

Figure 32. Subcycle sequence for zero-order and first-order nk-quantum selective excitation. Part a) shows the sequence of n phase cycled subcycles needed for one cycle of zero-order nk-quantum selective excitation, already shown on the left of Figure 24. Part b) shows how the phases are repeated in reverse order to obtain a symmetrized cycle twice as long, which is first-order nk-quantum selective. The extension to sequences selective to arbitrarily high order is obtained by additional levels of phase cycling and symmetrization. For example, repeating the sequence in b) n times with the overall phase cycled gives a second-order nk-quantum selective sequence.

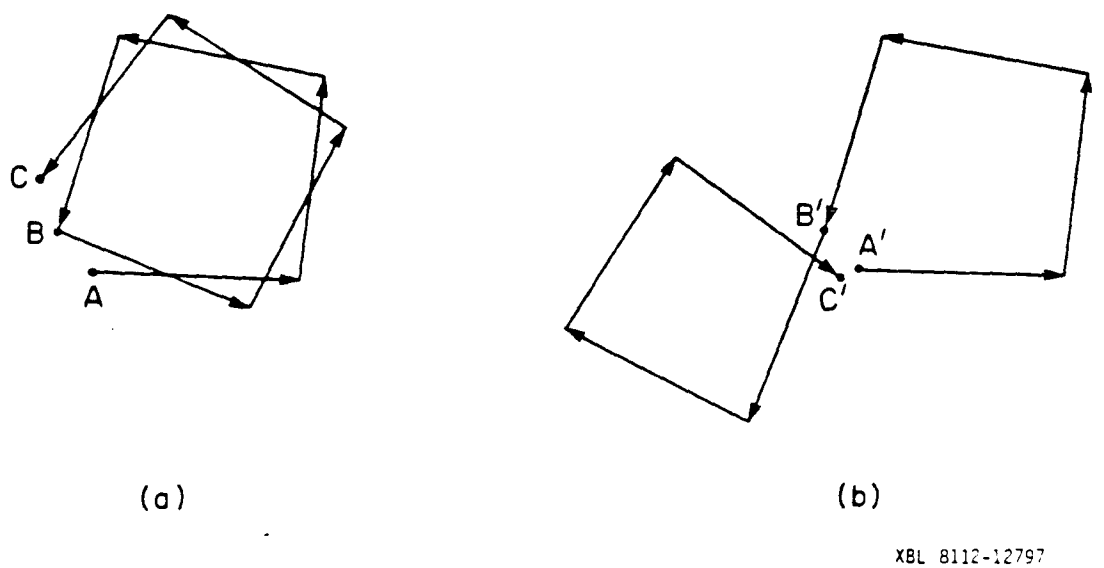

Figure 33. Illustration of the advantage of higher order selective excitation. Part (a) shows the excitation of a nonselected $n_{ij} = 1$ coherence by two repetitions of a zero-order 4k-quantum selective cycle (8 subcycles). The distance AC is a measure of the failure of selectivity. Part (b) shows the improvement of selectivity when the eight subcycles are symmetrized to form a first-order selective sequence. At point B' the phases of the first cycle are repeated in reverse order. The resulting selectivity is greater as indicated by the fact that A'C' < AC. Compare also with Figure 26.

preparation as on the left side of Figure 26, but with the difference that now the trajectory is followed through two cycles or eight subcycles. The distance AC between the final point and the origin is a measure of the failure of the sequence selectivity. In part b) the same eight subcycles occur, but now as a single first-order 4k-quantum selective cycle. Starting at the point marked B' the first four phases are repeated in reverse order. The result is that after the eighth subcycle the selectivity is better than with two zero-order cycles as indicated by the fact that A'C' is shorter than AC.

d. Higher order selectivity[144,145]. By the use of symmetrization and phase cycling, it is possible to construct sequences which are j-order nk-quantum selective for arbitrary j. With the additional assumption of perfect time reversal as used in Figure 30, this may also be done for n-quantum selective sequences. The construction procedure is an iterative one: a sequence which is (j-1)-order nk-quantum selective is used as a subcycle to form through phase cycling a longer cycle which is j-order nk-quantum selective.

Computer calculations[150,151] comparing cycles of different orders of selectivity generally confirm the AHT estimates[145] for the size of nonselective terms. One interesting feature is that when the AHT series (3.64) is not rapidly convergent, it is possible for a sequence which is selective to lower order to actually be more effective at exciting only the desired coherence.

8. Subspace Dynamics and Line Intensities

a. Overview. As demonstrated in Figure 31 order selective excitation leads to greater line intensities than the nonselective sequences. As alluded to in Section IIIB1, this is in part a consequence

of the reduction in the number N_T of possibly finite matrix elements in $\rho(\tau)$. At the same time, though to a lesser extent, the use of selective excitation restricts the fraction of the equilibrium magnetization which can appear in off diagonal elements. An estimate of achievable line intensities requires an assessment of both of these effects. Previous efforts along these lines[145] are corrected here in two respects. The fraction of the magnetization involved in the selective excitation sequences was overestimated for orders $|n| < N$ by overlooking some constants of the motion. On the other hand, a closer look at the dynamics reveals an unforeseen simplicity which indicates that the available magnetization may be efficiently directed to a subset of the selected coherences, thus increasing their magnitudes. The final result is a recalculation of the magnetization per transition optimally available in the high n spectra of systems of N spins 1/2.

b. The available magnetization. As noted in connection with (3.71), the application of an nk-quantum effective Hamiltonian to the equilibrium magnetization (itself an nk-quantum operator) results in an nk-quantum prepared density operator. The reason is easily seen by contemplation of an energy level diagram such as Figure 2. For concreteness ignore the ellipsis in that figure and let it represent an $N = 6$ system. Now imagine that some diagonal initial condition (population differences only) is acted on by a 2k-quantum excitation Hamiltonian. Any coherence prepared must be between states separated by 0, 2, 4, or 6 quanta. A corollary is that the problem decomposes into two independent subspaces even if, as we will assume, there is no permutation symmetry. One subspace involves states of even M (2,0,-2) and the other states of odd M (3,1,-1,-3). No allowed processes connect states in one set with

those in the other. The situation is similar to that of distinct irreducible representations of permutation groups (Sec. IIF1) except that here the extra symmetry is imposed by manipulation of the applied fields.

Now consider the same initial condition, but subjected to a 4k-quantum selective excitation. There are now subspaces consisting of the Zeeman manifolds (3,-1), (2,-2), (1,-3) while the $M=0$ manifold is unconnected to any other. There are now more subspaces but each is simpler. In fact, there are no dynamics in the $M=0$ manifold if $\rho(0) = I_z$, since there are no population differences within this manifold. Thus any off-diagonal elements in $\mathcal{H}$ which connect these equally populated states are not manifested in the dynamics.

Formally, these situations are described by an excitation Hamiltonian $\mathcal{H}$ which is the sum of commuting terms:

$$\mathcal{H} = \sum_q G_q \tag{3.78a}$$

$$[G_q, G_{q'}] = 0 \tag{3.78b}$$

Each of the G_q is also an nk-quantum operator.

The initial condition decomposes in a similar way

$$\rho(0) = \sum_q \rho_q(0) \tag{3.79}$$

and the dynamical problem of the preparation period (2.31) becomes

$$\rho(\tau) = \sum_q \exp(-iG_q\tau)\rho_q(0)\exp(iG_q\tau) \tag{3.80}$$

Now consider one of the subspaces q of interest consisting of two Zeeman manifolds M and M'. If $\rho(0) = I_z$, then

$$\rho_q(0) = M \sum_{M_i=M} |i><i| + M' \sum_{M_j=M'} |j><j| \tag{3.81}$$

Up until now, it has been possible to describe the terms of interest in the density operator by traceless operators. This is a consequence of having suppressed in (2.14) the term proportional to the identity. However,

$$\mathrm{Tr}\rho_q(0) = d_M M + d_{M'} M' \tag{3.82}$$

where d_M and $d_{M'}$ are the dimensions of the manifolds M and M'. The fact that (3.82) is not generally zero (unless M' = -M), means that the initial conditions $\rho_q(0)$ will usually contain a constant of the motion, which is the identity operator within the subspace. It represents magnetization which will never show up as coherence and thus must be disregarded in calculating line intensities.

In order to determine the actual available magnetization it is necessary to discard this subspace identity operator and examine what is left. In other words we are concerned with the subspace of traceless operators $SU(d_M + d_{M'})$. Define an operator within this subspace.

$$\sigma_q(0) \equiv \rho_q(0) - \alpha\, 1 \tag{3.83}$$

Its trace is

$$\mathrm{Tr}\sigma_q(0) = d_M M + d_{M'} M' - (d_M + d_{M'})\alpha \tag{3.84}$$

Setting this to zero and solving for α gives

$$\alpha = (d_M M + d_{M'} M')/(d_M + d_{M'}) \tag{3.85}$$

The relevant magnetization is proportional to

$$\mathrm{Tr}(\sigma_q^2(0)) = d_M(M-\alpha)^2 + d_{M'}(M'-\alpha)^2 \tag{3.86}$$

These are objects of the form of (3.22). After some preparation period has elapsed this quantity is distributed with the constraint

$$\sum_{ij} |\sigma_{qij}(\tau)|^2 = \mathrm{Tr}(\sigma_q^2(\tau)) = \mathrm{Tr}(\sigma_q^2(0)) \tag{3.87}$$

A convenient dimensionless way of expressing this quantity is as a fraction of the total magnetization:

$$f_q = \mathrm{Tr}(\sigma_q^2(0))/\mathrm{Tr}(I_z^2) \tag{3.88}$$

This quantity will now be evaluated for some of the cases relevant to selective excitation of high n transitions. The simplest case[145] is the total spin coherence n = N. The manifolds M = N/2 and M' = -N/2 contain only one state each and $\alpha = 0$. Setting the label q to N this is

$$f_N = 2(N/2)^2/(N2^N/4) = N/2^{N-1} \tag{3.89}$$

The next simplest case is the subspace formed by the level M = N/2 and M' = -(N/2) + 1 under (N-1)k-quantum selective excitation. Here $\alpha = N(3-N)/2(N+1)$ (if there is no permutation symmetry) and the available fraction of the total magnetization is

$$f_{N-1} = \frac{N(N-1)^2}{(N+1)} /(N2^N/4) = (N-1)^2/(N+1)2^{N-2} \tag{3.90}$$

An identical result holds for the (M = -N/2, M' = (N/2)-1) subspace.

The next case is that of (N-2)k-quantum selection. Here there are three contributing subspaces as already discussed above for the particular case N = 6. The two subspaces ($M = \pm N/2$, $M' = \mp((N/2)-2)$) give rise to $|n| = N-2$ lines which all belong to the A_1 irreducible representation. The calculation for these subspaces is similar to that above for $n = N-1$.

The other subspace ($M = (N/2)-1$, $M' = 1-(N/2)$) will include lines of other irreducible representations than A_1, if such exist, and thus allows location of $|M| = (N/2)-1$ states not involved in the $|n| = N-1$ spectrum. For concreteness, the case of no permutation symmetry (all A_1 states) will be adhered to. The calculation is particularly simple since $M' = -M$ and $\alpha = 0$. From (3.86) and (3.88)

$$f_{N-2,|M|=((N/2)-1)} = 2N((N/2)-1)^2/(N2^N/4) \tag{3.91a}$$

$$= 8((N/2)-1)^2/2N \tag{3.91b}$$

With the fraction f_q in hand for a given subspace the next step is to consider how it is distributed among the accessible matrix elements appearing in the sum (3.87). Without any further insight into the dynamics, the parsimonious approach is to apply the statistical model within each subspace. The number of independent operators is just

$$N_{Tq} = (d_M + d_{M'})^2 - 1 \tag{3.92}$$

and, of course, includes in general more $n = 0$ operators than the high n operators of primary interest. Dividing this into (3.86) gives a subspace analog of (3.23). Dividing it into (3.88) gives an estimate of the fraction of the total magnetization at $t_2 = 0$, which will oscillate at some selected ω_{ij} as a function of t_1.

c. Dynamical simplifications for n-quantum selection.

These statistical estimates assume that the subspace excitation dynamics are sufficiently complex that using one value of τ is as good as another. In Section IIIB1d a search method was discussed for nonselective excitation and similar methods are also appropriate with selective excitation. Since the Liouville space has been vastly constrained, the search becomes much easier than for nonselective excitation and thus applicable to larger systems.

In the remainder of this section it will be demonstrated that if the excitation Hamiltonian is not merely nk-quantum, but n-quantum (Sec. IIIC6d) then the dynamics of certain subspaces undergoes a great simplification which guarantees a more efficient excitation of high order coherence after a very simple search.

The subspaces for which this simplification is possible are those consisting of two Zeeman manifolds and for which $d_M = 1$ and $d_{M'}$ has any value. In the following $M = N/2$ will be assumed, but the same situation could occur with other manifolds, if there is only one state belonging to a particular irreducible representation.

Given these conditions the form of the effective excitation Hamiltonian within the subspace is

$$G_q = \sum_i c_i^* |N/2\rangle\langle i| + c_i |i\rangle\langle N/2| \tag{3.93a}$$

$$= (\omega_e/2)(|N/2\rangle\langle h_0| + |h_0\rangle\langle N/2|) \tag{3.93b}$$

where (3.93b) uses the definition

$$(\omega_e/2)|h_0\rangle = \sum_i c_i |i\rangle \tag{3.94}$$

Radiation-matter interactions of the form (3.93) have already been discussed as models of optical[152-153] excitation and have been called quasi-two-level systems (QTLS)[153]. The states $|i\rangle$ are the eigenstates of $\mathcal{H}_1$ in the M' manifold while $|N/2\rangle$ is the sole M = N/2 state. The form (3.93a) simply states that there are no diagonal elements in G_q and no off-diagonal elements within the M' manifold. These vanishing elements are zero quantum operators and are assumed to have been eliminated by construction of the excitation sequence. The state $|h_0\rangle$ is a linear combination of some or all of the M' eigenstates. If it is taken to be normalized then

$$\omega_e = 2\left(\sum_i |c_i|^2\right)^{\frac{1}{2}} \tag{3.95}$$

The calculational device being used here is sketched in Figure 34. Four states $|i\rangle$ are shown on the left in the manifold M'. The restriction M' < 0 is necessary, since if M' is not more than halfway up the energy level diagram there would be one or more manifolds above, which would also be part of the subspace q. The case M' = 0 is treated in Section IIIC9. In the center of the figure the transformation (3.94) has been indicated. The many states $|i\rangle$ are replaced by the one state $|h_0\rangle$ effectively making the dynamics like that of a two level system. This however, is not the basis relevant to the evolution period so a transformation back to the eigenbasis $\{|i\rangle\}$ of $\mathcal{H}_1$ is necessary to see exactly what has happened. As indicated by the arrows on the right, coherence between the manifolds has been created. Not indicated in the figure is that n = 0 coherence within M' is also created.

To see how all this comes out further calculation is needed. The form of (3.93b) is familiar. It shows that G_q is proportional to a

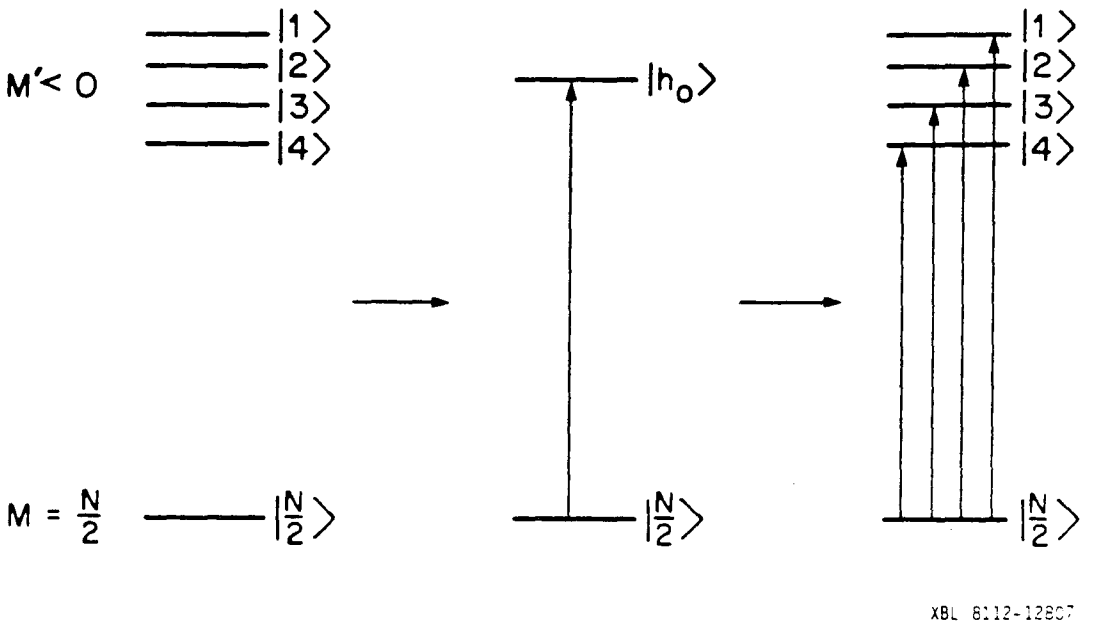

Figure 34. Schematic illustration of how n-quantum selective excitation leads to quasi-two-level dynamics. When the only matrix elements of the excitation Hamiltonian are between a single state and any manifold of states, the manifold can be replaced by a single state $|h_0\rangle$ as in the center and the dynamics occurs with a single frequency. Final expansion in the eigenbasis of the evolution period is indicated on the right and shows that coherence has been created between the single state and all those within the manifold which made finite contributions to $|h_0\rangle$.

single pseudo-spin operator:

$$I_x^{N/2,h_0} = (\tfrac{1}{2})(|N/2\rangle\langle h_0| + |h_0\rangle\langle N/2|) \tag{3.96}$$

The other operators needed to form an angular momentum are

$$I_y^{N/2,h_0} = -i/2(|N/2\rangle\langle h_0| - |h_0\rangle\langle N/2|) \tag{3.97}$$

and

$$I_z^{N/2,h_0} = (\tfrac{1}{2})(|N/2\rangle\langle N/2| - |h_0\rangle\langle h_0|) \tag{3.98}$$

This suggests rewriting the initial condition (3.83) to include $I_z^{N/2,h_0}$. This may be done using (3.81) and the subspace identity operator in the form

$$\underset{\approx}{1} = \sum_{k=0}^{d_{n'}-1} |h_k\rangle\langle h_k| + |N/2\rangle\langle N/2| \tag{3.99}$$

Here the set $\{|h_k\rangle\}$ is any orthonormal basis spanning the M' manifold and including $|h_0\rangle$. The desired form is

$$\sigma_q(0) = ((N/2)-\alpha)|N/2\rangle\langle N/2| + (M'-\alpha)\sum_{k=0}^{d_{m'}-1} |h_k\rangle\langle h_k| \tag{3.100a}$$

$$= ((N/2)-M')\, I_z^{N/2,h_0} + (\tfrac{1}{2})(N/2+M'-2\alpha)(|N/2\rangle\langle N/2| + |h_0\rangle\langle h_0|)$$

$$+ (M'-\alpha)\sum_{k=1}^{d_{M'}-1} |h_k\rangle\langle h_k| \tag{3.100b}$$

It is easy to see that the last two terms of (3.100b) commute with G_q and thus are constants of the motion. Only the first term develops in time and this is simply:

$$\exp(-iG_q\tau)I_z^{N/2,h_0}\exp(iG_q\tau) = I_z^{N/2,h_0}\cos\omega_e\tau + I_y^{N/2,h_0}\sin\omega_e\tau \quad (3.101)$$

Using this identity and rearranging terms gives

$$\begin{aligned}\sigma_q(\tau) = {} & ((N/2)-M')I_y^{N/2,h_0}\sin\omega_e\tau \\ & + \tfrac{1}{2}[((N/2)-M')(\cos\omega_e\tau-1) + (N-2\alpha)]|N/2\rangle\langle N/2| \\ & + \tfrac{1}{2}[((N/2)-M')(1-\cos\omega_e\tau)]|h_0\rangle\langle h_0| \\ & + (M'-\alpha)\sum_{k=0}^{d_{M'}-1}|h_k\rangle\langle h_k| \end{aligned} \quad (3.102)$$

The remarkable result for this QTLS model is that excitation dynamics occur with a single frequency ω_e. The time τ may be chosen as $(\pi/2\omega_e)$ to simultaneously maximize all of the $|n| = ((N/2)-M')$ coherences in the first term. At twice this length the $n = 0$ coherence within M' are maximized. These are contained in the $|h_0\rangle\langle h_0|$ term. The summation term is the identity operator within the M' manifold and contains no coherence.

In fact if preparation and mixing are identical (within a phase shift) then the $n = (N/2) - M'$ lines arising from this subspace have magnitudes

$$|\sigma_{qi(N/2)}(\tau)|^2 = n^2\sin^2(\omega_e\tau)|\langle i|I_y^{N/2,h_0}|N/2\rangle|^2 \quad (3.103a)$$

$$= n^2\sin^2(\omega_e\tau)c_i^2/4 \quad (3.103b)$$

The relative line intensities for these transitions are independent of τ and specify the magnitude of the coefficients c_i, which usually will not be known in advance because of the complexity of the pulse sequences giving rise to G_q.

Also, since (3.93) satisfies (3.7) with $\phi = \pi/n$, the lines can be obtained in phase.

A computer simulation of excitation dynamics of the type expressed in (3.102) is shown in Figure 35. The system is three dipolar coupled spins and the effective excitation Hamiltonian is $\mathcal{H} = (1/3)(\mathcal{H}_{II}^{D,yy} - \mathcal{H}_{II}^{D,xx})$ obtained by the sequence of Figure 29. The program, which is described elsewhere[118], actually calculates directly from the input pulse sequence and does not use AHT. The curves of Figure 35 are exactly what would be seen in an excitation function experiment (e.g., Fig. 21d) performed with this 2-quantum sequence and fixed t_1, as τ is incremented from 0 to 25 cycles. The solid line shows the sum over all n = 2 transitions. This is twice the sum over i in (3.103b) because the isomorphic (M = -3/2, M' = 1/2) subspace is also included. The dotted line shows the $(1-\cos\omega_e\tau)^2$ dependence of the n = 0 signal magnitude.

d. Optimum line intensities. It is important to note that the $|n|$ quantum transitions all arise from the first term of (3.100b) and their sum is not Tr $\sigma_q^2(0)$ but only the contribution to this quantity from this first term. This is just $n^2/2$ and is shared by the $2d_{M'}$ matrix elements within the subspace which correspond to ±n-quantum coherence

Similarly the n = 0 coherence comes entirely from the other two terms of (3.100b). An upper bound on its total intensity can be obtained from the fact that the trace of the square of the third term of (3.102) is n^2 when $\cos\omega_e\tau = -1$. However, this term also contains population operators when transformed back to the eigenbasis $\{|i\rangle\}$ and the fraction of its norm that corresponds to off-diagonal operators will depend on the distribution of the c_i.

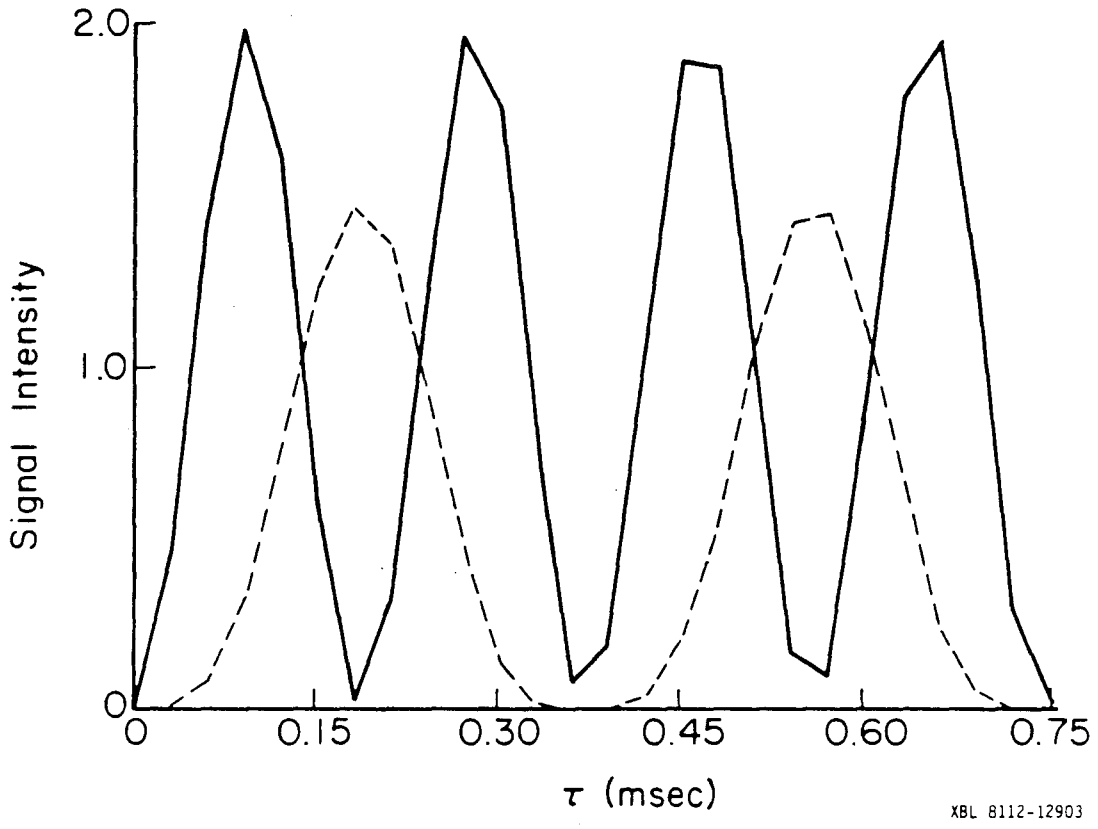

Figure 35. Computer simulation showing the simple dynamics for n-quantum selective excitation when one of the two Zeeman manifolds which form the subspace contains a single state. The system is three coupled spin 1/2 nuclei with dipolar couplings in Hz of $D_{12} = -500$, $D_{13} = 1000$, and $D_{23} = -750$. The excitation pulse sequence is that of Figure 29 with δ function pulses and $\tau'' = 5$ μsec. The curves are the $n = 2$ (solid) and $n = 0$ (dashed) excitation functions (Sec. IIIB1d) and are proportional to $\sin^2\omega_e\tau$ and $(1 - \cos\omega_e\tau)^2$, respectively, as explained in the text. Each curve is composed of 26 discrete points connected by straight lines. This illustrates the restriction that τ must be incremented in units of a cycle time in order to apply average Hamiltonian theory. The computer program calculates directly from the pulse sequence and does not use average Hamiltonian theory.

To summarize this in a useful form Figure 36 shows the log of the fractional magnetization per allowed transition for a system of N spins 1/2 with no permutation symmetry and assuming ideal n-quantum selective excitation. For the n = N and n = N-1 curves the QTLS considerations of the last paragraphs apply and perfect n-quantum $\pi/2$ pulses are assumed. This is also true for those n = N-2 transitions which involve the states $|M| = N/2$ and these give the lower of the two lines labelled n = N-2. The other n = N-2 transitions are between the manifolds $M = \pm(1-N/2)$ and the statistical model was applied within the subspace as described in Section IIIC8b. For these transitions the prediction would be the same for n-quantum or nk-quantum selective excitation, since no ability to preferentially direct coherence to particular operators within the subspace is assumed, though it seems likely the n-quantum selective dynamics might be simpler than nk-selective here also.

For comparison the totally nonselective multiple quantum experiment is also included in Figure 36. The ratios between the various high order lines and the nonselective line are the gain factors G of Section IIIB2. They grow exponentially with N.

The analogous quantity for n = 1 is also included in Figure 36. The comparison to the single quantum experiment is complicated by the fact that it is normally a one dimensional experiment and so does not suffer from the factor r_{2D} given by (3.34). For the multiple quantum and single quantum lines shown to be directly comparable, the single quantum experiment would need to be done two dimensionally. As noted in Section IIIA2 this could actually be advantageous for large N since it allows pulsed spin locking in t_2. To obtain a measure of relative experimental time needed for the different experiments, the quantities

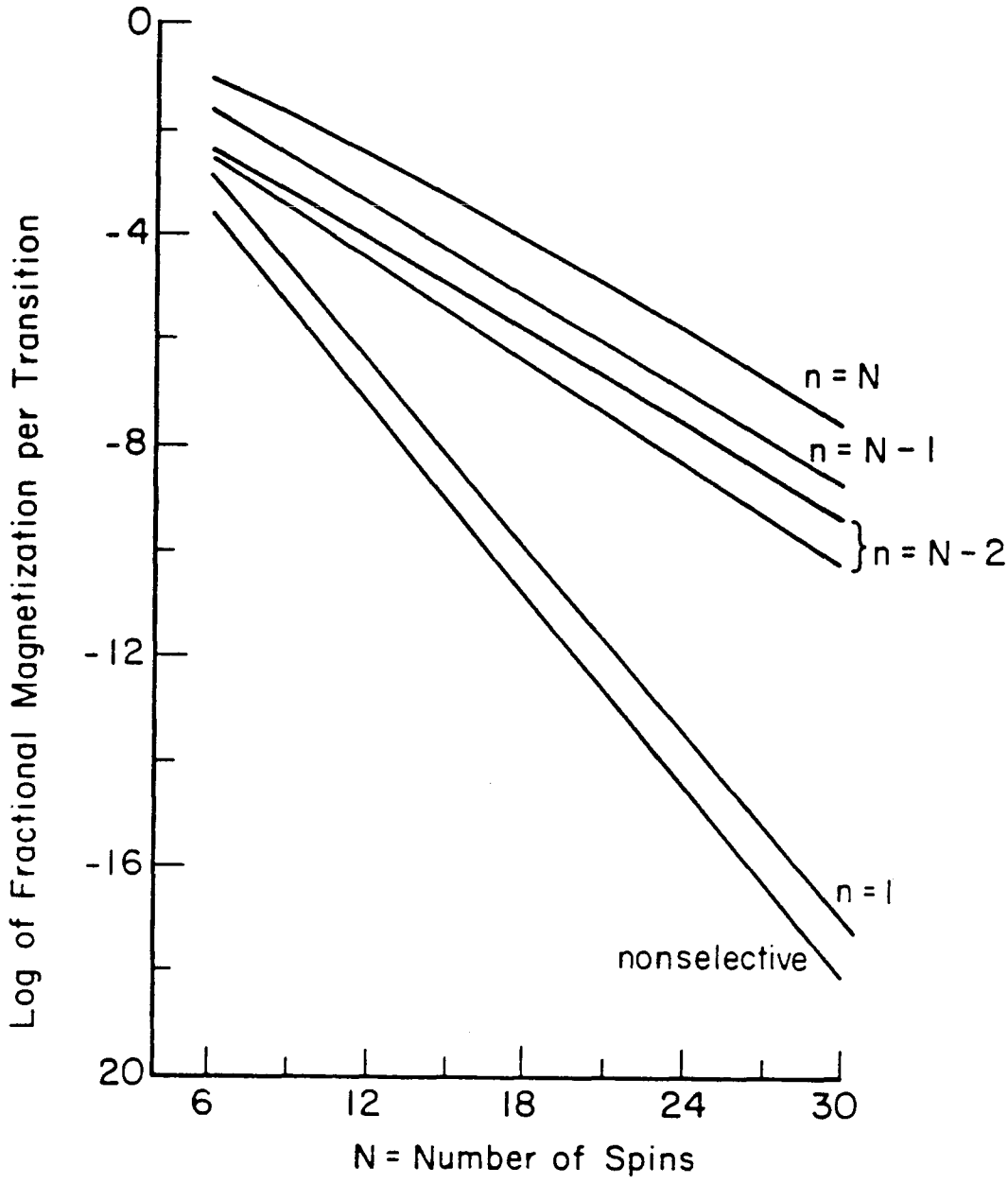

XBL 8112-12806

Figure 36. The logarithm of the fractional magnetization per transition for various ideal types of excitation as a function of the number of spins. In each case the ordinate is the logarithm of the observed signal magnitude of a nondegenerate resolved transition expressed as a fraction of the total magnetization of the coupled system of N spins 1/2, which is assumed to have no permutation symmetry. The highest curve is for the total spin transition n = N and is the function log ($N2^{-N}$). The curve

(cont. next page)

Figure 36 (cont.)

for n = N-1 assumes n-quantum selective excitation as does the lower of the two n = N-2 curves, which applies to the subspaces ($M = \pm N/2$, $M' = \mp((N/2)-2)$). These curves are $\log ((N-1)^2/N^2 2^{N-1})$ and $\log ((N-2)^2/N^2(N-1)2^{N-1})$ respectively. The upper n = N-2 curve applies to the subspace ($M = ((N/2)-1)$, $M' = -((N/2)-1)$) and assumes only nk-quantum selective excitation and gives equal weight to n = 0 operators within the subspace. The function is $\log ((N/2)-1)^2/(4N^2-1)2^{N-3})$. The next lowest curve is for single quantum excitation by a single $\pi/2$ pulse. The curve is $\log ((N-1)!(N+1)!/(2N)!)$. The lowest curve is nonselective excitation with the statistical model. The curve is $\log (1/(4^N-1))$. Comparison of the n = 1 curve with the curves for the multiple quantum experiments is complicated by factors of the order of unity, which arise from the one dimensional nature of the usual single quantum experiment,but more importantly the density of single quantum lines would prevent the observation of a resolved transition over nearly this entire range of N. Thus high order multiple quantum experiments are the only alternatives for such observations.

here would need to be squared so as to be proportional to signal energy (Sec. IIIA2).

Even taking into account the correction (3.34) needed to compare 1D and 2D signal energies, it is evident that the high order transitions are observable with greater sensitivity than the average, resolved single quantum transition in systems of several or more spins. This contradicts the common notion born of perturbation theory that higher order processes are in some sense always weak. On the other hand, it really should be no surprise that a transition between states separated by several times the Larmor frequency should be easier to detect than one involving a lesser energy. Of course, the foregoing assumes that the selective excitation can be achieved before irreversible relaxation dominates. This is discussed further in Section VA.

9. Selective Population Inversion

a. Motivation. The emphasis in the previous sections has been on the selective excitation of off-diagonal density matrix elements since it is these that lead to spectral information in ω_1. However, for T_1 studies (Sec. VB) it can be valuable to prepare various diagonal nonequilibrium initial conditions. The selective preparation of such conditions also serves as a simple model for optical frequency systems where nonequilibrium population could be the basis for laser action or selective photochemistry. Finally, it may prove possible to use such selectively inverted states as an initial condition for a single quantum experiment wherein only a small fraction of the lines are observed.

b. Two level and quasi-two-level systems. Population inversion of two levels by a frequency selective double quantum pulse[55]

was already mentioned in Section IIC2. For any of situations where the excitation dynamics is restricted to a subspace of two states, the inversion of their populations is an n-quantum π pulse and simply means exciting for twice as long as is necessary to optimally transfer a population difference to n-quantum coherence. In Figure 37 such a pulse is illustrated schematically for the total spin coherence of N spins 1/2. The equilibrium populations in the high temperature limit are suggested on the left by the constant increment in the number of circles in going from one Zeeman manifold to the next. Only one level is shown in each manifold. The situation after an ideal N-quantum π pulse is shown on the right. The populations of the extreme levels are exchanged without affecting those levels in between[145]. No coherence is prepared.

The situation is somewhat more complicated in the QTLS discussed in the previous section. Substituting $\omega_e \tau = \pi$ into (3.102) shows that the coefficients of $|N/2\rangle\langle N/2|$ and $|h_0\rangle\langle h_0|$ are exchanged, but this density operator is not purely diagonal within the M' manifold.

c. The quasi-four-level system (QFLS). There is another way of exchanging the populations of the extreme states which is illustrated in Figure 38. In part a) the N-quantum π pulse already discussed is indicated. In part b) an N/2 quantum process is indicated which proceeds via the intermediate M = 0 states. As will be demonstrated below, such a process is also capable of exchanging the populations of the extreme states. However, since there will be simultaneous N/2 excitation in other subspaces not indicated in Figure 38, this exchange will not leave the system in the diagonal state suggested by the right side of Figure 37. Rather there will be disturbances in certain of the intermediate manifolds.

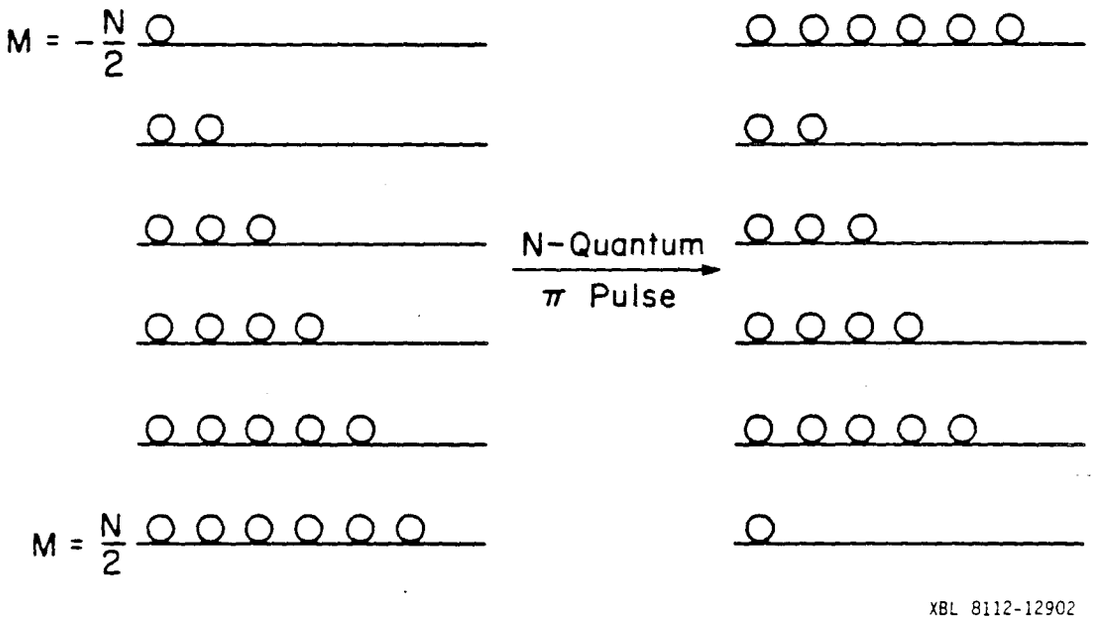

Figure 37. Population inversion by an N-quantum pulse. Order selective excitation ideally can exchange the populations of the extreme states without disturbing those of intermediate manifolds.

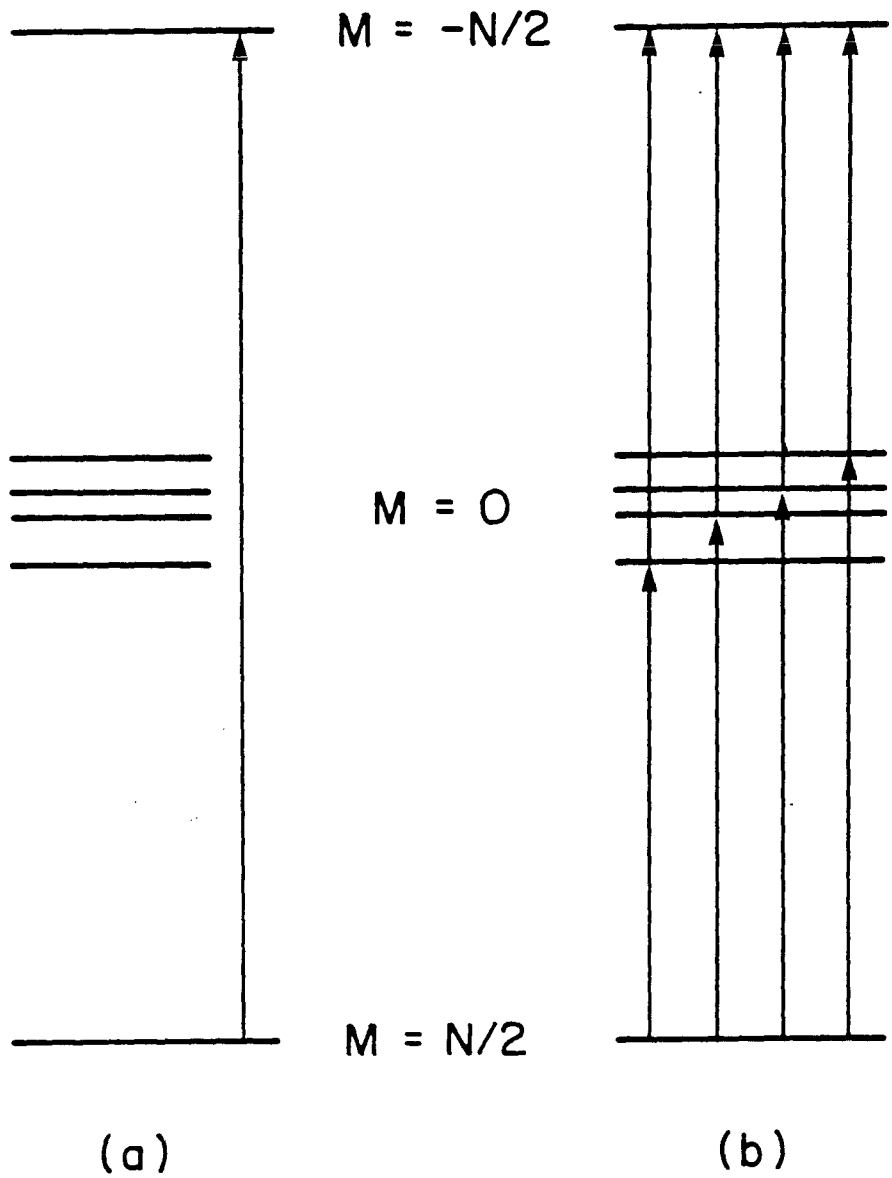

XBL 8112-12901

Figure 38. Two methods of exchanging the populations of the extreme states. In part a) N-quantum selective excitation is indicated as in Figure 37. In part b) N/2-quantum selective excitation is indicated. This also exchanges the extreme populations, but acts in addition to excite N/2 quantum coherence between other pairs of manifolds not shown.

The principle motivation for considering such a scheme at all is that the complexity and duration of a high order excitation sequence increases with N and may be ineffective when a sequence selective for $n \leqslant N/2$ is still practical. The N/2-quantum selective scheme discussed below could, because of its very simple dynamics be a useful ingredient in composite sequences for exciting high order coherence by juxtaposing sequences selective for lower orders.

To start, consider the possible form for an N/2-quantum Hamiltonian operator $G_{N/2}$ within the Liouville subspace formed by the three manifolds $M = N/2, 0, -N/2$. It will be convenient to use the operators of definite parity of the form tabulated in Table 1 (Sec. IIF2). Since $G_{N/2}$ is N/2-quantum, only the off-diagonal operators are relevant. Since any term involves either $|N/2\rangle$ or $|\overline{N/2}\rangle = |-N/2\rangle$, we can set $|i\rangle = |N/2\rangle$.

Now assume that G is not only N/2-quantum, but has definite parity. For concreteness assume

$$\Pi_x \, G_{N/2} \, \Pi_x^{\dagger} = G_{N/2} \tag{3.104a}$$

$$\Pi_y \, G_{N/2} \, \Pi_y^{\dagger} = (-)^{N/2} \, G_{N/2} \tag{3.104b}$$

This is not an unreasonable restriction, since for example, the subcycle average Hamiltonian (3.75) (Fig. 28a) satisfies this condition and it is easy to show that this property survives the process of phase cycling and time reversal. The average Hamiltonian for n-quantum selective cycles formed as in Figure 31 also can have definite parity.

Given (3.104) Table 1 shows that $G_{N/2}$ can be expanded in operators of the form $I_{x+}^{N/2,j}$ and $I_{y+}^{N/2,j}$ only. Recalling from Section IIIC3 that the $M = 0$ states may themselves be chosen to have definite parity, it is

convenient to use two labels within this manifold. Let j be used for the gerade states, which satisfy

$$\overline{|j\rangle} = |j\rangle \tag{3.105a}$$

and k be used for the ungerade states, which satisfy

$$\overline{|k\rangle} = -|k\rangle \tag{3.105b}$$

Thus $G_{N/2}$ is a sum of the form:

$$G_{N/2} = \sum_j (x_j\ I_{x+}^{N/2,j} + y_j\ I_{y+}^{N/2,j}) + \sum_k (x_k\ I_{x+}^{N/2,k} + y_k\ I_{y+}^{N/2,k}) \tag{3.106}$$

where together the indexes j and k span the M = 0 manifold.

With this understood, the relevant operators of definite parity take the form

$$I_{x+}^{N/2,j} = (\tfrac{1}{2})[(|N/2\rangle + |-N/2\rangle)\langle j| + |j\rangle(\langle N/2| + \langle -N/2|)] \tag{3.107a}$$

$$= (2)^{-\frac{1}{2}}\ (|N/2\rangle^{+}\langle j| + |j\rangle\langle N/2|^{+}) \tag{3.107b}$$

and similarly

$$I_{x+}^{N/2,k} = (2)^{-\frac{1}{2}}\ (|N/2\rangle^{-}\langle k| + |k\rangle\langle N/2|^{-}) \tag{3.108}$$

$$I_{y+}^{N/2,j} = -i(2)^{-\frac{1}{2}}\ (|N/2\rangle^{+}\langle j| - |j\rangle\langle N/2|^{+}) \tag{3.109}$$

$$I_{y+}^{N/2,k} = -i(2)^{-\frac{1}{2}}\ (|N/2\rangle^{-}\langle k| - |k\rangle\langle N/2|^{-}) \tag{3.110}$$

The new combinations of states

$$|N/2\rangle^{\pm} = (\tfrac{1}{2})^{-\frac{1}{2}}(|N/2\rangle \pm |N/2\rangle) \tag{3.111}$$

have been introduced, which are gerade (+) or ungerade (-). Now define within the M = 0 manifold the combinations

$$\omega_+|h_0^+\rangle = (2)^{-\frac{1}{2}} \sum_j (x_j + iy_j)|j\rangle \tag{3.112a}$$

and

$$\omega_-|h_0^-\rangle = (2)^{-\frac{1}{2}} \sum_k (x_k + iy_k)|k\rangle \tag{3.112b}$$

With this substitution (3.106) becomes

$$G_{N/2} = \omega_+(|N/2\rangle^+\langle h_0^+| + |h_0^+\rangle\langle N/2|^+)$$

$$+ \omega_-(|N/2\rangle^-\langle h_0^-| + |h_0^-\rangle\langle N/2|^-) \tag{3.113a}$$

$$= 2\omega_+ I_x^{(N/2)^+,h_0^+} + 2\omega_- I_x^{(N/2)^-,h_0^-} \tag{3.113b}$$

This is a sum of two commuting terms, which already suggests the dynamics will be simple. In order to make use of this form the relevant part of the initial condition $\rho(0) = I_z$ must be written in this basis set. The desired operator is

$$\sigma_{N/2}(0) = (N/2)(|N/2\rangle\langle N/2| - |-N/2\rangle\langle -N/2|) = NI_z^{N/2,-N/2} \tag{3.114a}$$

$$= (N/2)(|N/2\rangle^+\langle N/2|^- + |N/2\rangle^-\langle N/2|^+) = NI_x^{(N/2)^+,(N/2)^-} \tag{3.114b}$$

Notice that (3.114a) is the form that would be useful for treating the two level problem of N-quantum selection. Here the form (3.114b) propagated under (3.113b) leads to the prepared subspace density operator

$$\sigma_{N/2}(\tau) = N(I_x^{(N/2)^+,(N/2)^-} \cos\omega_+\tau \cos\omega_-\tau$$

$$- I_y^{(N/2)^+,h_0^-} \cos\omega_+\tau \sin\omega_-\tau$$

$$- I_y^{(N/2)^-,h_0^+} \sin\omega_+\tau \cos\omega_-\tau$$

$$+ I_x^{h_0^+,h_0^-} \sin\omega_+\tau \sin\omega_-\tau) \qquad (3.115)$$

The second and third terms of (3.115) are $|n| = N/2$ coherence involving, respectively, the ungerade and gerade states in $M = 0$. The last term is $n = 0$ coherence between gerade and ungerade states. Since there is no reason to expect ω_+ and ω_- to be commensurable, it is not necessarily possible to choose τ so that only one term of (3.115) survives. Nevertheless this situation can be closely approached.

The simplest example of such dynamics is provided by the effective Hamiltonian (3.74) in an $N = 4$ system. Figure 39 shows the computed dependence of the population difference between the extreme states for a system of four dipolar coupled spins. The displayed points are calculated at the end of integral numbers of cycles and closely trace out the expected $\cos\omega_+\tau \cos\omega_-\tau$ dependence. One of the frequencies happens to be about 9 times the other. At the point indicated by the arrow the slower function has proceeded through $\sim\pi$ radians and the faster one through $\sim 9\pi$ so that population inversion is nearly achieved.

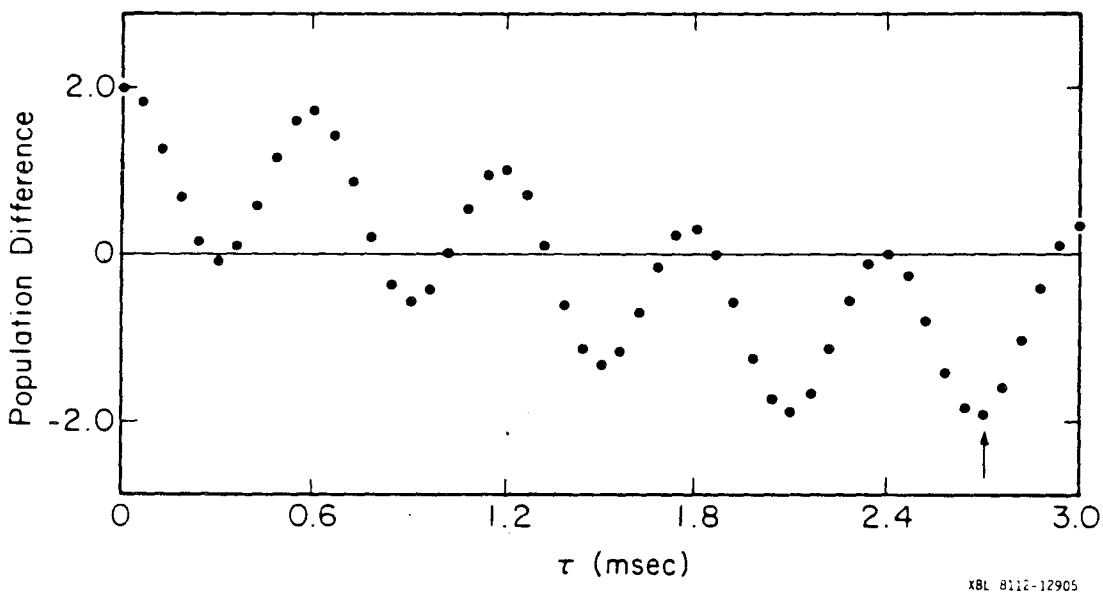

Figure 39. Inversion of the N-quantum population difference by (N/2)-quantum selective excitation. The population difference oscillates with only two Fourier components even though many intermediate levels in the M = 0 manifold are involved. The dynamics may be described in terms of a quasi-four-level system. The arrow indicates a point where the initial equilibrium population difference, which on this scale is 2.0, has nearly inverted to become -1.94. The system consists of four spin 1/2 nuclei with dipolar couplings in Hz of $D_{12} = -500$, $D_{13} = -1000$, $D_{14} = -750$, $D_{23} = -625$, $D_{24} = -250$ and $D_{34} = 750$. The population difference between the M = 2 and M = -2 levels was computed after each of 50 cycles of the pulse sequence of Figure 29 with $\tau'' = 5$ μsec.

IV. MULTIPLE QUANTUM PROCESSES WITH TWO SPIN SPECIES

A. Motivation

1. Doubly Rotating Frame Formalism

The possibilities for fruitful multiple quantum experiments multiply rapidly when two or more nuclear spin species are present in a coupled spin system. The heteronuclear topics covered here have as a common characteristic that at least one of the nuclear species evolves in a state of multiple quantum coherent superposition. Excluded are the many double resonance studies where the multiplicity of quanta is only a consequence of using a second frequency to tickle or decouple. The technique of double quantum decoupling was already reviewed in Section IIC2f. Included are the study of transitions in which one species flips in the field of another, in which the two coupled species flip independently, and in which the two species are coherently driven to exchange spin order in a concerted fashion.

In order to discuss these matters some additions to the notation introduced in Section II are needed. The starting point is the doubly rotating frame. This is the interaction representation in which the time dependence of the irradiation at or near each of the Larmor frequencies is removed. In typical applications the presence of two rf fields causes no particular complications; to a good approximation each spin species only responds to the one field which is nearly resonant. At high applied fields or in high resolution experiments, Bloch-Siegert shifts[62,154,155] of order $\omega_p^2/(\omega_o^I - \omega_o^S)$ may cause a noticeable shift of resonance of one species as the other is irradiated. Setting these aside, the Hamiltonian which replaces (2.7) is

$$\mathcal{H}_{rf} = -\omega_p^I I_{\psi_I} - \Delta\omega_I I_z - \omega_p^S S_{\psi_S} - \Delta\omega_S S_z \tag{4.1}$$

Similarly (2.9) is replaced by

$$\mathcal{H}^z = -\sum_i \omega_{zi} I_{zi} - \omega_z(\vec{r}) I_z - \sum_j \omega_{zj} S_{zj} - (\gamma_S/\gamma_I)\omega_z(\vec{r}) S_z \tag{4.2}$$

The applied magnetic field is assumed to be homogeneous over molecular dimensions, so the spatially dependent part of the field is proportional for the two species in the ratio of their gyromagnetic ratios (γ_S/γ_I).

The all important bilinear terms (2.10) become

$$\mathcal{H}^{zz} = (\mathcal{H}^D_{II} + \mathcal{H}^Q_I + \mathcal{H}^J_{II}) + (\mathcal{H}^D_{SS} + \mathcal{H}^Q_{SS} + \mathcal{H}^J_{SS}) + \mathcal{H}_{IS} \tag{4.3}$$

Only the last term is new in form. This is the coupling between unlike pairs

$$\mathcal{H}_{IS} = -\sum_i \sum_j 2F_{ij} I_{zi} S_{zj} \tag{4.4}$$

where $F_{ij} = (1/2)(J_{ij} + 2D_{ij})$. It is particularly simple since the flip-flop terms, which are present in the homonuclear couplings, are absent here. They are truncated for heteronuclei at high field by the large difference in Larmor frequencies.

The consequence is that there are independent Zeeman quantum numbers for the different spin species, which are conserved during free evolution. For the states $|i\rangle$ these are M_i^I and M_i^S, while for the density operator the two labels n^I and n^S will be useful. The generalization of (2.27) is

$$[I_z, |i\rangle\langle j|] = n_{ij}^I |i\rangle\langle j| \tag{4.5a}$$

$$[S_z, |i\rangle\langle j|] = n_{ij}^S |i\rangle\langle j| \tag{4.5b}$$

The relative size of the gyromagnetic moments is of great importance in the design of heteronuclear NMR experiments. Recall that it enters in several related but distinct ways. First of all it determines the difference between Larmor frequencies $\omega_o^I = \gamma_I H_o$ and $\omega_o^S = \gamma_S H_o$. It has already implicitly been assumed that the difference in these frequencies is much greater than any of the terms appearing in the doubly rotating frame Hamiltonians. The possible detection frequencies for the transverse magnetization are ω_o^I and ω_o^S and the induced voltage[18] is proportional to the frequency through Faraday's law. Furthermore a second power of γ enters the detection process through (2.19); regardless of the frequency, the magnetic moment is proportioned to γ. Finally the initial condition (2.14) now has two terms

$$\rho(0) = b_I I_z + b_S S_z \tag{4.6}$$

whose norms are also proportional to the respective gyromagnetic ratios.

2. Outline

Section IVB1 begins with a historical overview of the notion of multiple quantum spin flips in the communication between spin species in solids. This is followed in Section IIB2 by a proposal for a new method of cross polarization (SPETTERS) which clarifies the relations between number of quanta and thermodynamic constraints and may prove superior to existing methods in some circumstances. Section IVB3 returns to the more central issue of multiple quantum coherence as a chemical probe by reviewing several studies in which the multiple quantum coherence of quadrupolar nuclei is observed by way of proton magnetization.

Section IVC carries the applications further with a discussion of a variety of experiments in which both spins may be involved in the coherent

superposition during the evolution period. This class of heteronuclear multiple quantum (HMQ) NMR experiments shows promise of delivering information on molecular geometry and ordering with a simpler analysis than is possible for the homonuclear case.

B. Cross Polarization and Multiple Quantum Coherence

1. Background

a. Static fields. Multiple quantum processes have long been recognized as a mechanism for exchange of spin energy between nuclear species. In nearly every scheme where a flip-flop of one I spin and one S spin can occur through their mutual coupling, a small change in experimental conditions has been shown to lead to a flip of two or more I spins and a flop of one S spin. The discussion here will be limited to the common case where the two spin species are thermally isolated from the lattice by relaxation times T_1 considerably longer than that needed for them to interact with one another.

At very low static fields it is possible for the heteronuclear dipolar couplings alone to exchange energy between two spin species. At applied fields larger than these local fields, the simple flip-flop is forbidden by energy conservation. However, the ^{7}Li and ^{19}F magnetizations of LiF still approach a common spin temperature in several seconds at applied fields several times the local fields[156]. An explanation was found in a mechanism wherein two ^{7}Li spins, with their smaller gyromagnetic ratio, compensate for the flip of one ^{19}F spin[157].

b. Hartmann-Hahn matching. At very high static fields thermal contact between I and S spins requires strong rf fields. These create a new quantization axis perpendicular to the static field when ω_p exceeds the couplings between spins. One way of satisfying energy conservation for a flip-flop with such "rotating frame" or transverse

quantization is to simultaneously irradiate both spin species on resonance with matched nutation frequencies. This is the Hartmann-Hahn condition[158]:

$$\omega_p^I = \omega_p^S \ . \tag{4.7}$$

It allows exchange of spin locked I and S magnetization (SL method)[158-162], and is the most commonly used means of cross polarization, particularly of ^{13}C (S) by protons (I).

With respect to the transverse quantization axis, the cross-polarization proceeds by a single I spin flipping for each S spin which flops. This can be stated in terms of quantum numbers $\tilde{n}^I$ and $\tilde{n}^S$ analogous to those of (4.5), but now with the transverse, spin-locked components of magnetization $\tilde{I}_z$ and $\tilde{S}_z$ replacing I_z and S_z in the defining roles. The important difference between this transverse frame and the longitudinal doubly rotating frame is that the average Hamiltonian $\tilde{\mathcal{H}}^{(0)}$,[160-162] which remains after truncation by the rf terms, contains heteronuclear flip-flop terms arising from (4.4). Thus

$$[(\tilde{I}_z + \tilde{S}_z), \tilde{\mathcal{H}}^{(0)}] = 0, \tag{4.8}$$

but the individual operators $\tilde{I}_z$ and $\tilde{S}_z$ are not constants of the motion. In other words, $(\tilde{n}^I + \tilde{n}^S)$ is a good quantum number for evolution under intense resonant fields at the Hartmann-Hahn condition.

If $(\tilde{I}_z + \tilde{S}_z)$ is the only invariant having a finite projection on the initial condition, then the cross polarization dynamics are easily sketched. It is usual to assume that the equilibrium S magnetization is negligible or has been destroyed at the beginning of the experiment. Then the initial condition of spin locking for a system of N spins I = ½

and one spin S = ½ is

$$\rho(0) = I_z \tag{4.9a}$$

$$= N/(N+1)(\tilde{I}_z + \tilde{S}_z) + (1/(N+1)\tilde{I}_z - N/(N+1)\tilde{S}_z) \tag{4.9b}$$

The term in the first parentheses is a constant of the motion by (4.8), or more precisely a quasi-constant, good for times less than $\sim T_{1\rho}$. The other term develops in time under $\tilde{\mathcal{H}}^{(0)}$. If it undergoes a monotonic development into other unobserved degrees of freedom, then in a period of several times the cross polarization time T_{IS}[158-160], the only magnetization remaining is from the first term. This gives the quasi-equilibrium limit for the spin-locked S magnetization[158-160] with Hartmann-Hahn matching:

$$M_S = M_{OS}(\gamma_I/\gamma_S)(N/N+1) \tag{4.10}$$

M_{OS} is the thermal equilibrium S magnetization. The enhancement approaches (γ_I/γ_S) for large N. In the limit of a large system this result is usually derived using the concept of spin temperature and the last factor is the ratio of the I spin heat capacity to the total heat capacity.

For finite systems the S magnetization is often observed to oscillate [158,161,162]. This is a result of a change of sign in the coefficient of the terms in the second parentheses of (4.9). In the limit that this coefficient reaches a value equal and opposite to that in (4.9) then one attains the adiabatic (isentropic) limit for Hartmann-Hahn matching

$$M_S = M_{OS}(\gamma_I/\gamma_2)(2N/(N+1)). \tag{4.11}$$

This is just twice the magnetization in (4.10).

c. Multiple quantum cross polarization by spin-locking. There is a considerable body of literature on the study of multiple quantum transitions in transversely quantized systems; typically one strong resonant rf field determines the quantization axis and some number of photons from a second field is absorbed or emitted[163]. Such "multiple quantum" processes are possible with a single spin 1/2. Further references and the extension of such notions to time domain experiments may be found in a recent work[164]. Here we are concerned with multiple quantum processes with respect to a transverse quantization axis only in the context of cross polarization.

The generalization of the Hartmann-Hahn condition to one in which energy conservation is met only for multiple quantum processes has been shown also to lead to polarization exchange[165-170]. The generalized condition is

$$m'\omega_e^I = n'\omega_e^S \tag{4.12}$$

for some integers m' and n'. Generalization to the effective frequencies $\omega_e = \sqrt{\omega_p^2 + (\Delta\omega)^2}$ instead of ω_p is necessary, since off-resonance irradiation was used in these studies.

d. Cross polarization by ADRF. An alternative approach to the energy conservation requirement is to match the nutation frequency ω_e^S of the S spins with the dipolar eigenfrequencies of the I spins, which have been adiabatically demagnetized (ADRF method)[171]. The I spins are ordered not with respect to any quantization axis, but with respect to one another (dipolar order). The broad range of frequencies characteristic of the dipolar Hamiltonian mitigates against resolved matching conditions analogous to (4.12). The methods are more fruitfully compared according to their thermodynamic efficiency.

e. Total cross polarization. This problem is an old one: how can the magnetization of an abundant spin species I be transferred most efficiently to a dilute species S? For clarity it is convenient to assume that the equilibrium S magnetization is negligible or that it has been intentionally destroyed at the start of the experiment. Then, as usual, $\rho(0) = I_z$. The quantity to be maximized is $Tr(\rho(t)S_p)$ where p indicates the arbitrary direction of the S spin angular momentum vector operator.

An underlying constraint on any experiment designed to transfer order from one system to another is that the final order can be no greater than the initial order. This is the second law of thermodynamics: at best, entropy is conserved. Another form of this constraint was already encountered during the consideration of the maximum efficiency of excitation of coherence within various subspaces (Secs. IIIB1 and IIIC8). There the conservation of the trace of the square of the subspace density operator under unitary (and hence isentropic) evolution was used as a bound on the possible dynamics.

The best that can be done then in cross polarization is to convert the entirety of $\rho(0)$ to S_p so that at some time t:

$$\rho(t) = cS_p. \tag{4.13}$$

The maximum value of the constant can be evaluated from the constraint:

$$Tr(\rho(t)^2) = c^2 Tr(S_p^2) = Tr(I_z^2) = Tr(\rho(0)^2). \tag{4.14}$$

If there are N times as many I nuclei as S nuclei and all their spins are equal, then $c = \sqrt{N}$. This result is illustrated in Figure 40 for $N = 3$. It is nothing more than The Pythagorean Theorem in N dimensions.

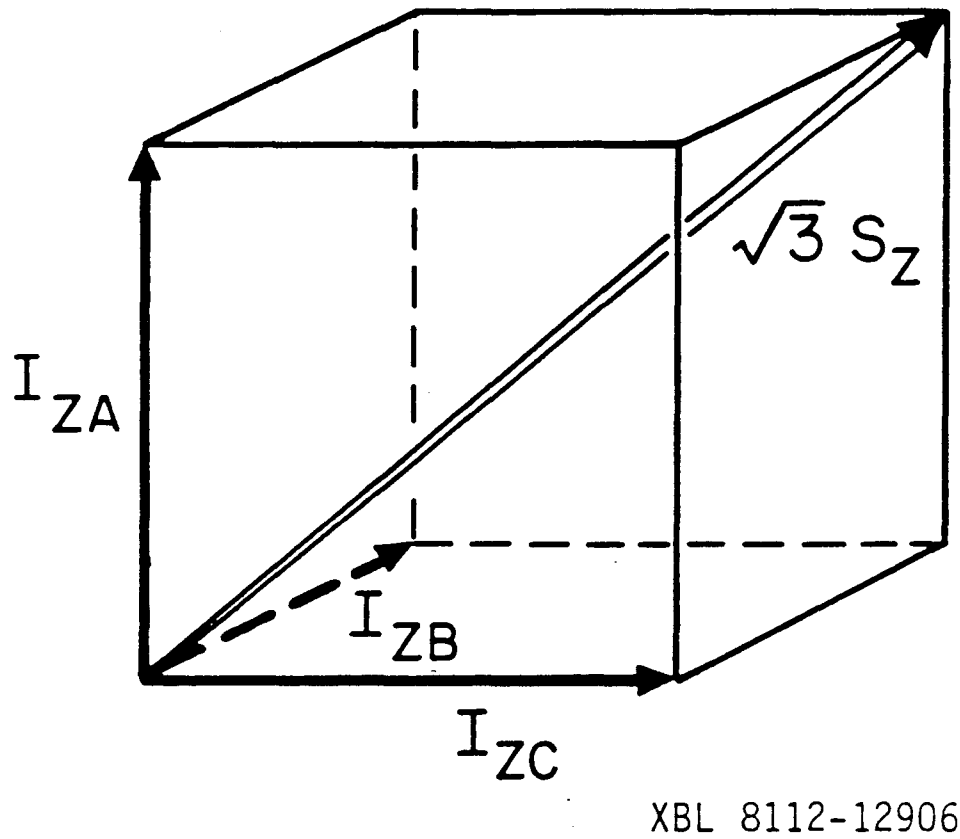

Figure 40. Geometric representation of the constraint on the maximum S magnetization obtainable by cross polarization. The case shown is that of N = 3 I = 1/2 spins coupled to a single S = 1/2 spin. An initial condition of $I_z = I_{zA} + I_{zB} + I_{zC}$ can at best be converted to $\sqrt{3}\ S_z$ as suggested by this construction where each of these vectors has the length of the body diagonal of the cube. The same constraint holds in N dimensions for arbitrary N and gives the adiabatic limit for cross polarization.

The initial condition $\rho(0)$ consists of three or thogonal vectors in Liouville space each having the same norm. The norm of their sum is $\sqrt{3}$ times their individual norms and this is the largest coefficient possible for any spin angular momentum component. This isentropic or adiabatic limit M_S^{ad} of the cross polarized magnetization of the S spin can be written[159] as a multiple of the equilibrium S magnetization without cross polarization, M_{0S}:

$$M_S^{ad} = \gamma_S \mathrm{Tr}(\rho(t) S_p) = (\gamma_I/\gamma_S)\ \sqrt{N}\ M_{0S} \tag{4.15}$$

Comparison with (4.11) shows that this about $\sqrt{N}/2$ better than is possible with Hartmann-Hahn matching.

The possibilities for realization of this total cross polarization in a complex spin system have been discussed theoretically[159,160] and explored experimentally. To date the closest approach to this limit for a solid appears to be by the ADRF method with adiabatically increasing ω_e^S[172,173]. The problem is that the rate of cross polarization decreases under those conditions where it is most nearly isentropic[160]. The cross polarization process competes with irreversible T_1 processes in the SL method and T_{1D} processes in the ADRF method. If these times are comparable or shorter than the cross polarization time T_{IS}, then total cross polarization is not possible.

2. Spin Polarization Exchange with Total Transfer of Entropy by Resonant Selection - (SPETTERS)

a. Motivation. In this section a possible approach to cross polarization is outlined which differs considerably from the SL or ADRF methods used to date. Here it is presented as a gedanken experiment in that details of the possible pulse sequences will not be pursued. It is of interest in that it clarifies the relationship between number of

quanta and cross polarization efficiency. We have seen in (4.10) and (4.11) that the Hartmann-Hahn condition (4.7) cannot lead to the total transfer of entropy necessary to obtain the total cross polarization limit given by (4.15). This can be traced to the fact that $(\tilde{n}^I + \tilde{n}^S)$ is a good quantum number so each S spin only flips one I spin. When the chemical ratio N of I spins to S spins is greater than one this wastes I spin magnetization. The multiple quantum generalization (4.12) seems to offer an adjustable exchange rate, but is expected to become prohibitively slow as the integer ratio n'/m' increases. This is because the average Hamiltonian for any such spin locking scheme is still linear in the coupling terms derived from $\mathcal{H}_{IS}$, S_p the higher order energy conserving processes which are needed appear either as correction terms in the effective Hamiltonian or nonlinearly in time.

b. Heteronuclear phase cycling. This problem is reminiscent of that encountered in order selective excitation (Sec. IIC) where it was found desirable to make the coupling between spins appear nonlinearly and with restricted combinations of raising and lowering operators in the average Hamiltonian. The principle trick needed there was phase cycling.

Figure 41 shows an extension of the phase cycling concept to the heteronuclear problem of cross polarization. The abundant I spins are put through a sequence of phase cycling with some increment $\Delta\phi_I = \Delta\phi$ in rf phase distinguishing successive subcycles. Within each subcycle the dilute S spin is also irradiated near its Larmor frequency, but the phase increment between subcycles is

$$\Delta\phi_S = K\Delta\phi_I. \tag{4.16}$$

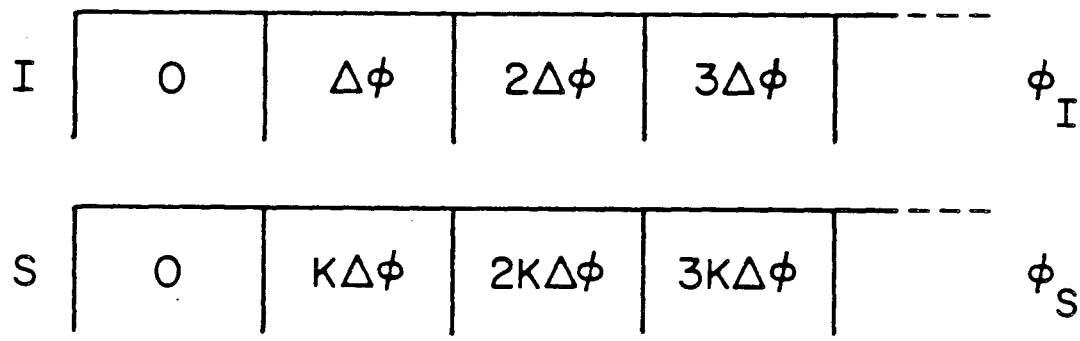

XBL 8112-12907

Figure 41. Phase cycling for SPETTERS. By incrementing the phase of the irradiation of the dilute S spins at K times the rate of the incrementation for the abundant I spins an average Hamiltonian is obtained under which cross polarization proceeds only by way of $n^S = \pm 1$, $n^I = \mp K$ coherence. The possible subcycle details, not shown here, are analogous to those discussed for order selective excitation in Section IIIC6.

Let each subcycle be characterized by an effective Hamiltonian $\mathcal{H}_{\phi_I,\phi_S}$. Then in analogy to (3.66), these are related to one another by

$$\mathcal{H}_{\phi_I,\phi_S} = \exp(i\phi_I I_z)\ \exp(i\phi_S S_z)\ \mathcal{H}_{0,0}\ \exp(-i\phi I_z)\ \exp(-\phi S_z) \tag{4.17}$$

For a particular matrix element with $\phi_S = K\phi_I$

$$\langle i|\mathcal{H}_{\phi_I,\phi_S}|j\rangle = \exp(i(n^I_{ij}\phi_I + n^S_{ij}\phi_S))\ \langle i|\mathcal{H}_{0,0}|j\rangle \tag{4.18a}$$

$$= \exp(i(n^I_{ij} + Kn^S_{ij})\phi_I)\ \langle i|\mathcal{H}_{0,0}|j\rangle \tag{4.18b}$$

Summing over Q different phases at intervals of $\Delta\phi_I = 2\pi/Q$ leaves only orders such that

$$(n^I + Kn^S) = kQ \tag{4.19}$$

If there are N spins $I = \frac{1}{2}$ and one spin $S = \frac{1}{2}$ then

$$|n^I + Kn^S| \leqslant N + K \tag{4.20}$$

Thus, if the choice

$$Q > N + K \tag{4.21}$$

is made, only $k = 0$ is possible in (4.19). This means that for all terms in the average Hamiltonian for the cycle

$$n^I = -Kn^S. \tag{4.22}$$

A smaller value of Q may suffice in practice, since statistically there are fewer operators which can satisfy (4.19) with $|k| > 0$ than with $k = 0$ for the range of K which will be of interest below. There is a close connection with the homonuclear order selective methods of Section IIIC5

to Sec. IIIC9. In analogy to the trick discussed in Section IIIC6d, time reversal in conjunction with a phase shift of π on the S spin could be used within the subcycles of Figure 41 to help keep $n^S = 0$ processes in check.

Assume then that an effective Hamiltonian $\mathcal{H}$ with all terms satisfying (4.22) is achieved. Evidently it can be used to excite heteronuclear coherence in an order selective manner starting from either I or S magnetizations. The focus here however, is on the cross polarization process in which the selected coherence plays only an intermediate role. The heteronuclear phase cycling amounts to a truncation of the subcycle Hamiltonian with respect to the operator $(I_z + KS_z)$, which is the generator for the propagator in (4.17) describing the phase shifts. Thus

$$[(I_z + KS_z), \mathcal{H}] = 0 \tag{4.23}$$

This should be compared with (4.8), which aside from the tilt to the transverse frame indicated by the tilde, is the $K = 1$ limit of (4.23).

The generalization of the cross polarization dynamics is now straightforward. Instead of (4.9) we have

$$\rho(0) = I_z \tag{4.24a}$$

$$= (N/(N+K^2))(I_z + KS_z) + [(K^2/(N+K^2)I_z - (NK/(N+K^2)S_z] \tag{4.24b}$$

If the dynamics of the second term causes its inversion at some time t_{opt}, then

$$\rho(t_{opt}) = ((N-K^2)/(N+K^2))I_z + (2NK/(N+K^2))S_z \tag{4.25}$$

Choosing $K = \sqrt{N}$ gives SPETTERS: spin polarization with total transfer of entropy by resonant selection. It is total cross polarization as

described by (4.13) and (4.15). Of course, since K is integral, it cannot always be set to $\sqrt{N}$, but the nearest integer values are nearly as good.

If only the constant term of (4.24) contributes to the S magnetization, then one obtains the quasi-equilibrium limit, which is half as great. Figure 42 shows the quasi-equilibrium magnetization in units of $(\gamma_I/\gamma_S)M_{0S}$ as a function of K for N = 1, 12, and 144.

The Hartmann-Hahn condition (4.7) has the same efficiency as K = 1. In the language of spin temperature theory, it suffers from a mismatch of heat capacities. When the I and S reservoirs have reached the same temperature most of the coolth or negentropy still resides in the I spin order. A transverse frame analog of $K \simeq \sqrt{N}$ is formally possible as a particular case of (4.12) with $(n'/m') \simeq \sqrt{N}$. The difficulty is in preventing decoupling of the two species in the presence of different nutation frequencies. By replacing nutation frequencies by phase shifts, SPETTERS increases the flexibility for designing a sequence with effective contact between reservoirs. In addition, by using the longitudinal magnetizations as reservoirs it offers the possibility of having the sometimes rapid I spin relaxation toward thermal equilibrium serve to replenish, rather than deplete, the I spin reservoir during cross polarization.

3. Multiple Quantum Cross Polarization of Quadrupolar Spins (174-178)

In the preceding sections the goal of the cross polarization processes discussed was to transfer magnetization on one spin species to magnetization on another. If the target species has $S \geqslant 1$, then it is useful to transfer the order of the I spins directly to multiple quantum coherence on the S spin[174-178]. This not only saves steps, but is often the most practical scheme since the large spectral

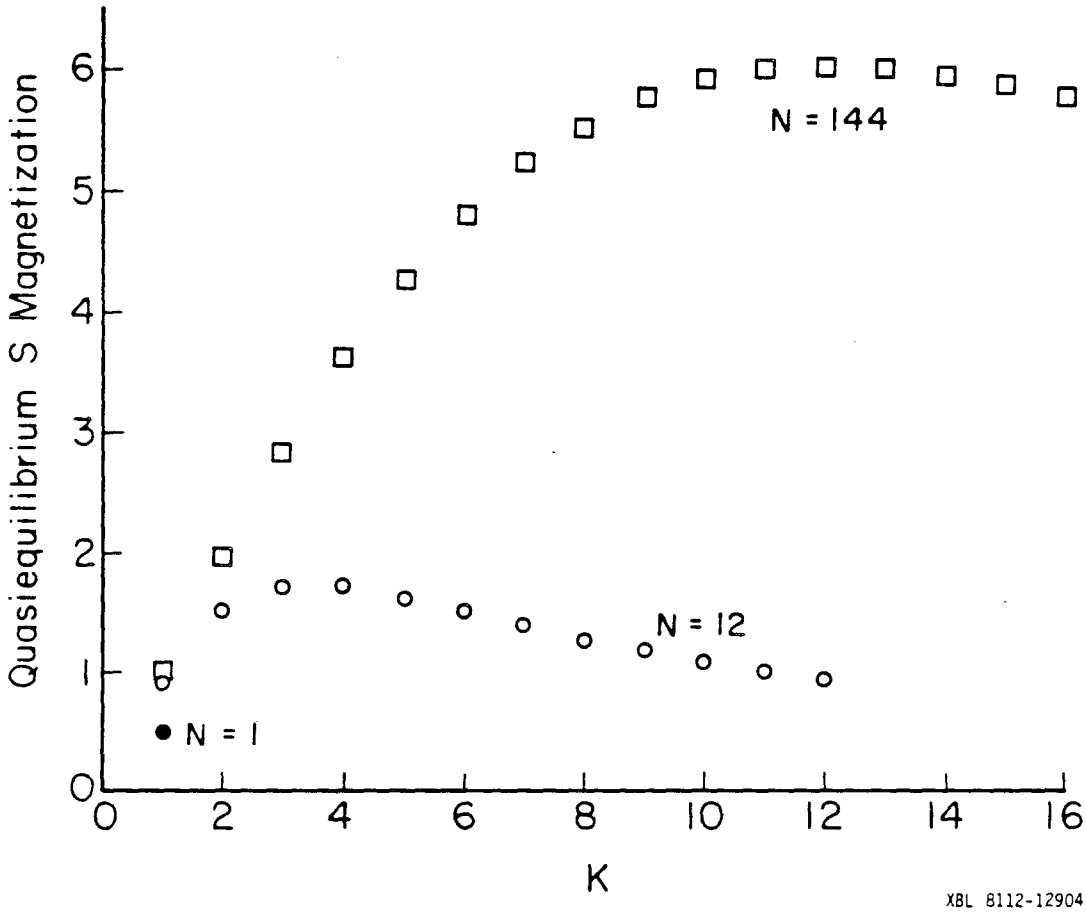

Figure 42. The dependence of the quasi-equilibrium magnetization on K and N for SPETTERS. The quasi-equilibrium magnetization in units of $(\gamma_I/\gamma_S)\ M_{0S}$ is shown as a function of K for N = 1, 12 and 144 I spins per S spin. For comparison, the Hartmann-Hahn condition is equivalent to K = 1.

range of quadrupolar nuclei frequently precludes spin locking of the entire magnetization.

The methods for direct cross polarization of the double quantum coherence of a several level system directly parallel those already discussed in Section IVB1 for S = 1/2. It is only necessary to substitute the S = 1/2 system by the pseudo-two-level system formed by the outer two levels. For a spin 1, the Hartmann-Hahn condition analogous to (4.7) is found by replacing ω_p^S by the effective double quantum nutation frequency in (2.40) thus obtaining

$$\omega_p^I = (\omega_p^S)^2/\omega_q^S. \tag{4.26}$$

With this condition met, the spin locked I spin magnetization is found to quasi-equilibrate with spin locked double quantum coherence on the S spin. Multiple quantum spin locking is discussed further in Section VC.

The analog of the ADRF method has also been demonstrated[174,175,177]. This has the advantage of cross polarizing effectively over a broader range of ω_Q and of being applicable to larger values of ω_Q. Furthermore, relative to the SL method, it is capable of more closely approaching the isentropic limit, just as is the case with ordinary cross polarization.

Applications with S = 1 have been made to both deuterium[174,175] and ^{14}N[176,177]. With S = 3/2, the cross polarization of both double and triple quantum transitions has been analyzed and demonstrated[178] in sodium ammonium tartarate.

C. The Spectroscopy of Heteronuclear Multiple Quantum Coherence

1. Overview

In the following sections a review is made of heteronuclear multiple quantum (HMQ) studies of systems with a well-defined number of

spins. A single S spin and N I spins will comprise the system in all the examples, but this will not be an important restriction for most of the techniques. What is important is that the number of spins in the coupled system be small enough so that there are at least some resolved high order spectra. This will allow a richer interplay among the spin species and in particular allow the parameters of $\mathcal{H}_{IS}$ to be measured with high resolution. This is in contrast to the situation of the preceding sections where the I spins only served as a source of magnetization for the dilute S spin, which then would usually be observed with I spin decoupling.

Several of the experiments reviewed here have in common with the cross polarization experiments the goal of obtaining chemical shift information on the S spin with the sensitivity of the I spin. They differ in one or both of two respects. First, spin locking is not necessary to transfer magnetization back and forth between nuclear species in small spin systems with resolved spectra. This may instead be achieved by rf pulses to both species preceded and followed by periods of free evolution of duration comparable to the inverse of the heteronuclear couplings[179]. Second, even for S = 1/2 it is not necessary for net S spin magnetization to be present at any time in order to measure the S chemical shift[8,83,180]. Such magnetization is a $(n^I = 0,\ n^S = \pm 1)$ operator. It can be advantageous to observe instead operators with various n^I and with $n^S \neq 0$, whose evolution frequencies are also sensitive to S chemical shifts.

The experiments may also be compared to cross polarization experiments and to pure S spin experiments with regard to signal-to-noise ratio[82,180,181]. A general comment is that whenever the coherence

during the evolution period is both prepared from I spin magnetization and mixed back to I spin magnetization for detection, the signal-to-noise ratio no longer has a necessary dependence on γ_S as is the case when S magnetization is detected and line intensities depend on magnetization transfer in one direction. Instead, γ_S enters only through the heteronuclear couplings, which determine the timing of the excitation periods. So long as these periods can be optimized, while still remaining short compared to irreversible relaxation times, then γ_S does not figure in the line intensities.

In such a case, the line intensity considerations are little changed from the homonuclear case; the magnetization available to a certain order must be assessed according to the excitation dynamics and apportioned among the lines (Secs. IIE4, IIIB1, and IIIC8). Several cases of HMQ spectroscopy with I spin magnetization have been discussed where absolute or relative line intensities can be calculated[82,83,85,180].

2. Pulse Sequences for HMQ Spectroscopy

The similarities and differences between the homonuclear and heteronuclear time domain multiple quantum experiments can be brought out by examining some of the pulse sequences which have been used. The survey here will not be exhaustive. Some heteronuclear sequences involving frequency selective pulses were already mentioned in Section IIC2[47,48]. Tables of sequences and further discussion can be found in several of the primary references[83,180,181].

Figure 43 shows a typical example of a HMQ pulse sequence[82]. The approach is closely analogous to the homonuclear sequences of Figures 3, 4, and 13. For the most part, there is a pulse on the S spins for each one on the I spins. These strong pulses may be given

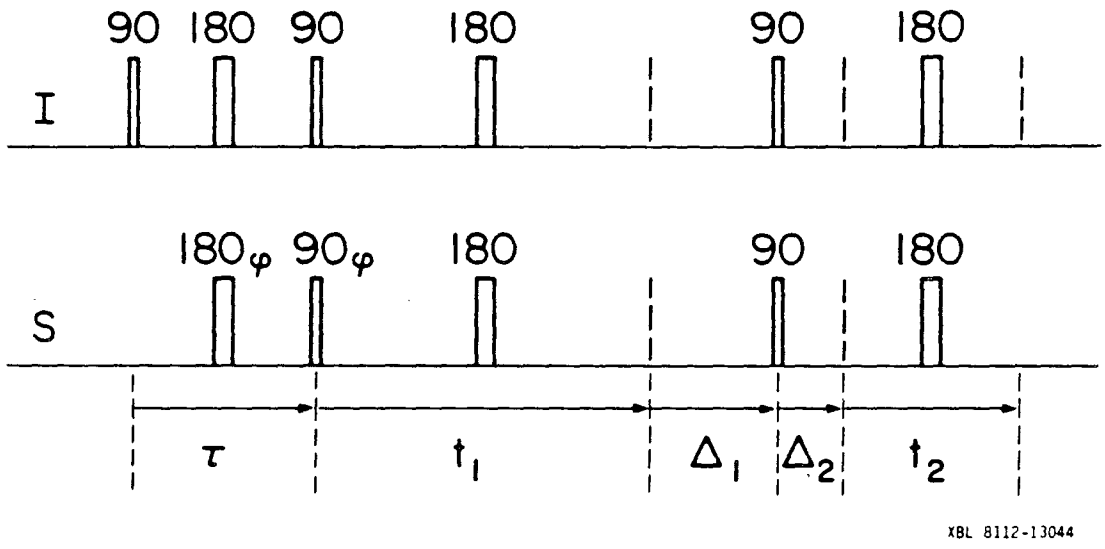

Figure 43. Simple pulse sequence for HMQ spectroscopy in an inhomogeneous field. Except for the (optional) absence of the first $\pi/2$ pulse on the S spin the two species are treated symmetrically. The phase shifts between shots indicated by ϕ on the S preparation pulses would in other applications be on the I preparation pulses or on both spins to separate spectra according to n^I and n^S. The initial and detected magnetization here is that of the I spins. A heteronuclear coherence transfer echo is also incorporated and the particular coherence observed selected by choice of the periods Δ_1 and Δ_2.

simultaneously or in rapid succession without changing the propagator, since the rotation operators for the different species commute. The excitation and evolution periods include π pulses to eliminate effects of static magnetic field inhomogeneity. The π pulses in the excitation periods also serve to make the sequence even (or odd) selective (Sec. IIIC2 and Ref. 180) if the I spins are fully equivalent or if the weak coupling limit between inequivalent spins pertains. In this context the even (or odd) character refers to the quantity $(n^I + n^S)$ and not to the individual quantum numbers. The initial $(\pi/2)_S$ pulse is omitted, so the even or odd selection does not apply to coherence arising from the equilibrium S magnetization. It contributes here only to orders $(n^I = 0, n^S = \pm 1)$, as can be seen by noting that the first π_S pulse merely inverts it and the first $(\pi/2)_S$ pulse gives $S_{\phi+\pi/2}$ transverse magnetization at the beginning of the evolution period t_1.

The phase ϕ of the S spin preparation pulses was incremented between shots to differentially label orders (n^I, n^S) with different values of n^S. In the general case, independent incrementation of the preparation phase at the two applied frequencies is necessary to separate by all values of n^I and n^S using extensions of either PFT or TPPI (Sec. IID2).

The sequence of Figure 43 also includes a heteronuclear coherence transfer echo[80,82,83] to separately echo the signals in t_2 from different orders as is illustrated for the homonuclear case in Figure 14. The echo condition for detection through the I magnetization is

$$\Delta_2 = (n^S\gamma_S + n^I\gamma_I)/\gamma_I. \tag{4.27}$$

This sequence was used to obtain the ^{14}N double quantum $(n^I = 0, n^S = 2)$ spectrum of the I_4S system of the ammonium ion in isotropic

solution using only the proton magnetization[82]. The lack of quadrupolar splitting in liquids makes it impossible to excite such multiple quantum coherence by irradiation of the S spin alone. This problem had earlier been approached by spin tickling of the protons, which allowed the ^{14}N magnetization to be interconverted with the same coherence[182].

Other HMQ sequences involving coherence transfer by $(\pi/2)_{I,S}$ pulses have been demonstrated on the I_3S system of $^{13}CH_3I$ in isotropic solution[180] and the I_2S of d_1-acetonitrile oriented in a nematic liquid crystal[181].

A somewhat different approach to exciting HMQ coherence is exemplified in Figure 44[83]. Here the heteronuclear interaction $\mathcal{H}_{IS}$ is initially eliminated by S spin decoupling, while the homonuclear interactions are used during τ to prepare coherence characterized by one or more values of n^I, but with $n^S = 0$. The simplest two pulse preparation sequence on the I spins is depicted, but for more than a few I spins the order selective methods of Section IIIC should be used during the decoupling. Preparation is completed by a period of free evolution τ_{IS} followed by a $\pi/2$ pulse to the S spin. This has the effect of appending the $n^S = \pm 1$ quantum number to what had been I spin coherence. The mixing period is similar and simply reverses the two step procedure.

This approach is particularly valuable when the sample consists of a collection of systems differing only in the terms of the Hamiltonian involving the S spin. The most important such situation is that of organic molecules where the protons (I) are accompanied by ^{13}C (S) at a natural abundance of ~1%. A typical molecule will have a single ^{13}C located in any one of the carbon positions. The decoupling renders these isomers equivalent to a good approximation, so the I spin

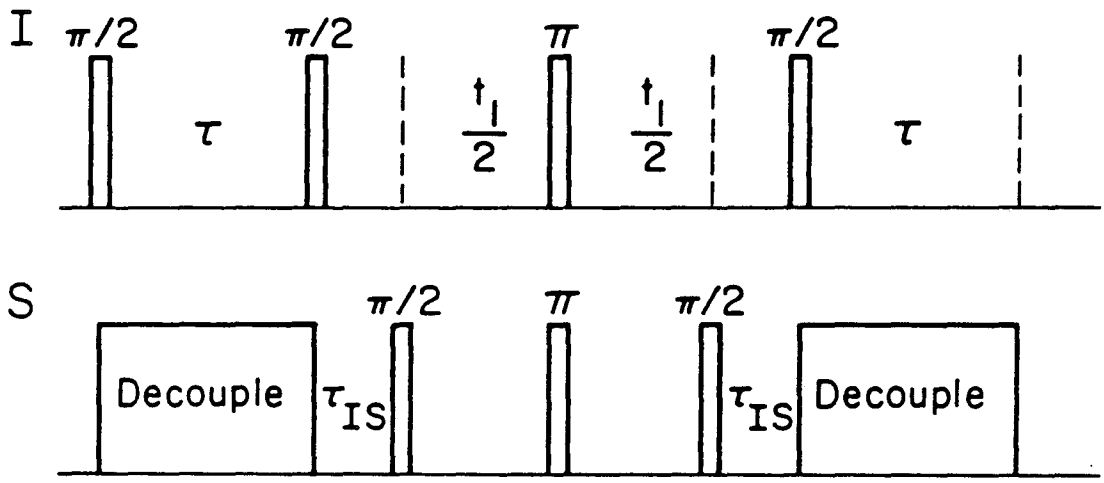

XBL 8112-13045

Figure 44. Pulse sequence for sequential excitation of $n^S = \pm 1$ HMQ coherence. The decoupling of the S spins during the periods τ leads to simplification of the excitation dynamics. The heteronuclear couplings are necessary and are allowed to act during the periods τ_{IS}.

excitation is simultaneously optimized for all of them. This optimization does not require any S participation, so even the unlabeled molecules contribute their signal at this preliminary stage. Decoupling of the S spin during excitation can also lead to simpler line intensity calculations[83].

3. Techniques for Determining $\mathcal{H}_{IS}$ in Anisotropic Phases

One of the most promising avenues for the application of HMQ spectroscopy is in the determination of molecular geometry in anisotropic phases. This information is contained in the direct dipolar coupling between spins as noted already in Section IIF3e. Systems of two nuclear species, usually protons and a chemically dilute nucleus, offer important advantages over the purely homonuclear case.

The first of these advantages is simply that the number of unknowns is smaller. Instead of the $N(N-1)/2$ homonuclear couplings determining $\mathcal{H}^D_{II}$, one has only N couplings in $\mathcal{H}_{IS}$ for a system of N spins I and one spin S. Because these Hamiltonians do not in general commute, these problems are only separable if $\mathcal{H}^D_{II}$ is eliminated by multiple pulse homonuclear decoupling techniques[61-63,148,149].

A second advantage is that the various candidates for the role of S spin (e.g., ^2H, ^{13}C, ^{14}N, ^{15}N, ^{31}P, ^{29}Si) have either a range of quadrupole splittings or a large chemical shift range. By correlating the dipolar spectral structure with either of these quantities, the job of assigning the parameters D_{ij} to particular pairs of nuclei is made far easier than in the case of nearly isochronous protons.

These advantages motivated a number of studies over the past decade, which are often referred to as local field spectroscopy[52,110,183-195]. These were among the earliest applications of two dimensional NMR. By

combining homonuclear decoupling in one time dimension with heteronuclear decoupling in a second, the correlation of $\mathcal{H}_{IS}$ with the spreading parameters is achieved.

Possibilities for combining homonuclear decoupling with HMQ spectroscopy and comparison of such methods with the single quantum local field experiments have recently been discussed at some length[83]. Figure 45 is a schematic comparison of the way in which the local-fields are probed by the single quantum and multiple quantum experiments. In part (a) the situation ideally attained in single quantum local field experiments is suggested. The ^{13}C spins experiences the 2^N possible local fields of the N protons. While the resulting spectrum of 2^N lines is a simplification over that obtained with couplings between the protons present, it is still growing exponentially more dense with N. Furthermore, such a picture only holds rigorously when all couplings between I spins are absent, while in fact the homonuclear J couplings are not eliminated by multiple pulse methods. The consequence is that in practice only the nearest or next nearest protons are resolved in the ^{13}C local-field spectrum. The accuracy with which even these are measurable is well below that set by irreversible relaxation, since one is in fact observing not single transitions but unresolved multiplets.

A somewhat more favorable situation prevails in principle if the I spin single quantum spectrum is observed. Here in the local field limit one predicts only 2N lines, since each proton sees only the lone ^{13}C and it may be up or down. Again homonuclear J couplings spoil the picture, broadening each of these lines into unresolved multiplets[83].

The situation encountered in HMQ spectroscopy is very different. Even if the couplings between protons were completely absent during the evolution period, the prior coherent preparation is such that their local

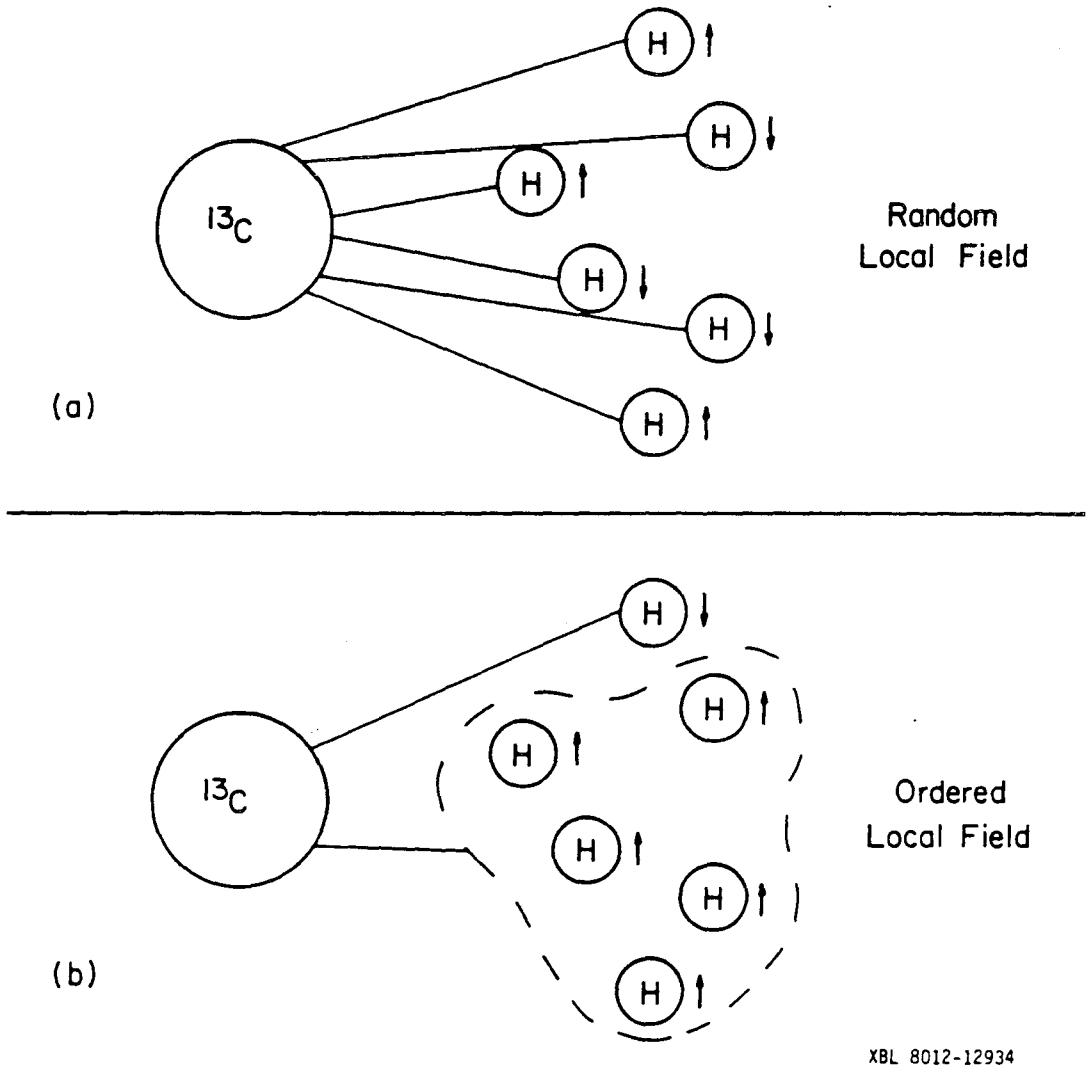

Figure 45. Schematic representation of the single quantum random local field and multiple quantum ordered local field for a system of one ^{13}C and N protons. (a) In the single quantum experiment the protons are assumed to be uncoupled from one another. A total of 2^N different proton configurations are possible, one of which is shown. The ^{13}C heteronucleus may experience any of these different proton local fields. (b) In the heteronuclear multiple quantum experiments the protons are excited as a coherent group. One of the six possible groups of 5 protons is illustrated. This fewer number of ordered local fields enhances spectral resolution by reducing the number of possible transition frequencies. These frequencies measure sums and differences of individual heteronuclear couplings, thus providing information on relative signs to which the single quantum spectra are insensitive.

fields appear to the ^{13}C as being ordered in only a small number of ways. The grouping sketched in Figure 45 (b) shows one of the N ways in which (N - 1) of the I spins can be singled out. Thus, for example, the (n^I = (N-1), n^S = 1) spectrum has in general 2N lines. This number is not affected by the unavoidable J couplings between the I spins and so resolution at the level of single transitions is possible.

Another feature of the HMQ spectra is that the line positions are sensitive to the relative algebraic signs of the heteronuclear couplings. This is analogous to the case of weak coupling in liquids discussed in Section IIF3c. These signs are crucial to geometric interpretation of the direct dipolar couplings, but are not manifest in the local field limit of the single quantum I or S spectrum.

Figure 46 shows the partial energy level diagram of partially oriented 1- ^{13}C-benzene which is necessary to explain the high order HMQ spectra[83]. The case depicted is relevant to the case where $\mathcal{H}_1$ is the unperturbed Hamiltonian $\mathcal{H}_{int}$ or, with a change in the exact positions of the levels, to the case where the effective multiple pulse Hamiltonian commutes with both I_z and S_z[61,83]. Transitions between states on the left or between states on the right correspond to n^S = 0 transitions and may be observed without any irradiation at the ^{13}C frequency. Those transitions between states on different sides of the figure are characterized by n^S = ±1 and are excited, for example, by the sequence of Figure 44. Only the A_1 states of the extreme Zeeman manifolds are shown. Their positions are determined by the spectra (n^I = 6,5; n^S = 0,1) which in turn is the minimum data necessary to characterize the heteronuclear couplings F_{iS}. Usually lower order spectra will also be desirable.

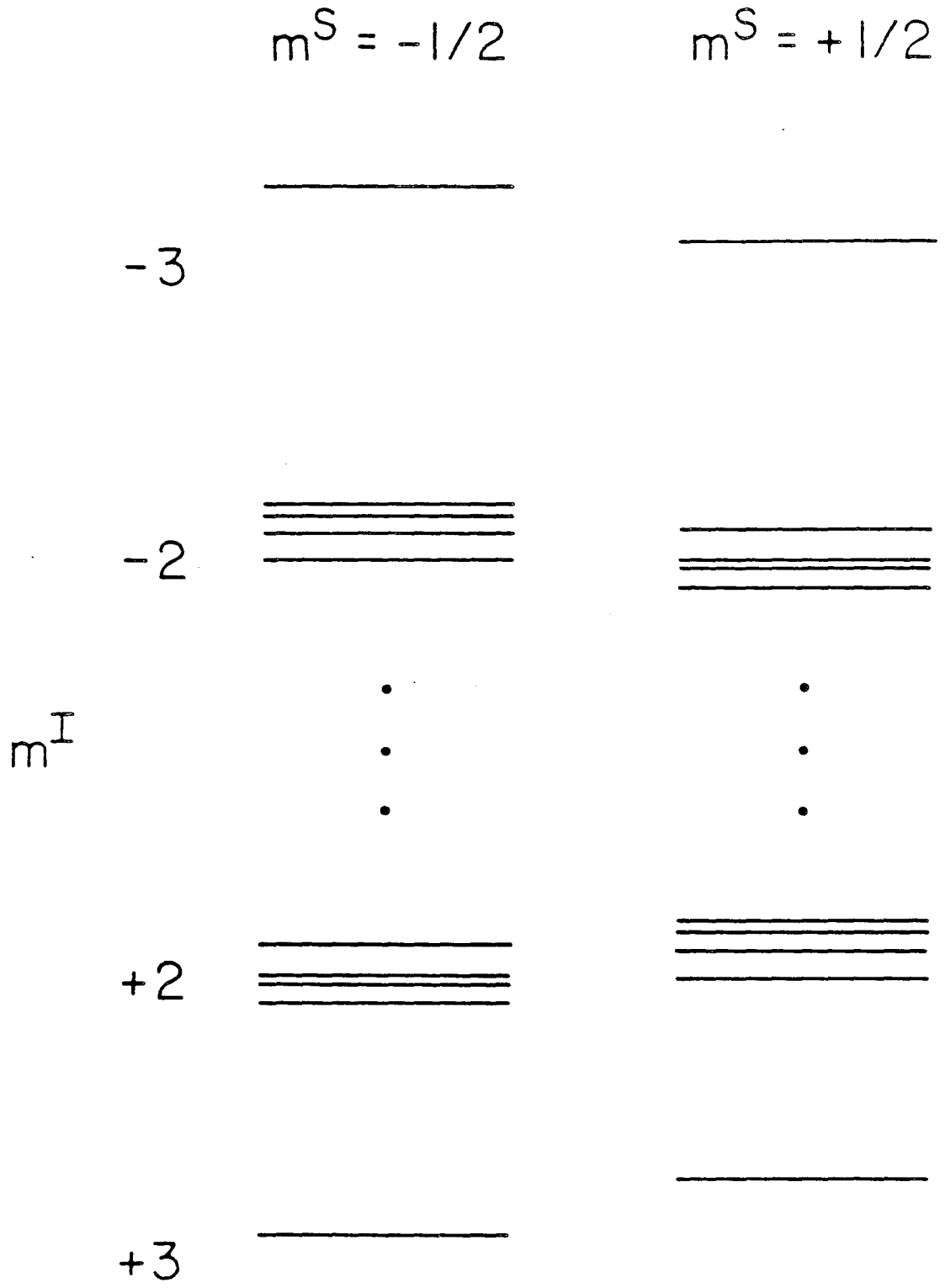

XBL 8110-7174 A

Figure 46 (Caption next page).

Figure 46. Partial energy level diagram of the A_1 states of ^{13}C benzene. This is a typical heteronuclear energy level diagram. The states may be grouped according to both M^I and M^S (lower case m in the figure). Transitions within a column are characterized by $n^S = 0$ while those between columns are $n^S = \pm 1$ transitions.

V. RELAXATION

A. Overview

1. Reversibility and Irreversibility

The resolution and the sensitivity of multiple quantum experiments is ultimately constrained by irreversible processes of relaxation. In some ways these constraints are looser than those of the single quantum experiments and in other ways they are more severe. Before making these comparisons it is useful to review some notions of reversibility and irreversibility in NMR.

Consider once again the fundamental phenomenon of the f.i.d. after a single strong pulse. The decay of this transient is often loosely referred to as transverse relaxation and characterized by a time T_2, but it has long been recognized that in fact the observed disappearance of the signal can in different circumstances be due to a number of distinct phenomena. The most trivial cause of decay, static magnet inhomogeneity, has already been discussed in relation to the multiple quantum experiments (Sec. IIE). It is the most obviously reversible cause of transverse decay.

A more subtle case is the decay of the f.i.d. for a large system of coupled spins with an unresolved single quantum spectrum. Here the f.i.d. vanishes on a time scale set by $M_2^{-\frac{1}{2}}$. That such a system is not necessarily undergoing rapid irreversible dephasing on this time scale is clear from several types of experiments.

One of the earliest and experimentally simplest demonstrations of this is the phenomenon of spin locking[133-137]. The spin locked magnetization decays with an exponential time constant $T_{1\rho}$ which is often orders of magnitude longer than $M_2^{-\frac{1}{2}}$. The consequences of this

fact for signal energy were discussed in Section IIIB2. Another class of experiments which demonstrate long lived coherence in broad line systems are the various multiple pulse dipolar line narrowing sequences (61-63,148,149).

In the spin locking and multiple pulse experiments the intense continuous or rapidly repeated irradiation might be thought to be preventing irreversible dephasing by decoupling the spin system from the very processes responsible for relaxation. An analogy would be the irreversible dephasing in liquids which arises from random diffusion in a field gradient. Such relaxation is indeed eliminated by spin locking and also by the more familiar rapid sequence of π pulses[86].

That this analogy is flawed is demonstrated by the magic echo[121] and other time reversal experiments[145,196] already mentioned in Sections IIIA2 and IIIC6. In these experiments the system may evolve far from the observable initial condition of transverse magnetization and still be retrieved. This single quantum evolution was described in Section IIA3 as a unitary conversion of the "visible" $\ell = 1$ tensor operator into "invisible", multipolar single quantum operators characterized by higher values of the angular momentum quantum number ℓ.

On the other hand, loss of coherence due to translational diffusion in a field gradient is truly irreversible; to recover it would require reversing the spatial trajectories of the molecules themselves.

The viewpoint taken here then is that any evolution of the system due to a static spin Hamiltonian is in principle reversible; it is not described by a reduction in $Tr(\rho^2)$. The entropy of the spin system is conserved under unitary time development of its density operator, regardless of the complexity of this time development. Thus there is no

thermodynamic inconsistency. The practicality of actually reversing the spin dynamics in a particular case is a separate matter.

This still leaves the question of the mechanism of the various truly irreversible relaxation processes. Radiative mechanisms both coherent and spontaneous, are almost always negligible in NMR. In nearly all cases the irreversible decay is due to fluctuations of diagonal or off-diagonal terms of the spin Hamiltonian due to random motion of the lattice. The theory of this relaxation is well established [18,26,28,197-201] and is totally applicable without fundamental modification to any observation made with multiple quantum NMR.

This is not to say that there is nothing new in multiple quantum relaxation studies. Novel features arise because of the greater variety of observables which are measurable in practice. This is the subject of Sections VB and VC and of previous discussions[13,29]. In the remainder of this section we consider the role of the familiar phenomenological relaxation times as constraints on the multiple quantum experiments already discussed.

2. Relaxation Times as Constraints

In the many level systems necessary for multiple quantum phenomena there are of course a great number of different relaxation times. In this section it will be useful to refer to exponential time constants T_1, T_2, and $T_{1\rho}$ even though the closer analysis, which will be necessary subsequently, shows that there are many times of each type.

The spin lattice relaxation time T_1 is the longest of these times and limits the repetition rate and thus the sensitivity of the multiple quantum experiment much as in the single quantum case. The major difference is that the two dimensional nature of the experiment and the

greater complexity of the pulse sequences can lead to subtle line amplitude anomalies when the repetition period is less than several T_1. On the other hand, these are frequently not a concern and more rapid repetition is common and particularly advantageous in the presence of multiplicative noise (Sec. IIB3).

The transverse relaxation time T_2 constrains the multiple quantum experiment in diverse ways. The most obvious is that it sets an upper limit on the useful length of t_1, which must vary over several times T_2 to allow accurate linewidth. The more difficult question is the way in which T_2 processes limit the length of the preparation and mixing periods and consequently the number of quanta n. It is evident from the discussions of the preceding sections that the length of the excitation periods can not be much longer than some T_2 since off diagonal elements dominate in ρ during these times. For the simplest sequences, only single quantum coherence is relevant during τ and τ'. In general, however, the various orders are rapidly interconverted by rf pulses and no easy prescription for the relevant decay time is available, though the ordinary $T_{1\rho}$ is of the right magnitude and is experimentally accessible.

If some such estimate of the maximum length allowed for excitation is made one is left with the problem of how long it takes to excite lines of a certain order. Again, there is no simple rule, but some rough guidelines have emerged. The greatest number of calculations have been done for dipolar coupled systems of up to eight protons[118,126]. For the sequence of three $\pi/2$ pulses the high order coherence typically reaches a first maximum in a time τ of less than several times $M_2^{-\frac{1}{2}}$. This maximum will usually be far less than the ideal order selective maximum (Sec.IIIC8), which in larger systems becomes increasingly unlikely

to be approached nonselectively even in a time T_2. For such systems, the quantity $M_2^{-\frac{1}{2}}$ serves as an approximate correlation time, in the sense of Section IIIB1. An effective subcycle of an order selective sequence (Sec. IIIC6) will also extend for comparable time or longer, so that a period $\tau \gtrsim n\, M_2^{\frac{1}{2}}$ is an optimistic lower bound on the time needed for a selective excitation period. Since higher order sequences (Sec. IIIC7) are anticipated[145] to be increasingly necessary for larger systems a more cautious estimate is $\tau \gtrsim (4n)^2\, M_2^{-\frac{1}{2}}$. For $\tau = T_2$ and $(T_2/M_2^{-\frac{1}{2}}) = 10^3$ this suggests a maximum n in the neighborhood of 15.

Lacking still is a comprehensive understanding of how the production of higher order coherence depends on the distribution of dipolar couplings so it is not clear that an estimate in terms of a single parameter like $M_2^{-\frac{1}{2}}$ will be generally useful. Roughly speaking, the smaller the range of the parameters D_{ij} the easier it is to create high order coherence. In the limiting case of an A_N system where all D_{ij} are equal, then $n = N$ quantum coherence is created with perfect efficiency in a time $\tau = (\pi/3D)$ with two pulse preparation[126]. In adamantane, where $\mathcal{H}^D_{II}$ is dominated by only a few near neighbor intermolecular couplings, spectra with $n > 20$ have been observed using a two-quantum selective sequence[196].

B. Longitudinal Relaxation Times

1. Master Equation Description for the Individual Populations

The relaxation of the populations of an ensemble of spin systems has the form of a set of coupled first order differential equations with constant coefficients[18]

$$\dot{\rho}_{ii} = \sum_j W_{ij}(\rho_{jj} - \rho_{jj}(0)) \tag{5.1}$$

The number of independent rates is constrained by the conservation of

$Tr(\rho)$, by detailed balance, and by the particular mechanisms responsible for the coupling to the lattice. In high field the only significant mechanisms involve an exchange of phonons at ω_0 or $2\omega_0$ between the spins and the lattice. For heteronuclear systems, energy exchange at the sums and differences of Larmor frequencies may also enter. The rates W_{ij} are particular sums of spectral densities at these frequencies. These spectral densities are the Fourier components of the various correlation functions between nonsecular terms of the spin Hamiltonian. The time dependence is a result of the motion of the lattice.

The applications of this formalism to spin systems with several levels have been reviewed[202,203]. One approach to making sufficient measurements to measure all the independent rates is to prepare the system with a variety of different nonequilibrium population distributions and monitor the recovery of these populations toward equilibrium by transferring population differences to coherence in a known way.

To date, multiple quantum excitation techniques have been used to prepare nonequilibrium population distributions for relaxation studies only in nearly isolated quadrupole nuclei[5,55]. In principle, both the order selective excitation of Section IIIC and the simple nonselective excitation sequences can be used to prepare various nonequilibrium population distributions in more complex systems. The efficiency of these schemes is low, particularly in systems of many spins. This is because most of the equilibrium population differences are either unperturbed (with high order selective sequences) or are converted to coherence (with nonselective sequences). Nevertheless, the strong pulse excitation methods offer an alternative means of preparing combinations of population differences which are not attainable with frequency

selective inversion when the single quantum line density becomes great.

Once some nonequilibrium population difference has been prepared the next step in any spin lattice relaxation experiment is to convert it to coherence after a variable delay. Usually this is single quantum coherence, since this is directly observable as magnetization. Furthermore the single quantum lines have the great advantage of being linearly dependent on individual population differences for small pulse angles[21]. These individual measurements become inaccessible when the single quantum lines are unresolved. One possibility, mentioned already in Section IIIC9, is to label population differences by a prior period of high quantum evolution so that the single quantum coherence resulting from them is separable from the bulk of the single quantum coherence.

Of course, the nonequilibrium population differences are also in principle measurable through the particular multiple quantum line intensities which result from them when they are used as initial conditions. The analysis is highly nonlinear in general and requires a quantitative characterization of the excitation propagators as is obtained by exact dynamical calculation for well characterized internal and rf Hamiltonians (Sec. IIIB1).

2. Other Descriptions of the Quasi-constants

The use of the individual state populations to describe the diagonal part of the density operator loses much empirical import when the system is too complex to resolve individual lines. It is well-known[18,31,204] that even in macroscopic spin systems, as occur for abundant spins in solids, there are at least two experimentally accessible constants of the motion. These are the longitudinal magnetization or Zeeman order and the energy of interaction between the spins or dipolar order.

An experimentally convenient way of preparing and monitoring dipolar order is the three pulse sequence $(\pi/2)_x-\tau-(\pi/4)_y-t_1-(\pi/4)-t_2$[205]. For short t_1 the measurement is complicated by interference from double quantum coherence[206,207]. In fact such a sequence is a nonselective multiple quantum experiment and must be expected, in general, to monitor a variety of coherences and nonequilibrium population differences. The coherence, including n = 0, is easily avoided in systems with unresolved spectra by keeping t_1 long. Signal arising from Zeeman order during t_1 is also easily accounted for since it appears immediately after and orthogonal to the final pulse. These are the usual considerations for using the sequence to measure the decay time T_{1D} of the dipolar order[205].

The more subtle question is whether the sequence does not also monitor other non-equilibrium population differences which, like dipolar order, are nearly constants of the motion for times t_1 much greater than the inverse spectral width $M_2^{-\frac{1}{2}}$. Some evidence for such other quasi-constants has been seen in the proton signals from liquid crystals[208] and partially deuterated solids[209]. In each case, even for long t_1, the signal evoked in t_2 by the final pulse was found to depend not only in size, but also in shape, on the length of the preparation period τ.

Such observations suggest that the density operator contains during t_1 quasi-constants orthogonal to $\mathcal{H}^{zz}$ and I_z and that these have different dependences on τ and t_2 than either dipolar or Zeeman order. The change in their relative contributions to the signal with τ, leads to the different signal shapes in t_2 or ω_2.

That such quasi-constants exist can be easily seen from the fact that any operators of the form $(I_z)^p\ (\mathcal{H}_{int})^q$ with integers p and q contain only diagonal elements regardless of the size of the system. Though not

an orthogonal basis, this set certainly contains operators which are neither linear nor bilinear in the individual spin operators and which are orthogonal to I_z and $\mathcal{H}^{zz}$. The unanswered question is whether such terms can be experimentally isolated and theoretically analyzed in systems with unresolved single quantum spectra so as to provide additional relaxation parameters. The principle difficulty, of course, is that the ratio of diagonal to off-diagonal density matrix elements decreases as $(2I+1)^{-N}$ for N spins I. Any nonselective approach soon runs into problems of signal to noise as N increases, since the greatest part of the original order $Tr(\rho^2)$ becomes coherence.

C. Transverse Relaxation Times

1. Complete Characterization of the Spectral Densities

Perhaps the most fundamental fact about time domain multiple quantum studies is that they allow one to measure more quantities on a given system. Even for systems of only several levels this becomes invaluable for a complete characterization of the relaxation. Once a model of the relaxation process has been adopted any Lorentzian linewidth can be expressed in terms of some number of independent spectral densities. The number of independent spectral densities will generally exceed the number of single quantum lines. In some cases the multiple quantum linewidths will suffice to complete the characterization. In any case, they provide a fuller picture. This point has been a motivation for a number of multiple quantum relaxation studies in liquids[8, 29,47-49].

The relaxation of deuterons on small molecules dissolved in liquid crystal solvents has been the subject of a number of studies using multiple quantum techniques in order to obtain a complete characterization

of spectral densities. The advantage of deuterated systems is that the relaxation is dominated by the fluctuating quadrupole Hamiltonian. Intermolecular dipolar relaxation is often negligible, allowing a model based on the orientational dynamics of a single molecule.

Expressions needed for a single deuteron, for the various relaxation rates in terms of spectral densities were given even before the value of the time domain multiple quantum experiment for such studies was appreciated[210-213]. In a series of studies combining both spin lattice relaxation time measurements and various single and multiple quantum transverse measurements, one[73,214-216], two[217,218] and three[123,219] deuteron systems have been examined. The measured spectral densities are modeled in terms of rapid anisotropic reorientation and slower fluctuations in molecular ordering due to director fluctuations of the liquid crystals and translational diffusion of the solutes.

2. Enhanced and Reduced Sensitivity to Fluctuations

The different sensitivity of various lines to particular relaxation mechanisms is particularly easy to visualize for the adiabatic contribution to the linewidths. This is the pure dephasing contribution, which is proportional to zero frequency spectral densities and which originates from fluctuations of diagonal terms of the Hamiltonian. Figure 47 illustrates the way in which certain transitions can have an enhanced or a reduced sensitivity to particular relaxation mechanisms. The energy level diagram in the center (part b) is that of the time averaged Hamiltonian which determines the line centers. In part a) the energy level diagram is redrawn with some dipolar terms varying from left to right over some small range. The slope of each energy level is a measure of its sensitivity to the terms which vary. Note, for example,

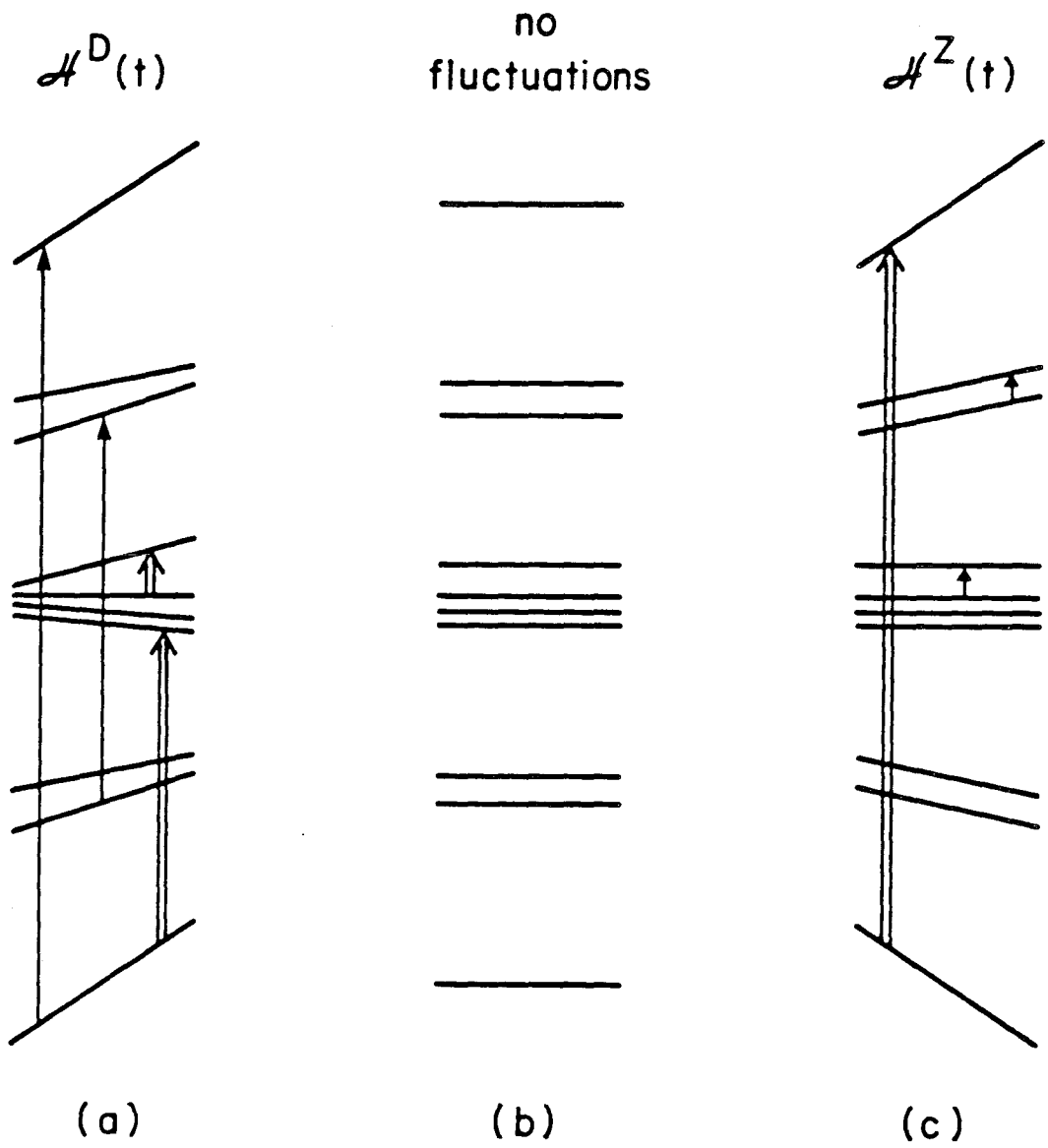

XBL 8112-12900

Figure 47. Enhanced and reduced sensitivity of transitions to linear and bilinear fluctuations. The sensitivity of the transverse relaxation times of particular transitions to low frequency fluctuations is apparent in the extent to which the transition frequency changes as a term in the Hamiltonian is varied. In part a) the dipolar terms vary from left to right. In part b) the average energies are shown. In part c) the total Zeeman energy varies. Single arrows represent transitions which are insensitive to the particular fluctuation. Double arrows represent transitions which are particularly sensitive.

that the extreme energy levels vary in the same way with any change in dipolar couplings. Transitions connecting energy levels which vary identically with the changing Hamiltonian have a constant frequency. These are indicated by single arrows. Thus the spin inversion transitions (Sec. IIIA4), such as the total spin transition, are insensitive to dipolar fluctuations. This applies not only to their line positions, but also to the adiabatic contribution to their linewidth. Other transitions, indicated by double arrows, are particularly sensitive to dipolar fluctuations, because the energy levels which they connect move in opposite directions as these terms change.

In part c) a similar picture is drawn for the case of a fluctuating Zeeman term, as would be experienced by a molecule diffusing through an inhomogeneous field (Sec. IIE5) or diffusing with respect to a distant paramagnetic center. For a fluctuating field which is homogeneous over the dimensions of the observed spin system, the sensitivity of the line positions to the time average field is proportional to n (Sec. IID1), while the sensitivity of the adiabatic dephasing rate to the fluctuations in the field is proportional to n^2[220]. Thus the total spin transition which is insensitive to bilinear intramolecular fluctuations is most sensitive to external fluctuations.

3. Correlations in Fluctuating Fields

A more interesting case arises when the fluctuating field may vary across the system dimensions. This occurs when this dimension is comparable to the distance of closest approach to a paramagnetic center. In such a situation the relaxation rates may be used to evaluate the degree of correlation of the fluctuating field at the different spins of the system[29,220]. This effect has been studied in the AB proton

system of 2,3-dibromothiophene in the presence of either dissolved O_2 or the bulkier paramagnet 1,1-diphenyl-2-picryl-hydrazyl[29]. It was found using single and double quantum linewidths that the correlation in the fluctuations was greater for the larger relaxation agent.

This question of the degree of correlation in paramagnetic relaxation has also been investigated in the oriented system of acetonitrile and di-t-butylnitroxide in the liquid crystal EBBA (p-ethoxy-benzylidine n-butylaniline). Figure 48 shows the ratio of the transverse relaxation rates of the n = 2 and n = 3 transitions to that of the n = 1 transitions for the acetonitrite methyl group as a function of a correlation factor ξ[220]. This factor is a measure of the extent to which the relaxation process retains the C_3 symmetry of the time averaged Hamiltonian. The various lines are for different limits of the electronic and nuclear correlation times. The experimental dependence of the multiple quantum linewidths on concentration of the paramagnet demonstrated that the curves C and C' applied and that the relaxation was nearly fully symmetric ($\xi = 1$). Calculations have also been performed for two methyl groups[221].

4. Spin Locking of Multiple Quantum Coherence

In Section IIIB2 spin locking of transverse magnetization was discussed as a way of stopping the dynamics of the system due to $\mathcal{H}_{int}$ in order to prolong a state of high signal power in the detection period. The more usual motivation for such single quantum spin locking with intense fields is the measurement of the irreversible decay of coherence, characterized by $T_{1\rho}$, without the complication of reversible, unitary dynamics. In addition, it is sometimes possible to characterize the spectral densities of low frequency motions by measuring $T_{1\rho}$ as a function of the rotating frame frequency $\omega_p = \gamma H_1$[26].

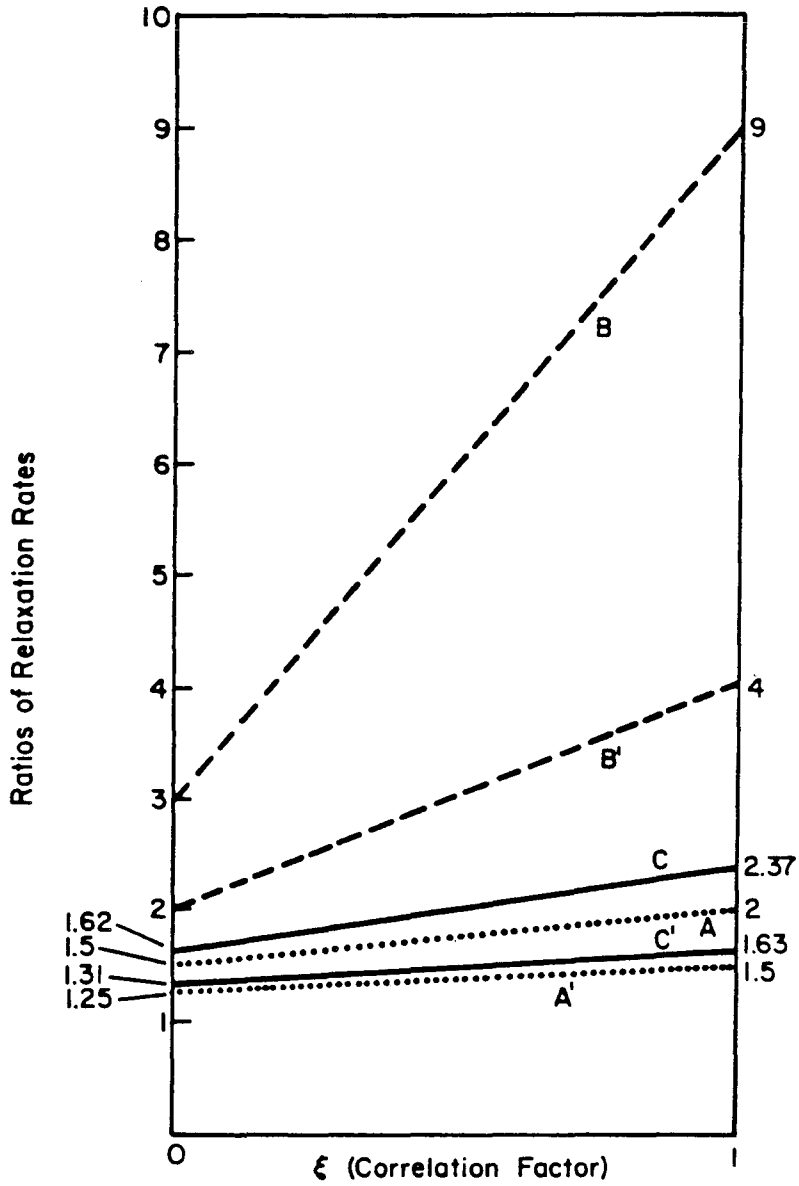

Figure 48. The ratios of transverse relaxation rates of an oriented methyl group (I) due to a fluctuating paramagnetic center(S). The unprimed letters indicate the ratio of double to single quantum rates. The primed letters indicate the ratio of triple to single quantum rates. The three letters distinguish different regimes for the correlation time τ_c of the interaction relative to the Larmor frequencies ω_I and ω_S: A, $\tau_c^2 \ll \omega_S^{-2}$; B, $\tau_c^2 \gg \omega_I^{-2}$ and C, $\omega_I^{-2} \gg \tau_c^2 \gg \omega_S^{-2}$. Each curve is shown as a function of a correlation factor ξ which measures the extent to which the fluctuating field of S is the same at each of the three methyl protons over periods of $\sim\tau_c$. [By permission from J. Tang and A. Pines, J. Chem. Phys. 72, 3290 (1980).]

In Section IIC2 a variety of studies were reviewed involving frequency selective double quantum irradiation on a three-level system. Analysis of these experiments is conveniently approached by replacing the usual Liouville space operators of a dipole allowed two level system (I_x, I_y, and I_z) by their double quantum analogs. The double quantum analog of ω_p is (ω_p^2/ω_Q), which already appeared in (2.40). The double quantum analog of spin locking is illustrated in Figure 49[7]. The spin system is the carboxyl deuterons of crystalline oxalic acid dihydrate. The pulse sequence is shown in the inset. The first segment of 58 μsec is a $\pi/2$ $(\frac{1}{2}\omega_{13})$ pulse (Sec. IIC2) which prepares the double quantum coherence. A phase shift of the rf by 45° follows. This is analogous to one of 90° for a two level system; it makes the effective radiation interaction Hamiltonian proportional to the density operator. This weak irradiation is sustained for a variable evolution time (τ in Fig. 49) followed by mixing and detection.

If the couplings between spins are less than (ω_p^2/ω_Q), they are truncated with respect to the radiation operator during evolution and cease to effect the dynamics. In this example this effect resulted in a decay time of 2.2 msec. This a factor of ten longer than the apparent decay of the coherence in the absence of the spin locking.

The extension of this concept to the total spin coherence of any system is straightforward since an order selective pulse sequence will always reduce the problem to a two level problem. Similarly, for all QTLS (Sec. IIIC8c) and QFLS (Sec. IIIC9c), the form of the prepared high quantum operator is related to the effective preparation period Hamiltonian by a phase shift of $\pi/2n$. Alternatively, multiple quantum spin-locking could be achieved by adiabatically bringing an order selective

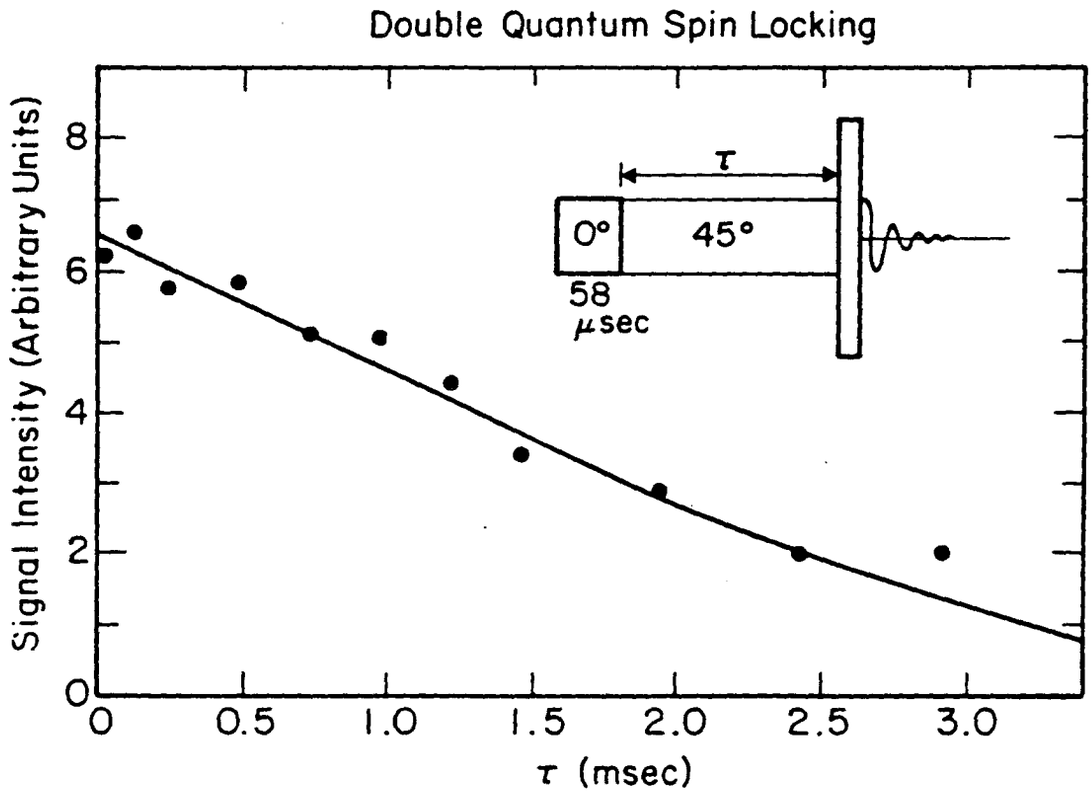

XBL 7710-6865

Figure 49. Double quantum spin locking on a spin 1 nucleus. A double quantum $\pi/2$ pulse is followed by a phase shift of $\pi/4$ in the rf phase and continued irradiation. The effective radiation interaction operator is proportional to the density operator, resulting in spinlocking of the double quantum coherence. The decay time, which is a double quantum analog of $T_{1\rho}$, is measured through the signal which develops after a mixing pulse. The system is the carboxyl deuterons of crystalline oxalic acid dihydrate. [By permission from S. Vega and A. Pines, in "Magnetic Resonance and Related Phenomena", (H. Brunner, K. Hausser, and D. Schweitzer, eds.), p. 395, Bettz Offsetdruck, Hemsbach, 1976.]

sequence from far off resonance into resonance. In this case no phase shift between preparation and locking is used. The subcycles of Section IIIC6c are particularly applicable for adiabatic spin locking, since the offset term is effective.

In all of these cases the selective multiple quantum spin locking method is only of obvious utility for relaxation studies if there exists some broadening mechanism, such as intramolecular couplings, to be eliminated and if the effective multiple quantum nutation frequency is large enough to truncate it. For a dipolar coupled system of spins 1/2 this nutation frequency is difficult in general to estimate beforehand, but it is likely to be inadequate in many cases since it is comparable to or less than typical dipolar couplings.

An alternative possibility for spin locking of multiple quantum coherence is to use an intense pulse of constant phase as in ordinary spin locking. Under such irradiation there must be a class of quasi-constants since any operator of the form $(I_y)^p\ (\mathcal{H}^{yy})^q$ is in this class for radiation of phase y. $\mathcal{H}^{yy}$ is given by (3.54). This class contains coherence of all orders n, but it is not obvious without calculation which particular linear combinations of lines would be spin locked nor under what conditions the decay times observed would provide information complementary to the ordinary $T_{1\rho}$.

5. Exchange

A variety of rather different processes can be loosely grouped as exchange phenomena. These have the common feature that magnetization or coherence is transferred from one transition to another during a period of free evolution. Thus the simple picture of resolved transitions, each with its own T_2 is inapplicable. The different

situations where this occurs are variously viewed as population processes (spin diffusion) or off-diagonal processes (exchange broadening and narrowing). Recently 2D Fourier transformation has been applied to these problems[222].

A great many applications of NMR relaxation theory have been made to the problem of chemical exchange and the field is frequently reviewed[223-226]. Here an incoherent thermally activated motion of the lattice randomly exchanges spins between different environments either within or between molecules. One application of time domain multiple quantum NMR has been made to such a problem: the $n = 6$ proton spectrum of cyclooctatetraene in a nematic solvent was used to measure the rate of intramolecular bond shift exchange[150]. This process had previously been analyzed through the spectrum of proton pairs in the partially deuterated compound[227]. The motivation for the multiple quantum study was that the relatively sparse high order spectra provides resolved lines without isotopic labeling. A difficulty encountered in practice is that the T_2 due to the exchange process itself limits the efficiency of multiple quantum excitation. This decreases the signal-to-noise ratio sharply in the interesting region of exchange broadening.

Another case where the simple analysis in terms of isolated lines fails is when two transitions are degenerate. In such a case relaxation mechanisms can transfer population differences or coherence between pairs of levels[200]. This may occur even between different irreducible representations if the time dependent mechanism breaks the symmetry of the average Hamiltonian. Exchange between degenerate multiple quantum transitions has been noted by several authors[48,49,218]. This is a situation where representation of the data in two frequency dimensions

is particularly useful, since exchanging transitions which are degenerate in ω_1 may be separable in ω_2 by the single quantum frequencies which carry their signals[73].

Spin diffusion, either spatially or between different frequency regions of a spectrum, is also a form of exchange phenomenon, but one which persists even in the absence of random lattice fluctuations. It is usually viewed as change in the populations of some localized system of a few levels, but can also be viewed as zero quantum coherence within the larger system. As a process dependent only on the static spin Hamiltonian, it is not irreversible in the sense of Section VA1.

Recently spin diffusion between $S = 1$ nuclei in solids has received renewed attention. It is relevant to the effectiveness of cross polarization of quadrupolar nuclei as the magnetization gained from the I spins will be to some extent shared even by those S spins not directly cross polarized[228]. The surprising feature is that spin diffusion is reasonably effective even between $I = 1$ spins with different values of ω_Q[228-230]. This would appear to violate energy conservation, since the single quantum transitions do not overlap. Sample rotation[228] and heteronuclear couplings[229,230] have been implicated in mechanisms for making up this mismatch.

A simpler mechanism has been advanced[231] which involves only the homonuclear coupling among the I spins. The condition that the quadrupolar satellites are well resolved turns out to be a poor criterion for whether the Zeeman order associated with a particular ω_Q is a constant of the motion. The coupling between such different sites can be formulated as an effective double quantum flip-flop operator with a reduced, but significant, coupling constant. Further

work is necessary to sort out the role of the various mechanisms in the experimental situations of interest.

References

1. E. L. Hahn, Phys. Rev. 80, 580 (1950).

2. E. L. Hahn and D. E. Maxwell, Phys. Rev. 88, 1070 (1952).

3. I. Solomon, Phys. Rev. 110, 61 (1958).

4. J. Jeener, Ampere International Summer School, Basko Polje, Yugoslavia, 1971 (unpublished).

5. H. Hatanaka, T. Terao and T. Hashi, J. Phys. Soc., Japan, 39, 835 (1975).

6. H. Hatanaka and T. Hashi, J. Phys. Soc., Japan, 39, 1139 (1975).

7. S. Vega and A. Pines, in "Magnetic Resonance and Related Phenomena" (H. Brünner, K. Hausser, and D. Schweitzer, eds.), p. 395. Beltz Offsetdruck, Hemsbach, 1976.

8. M. E. Stoll, A. J. Vega and R. W. Vaughan, J. Chem. Phys. 67, 2029 (1977).

9. W. P. Aue, E. Bartholdi and R. R. Ernst, J. Chem. Phys. 64, 2229 (1976).

10. R. Freeman and G. A. Morris, Bull. Magn. Reson. 1, 5 (1979).

11. R. Freeman, Proc. R. Soc. Lond. A 373, 149 (1980).

12a. K. Nagayama, Adv. Biophys. 14, 139 (1981).

12b. A. Bax, "Two Dimensional NMR", Delft University Press, 1982.

13. G. Bodenhausen, Prog. in NMR Spec. 14, 137 (1981).

14. A. Pines, D. Wemmer, J. Tang and S. Sinton, Bull. Amer. Phys. Soc. 23, 21 (1978).

15. G. Drobny, A. Pines, S. Sinton, D. P. Weitekamp and D. Wemmer, Faraday Symp. Chem. Soc. 13, 49 (1979).

16. S. Sinton, "NMR Studies of Oriented Molecules", Ph.D. dissertation, University of California, Berkeley, 1981, published as Lawrence Berkeley Laboratory Report LBL-13604.

17. A. Saupe, Z. Naturforsch 20a, 572 (1965).

18. A. Abragam, "The Principles of Nuclear Magetism", Oxford University Press, 1961.

19. I. J. Lowe and R. E. Norberg, Phys. Rev. 107, 46 (1957).

20. S. Schäublin, A. Höhener, and R. R. Ernst, J. Magn. Reson. 13, 196 (1974).

21. R. R. Ernst, W. P. Aue, E. Bartholdi, A. Höhener and S. Schäublin, Pure Appl. Chem. 37, 47 (1974).

22. W. A. Anderson, Phys. Rev. 104, 850 (1956).

23. J. I. Kaplan and S. Meiboom, Phys. Rev. 106, 499 (1957).

24. S. Yatsiv, Phys. Rev. 113, 1522 (1959).

25. U. Fano, Rev. Mod. Phys. 29, 74 (1957).

26. C. P. Slichter, "Principles of Magnetic Resonance", Springer, Berlin, 1978.

27. M. Silver, "Irreducible Tensor Methods", Academic Press, New York, 1976.

28. R. A. Hoffman, Advan. Magn. Reson. 4, 87 (1970).

29. A. Wokaun and R. R. Ernst, Molec. Phys. 36, 317 (1978).

30. A. G. Anderson and S. R. Hartmann, Phys. Rev. 128, 2023 (1962).

31. A. Abragam and M. Goldman, "Magnetism, Order and Disorder", Oxford University Press, 1982.

32. S. Emid, J. Smidt and A. Pines, Chem. Phys. Lett. 73, 496 (1980).

33. R. N. Bracewell, "The Fourier Transform and Its Applications", McGraw Hill, New York, 1978.

34. A. A. Maudsley, L. Müller, and R. R. Ernst, J. Magn. Reson. 28, 463 (1977).

35. A. Wokaun and R. R. Ernst, J. Chem. Phys. 67, 1752 (1977).

36. S. Vega, J. Chem. Phys. 68, 5518 (1978).

37. R. G. Brewer and E. L. Hahn, Phys. Rev. A. 11, 1641 (1975).

38. S. Vega and A. Pines, J. Chem. Phys. 66, 5624 (1977).

39. M. M. T. Loy, IBM J. Res. Develop. 23, 504 (1979).

40. M. Mehring, E. K. Wolff and M. E. Stoll, J. Magn. Reson. 37. 475 (1980).

41a. S. B. Ahmad and K. J. Packer, Mol. Phys. 37, 47 (1979).

41b. S. B. Ahmad and K. J. Packer, Mol. Phys. 37. 59 (1979).

41c. G. L. Hoatson and K. J. Packer, Mol. Phys. 40, 1153 (1980).

41d. J. Stepisnik, Physica 100 B+C, 245 (1980).

42. H. Hatanaka, T. Ozawa, and T. Hashi, J. Phys. Soc., Japan, 42, 2069 (1977).

43. H. Hatanaka and T. Hashi, Phys. Lett. 67A, 183 (1978).

44. H. Hatanaka and T. Hashi, Phys. Rev. B., 21, 2677 (1980).

45. S. Vega, T. W. Shattuck and A. Pines, Phys. Rev. Lett. 37, 43 (1976).

46. E. Y. C. Lu and L. E. Wood, Phys. Lett. 44A, 68 (1973).

47. P. M. Henrichs and L. J. Schwartz, J. Magn. Reson. 28, 477 (1977).

48. P. M. Henrichs and L. J. Schwartz, J. Chem. Phys. 69, 622 (1978); J. Chem. Phys. 70, 2586 (1979).

49. R. Kaiser, J. Magn. Reson. 40, 439 (1980).

50. M. E. Stoll, A. J. Vega, and R. W. Vaughan, Phys. Rev. A 16, 1521 (1977).

51a. M. E. Stoll, E. K. Wolff and M. Mehring, Phys. Rev. A 17, 1561 (1978).

51b. E. K. Wolff and M. Mehring, Phys. Lett. 70A, 125 (1979).

52. M. E. Stoll, Phil. Trans. R. Soc. Lond. A, 299, 565 (1981).

53. S. Vega and Y. Naor, J. Chem. Phys. 75, 75 (1981).

54. D. E. Wemmer, "Some Double Resonance and Multiple Quantum NMR Studies in Solids", Ph. D. dissertation, University of California, Berkeley, 1978, published as Lawrence Berkeley Laboratory Report LBL-8042.

55. D. G. Gold and E. L. Hahn, P. Rev. A 16, 324 (1977).

56. H. C. Torrey, Phys. Rev. 76, 1059 (1949).

57. R. C. Hewitt, S. Meiboom and L. C. Snyder, J. Chem. Phys. 58, 5089 (1973).

58. L. C. Snyder and S. Meiboom, J. Chem. Phys. 58, 5096 (1973).

59. J. W. Emsley, J. C. Lindon and J. M. Tabony, J. Chem. Soc. Faraday Trans. 269, 10 (1973).

60. A. Pines, D. J. Ruben, S. Vega and M. Mehring, Phys. Rev. Lett. 36, 110 (1976).

61. U. Haeberlen and J. S. Waugh, Phys. Rev. 175, 453 (1968).

62. U. Haeberlen, "High Resolution NMR in Solids, Selective Averaging", Academic Press, New York, 1976.

63. M. Mehring, "High Resolution NMR Spectroscopy in Solids", Springer, Berlin, 1976.

64. A. Pines, S. Vega and M. Mehring, Phys. Rev. B 18, 112 (1978).

65. D. Suwelack, M. Mehring and A. Pines, Phys. Rev. B. 19, 238 (1979).

66. E. R. Andrew, Int'l Rev. Phys. Chem. 1, 195 (1981).

67. J. L. Ackerman, R. Eckman and A. Pines, Chem. Phys. 42, 423 (1979).

68. R. Eckman, M. Alla and A. Pines, J. Magn. Reson., 41, 440 (1980).

69. R. Eckman, L. Müller and A. Pines, Chem. Phys. Lett. 74, 376 (1980).

70. A. Wokaun and R. R. Ernst, Molec. Phys. 38, 1579 (1979).

71. G. Baym, "Lectures on Quantum Mechanics", Chapter 5, W. A. Benjamim, Inc., Reading, Massachusetts, 1969.

72. A. Wokaun and R. R. Ernst, Chem. Phys. Lett. 52, 407 (1977).

73. G. Bodenhausen, R. L. Vold, and R. R. Vold, J. Magn. Reson. 37, 93 (1980).

74. G. Bodenhausen, J. Magn. Reson. 34, 357 (1979).

75. J. B. Murdoch, personal communication, 1978.

76a. R. Freeman, T. A. Frenkiel, and M. H. Levitt, J. Magn. Reson. 44, 409 (1981).

76b. T. A. Frenkiel, M. H. Levitt and R. Freeman, J. Magn. Reson. 47, 328 (1982).

77. R. Freeman and H. D. W. Hill, J. Chem. Phys. 54, 301 (1971).

78a. A. Kumar. J. Magn. Reson. 30, 227 (1978).

78b. M. A. Thomas and A. Kumar, J. Magn. Reson. 47, 535 (1982).

79. J. B. Murdoch, personal communication, 1981.

80. A. A. Maudsley, A. Wokaun and R. R. Ernst, Chem. Phys. Lett. 55, 9 (1978).

81. A. Bax, P. G. De Jong, A. F. Mehlkopf and J. Smidt, Chem. Phys. Lett. 69, 567 (1980).

82. Y. S. Yen and D. P. Weitekamp, J. Magn. Reson. 47, 476 (1982).

83. D. P. Weitekamp, J. R. Garbow, and A. Pines, J. Chem. Phys. 77, 2870 (1982).

84. D. P. Weitekamp, J. R. Garbow, J. B. Murdoch and A. Pines, J. Amer. Chem. Soc. 103, 3578 (1981).

85. J. R. Garbow, D. P. Weitekamp and A. Pines, in preparation.

86. H. Y. Carr and E. M. Purcell, Phys. Rev. 94, 630 (1954).

87a. J. F. Martin, L. S. Selwyn, R. R. Vold and R. L. Vold, J. Chem. Phys. 76, 2632 (1982).

87b. D. Zax and A. Pines, submitted for publication.

88. G. Pouzard, S. Sukumar, and L. D. Hall, J. Amer. Chem. 103, 1209 (1981).

89. R. L. Strombotne and E. L. Hahn, Phys. Rev. 133, A1616 (1964).

90. S. Schäublin, A. Wokaun and R. R. Ernst, Chem. Phys. 14, 285 (1976).

91. G. L. Closs, Advan. Magn. Reson. 7, 157 (1974).

92. A. Bax, T. Mehlkopf, J. Smidt, and R. Freeman, J. Magn. Reson. 41, 502 (1980).

93. J. W. Emsley, J. Feeney and L. H. Sutcliffe, "High Resolution Nuclear Magnetic Resonance Spectroscopy", Pergamon Press, Oxford, 1965.

94. P. L. Corio, "Structure of High Resolution NMR Spectra", Academic Press, New York, 1966.

95. J. W. Emsley and J. C. Lindon, "NMR Spectroscopy Using Liquid Crystal Solvents", Pergamon Press, Oxford, 1975.

96. S. Sinton and A. Pines, Chem. Phys. Lett. 76, 263 (1980).

97. W. S. Warren and A. Pines, J. Amer. Chem. Soc. 103, 1613 (1981).

98. G. Drobny, A. Pines, S. Sinton, W. S. Warren and D. P. Weitekamp, Phil. Trans. R. Soc. Lond. A 299, 585 (1981).

99a. G. Drobny, D. P. Weitekamp and A. Pines, submitted to Chem. Phys. Lett.

b. G. Drobny, "NMR Studies of Liquid Crystals and Molecules Dissolved in Liquid Crystal Solvents", Ph.D. Dissertation, University of California, Berkeley, 1982.

100. Y. S. Yen, personal communication (1980).

101. A. Messiah, "Quantum Mechanics", Chapter XV, John Wiley & Sons, New York, 1959.

102. A. Bax, R. Freeman and S. P. Kempsell, J. Amer. Chem. Soc. 102, 4849 (1980).

103. A. Bax, R. Freeman and S. P. Kempsell, J. Magn. Reson. 41, 349 (1980).

104. A. Bax and R. Freeman, J. Magn. Reson. 41, 507 (1980).

105. A. Bax, R. Freeman, T. A. Frenkiel and M. H. Levitt, J. Magn. Reson. 43, 478 (1981).

106. A. Bax, R. Freeman and T. A. Frenkiel, J. Am. Chem. Soc., in press.

107. D. W. Sorensen, R. Freeman, T. Frenkiel and T. H. Mareci, J. Magn. Reson. 46, 180 (1982).

108. P. Diehl and C. L. Khetrapal, "NMR, Basic Principles and Progress", 1, 1, (1969).

109. C. L. Khetrapal and A. C. Kunwar, Advan. Magn. Reson. 9, 301 (1977).

110. R. W. Vaughan, Ann. Rev. Phys. Chem. 29, 397 (1978).

111. C. L. Khetrapal and A. C. Kunwar, Specialist Periodical Reports, NMR 9, 245 (1980).

112. T. Terao and R. Ikeda, Specialist Periodical Reports, NMR 10, 132 (1981).

113. G. J. T. Tiddy, Specialist Periodical Reports, NMR 10, 267 (1981).

114. S. Hsi, H. Zimmermann and Z. Luz, J. Chem. Phys. 69, 4126 (1978).

115. P. Diehl, H. Kellerhals and E. Lustig, "NMR Basic Principles and Progress", 6, 1 (1972).

116. P. Diehl, S. Sykora and J. Vogt, J. Magn. Reson. 19, 67 (1975).

117a. D. S. Stephenson and G. Binsch, J. Magn. Reson. 37, 395 (1980).

117b. D. S. Stephenson and G. Binsch, J. Magn. Reson. 37, 409 (1980).

118. J. B. Murdoch, "Computer Studies of Multiple Quantum Spin Dynamics", Ph. D. Dissertation, University of California,Berkeley, 1982.

119. J. Tang and A. Pines, J. Chem. Phys. 73, 2512 (1980).

120. P. J. Flory, "Statistical Mechanics of Chain Molecules", Interscience, New York, 1969.

121. W. -K. Rhim, A. Pines and J. S. Waugh, Phys. Rev. B 3, 684 (1971).

122. J. B. Murdoch, personal communication, 1980.

123. D. Jaffe, R. R. Vold and R. L. Vold, J. Magn. Reson. 46, 475 (1982).

124. K. J. Packer, Mol. Phys. 39, 15 (1980).

125. L. Müller, J. Magn. Reson. 42. 324 (1981).

126. J. B. Murdoch, W. S. Warren, D. P. Weitekamp and A. Pines, "Computer Simulations of Multiple Quantum NMR Experiments", in preparation.

127. A. D. Bain and S. Brownstein, J. Magn. Reson. 47, 409 (1982).

128. D. P. Weitekamp, J. R. Garbow and A. Pines, J. Magn. Reson. 46, 529 (1982).

129. J. B. Murdoch, personal communication, 1981.

130. R. R. Ernst, Advan. Magn. Reson. 2, 1 (1966).

131. W. P. Aue, P. Bachmann, A. Wokaun and R. R. Ernst, J. Magn. Reson. 29, 523 (1978).

132. P. Diehl, C. L. Khetrepal, H. P. Kellerhals, J. Magn. Reson. 1, 257 (1968).

133. E. D. Ostroff and J. S. Waugh, Phys. Rev. Lett. 16, 1097 (1966).

134a. W. -K. Rhim, D. P. Burum and D. D. Elleman, Phys. Rev. Lett. 37, 1764 (1976).

134b. M. Maricq, Phys. Rev. B. 25, 6622 (1982).

135. A. G. Redfield, Phys. Rev. 98, 1787 (1955).

136. I. Solomon, Compt. Rend. 248, 92 (1959).

137. S. R. Hartmann and E. L. Hahn, Phys. Rev. 128, 2042 (1962).

138. Y. S. Yen, D. P. Weitekamp, and A. Pines, to be published.

139. K. Nagayama, P. Bachmann, K. Wuthrich and R. R. Ernst, J. Magn. Reson. 31, 133 (1978).

140. A. F. Mehlkopf, personal communication, 1982.

141. J. S. Waugh, J. Mol. Spectrosc. 35, 298 (1970).

142. J. Tang, personal communication, 1977.

143. W. S. Warren, S. Sinton, D. P. Weitekamp and A. Pines, Phys. Rev. Lett. 43, 1791 (1979).

144. W. S. Warren, D. P. Weitekamp and A. Pines, J. Magn. Reson. 40, 581 (1980).

145. W. S. Warren, D. P. Weitekamp and A. Pines, J. Chem. Phys., 73, 2084 (1980).

146. W. S. Warren and A. Pines, J. Chem. Phys. 74, 2809 (1980).

147. W. S. Warren and A. Pines, Chem. Phys. Lett. 88, 441 (1982).

148. D. P. Burum and W. -K. Rhim, J. Chem. Phys. 71, 944 (1979).

149. D. P. Burum, M. Linder and R. R. Ernst, J. Magn. Reson. 44, 123, (1981).

150. W. S. Warren, "Selectivity in Multiple Quantum Nuclear Magnetic Resonance", Ph.D. dissertation, University of California, Berkeley, 1980, published as Lawrence Berkeley Laboratory Report LBL-11885.

151. W. S. Warren, J. B. Murdoch and A. Pines, to be published.

152. J. T. Yeh and J. H. Eberley, Phys. Rev. A 22, 1124 (1980).

153. J. L. Skinner, H. C. Andersen and M. D. Fayer, Phys. Rev. A 24, 1994 (1981).

154. F. Bloch and A. Siegert, Phys. Rev. 57, 522 (1940).

155. J. S. Waugh, NMR Basic Principles and Progress 13, 23 (1976).

156. A. Abragam and W. G. Proctor, Phys, Rev. 109, 1441 (1958).

157. N. Bloembergen, S. Shapiro, P. S. Pershan and J. O. Artmann, Phys. Rev. 114, 445 (1959).

158. S. R. Hartmann and E. L. Hahn, Phys. Rev. 128, 2042 (1962).

159. A. Pines, M. G. Gibby and J. S. Waugh, J. Chem. Phys. 59, 569 (1973).

160. D. E. Demco, J. Tegenfeldt and J. S. Waugh, Phys. Rev. B 11, 4133, (1974).

161. L. Müller, A. Kumar, T. Baumann and R. R. Ernst, Phys. Rev. Lett. 32, 1402 (1974).

162. L. Müller and R. R. Ernst, Molec. Phys. 38, 962 (1979).

163. J. R. Franz and C. P. Slichter, Phys. Rev. 148, 287 (1966).

164. Y. Zur, M. H. Levitt and S. Vega, J. Chem. Phys., in press.

165. Y. Tsutumi, M. Kunitomo and T. Hashi, J. Phys. Soc. Japan 20, 2095 (1965).

166. P. Mansfield and G. P. Cant, Phys. Lett. 33A, 130 (1970).

167. M. Kunitomo, J. Phys. Soc. Japan 30, 1059 (1971).

168. M. Kunitomo and T. Hashi, Phys. Lett. A 41, 231 (1972).

169. M. Kunitomo, H. Hatanaka and T. Hashi, J. Phys. Soc. Japan 42, 453 (1977).

170. M. A. B. Whitaker, Phys. Status Solidi B, 98, 449 (1980).

171. F. M. Lurie and C. P. Slichter, Phys. Rev. A 133, 1108 (1964).

172. A. Pines and T. W. Shattuck, J. Chem. Phys. 61, 1255 (1974).

173. T. Terao, S. Matsui and S. Saika, Chem. Phys. Lett. 64, 582 (1979).

174. T. W. Shattuck, "Carbon and Deuterium Nuclear Magnetic Resonance in Solids", Ph.D. dissertation, University of California, Berkeley, 1976, published as Lawrence Berkeley Laboratory Report LBL-5458.

175. S. Vega, T. W. Shattuck and A. Pines, Phys. Rev. A 22, 638 (1980).

176. P. Brünner, M. Rheinhold and R. R. Ernst, J. Chem. Phys. 73, 1086 (1980).

177. M. Rheinhold, P. Brünner and R. R. Ernst, J. Chem. Phys. 74, 184 (1980).

178. S. Vega, Phys. Rev. A 23, 3152 (1981).

179. A. A. Maudsley and R. R. Ernst, Chem. Phys. Lett. 50, 368 (1977).

180. L. Müller, J. Amer. Chem. Soc. 101, 4481 (1979).

181. A. Minoretti, W. P. Aue, M. Rheinhold and R. R. Ernst, J. Magn. Reson. 40, 175 (1980).

182. V. W. Miner and J. H. Prestegard, J. Amer. Chem. Soc. 103, 5979 (1981).

183. R. K. Hester, J. L. Ackerman, V. R. Cross and J. S. Waugh, Phys. Rev. Lett. 34, 993 (1975).

184. R. K. Hester, V. R. Cross, J. L. Ackerman and J. S. Waugh, J. Chem. Phys. 63, 3606 (1975).

185. J. S. Waugh, Proc. Natl. Acad. Sci. 73, 1394 (1976).

186. M.E. Stoll, A. J. Vega and R. W. Vaughan, J. Chem. Phys. 65, 4093 (1976).

187. E. F. Rybaczewski, B. L. Neff, J. S. Waugh and J. S. Sherfinski, J. Chem. Phys. 67, 1231 (1977).

188. J. A. Reimer and R. W. Vaughan, Chem, Phys. Lett 63, 163 (1978).

189. J. A. Reimer and R. W. Vaughan, J. Magn. Reson. 41, 483 (1980).

190. A. Höhener, L. Müller and R. R. Ernst, Molec. Phys. 38, 909 (1979).

191. M. Linder, A. Höhener and R. R. Ernst, J. Chem. Phys. 73, 4959 (1980).

192. M. G. Munowitz, R. G. Griffin, G. Bodenhausen and T. H. Huang, J. Amer. Chem. Soc. 103, 2529 (1981).

193. M. G. Munowitz and R. G. Griffin, J. Chem. Phys. 76, 2848 (1982); 77, 2217 (1982).

194. M. Munowitz, W. P. Aue and R. G. Griffin, J. Chem. Phys. 77, 1686 (1982).

195. T. Terao, H. Miura and A. Saika, J. Chem. Phys. 75, 1573 (1981).

196. Y. S. Yen and A. Pines, J. Chem. Phys. (accepted for publication).

197. N. Bloembergen, E. M. Purcell and R. V. Pound, Phys. Rev. 73, 679 (1948).

198. R. K. Wangsness and F. Bloch, Phys. Rev. 89, 728 (1953).

199. F. Bloch, Phys. Rev. 102, 104 (1956).

200. A. G. Redfield, Advan. Magn. Reson. 1, 1 (1965).

201. A. G. Redfield, IBM J. Res. Develop. 1, 19 (1957).

201. A. G. Redfield, IBM J. Res. Develop. 1, 19 (1957).

202. L. G. Werbelow and D. M. Grant, Advan. Magn. Reson. 9, 189 (1977).

203. R. L. Vold and R. R. Vold, Prog. in NMR Spectrosc. 12, 79 (1978).

204. M. Goldman, "Spin Temperature and Nuclear Magnetic Resonance in Solids" (Oxford University Press, 1970).

205. J. Jeener and P. Broeckaert, Phys. Rev. 157, 232 (1967).

206. S. Emid, A. Bax, J. Konijnendijk, J. Smidt and A. Pines, Physica 96B, 333 (1979).

207. S. Emid, J. Konijnendijk, J. Smidt and A. Pines, Physics 100B, 215 (1980).

208. J. Jeener, personal communication (1981).

209. M. Bloom, personal communication (1981).

210. H. Bildsoe, J. P. Jacobsen and K. Schaumburg, J. Magn. Reson. 23, 137 (1975).

211. J. P. Jacobsen, H. K. Bildsoe and K. Schaumburg, J. Magn. Reson. 23, 153 (1975).

212. J. P. Jacobsen and K. Schaumburg, J. Magn. Reson. 24, 173 (1976).

213. R. R. Vold and R. L. Vold, J. Chem. Phys. 66, 4018 (1977).

214. G. Bodenhausen, N. M. Szeverenyi, R. L. Vold and R. R. Vold, J. Amer. Chem. Soc. 100, 6265 (1978).

215. R. R. Vold and G. Bodenhausen, J. Magn. Reson. 39, 363 (1980).

216. R. R. Vold, R. L. Vold and N. M. Szeverenyi, J. Phys. Chem. 85, 1934 (1981).

217. R. Poupko, R. L. Vold and R. R. Vold, J. Magn. Reson. 34, 67 (1979).

218. R. L. Vold, R. R. Vold, R. Poupko and G. Bodenhausen, J. Magn. Reson. 38, 141 (1980).

219. D. Jaffe, R. L. Vold and R. R. Vold, J. Magn. Reson. 46, 496 (1982).

220. J. Tang and A. Pines, J. Chem. Phys. 72, 3290 (1980).

221. T. Tang, "Study of Correlations in Molecular Motion by Multiple Quantum NMR", Ph. D. dissertation, University of California, Berkeley, 1981, published as Lawrence Berkeley Laboratory Report LBL-13605.

222. J. Jeener, B. H. Meier, P. Buchmann and R. R. Ernst, J. Chem. Phys. 71, 4546 (1979).

223. C. S. Johnson, Jr., Advan. Magn. Reson. 1, 33 (1965).

224. L. M. Jackson and F. A. Cotton, "Dynamical Nuclear Magnetic Resonance Spectroscopy", (Academic, New York, 1975).

225. A. Steigel, "NMR Basic Principles and Progress", 15, 1 (1978).

226. H. W. Speiss, "NMR Basic Principles and Progress", 15, 55 (1978).

227. Z. Luz and S. Meiboom, J. Chem. Phys. 59, 1077 (1973).

228. M. Alla, R. Eckman and A. Pines, Chem. Phys. Lett. 71, 148 (1980).

229. W. Schajor, N. Pislewski, H. Zimmermann and U. Haeberlen, Chem. Phys. Lett. 76, 409 (1980).

230. D. Suter and R. R. Ernst, Phys. Rev. B. 25, 6038 (1982).

231. R. Eckman, A. Pines, R. Tycko and D. P. Weitekamp, submitted for publication.